Determining Seismic Response of Mid-rise Building Frames Considering Dynamic Soil-Structure Interaction

By

Seyed Hamid Reza Tabatabaiefar

A thesis submitted in fulfilment
of the requirement for the degree of
Doctor of Philosophy

Faculty of Engineering and Information Technology
University of Technology Sydney (UTS)

December 2012

CERTIFICATE OF AUTHORSHIP/ORIGINALITY

I certify that the work in this thesis has not previously been submitted for a degree nor has it been submitted as part of requirements for a degree except as fully acknowledged within the text.

I also certify that the thesis has been written by me. Any help that I have received in my research work and the preparation of the thesis itself has been acknowledged. In addition, I certify that all information sources and literature used are indicated in the thesis.

Seyed Hamid Reza Tabatabaiefar

Sydney, December 2012

ABSTRACT

Structures are often mounted on layers of soil unless bedrock is very close to the ground surface. Based on the fact that seismic waves pass through kilometres of bedrock and usually less than 100 meters of soil, soil layers play a significant role in assigning the characteristics of the ground surface movement. When the ground is stiff enough, the dynamic response of the structure will not be influenced significantly by the soil properties during the earthquake, and the structure can be analysed under the fixed base condition. When the structure is resting on a flexible medium, the dynamic response of the structure will be different from the fixed base condition owing to the interaction between the soil and the structure. This difference in behaviour is because of the phenomenon, commonly referred to as soil-structure interaction (SSI), which if not taken into account in analysis and design properly; the accuracy in assessing the structural safety, facing earthquakes, could not be reliable. Performance-based engineering (PBE) is a technique for seismic evaluation and design using performance level prediction for safety and risk assessment. Soil-structure interaction particularly for unbraced structures resting on relatively soft soils may significantly amplify the lateral displacements and inter-storey drifts. This amplification of lateral deformations may change the performance level of the building frames. Thus, a comprehensive dynamic analysis to evaluate the realistic performance level of a structure should consider effects of SSI in the model.

In this study, an enhanced numerical soil-structure model has been developed which treats the behaviour of soil and structure with equal rigor. Structural elements of the soil-structure model are capable of capturing both elastic and inelastic structural behaviour as well as structural geometric nonlinearity (large displacements) in dynamic analysis. Adopting direct method of analysis, the numerical model can perform fully nonlinear time history dynamic analysis to simulate realistic dynamic behaviour of soil and structure under seismic excitations accurately. Fully nonlinear method precisely follows any prescribed nonlinear constitutive relation and adopts hysteretic damping algorithm enabling strain-dependent modulus (G/G_{max} - γ) and damping functions (ξ - γ) to be incorporated directly to capture the hysteresis curves and energy-absorbing characteristics of the real soil. In order to avoid reflection of outward propagating waves back into the model, viscous boundaries comprising independent dashpots in the normal and shear directions are placed at the lateral boundaries of

the soil medium. In addition, the lateral boundaries of the main grid are coupled to the free-field grids at the sides of the model to simulate the free-field motion which would exist in the absence of the structure.

The proposed numerical soil-structure model has been verified and validated by performing experimental shaking table tests at the UTS civil laboratories. For this purpose, a prototype soil-structure system including a building frame resting on a clayey soil has been selected and scaled with geometric scaling factor of 1:30. The soil-structure physical model consists of 15 storey steel structural model, synthetic clay mixture consists of kaolinite, bentonite, class F fly ash, lime, and water, and laminar soil container, designed and constructed to realistically simulate the free field conditions in shaking table tests. A series of shaking table tests were performed on the soil-structure physical model under the influence of four scaled earthquake acceleration records and the results, in terms of maximum structural lateral and vertical displacements, were measured and compared with the numerical predictions. Comparing the predicted and observed values, it is noted that the numerical predictions and laboratory measurements are in a good agreement. Therefore, the numerical soil-structure model can replicate the behaviour of the real soil-structure system with acceptable accuracy.

In order to determine the elastic and inelastic structural response of regular mid-rise building frames under the influence of soil-structure interaction, three types of mid-rise moment resisting building frames, including 5, 10, and 15 storey buildings are selected in conjunction with three soil types with the shear wave velocities less than 600m/s, representing soil classes C_e (V_s=600*m/s*), D_e *(Vs=320m/s)*, and E_e *(Vs=150m/s)* according to Australian Standards, having three bedrock depths of 10, 20, and 30 metres. The structural sections are designed after conducting nonlinear time history analysis, based on both elastic method, and inelastic procedure considering elastic-perfectly plastic behaviour of structural elements. The designed frame sections are modelled and analysed, employing Finite Difference Method adopting FLAC2D software under two different boundary conditions: (i) fixed base (no soil-structure interaction), and (ii) flexible base considering soil-structure interaction. Fully nonlinear dynamic analyses under the influence of four different earthquake records are conducted and the results in terms of lateral displacements, inter-storey drifts, and base shears for both mentioned boundary conditions are

obtained, compared, and discussed. According to the numerical and experimental investigations, conducted in this study, soil-structure interaction has significant effects on the elastic and inelastic seismic response and performance level of mid-rise moment resisting building frames resting on soil classes D_e and E_e. Thus, the conventional elastic and inelastic design procedures excluding SSI may not be adequate to guarantee the structural safety of regular mid-rise moment resisting building frames resting on soft soil deposits.

Based on the numerical results, a simplified design procedure is proposed in which inter-storey drifts under the influence of soil-structure interaction for each two adjacent stories can be determined and checked against the criterion of life safe performance level. This can be used to ensure the performance levels of the mid-rise moment resisting building frames under the influence of SSI remain in life safe level, and the seismic design is safe and reliable. Structural engineers and engineering companies could employ the proposed simplified design procedure for similar structures as a reliable and accurate method of considering SSI effects in the seismic design procedure instead of going through the whole numerical procedure which could be complicated and time consuming.

ACKNOWLEDGMENT

This PhD project could not have been possible without the assistance, understanding, and guidance rendered by numerous people throughout the project. The author would very much like to express his appreciation and gratitude to his principal supervisor, Dr. Behzad Fatahi, for his limitless support, tireless contributions, and guidance throughout this work. The author would also like to very much thank his co-supervisor, Professor Bijan Samali, for his invaluable advice and unfailing assistance throughout the years.

Furthermore, the author would like to thank staff of the UTS Structures Laboratory, Rami Haddad, David Dicker, David Hooper, and Laurence Stonard for their extensive assistance in conducting the experimental works. Special thanks go to Peter Brown, for his remarkable help in all technical matters concerning experimental shaking table tests.

Warm thanks to my friends and colleagues for sharing their time and friendship with the author and rendered precious help. Special thanks to Aslan Sadeghi Hokmabadi (PhD candidate at UTS) for his collaboration and kind assistance during the experimental phase of the project. Aslan and I conducted the experimental part of this research together to be used in our theses. The author also feels a deep sense of gratitude to all the academic and non-academic staff in the Faculty of Engineering and Information Technology for the help rendered.

Words are not enough to thank my family for the support they have given me during this long and sometimes difficult journey. The author would very much like to express his love and gratitude to his mother and father for their love and support, and for instilling in me the value of learning and providing me outstanding opportunities to do so throughout my life. Without their endless help, I would not be able to achieve and enjoy these successes.

LIST OF REFEREED PUBLICATIONS BASED ON THIS RESEARCH

Journal Articles

1. **Tabatabaiefar, H.R.**, Fatahi, B. & Samali, B. 2012, 'Seismic Behaviour of Building Frames Considering Dynamic Soil-Structure Interaction', *International Journal of Geomechanics*, ASCE, doi:10.1061/ (ASCE) GM.1943-5622.0000231 (Accepted on June 5, 2012).
2. **Tabatabaiefar, H.R.**, Fatahi, B. & Samali, B. 2012, 'Idealisation of Soil-Structure System to Determine Inelastic Seismic Response of Mid-Rise Building Frames', *Soil Dynamics and Earthquake Engineering*, Elsevier Ltd (Accepted on March 24, 2012).
3. **Tabatabaiefar, H.R.**, Fatahi, B. & Samali, B. 2012, 'Finite Difference Modelling of Soil-Structure Interaction for Seismic Design of Moment Resisting Building Frames', *Australian Geomechanis Journal*, vol. 47, no. 3, pp.113-120.
4. **Tabatabaiefar, H.R.**, Fatahi, B. & Samali, B. 2012, 'An Empirical Relationship to Determine Lateral Seismic Response of Mid-Rise Building Frames under Influence of Soil-Structure Interaction', *The Structural Design of Tall and Special Buildings*, DOI: 10.1002/tal.1058, Wiley-Blackwell (Accepted on August 9, 2012).
5. **Tabatabaiefar, H.R.**, Fatahi, B. & Samali, B. 2012, 'Lateral Seismic Response of Mid-Rise Building Frames under Influence of Dynamic Soil-Structure Interaction', *Structural Engineering and Mechanics*, Techno Press (Accepted on November 30, 2012).

Peer-reviewed Conference Papers

6. **Tabatabaiefar, H.R.**, Fatahi, B. & Samali, B. 2012, 'Inelastic Lateral Seismic Response of Building Frames under Influence of Bedrock Depth Variations Incorporating Soil-Structure Interaction', *The 22nd Australasian Conference on the Mechanics of Structures and Materials, Materials to Structures : Advancement through Innovation (ACMSM22)*, 11-14 December 2012, Sydney, Australia, pp. 587-592.

7. Hokmabadi, A.S., Fatahi, B., **Tabatabaiefar, H.R.** & Samali, B. 2012, 'Effects of Soil-Pile-Structure Interaction on Seismic Response of Moment Resisting Buildings on Soft Soil', *Proceedings of The Third International Conference on New Developments in Soil Mechanics and Geotechnical Engineering*, Near East University, pp. 337-384.

8. Fatahi, B., **Tabatabaiefar, H.R.**, Hokmabadi, A.S. & Samali, B. 2012, 'Significance of Bedrock Depth in Dynamic Soil-Structure Interaction Analysis for Moment Resisting Frames', *Proceedings of the Second International Conference on Performance-based Design in Earthquake Geotechnical Engineering*, Associazione Geotecnica Italiana, pp. 1396-1406.

9. **Tabatabaiefar, H.R.**, Fatahi, B. & Samali, B. 2012, 'Effects of Soil Dynamic Properties and Bedrock Depth on Seismic Response of Building Frames Incorporation Soil-Structure Interaction', *Proceedings of the 5th Asia-Pacific Conference on Unsaturated Soils Theory and Practice*, pp. 597-603.

10. **Tabatabaiefar, H.R.**, Fatahi, B. & Samali, B. 2011, 'Effects of Dynamic Soil-Structure Interaction on Performance Level of Moment Resisting Buildings Resting on Different Types of Soil', *Proceedings of the 2011 Pacific Conference on Earthquake Engineering (PCEE)*, New Zealand Society for Earthquake Engineering Inc, pp. 1-8.

11. Samali, B., Fatahi, B. & **Tabatabaiefar, H.R.** 2011, 'Seismic behaviour of Concrete Moment Resisting Buildings on Soft Soil Considering Soil-Structure Interaction', *Proceedings of the 21st Australasian Conference on the Mechanics of Structures and Materials (ACMSM21)*, pp. 407-412.

12. Fatahi, B., **Tabatabaiefar, H.R.** & Samali, B. 2011, 'Performance Based Assessment of Dynamic Soil-Structure Interaction Effects on Seismic Response of Building Frame', *Proceedings of Georisk 2011 - Geotechnical Risk Assessment & Management (Geotechnical Special Publication No. 224)*, American Society of Civil Engineers (ASCE), pp. 344-351.

13. **Tabatabaiefar, H.R.** Samali, B., & Fatahi, B. 2010, 'Effects of Dynamic Soil-Structure Interaction on Inelastic Behaviour of Mid-Rise Moment Resisting Buildings on Soft Soils', *Proceedings of the Australian Earthquake Engineering Society 2010 Conference*, Australian Earthquake Engineering Society, pp. 1-11.

14. Fatahi, B., **Tabatabaiefar, H.R.** & Samali, B. 2010, 'Influence of Soil Characteristics on Seismic Response of Mid-Rise Moment Resisting Buildings Considering Soil-Structure Interaction', *Proceedings of the 2010 Symposium on Seismic Engineering Design for Management of Geohazards,* Australian Geomechanics Society, pp. 67-74.

15. **Tabatabaiefar, H.R.** Samali, B., & Fatahi, B. 2010, 'Seismic Behaviour of Steel Moment Resisting Buildings on Soft Soil Considering Soil-Structure Interaction', *Proceedings of the 14 European Conference on Earthquake Engineering 2010*, Macedonian Association for Earthquake Engineering (MAEE), pp.1720-1727.

TABLE OF CONTENTS

LIST OF FIGURES

LIST OF TABLES

LIST OF NOTATIONS

A foundation area

B foundation width

c damping coefficient of the structure

C cohesion

$[C]$ damping matrix

C_h horizontal damping coefficient of the subsoil

C_r rocking damping coefficient of the subsoil

E modulus of elasticity

E_{str} modulus of elasticity of the structural material

f natural frequency of fixed base structure

$\tilde{f}$ natural frequency of soil-structure system

f_c' specified compressive strength

f_m natural frequency of the model

f_p natural frequency of the prototype

F_s total shear force

F_n total normal force

F_x unbalanced forces in x direction from the free-field grid

F_y unbalanced forces in y direction from the free-field grid

$\{F_v\}$ force vector

G shear modulus of the soil

G_{max} largest value of the shear modulus

h height of the structure

h_s bedrock depth

$h\theta$ lateral displacement at the top of the structure due to rotation of the base

I_c flexural rigidity of the building columns

I_r moment of inertia for rocking motion

k stiffness of the structure

k_s shear spring stiffness

k_n normal spring stiffness

K bulk modulus

$[K]$ stiffness matrix

K_h horizontal stiffness coefficient of the subsoil

K_r rocking stiffness coefficient of the subsoil

K_{ss} soil-structure relative rigidity

k_x lateral stiffness of the subsoil foundation

k_θ rocking stiffness of the subsoil foundation

L effective contact length

m mass of the structure

$[M]$ mass matrix

M_p plastic moment capacity

N_s number of stories

r radius of the foundation base

S_p performance factor

S_u soil shear strength

T natural period of fixed-base structure

$\tilde{T}$ natural period of soil-structure system

T_n normal traction at the model boundaries

T_s shear traction at the model boundaries

u lateral displacement at the top of the structure due to structural distortion

u_n incremental relative displacement vector in normal direction

u_s incremental relative displacement vector in shear direction

u_0 lateral displacement at the top of structure due to translation of the base

u_0^t total displacement of the base

u^g horizontal seismic excitation

$\tilde{u}^g$ effective input motion

$\{u\}$ nodal displacement

$\{\dot{u}\}$ nodal velocity

$\{\ddot{u}\}$ nodal acceleration

V base shear of fixed base structure

$\tilde{V}$ base shear of the structure in soil-structure system

V_p compression wave velocity of the soil

V_s shear wave velocity of the soil

W_D dissipated energy in one hysteresis loop

W_S ### maximum strain energy

γ shear strain

γ_{ref} numerical fitting parameter

δ maximum lateral deflection of fixed base structure

$\tilde{\delta}$ maximum lateral deflection of the structure in soil-structure system

Δt time-step

ΔS_y mean vertical zone size at boundary grid point

η material viscosity

θ foundation rotation

λ analysis type factor

μ structural ductility factor

υ Poisson's ratio of the soil

v_x^m *x*-velocity of the grid point in the main grid

v_y^m *y*- velocity of the grid point in the main grid

v_x^{ff} *x*-velocity of the grid point in the free-field grid

v_y^{ff} *y*- velocity of the grid point in the free-field grid

ξ equivalent viscous damping ratio

$\tilde{\xi}$ effective damping ratio

ξ_g hysteretic material damping of the soil

ρ soil density

σ_y yield stress

σ_{xx}^{ff} mean horizontal free-field stress at the grid point

σ_{xy}^{ff} mean free-field shear stress at the grid point

ϕ friction angle

$\tilde{\omega}$ effective natural frequency

ω_s natural frequency of the fixed base structure

CHAPTER ONE

1. INTRODUCTION

1.1 General

The problem of soil-structure interaction in the seismic analysis and design of structures has become increasingly important, as it may be inevitable to build structures at locations with less favourable geotechnical conditions in seismically active regions. The 28 December 1989 Newcastle (Australia) earthquake killed and injured over 150 people and damage bill was about $4 billion. Recently, a similar disaster hit Haiti on 12 January 2010 causing over 200,000 deaths, and leaving over 3 million people homeless. The similarity of these two earthquakes is that both of them are intra-plate earthquakes occurring in the interior of a tectonic plate. In both cases, many mid-rise buildings (approximately 5-15 stories) were severely damaged. The scarcity of land compels engineers to construct major structures over soft deposits. Therefore, there is a need to design structures safely but not costly against natural disasters such as earthquakes. Effects of dynamic soil-structure interaction under extreme loads due to strong earthquakes are significant for many classes of structures and must be included precisely in the design.

Soil-structure interaction (SSI) includes a set of mechanisms accounting for the flexibility of the foundation support beneath a given structure resulting in altering the ground motion in the vicinity of the foundation compared to the free-field. It determines the actual loading experienced by the soil-structure system resulting from the free-field seismic ground motions. The seismic excitation experienced by structures is a function of the earthquake characteristics, travel path effects, local site effects, and soil-structure interaction effects. The result of the first three of these factors can be summarised as free-field ground motion. Structural response to the free-field motion is influenced by SSI. In particular, accelerations within the structure are affected by the flexibility of the foundation support and the difference between foundation support and free-field motions. Consequently, an accurate assessment of the inertial forces and displacements in structures requires a rational treatment of SSI effects.

1.2 Significant of Soil-Structure Interaction

The seismic response of an engineering structure is influenced by the medium on which it is founded. On the solid rock, a fixed base structural response occurs which can be evaluated by subjecting the foundation to the free-field ground motion occurring in the absence of the structure. However, on a deformable soil, a feedback loop exists. In the other words, when the feedback loop exists, the structure responds to the dynamics of the soil, while the soil also responds to the dynamics of the structure. Structural response is then governed by the interplay between the characteristics of the soil, the structure and the input motion.

The Mexico City earthquake in 1985 (Gazetas and Mylonakis, 1998) and Christchurch-New Zealand earthquake in 2011 (Bray & Dashti, 2012) clearly illustrate the importance of local soil properties on the earthquake response of structures. These earthquakes demonstrated that the rock motions could be significantly amplified at the base of the structure. Therefore, there is a strong engineering motivation for a site-dependent dynamic response analysis for many foundations to determine the free-field earthquake motions.

The determination of a realistic site-dependent free-field surface motion at the base of the structure can be the most important step in the earthquake resistant design of structures. For determining the seismic response of building structures, it is a common practice to assume the structure is fixed at the base. However, this is a gross assumption since flexibility of the foundation could be overlooked and underestimated in this case. This assumption is realistic only when the structure is founded on solid rock. The main concept of site response analysis is that the free field motion is dependent on the properties of the soil profile including stiffness of soil layers. The stiffness of the soil deposit can change the frequency content and amplitude of the ground motion. Likewise, on the path to the structure, wave properties might be changed due to the stiffness of the foundation. In general, the subsoil foundation response subjected to seismic ground motion has been dictated by the soil attributes, the soil conditions, and the characteristics of the earthquake. Wave propagation theory denotes that soil layers modify the attribute of the input seismic waves while passing through the soil, so that the acceleration record will be affected.

Soil-structure interaction particularly for unbraced structures resting on relatively soft soils may significantly amplify the lateral displacements and inter-storey drifts.

Considering performance-base design approach, the amplification of lateral deformations due to SSI may noticeably change the performance level of the building frames. Consequently, the safety and integrity of the building would be endangered.

National and international design codes e.g. Australian Standards (AS 1170.4-2007), International Building Code (IBC, 2012) and National Building Code of Canada (NBCC, 2010) permit the use of alternate methods of design to those prescribed in their seismic requirements with the approval of regularity agency having due jurisdiction. The ground motions in seismic regions in Asia-Pacific such as New Zealand, Indonesia, and some parts of Australia will most probably govern the design of lateral resisting systems of buildings. As a result, there is a strong need to develop design tools to evaluate seismic response of structures considering the foundation flexibility and sub-soil conditions.

In this study, numerical and experimental investigations are employed to study effects of dynamic soil-structure interaction on seismic response of regular mid-rise moment resisting building frames. To achieve this goal, an enhanced numerical soil-structure model is developed which has been verified by a series of experimental shaking table tests conducted at the University of Technology Sydney (UTS). Adopting the developed numerical soil-structure model, a comprehensive parametric study has been undertaken to determine elastic and inelastic responses of mid-rise moment resisting building frames under the influence of soil-structure interaction. Based on the results, a simplified procedure is proposed in which inter-storey drifts under the influence of soil-structure interaction for each two adjacent stories can be determined and checked against the seismic code requirements.

1.3 Objectives and Scope of Study

The main objective of this study is to propose a simplified but practical design procedure which enables structural engineers to consider detrimental effects of soil-structure interaction in seismic design of regular mid-rise moment resisting building frames in order to ensure the design safety and reliability. The research work comprises four parts, (a) developing an enhanced numerical soil-structure model, (b) validation of the soil-structure model and experimental investigations using a series of laboratory shaking table tests, (c) conducting numerical parametric study utilising

the validated numerical soil-structure model, and (d) developing a simplified design procedure to predict the seismic response of mid-rise building frames under the influence of soil-structure interaction.

The specific objectives to develop an enhanced soil-structure model in this study are as follows:

- Simulating the complex nature of dynamic soil-structure interaction as accurate and realistic as possible.
- Treating the dynamic behaviour of both soil and structure with equal rigor simultaneously.
- Incorporating hysteretic damping algorithm in the dynamic analysis enabling strain-dependent modulus (G/G_{max} -γ) and damping functions (ξ - γ) to be included directly in order to capture the hysteresis curves and energy-absorbing characteristics of the soil.
- Determining elastic and inelastic structural response under the influence of soil-structure interaction rigorously.
- Employing a Multi Degree of Freedom (MDOF) structure in order to determine inter-storey drifts directly to be used for investigating the performance levels of the building structures under the influence of dynamic soil-structure interaction.

The main objectives of the experimental investigations are:

- Investigating the significance of soil-structure interaction on the seismic response of building frames resting on a deep soil deposit using experimental shaking table tests.
- Verifying the developed numerical soil-structure model as a qualified model which can be employed for further dynamic soil-structure interaction numerical investigations.
- Designing and constructing the soil-structure model components including structural model, soil mix, and laminar soil container.

The key objectives of the numerical parametric study and developing a simplified design approach are:

- Studying, in depth, the seismic behaviour and response of regular mid-rise moment resiting building frames subjected to earthquake action embracing the influence of dynamic soil-structure interaction.
- Acquiring better understanding of key parameters influencing soil-structure interaction under seismic loads.
- Finding the detrimental effects of soil-structure interaction on seismic behaviour of regular mid-rise moment resisting building frames.
- Examining the adequacy of conventional elastic and inelastic design procedures excluding SSI to guarantee the structural safety.
- Proposing a simplified design procedure enabling structural engineers to determine seismic response of regular mid-rise moment resisting building frames under influence of soil-structure interaction utilising fixed base analysis results as well as other basic site and structural characteristics.
- Capturing the detrimental effects of soil-structure interaction in the seismic design procedure of regular mid-rise moment resisting building frames to ensure the design safety and reliability.

1.4 Organisation of the Thesis

Following this introduction, Chapter 2 provides a comprehensive literature review of past research on the effects of soil-structure interaction on seismic behaviour of building frames, theoretical background, analytical and numerical methods, building codes recommendations, proposed relationships for considering soil-structure interaction in seismic design of building frames, and experimental shaking table test techniques for simulation of soil-structure interaction.

Chapter 3 describes characteristics, theoretical concepts, and boundary conditions of the different components of the developed numerical soil-structure model. In addition, adopted methodology for dynamic soil-structure analysis considering soil nonlinear behaviour and hysteretic damping algorithm using backbone curves are discussed.

Chapter 4 depicts adopted laboratory shaking table tests procedure for verifying the proposed numerical soil-structure model and investigating the seismic behaviour of the studied structural model under the influence of soil-structure interaction.

Furthermore, the scaling methodology and utilised scaling factors, design and construction of the soil-structure model components, instrumentations of the model as well as test preparations and set up are described.

Chapter 5 presents a comprehensive parametric study on elastic and inelastic response of regular mid-rise moment resisting building frames under the influence of soil-structure interaction and discusses the results. In the numerical parametric study, height of the structure (h), bedrock depth (h_s), and shear wave velocity of the subsoil (V_s) have been changed. Adopted characteristics of the employed structural frames, subsoils, and earthquake records as well as elastic and inelastic procedures for structural section design of the models are presented as well.

Chapter 6 explains the developed empirical relationships, based on the results of the parametric study, and describes the proposed simplified design procedure for practical applications in order to consider the amplification of inter-storey drifts under the influence of soil-structure interaction in seismic design of mid-rise moment resisting building frames.

Chapter 7 presents the conclusions of the current research and recommendations for further research, followed by References and Appendix A.

CHAPTER TWO

2. LITERATURE REVIEW ON SOIL-STRUCTURE INTERACTION

2.1 Background

Soil-Structure Interaction (SSI) is an interdisciplinary field of endeavour. It lies at the intersection of soil and structural mechanics, soil and structural dynamics, earthquake engineering, geophysics and geomechanics, material science, computational and numerical methods, and other diverse technical disciplines. Its origins trace back to the late 19th century, evolving and maturing gradually in the ensuing decades and during the first half of the 20th century. SSI progressed rapidly in the second half stimulated mainly by the needs of the nuclear power and offshore industries, by the debut of powerful computers and simulation tools such as finite elements, and by the desire for improvements in seismic safety.

The importance of soil-structure interaction both for static and dynamic loads has been well established and the related literature covers at least 30 years of computational and analytical approaches for solving soil–structure interaction problems. Since 1990s, great effort has been made for substituting the classical methods of design by the new ones based on the concept of *performance-based seismic design*. In addition, the necessity of estimating the vulnerability of existing structures and assessing reliable methods for their retrofit have greatly attracted the attention of engineering community in most seismic zones throughout the world.

Several researchers (e.g. Iwan et al., 2000; Krawinkler et al., 2003; Galal and Naimi, 2008; El Ganainy and El Naggar, 2009; Tabatabaiefar and Massumi, 2010; Tavakoli et al., 2011) studied structural behaviour of un-braced structures subjected to earthquake under the influence of soil-structure interaction. Various analytical formulations have been developed to solve complex practical problems assuming linear and elastic SSI (e.g. Stewart et al., 1999; Dutta et al., 2004; Khalil et al., 2007; Tabatabaiefar and Massumi, 2010; Maheshwari and Sarkar, 2011). However, effects of nonlinear behaviour of the supporting soil and inelastic seismic response of structures have not been fully addressed in the literature. In addition, during the recent decades, the importance of dynamic soil-structure interaction for several structures

founded on soft soils has been well recognised. Examples are given by Gazetas and Mylonakis (1998) including evidence that some structures founded on soft soils are vulnerable to SSI.

According to available literature, generally when the shear wave velocity (average shear wave velocity) of the supporting soil is less than 600 m/s, the effects of soil-structure interaction on the seismic response of structural systems, particularly for moment resisting building frames, are significant (e.g. Veletsos and Meek, 1974; Hosseinzadeh and Nateghi, 2004; Galal and Naimi, 2008). Wolf and Deeks (2004) summarised these effects as: (i) increase in the natural period and damping of the system, (ii) increase in the lateral displacements of the structure, and (iii) change in the base shear force depending on the frequency content of the input motion and dynamic characteristics of the soil and the structure. Thus, especially for ordinary building structures, which are the most vulnerable among the built environment, the necessity of a better insight into the physical phenomena involved in SSI problems has been recognised.

2.2 Soil-Structure Interaction (SSI)

Recent improvements in seismological source modelling, analysis of travel path effects, and characterisation of local site effects on the strong shaking, have led to significant advances in both simplified code-based and more advanced procedures for evaluating the seismic demand for structural design. However, a missing link has been an improved and empirically verified treatment of soil-structure interaction.

The estimation of earthquake motions at the construction sites is the most important phase of design to retrofit the performance of the structures. When the structure resting on the hard rock is subjected to seismic loads of an earthquake, the high stiffness of the rock compels the rock motion to be very close to the free field motion. Structures founded on the rock are assumed to be fixed base structures for the structural analysis purposes. However, the same structure would respond differently when supported on the soft soil deposit rather than the hard rock. The inability of the foundation to conform to the deformations of the free field motion would cause the motion of the base of the structure to deviate from the free field motion. Obviously, the dynamic response of the structure itself would induce deformation of the supporting soil. The structural response of buildings subjected to dynamic loads is affected by the interaction between the

structure and the supporting soil media. Dynamics of structures and dynamics of soil define time dependant behaviour of structures and soil under the influence of external loads. This process, in which the response of the soil influences the motion of the structure and response of the structure influences the motion of the soil, is referred to as *Soil-Structure Interaction (SSI).*

For the structures resting on soft soils, the foundation motion is usually different from the free field motion, and a rocking component, caused by the support flexibility, is added. In addition to the rocking component, a part of the structural vibration energy transmits to the soil layer and can be dissipated due to the radiation damping resulting from the wave propagation and hysteresis damping of the soil materials. However, in classical methods for the rigid base structures, this energy dissipation has not been considered.

Seismic analysis of buildings and other engineering structures is often based on the assumption that the foundation corresponds to a rigid half-space, which is subjected to a horizontal, unidirectional acceleration. Such a model constitutes an adequate representation of the physical situation in case of average size structures founded on sound rock. Under such conditions, it has been verified that the free field motion at the rock surface, i.e., the motion that would occur without the building, is barely influenced by building's presence. The hypothesis loses its validity when the structure is founded on soft soil deposits, since the motion at the soil surface, without the building, may be significantly altered by the presence of the structure. Structure rested on soft soil, has its dynamic characteristics, namely the vibration modes and frequencies modified by the flexibility of the supports (Wolf and Deeks, 2004).

2.2.1 Principles of Soil-Structure Interaction

Wolf (1985) indicated that a simple analysis is adequate to demonstrate the important effects of soil-structure interaction. In case of considering a simple SDOF (single degree of freedom) system including a structure characterised by its mass (m), stiffness (k), and damping coefficient (c), resting on a rigid soil deposit, the natural frequency of the resulting fixed base system (ω_0) depends only on the mass and stiffness of the structure and can be determined as:

$$\omega_0 = \sqrt{\frac{k}{m}} \tag{2.1}$$

The equivalent viscous damping ratio (ξ) can be calculated using:

$$\xi = \frac{c\omega_0}{2k} \tag{2.2}$$

If the supporting soil is compliant, the foundation can translate and rotate. Characteristic of such a system was presented by Wolf (1985) as a simple coupled dynamic model (Figure 2.1) consisting of a vertical rigid bar with the horizontal and rocking springs and dashpots with frequency-dependent coefficients denoting the soil attached at one end, and at the other end, at the height equal to h, a spring with coefficient (k) connected to a mass (m), modelling the structure. This system captures the essential effects of soil-structure interaction for a horizontal seismic excitation (u^g), correctly.

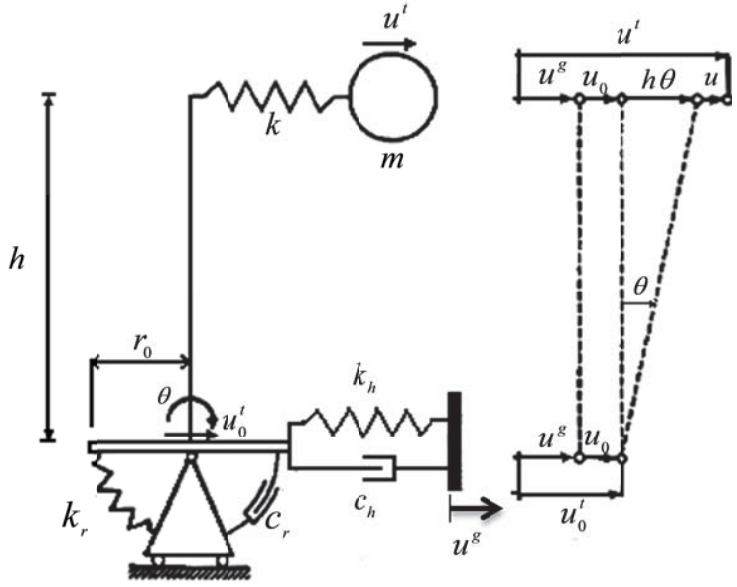

Figure 2.1: Coupled dynamic model of structure and soil for horizontal and rocking motions proposed by Wolf (1985)

In Figure 2.1, r_0 is the radius of the foundation base, θ is the foundation rotation, u_0^t is the total displacement of the base, K_h is the horizontal stiffness coefficient of the subsoil, K_r is the rocking stiffness coefficient of the subsoil, C_h is the horizontal damping coefficient of the subsoil, C_r is the rocking damping coefficient of the subsoil, u_0 is the lateral displacement at the top of structure due to translation of the base, $h\theta$ is

the lateral displacement at the top of the structure due to rotation of the base, and *u* is the lateral displacement at the top of the structure due to structural distortion. Wolf (1985) elucidated that the coupled system (Figure 2.1) can be replaced by an equivalent one-degree-of-freedom system (Figure 2.2) enforcing the same structural distortion (u) as in the coupled dynamic system with the same attributes.

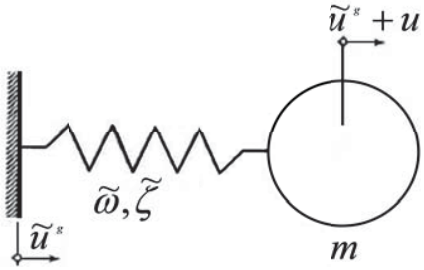

Figure 2.2: Equivalent one-degree-of-freedom system presented by Wolf (1985)

For the above mentioned system, the effective natural frequency ($\tilde{\omega}$), the effective damping ratio ($\tilde{\xi}$), and the effective input motion ($\tilde{u}^g$) are as follows:

$$\frac{1}{\tilde{\omega}^2} = \frac{1}{\omega_s^2} + \frac{1}{\omega_h^2(\tilde{a}_0)} + \frac{1}{\omega_r^2(\tilde{a}_0)} \tag{2.3}$$

$$\tilde{\xi} = \frac{\tilde{\omega}^2}{\omega_s^2}\xi + \left[1 - \frac{\tilde{\omega}^2}{\omega_s^2}\right]\xi_g + \frac{\tilde{\omega}^2}{\omega_h^2(\tilde{a}_0)}\xi_h(\tilde{a}_0) + \frac{\tilde{\omega}^2}{\omega_r^2(\tilde{a}_0)}\xi_r(\tilde{a}_0) \tag{2.4}$$

$$\tilde{u}^g = \frac{\tilde{\omega}^2}{\omega_s^2}u^g$$

(2.5) where,

ω_s = Natural frequency of the fixed base structure;

$\omega_h(\tilde{a}_0)$ = Natural frequency for the translational vibration where the structure is rigid and the foundation is unable to rotate (rocking motion prevented);

$\omega_r(\tilde{a}_0)$ = Natural frequency for rocking where the structure is rigid and the foundation is unable to translate (horizontal motion prevented);

$\xi_h(\tilde{a}_0)$ = Horizontal radiation damping;

$\xi_r(\tilde{a}_0)$ = Rocking radiation damping;

ξ= Hysteretic material damping of the structure; and

ξ_g = Hysteretic material damping of the soil.

For a redundant coupled soil-structure system where the mass of the structure can only displace horizontally without rotating, as illustrated in Figure 2.3, the equivalent one-degree-of-freedom system for horizontal seismic excitation is defined by the effective natural frequency ($\tilde{\omega}$) and the effective damping ratio ($\tilde{\xi}$) as follows:

$$\frac{1}{\tilde{\omega}^2} = \frac{1}{\omega_s^2} + \frac{1}{\omega_h^2(\tilde{a}_0)} + \frac{1}{\omega_s^2 + 12\omega_r^2(\tilde{a}_0)} \tag{2.6}$$

$$\tilde{\xi} = \xi - \frac{\tilde{\omega}^2}{\omega_h^2(\tilde{a}_0)}\left[\xi - \xi_g - \xi_h(\tilde{a}_0)\right] - \frac{36\tilde{\omega}^2\omega_r^2(\tilde{a}_0)}{(\omega_s^2 + 12\omega_r^2(\tilde{a}_0))^2}\left[\xi - \xi_g - \xi_r(\tilde{a}_0)\right] \tag{2.7}$$

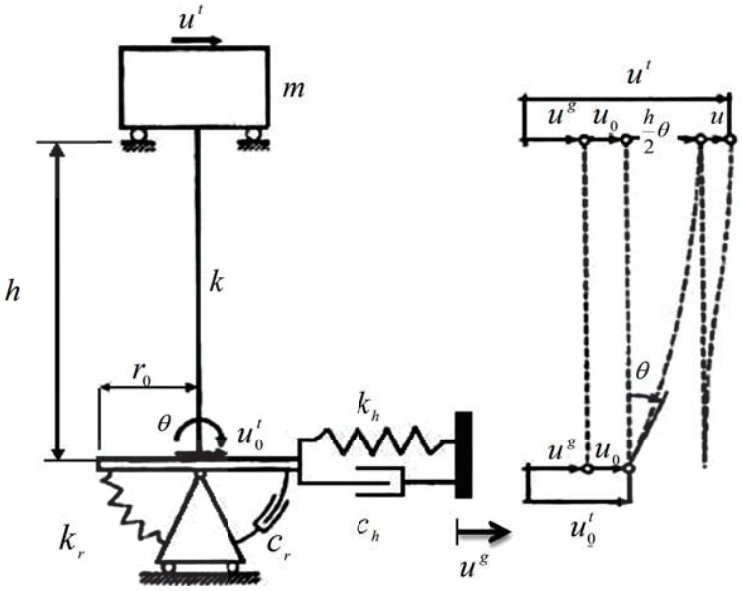

Figure 2.3: Redundant coupled dynamic model of structure with zero rotation of mass and of soil for horizontal and rocking motions (Wolf, 1985)

The effective input motion ($\tilde{u}^g$) for this system can be determined from Equation (2.5). Based on the above mentioned principles, when SSI comes to play, natural frequency of the system decreases (Equations 2.3 and 2.6), while damping of the system increases (Equations 2.4 and 2.7). Therefore, natural period of the system lies in the long period region of the response spectrum curve due to the natural frequency reduction. Consequently, the displacement response (S_d) tends to increase, leading to amplification of the lateral displacements of the system, as denoted by Equation (2.5), while the acceleration response (S_a) tends to reduce. Reduction of

the acceleration response as well as increment of the damping, evidently decrease the base shear and internal forces of the structure.

2.3 Modelling Soil Medium for Soil-Structure Interaction Analysis

Modelling the soil medium beneath the structure in the soil-structure system is one of the most important parts of the dynamic soil-structure interaction analysis. If the soil medium is modelled properly using an appropriate modelling methodology, the seismic response resulting from the dynamic soil-structure analysis can be realistically determined. Several research have been conducted in the subject of soil medium modelling and generally the soil medium can be represented using the following methods:

- Winkler model (spring model);
- Lumped parameter on elastic half-space; and
- Numerical methods.

The above mentioned methods are explained below.

2.3.1 Winkler Model (Spring Model)

According to Bowles (1996), Winkler model denotes the soil medium as a system of interchangeable but independent, closely spaced, discrete and linearly elastic springs. According to this method, deformation of the foundation due to the applied loads is limited to the loaded area. In this method, the subsoil is modelled by linear springs. Figure 2.4 shows the physical representation of the Winkler foundation model. The pressure-deflection relation at any point is given by

$$p = kw \tag{2.8}$$

where, p is the pressure, k is the coefficient of sub-grade reaction or sub-grade modulus, and w is the deformation.

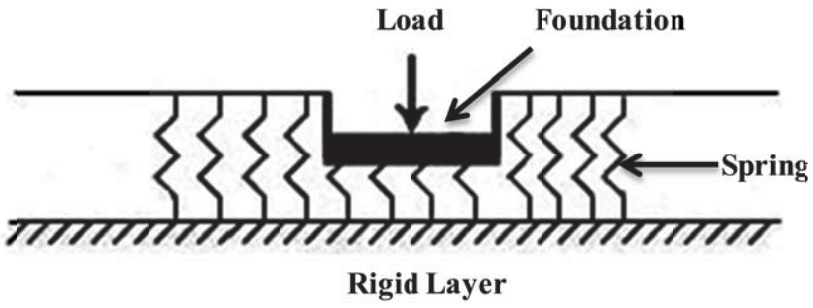

Figure 2.4: Winkler foundation model

Baker (1957), Vesic (1961), Kramrisch et al. (1961), Bowles (1996), and Brown (1977) conducted research on the basis of Winkler hypothesis due to its simplicity.

Dutta and Roy (2002) realised that the basic limitation of Winkler hypothesis lies in the fact that it considers *linear stress–strain behaviour of soil*. The most serious demerit of Winkler model is the one pertaining to the independence of the springs. In addition, they pointed out that despite the simplicity and low computational cost of the Winkler idealisation, another fundamental problem is the determination of the stiffness of the associated elastic springs replacing the soil sub-domain. As a coupled problem, the value of the sub-grade reaction is not only dependent on the sub-grade but also on the parameters of the loaded area as well. However, the sub-grade reaction is the only parameter in Winkler idealisation. Therefore, great care should be practiced in determination of the sub-grade parameter.

The mathematically and computationally attractive but physically inadequate Winkler hypothesis has attracted several attempts over time to develop modified models to overcome its shortcomings. Amongst many are Filonenko-borodich foundation model (Filonenko, 1940), Hetenyi's foundation model (Hetenyi, 1946), Kerr foundation model (Kerr, 1967), and Beam-column analogy model (Horvath, 1993) in order to make it mathematically simpler and physically more realistic. New enhanced methods (e.g. Ter-Martirosyan, 1992; Hashiguchi and Okayasu, 2000) represent the rheological properties of the soil skeleton by combination of elastic, viscous, and plastic elements to consider nonlinear behaviour of the springs.

Dutta and Roy (2002) recommended that Winkler hypothesis, despite its obvious limitations, yields reasonable performance and it is very easy to exercise. Thus, for practical purposes, this idealisation should, at least, be employed instead of carrying out an analysis with fixed base idealisation of structures.

2.3.2 Lumped Parameter on Elastic Half-Space

In this method, three translational and three rotational springs are attached along three reciprocally perpendicular axes and three rotational degrees of freedom about the same axes below each of the foundations of the structure. In addition, dashpots are added to the system in order to consider soil damping of the system (Figure 2.5).

In this method, the spring's stiffness is dependent on the frequency of the forcing function, especially when the foundation is long and resting on saturated clay. In

fact, the inertia force exerted by a time varying force imparts a frequency dependent behaviour, which seems to be more conveniently incorporated in stiffness in the equivalent sense. Thus, the dependence of the spring stiffness, denoting the deformable behaviour of soil, is due to the incorporation of the influence that frequency exerts on the inertia, though original stiffness properties are frequency independent.

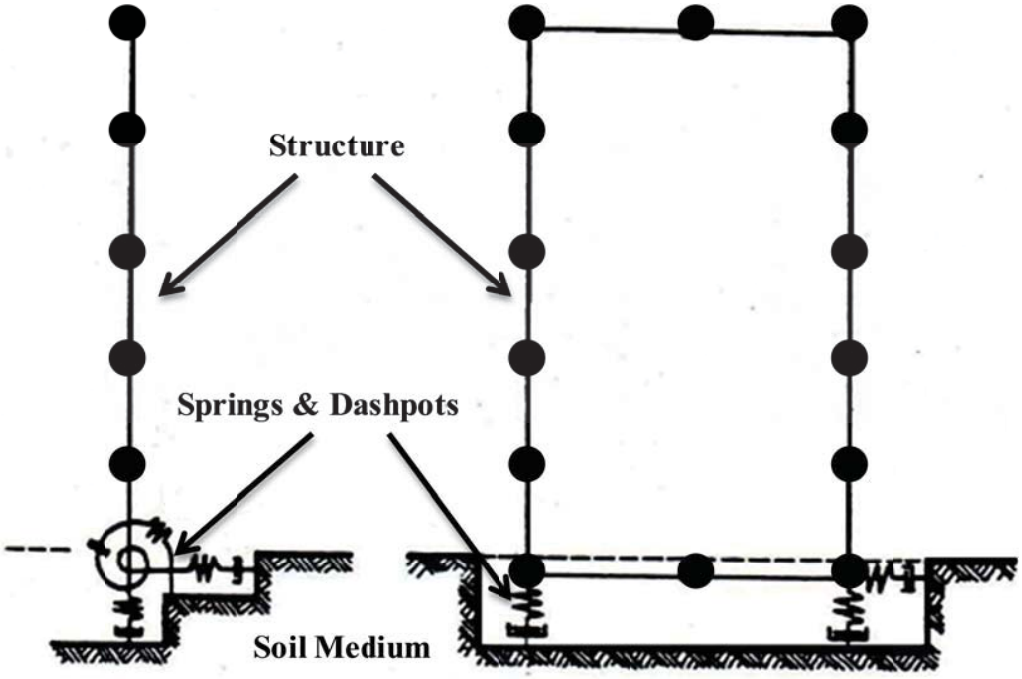

Figure 2.5: Soil modelling in Lumped Parameter method

For the first time, the stiffness values of these springs for arbitrary shaped footings resting on homogeneous elastic half-space were suggested by Lysmer (1965). The stiffness parameters for horizontal, rocking and torsional degrees of freedom were developed later by Gazetas (1991).

The damping coefficients which are proportional to the wave velocity in the soil and the foundation area were proposed by Wolf (1994) as follows:

$$c = \rho v A_0 \tag{2.9}$$

where, c is the damping coefficient taking into account the radiation damping of the soil and foundation, ρ is the soil density, v is the wave velocity of the soil, and A_0 is the foundation area.

Wolf (1994) developed a series of cone model parameters, which have been widely used in practical applications. Foundation stiffness coefficients of the proposed cone model are similar to the stiffness parameters proposed by Gazetas (1991). The cone model parameters proposed by Wolf (1994) are summarised in Table 2.1.

Table 2.1: The cone model properties proposed by Wolf (1994)

Motion		Spring Stiffness Coefficient (k)	Viscous Damping Coefficient (c)
Vertical	$\upsilon \leq 1/3$	$4Ga / (1-\upsilon)$	$\rho.V_p.A$
	$1/3 < \upsilon \leq 1/2$		$\rho.(2V_s).A$
Horizontal		$8Ga / (2-\upsilon)$	$\rho.V_s.A$
Rocking	$\upsilon \leq 1/3$	$8Ga^3 / 3(1-\upsilon)$	$\rho.V_p.I_r$
	$1/3 < \upsilon \leq 1/2$		$\rho.(2V_s).I_r$

In Table 2.1, A is the foundation area, I_r is the moment of inertia for rocking motion, G is the shear modulus of the soil, υ is the Poisson's ratio of the soil, V_s is the shear wave velocity of the soil, and V_p is the compression wave velocity of the soil.

Bowles (1996) describes that, in the Lumped Parameter method, the effect of frequency dependent soil-flexibility on the behaviour of overall structural system is higher than what is obtained from the frequency independent behaviour determined by Winkler model. The additional damping effect imparted by the soil to the overall system may also be conveniently accounted for in this method of analysis. However, he concluded that the accuracy of this method is not adequate for complex problems.

Dutta and Roy (2002) elucidated that the effects of soil-structure interaction on the dynamic behaviour of structures may conveniently be analysed using the Lumped Parameter approach. However, resorting to the numerical modelling may be required for important structures where more rigorous analyses are necessary.

Jahromi (2009) concluded that this method cannot deal accurately with geometric and material nonlinearity, hence modelling the nonlinear response of both soil and structure becomes complex for which more sophisticated modelling approaches would

be required. In addition, he mentioned that with the increasing availability of powerful computers and the wider applicability of numerical methods compared to analytical approaches, the use of the numerical methods has become a common means for modelling such complex interactive behaviour.

2.3.3 Numerical Methods

The advent of powerful computers has significantly changed computational aspects. As the scope of numerical methods has been wider than analytical methods, the use of finite element method (FEM) or finite difference method (FDM) has become more popular for studying complex and complicated interactive behaviour. Both methods produce a set of algebraic equations which may be identical for the two methods to be solved. According to Cundall (1976), it is pointless to argue about the relative merits of finite element or finite difference approaches as the resulting equations are the same. Finite element programs often combine the element matrices into a large global stiffness matrix, while this is not usually done with finite difference because it is relatively more efficient to regenerate the finite difference equations at each step.

Most of the numerical methods (e.g. FDM and FEM) include extended form of matrix analysis based on variational approach, where the whole perpetual is divided into a finite number of elements connected at different nodal points. The general principles and use of finite element method and finite difference method is well documented and explained by Desai and Abel (1987).

Another well known numerical method is boundary element method (BEM) which is based on boundary integral equations which presents an attractive computational framework especially for problems involving singularity and unbounded domains. A detailed literature on the formulation of the method and its applications in different fields is addressed in the book by Brebbia et al. (1984). The basic idea of this method is to formulate the equation of motion of the unbounded domain in the form of an integral equation instead of a differential equation. Finally, this integral equation is solved numerically. Katsikadelis (2002) indicated that boundary element method has been applied in various areas of engineering and science. However, for many complex problems boundary element method is significantly less efficient than finite element and finite difference methods.

Employing numerical methods, researchers are able to model complicated geometries and conditions of soil medium with a high degree of accuracy using two or three dimensional elements (Figure 2.6).

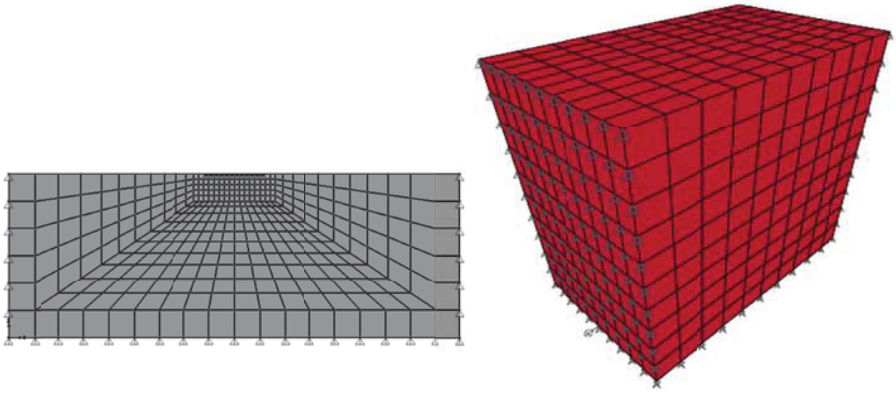

(a) **(b)**

Figure 2.6: Modelling soil medium using numerical methods; (a) 2D model; (b) 3D model

Chopra and Gutierres (1978) pointed out that numerical methods are most appropriate and accurate methods for soil-structure interaction analysis. Dutta and Roy (2002) after conducting a comprehensive critical review on idealisation and modelling of the soil medium for dynamic soil-structure interaction problems concluded that modelling the system through discretisation into a number of elements and assembling the same using the concept of numerical methods have proved to be very useful method, which is recommended to be employed for studying the effect of soil-structure interaction.

According to Bowles (1996) and Dutta and Roy (2002), numerical techniques can incorporate the effects of material nonlinearity (nonlinear stress-strain behaviour), heterogeneous material conditions, stress anisotropy, material and radiation dampings as well as changes in geometry of the supporting soil medium in the dynamic soil-structure interaction analysis, due to the case specific nature of any particular problem. Thus, considering the mentioned merits of using numerical methods for dynamic analysis of soil-structure systems over the other mentioned approaches, and in order to attain rigorous and realistic results, this method is adopted in this study for dynamic analysis of soil-structure interaction.

In general, in order to quantify soil-structure interaction effects using numerical methods, the following two approaches may be utilised:

I). *Substructure method*: In substructure method, the SSI problem is decomposed into three distinct steps which are combined to formulate the complete solution. As reported

by (Kramer, 1996), the superposition inherent to this approach requires an assumption of linear soil and structure behaviour. Varun (2010) described the three mentioned steps in the analysis as follows:

Step 1: Evaluation of a Foundation Input Motion (FIM), which is the motion that would occur on the base-slab if the structure and foundation had no mass.

Step 2: Determination of the impedance function. The impedance function describes the stiffness and damping characteristics of foundation-soil system.

Step 3: Dynamic analysis of the structure supported on a compliant base represented by the impedance function and subjected to a base excitation consisting of the FIM.

Numerous numerical studies (e.g. Kutan and Elmas, 2001; Yang et al., 2008; Carbonari et al., 2012) have been carried out adopting substructure method in assessing the seismic response of structural systems considering soil-structure interaction. Chopra and Gutierres (1978) reported that the principal advantage of the substructure approach is its flexibility. As each step is independent of the others, the analyst can focus resources on the most significant aspects of the problem. However, according to Wolf (1998), as the method is based on the superposition principle, which is exact only for linear soil and structure behaviour, approximations of the soil nonlinearity by means of iterative wave propagation analyses, allow the superposition to be applied for moderately-nonlinear systems. Therefore, taking into account the exact nonlinearity of the subsoil in the dynamic analysis may not be easily achievable using this technique. Kutan and Elmas (2001) noted that much has to be done in investigating the performance of the model and the numerical procedures of substructure method as well as the various influence factors on the response of a soil-structure system. Moreover, the material damping of foundation media in the time domain needs to be improved.

II). *Direct method*: In direct method, the soil and structure are simultaneously accounted for in the mathematical model and analysed in a single step. Typically, the soil is discretised with solid finite elements and the structure with finite beam elements. Principles of this method are described in Section 3.1. Several researchers (e.g. Desai et al., 1982; Mirhashemian et al., 2009; Tabatabaiefar and Massumi, 2010; Gouasmia1 and Djeghaba, 2010) have studied dynamic response of soil-structure systems adopting direct method for modelling soil-structure interaction to achieve accurate and realistic analysis outcomes.

Carr (2008) believes that the advantage of this method in fact is its versatility to deal with complex geometries and material properties. However, data preparation and complexity of the modelling makes it difficult to implement it in every-day engineering practice. In addition, more advanced computer programs are required in this method. Since assumptions of superposition are not required, true and accurate nonlinear analyses are possible in this case (Borja et al., 1992). Therefore, direct method, which is more capable in modelling the complex nature of the soil-structure interaction in dynamic analysis, is employed in this study.

2.4 Effects of Soil-Structure Interaction on Seismic Behaviour of Building Frames

When SSI is taken into consideration, the ground motions imposed at the foundation of the structure are influenced by the soil properties, travel path, local site effects, and the geometry of the soil medium (Wolf and Deeks, 2004). The conventional design practice for seismic analysis assumes the building frames to be fixed at their bases. However, supporting soil medium allows movement due to natural ground flexibility. This may reduce the overall stiffness of the structural system and hence, may increase the natural periods of the system. Such influence of partial fixity of structures at the foundation level due to soil flexibility in turn alters the response. According to Veletsos and Meek (1974), compared with the counterpart fixed-base system, SSI has two basic effects on structural response:

- The soil-structure system has an increased number of degrees of freedom and thus modified dynamic characteristics; and
- A significant part of the vibration energy of the soil-structure system may be dissipated either by radiating waves, emanating from the vibrating foundation-structure system back into the soil, or by hysteretic material damping in the soil.

The result is that soil-structure system has longer natural period of vibration than the fixed-base counterpart.

In addition, Veletsos and Meek (1974) elucidated that the role of the soil-structure interaction may look beneficial to the structural system under seismic loading since it lengthens the lateral fundamental period and leads to higher damping of the system; however, this conclusion is misleading. Gazetas and Mylonakis (1998) pointed out that in reality, supporting soil medium allows some movements due to its natural

flexibility. This may reduce the overall stiffness of the structural system and hence, may increase the natural periods of the system. Such influence of partial fixity of structures at the foundation level due to soil flexibility in turn alters the response. Indeed, case studies and post seismic observations (e.g. Kobayashi et al., 1986; Stewart and Seed, 1998; Gazetas and Mylonakis, 1998) suggest that the SSI can be detrimental and neglecting its influence could lead to unsafe design for both the superstructure and the foundation especially for structures founded on soft soil deposits.

Several researchers (e.g. Veletsos and Prasad, 1989; Balendra and Heidebrecht, 1986) showed that soil-structure interaction effects are significant for medium and long period structures when the predominant site period is large. Recent recorded earthquake spectra demonstrate that SSI will become an important factor for the maximum acceleration occurring at a period greater than 1.0 second. If the fundamental period is lengthened due to SSI, it would increase the response rather than decreasing it, which goes against the conventional design spectra.

Gazetas and Mylonakis (1998) reported three cases of earthquakes, namely, Bucharest 1977, Mexico City 1985 and Kobe 1995, where SSI caused an increase in the seismic-induced response of structures despite a possible increase in damping. They reported that Mexico earthquake was particularly destructive to l0-12 storey unbraced buildings founded on soft clay, whose period increased from about 1.0s (assumption of a fixed base structure) to nearly 2.0 s due to the SSI.

Stewart and Seed (1998) carried out a comprehensive study including soil-structure interaction effects for 77 strong motion data sets at 57 actual building sites that encompass a wide range of structural and geotechnical conditions. The results of the investigation revealed that inertial SSI effects can be expressed by a fundamental natural period lengthening ratio and foundation damping factor, consequently fundamental natural period of the overall system and total damping will be increased by considering SSI effects. In addition, their research indicated that the period lengthening for long-period structures (T > 2 s) with significant higher-mode responses, maybe negligible. They concluded that approaches proposed by Velestos and Meek (1974) to predict $\tilde{T}/T$ can reliably predict the effect of inertial interaction but are limited to single degree of freedom (SDOF) oscillators. The relationship

between the natural period of soil-structure system ($\tilde{T}$) and fixed-base structure (T) proposed by Veletsos and Meek (1974) is as follows:

$$\frac{\tilde{T}}{T} = \sqrt{1 + \frac{k}{k_x}\left(1 + \frac{k_x}{k_\theta}\frac{h^2}{r^2}\right)} \tag{2.10}$$

where, k is the stiffness of the structure, k_x is the lateral stiffness of the subsoil foundation, k_θ is the rocking stiffness of the subsoil foundation, r is the radius of the foundation base (equal to B/2 where B is the foundation width), and h is the height of the structure. Equation (2.10) denotes that by reducing the soil and foundation parameters such as k_θ and r or increasing the structural characteristics such as k and h, the natural period of soil-structure system ($\tilde{T}$) increases.

The objective of Stewart and Seed (1998) research concerns the elaboration of a simple procedure for taking into account the influence of the SSI in the determination of the fundamental frequency of buildings. Analyses conducted by Stewart and Seed (1998) for both one-storey and multi-storey buildings for various geotechnical conditions led to comprehensive charts that give the fundamental frequency of a wide range of buildings in terms of the relative soil-structure stiffness. Research results conducted by Kumar and Prakash (1998) denoted that the fundamental natural period of a soil-structure system reduces nonlinearly with the increase in the soil shear modulus. The effect of considering nonlinear behaviour of the soil on the natural period response of structures depends on the level of strains in the soils. The higher the strain in the soil, the greater is the effect of soil nonlinearity. Kumar and Prakash (1998) have utilised the above mentioned factors (natural period and damping) to derive flexible base fundamental-mode parameters, which are used in response based approaches for evaluating the base shear forces and deformations in structures.

2.4.1 Effects of Shear Wave Velocity of Subsoil on Seismic Response

Soil medium beneath the structure influences the seismic behaviour and response of the structure when an earthquake occurs. If the supporting soil is stiff enough, the response of the structure will not be much affected by the support condition. Therefore, the structure can be assumed as fixed-base. If the foundation soil is flexible, it affects the overall structural response, and consequently, soil-structure interaction effects are considerable. Veletsos and Meek (1974) concluded that

generally when shear wave velocity of the supporting soil is less than 600 m/sec, the effects of soil-structure interaction are significant. This conclusion has been broadly used by other researchers focusing on soil-structure interaction problems (e.g. Stewart et al., 1999; Hosseinzadeh and Nateghi, 2004; El Ganainy and El Naggar, 2009; Tabatabaiefar and Massumi, 2010).

Galal and Naimi (2008) conducted a comprehensive numerical study on moment resisting building frames up to 20 stories under the influence of soil-structure interaction resting on site classes B, C, D, and E according to site classifications of International Building Code (IBC 2009). IBC2009 site subsoil classifications are presented in Table 2.2.

Table 2.2: Site subsoil classifications according to IBC2009

Site Class	Soil profile name	Soil shear wave velocity V_s (m/s)	Soil undrained shear strength, S_u (KPa)	Standard Penetration Resistance N
A	Hard Rock	1500> Vs	N/A	N/A
B	Rock	750 < Vs < 1500	N/A	N/A
C	Very dense soil	360 < Vs < 750	S_u > 100	N > 50
D	Stiff soil profile	180 < Vs < 300	50 < S_u < 100	15 < N < 50
E	Soft soil profile	Vs < 180	S_u < 50	N < 15

Based on the mentioned results, when the supporting rock or very dense soil exists (site class A, B and C), the structure can be assumed as fixed base. For the structures constructed on the other softer soils with shear wave velocity less than 600 m/sec comprising site class E, D and lower limit of C (360 m/s < Vs < 600 m/s), overall structural response might be affected by soil-structure interaction, while for the structures resting on site classes A, B, and upper limit of soil C (600 m/s < Vs < 750 m/s), SSI effects on structural response would be negligible. Thus, in order to find reliable and accurate results, soil-structure interaction effects are needed to be taken into consideration in dynamic analysis of the structures resting on site class E, D and lower limit of C.

2.4.2 Effect of SSI on Seismic Response of Braced Building Frames

Stewart et al. (1999) performed two different simulations procedures to investigate behaviour of steel braced building frames resting on soft soil deposit with shear wave velocity of 190 m/s. SHAKE software was employed to validate the analytical

procedure. It was concluded that structural design based on fixed base assumption is more conservative for the laterally braced building frames. Thus, soil-structure interaction effects for the braced building frames are beneficial and can be ignored.

Azarbakhti and Ashtiani (2008) conducted a comprehensive numerical analysis for a wide range of braced building frames with steel brace or shear wall lateral resisting systems in order to evaluate the effects of soil-structure interaction on the seismic structural seismic response. They concluded that considering influence of SSI in seismic design of laterally braced buildings provides a cost effective design since the sections required are smaller in size.

It can be concluded that considering effects of soil-structure interaction in seismic design of the braced building frames will lead to more economic structural sections which means time, energy and cost saving. Therefore, assuming fixed base structure based on the conventional methods of structural analysis is deemed to be conservative and adequate to guarantee the structural safety.

2.4.3 Effect of SSI on Seismic Response of Unbraced Building Frames

Several studies (e.g. Sivakumaran and Balendra, 1994, Adam et al., 2005, Alavi and Krawinkler, 2004; Galal and Naimi, 2008; Massumi and Tabatabaiefar, 2008; Tavakoli et al., 2011) have reported that soil-structure interaction can increase the lateral deflections and corresponding inter-storey drifts of the structure, forcing the structure to behave in the inelastic range, leading to severe damage of the structure.

Dutta et al. (2004) carried out a numerical study on low-rise unbraced buildings up to 6 stories. They adopted Winkler method for modelling the soil medium, which its demerits in soil modelling was described in Section 2.3.1, using equivalent linear method for dynamic analysis of soil-structure interaction assuming elastic behaviour for the structure. In addition, all the employed soil parameters were assumed parameters rather than real soil parameters determined from actual geotechnical studies. Their results showed that, generally, for low-rise unbraced buildings, the lateral natural period is very small and may lie within the sharply increasing zone of response spectrum. Hence, an increase in lateral natural period due to the effect of soil-structure interaction may cause an increase in the spectral acceleration ordinate. Dutta et al. (2004) concluded that the effect of soil-structure interaction may play a significant role in increasing the seismic base shear of low-rise building frames.

However, seismic response generally decreases due to the influence of soil-structure interaction for medium to high rise buildings.

Galal and Naimi (2008), El Ganainy and El Naggar (2009), and Tavakoli et al. (2011), in their numerical investigations, adopted Lumped Parameter approach, which as explained in Section 2.3.2, is not adequately accurate for rigorous analyses of soil-structure interaction. Additionally, they utilised equivalent linear method for dynamic analysis assuming elastic behaviour for the structure, and assumed soil parameters which may not be completely reflecting the nature of the real soil.

Galal and Naimi (2008) analysed 6 and 20 storey building frames resting on subsoil classes B (750 m/s < *Vs* < 1500 m/s), C (360 m/s < *Vs* < 750 m/s), D (180 m/s < *Vs* < 300 m/s), and E (*Vs* < 180 m/s) according to IBC2000. The results showed that the effects of SSI on the seismic performance of concrete moment resisting building frames up to 20 stories, resting on soft and medium soil types, are significant while those effects are negligible for stiff soils and rocks.

El Ganainy and El Naggar (2009) studied seismic behaviour of steel moment resisting building frames resting on subsoil classes C (360 m/s < *Vs* < 750 m/s) and E (*Vs* < 180 m/s) in accordance with IBC2000 under the influence of soil-structure interaction. They concluded that structural deformations of the buildings were substantially influenced by soil-structure interaction. Lateral deformations of the buildings with flexible bases, experienced considerable amplification ranging from 50% to about 300% in comparison to the fixed bases for buildings founded on soil class E (*Vs* < 180 m/s).

Tavakoli et al. (2011) after conducting a comprehensive numerical study on moment resisting building frames elucidated that, in general, as the soil under the structure becomes softer, SSI influences lateral deflections, inter-storey drifts, base shear, period of the structure, and the earthquake field effects more significantly. According to their results, the importance of soil-structure interaction could be neglected for moment resisting frames resting on rock or very stiff soil while considering SSI for structures supported on relatively soft soil is necessary.

Nevertheless, all the above mentioned researchers (Dutta et al., 2004; Galal and Naimi, 2008; El Ganainy and El Naggar, 2009; and Tavakoli et al., 2011) carried out functional research regarding SSI effects on moment resisting building frames

- They only considered conventional elastic method for structural analysis which can only predict the performance levels implicitly, rather than utilising inelastic method that estimates the magnitude of inelastic deformations and distortions directly and accurately;
- They adopted equivalent linear method (and not nonlinear method) for dynamic analysis of soil-structure interaction. Equivalent linear method has been in use for many years to calculate the wave propagation (and response spectra) in soil and rock at sites subjected to seismic excitation. This method does not capture directly any soil nonlinearity effects because it is based on linear behaviour during the solution process; strain-dependent modulus and damping functions are only taken into account in an average sense, in order to approximate some effects of nonlinearity (damping and material softening); and
- They have adopted Winkler model or Lumped Parameter approach which, as described in Sections 2.3.1 and 2.3.2, cannot realistically capture the dynamic behaviour of the subsoil in the dynamic analysis of soil-structure interaction in comparison to numerical methods.

Therefore, the results of the above mentioned numerical investigations on seismic behaviour of moment resisting building frames can be significantly improved.

In general, considering the above mentioned studies and other available literature, soil-structure interaction, particularly for unbraced structures resting on relatively soft soils, creates large lateral displacements and inter-storey drifts which may change the performance level of the buildings.

In this research, in order to conduct a rigorous, comprehensive, and more realistic investigation on seismic response of moment resisting building frames under the influence of soil-structure interaction and to achieve the most accurate outcomes, the following points are adopted:

- Structural models, representing the range of mid-rise moment resisting frames, will be utilised in conjunction with various types of soil from stiff to soft having the properties extracted directly from actual geotechnical studies of some existing projects. Such data have merit over the assumed parameters

adopted by many researchers which may not be completely conforming to reality;

- Numerical approach using direct method, which could model the complex nature of the soil-structure interaction in dynamic analysis in a realistic way, will be employed;
- Fully nonlinear method of analysis will be adopted in the numerical investigation which correctly represents the physics associated with the problem and follows any stress-strain relation in a realistic way. In this method, small strain shear modulus and damping degradation of soil with strain level can be captured in the modelling precisely; and
- Inelastic structural analysis and P-Delta effects will be taken into account.

2.5 Building Codes Recommendations

Although some international seismic design codes investigated incorporation of simplified soil-structure interaction analysis methods, they acknowledge the need for site specific studies on soft soils subject to strong levels of shaking. Based on design codes, seismic analysis of structures resting on soft soil deposits requires a careful consideration of the site effect and soil-structure interaction. The site effect refers to the scattering and diffraction of the incident waves by the soil layers overlaying the bedrock which are reflected in the values of seismic design coefficients. Soil-structure interaction refers to the relationship between the characteristics of both the structure and the soil stratum, and is usually presented by one of the following methods;

- Modifying the dynamic properties of the structure; or
- Modelling the subsoil with springs and dashpots (Lumped Parameter method).

The 2003 NEHRP, Recommended Provisions for New Buildings and other Structures (BSSC, 2003), includes detailed procedure for incorporating the effects of soil-structure interaction in the determination of design earthquake forces and lateral deflections in the structure. Incorporating these effects has direct result on reducing the base shear applied to the structure, and consequently the lateral forces and overturning moments, while those effects can either increase or reduce the lateral deflections. The NEHRP guidelines for new buildings employ a force-based

specification of structural capacity and seismic demand. Seismic demand is represented by a base shear force that is proportional to the product of building mass and first mode spectral acceleration. Inertial interaction effects are accounted for through analysis of a period lengthening ratio and foundation damping factor which modify the base shear and lateral deflections. BSSC (2003) allows for up to 30% base shear reduction due to SSI, presenting modified base shear value under the influence of soil-structure interaction ($\tilde{V}$). The ratio of the modified base shear to the base shear of the fixed-base structure ($\tilde{V}$ / V) as well as the structural height (h), and the rocking stiffness of the subsoil foundation (k_θ) are employed by the code to determine the modified lateral deflections of the structure due to SSI.

International Building Code 2012 (IBC, 2012) provides minimal design guidance for foundation construction in high risk seismic zones. An emphasis is placed on the capacity of the foundation to sustain the base shear and overturning moments transmitted from the superstructure, and adequacy of superstructure to foundation connections. Chapter 16 of the IBC (Structural Design) provides both response spectrum and time history analyses for earthquake design. However, there are no provisions to account for soil-structure interaction in either method. The current IBC provisions call for the use of the fundamental vibration period which depends on a building's vibration period on a fixed base and a period lengthening ratio. The period lengthening ratio depends on the lateral stiffness and height of the building as well as horizontal, translational, and rotational stiffness of the soil, and is never less than one since flexibility always increases the period. Compared to the simple fixed-base case, the modified system now takes into account a lengthened period and increased damping.

The New Zealand structural design actions for Earthquake actions (NZS1170.5, 2007), adopts a similar approach to IBC (2012) in which the period and the damping of the structure are modified to consider soil-structure interaction effects in seismic design of structures.

For code-designed buildings based on the three above mentioned seismic design codes, it is deemed adequate to consider the site effects due to surface layering and inertial interaction effects on the fundamental mode of vibration which is expressed

by an increment in the fundamental period of the structures and a change in the associated damping.

The 2010 National Building Code of Canada (NBCC, 2010), postulates that the effects of soil-structure interaction on the seismic response of most buildings are favourable, and thus ignoring it, is considered to be conservative. Therefore, the seismic provisions of the proposed NBCC (2010) recommend performing soil-structure interaction analysis for unconventional structures only.

Eurocode 8, Design of Structures for Earthquake Resistance (DIN EN 1998-5, 2010-12), highlights that considering soil-structure effects on the seismic design of structures is only necessary for

- Structures sensitive to P-δ effects;
- Massive or deep seated structures;
- Slender tall structures; and
- Structures supported on very soft soil (V_s< 100 m/s).

For the mentioned structures, the code provides a design procedure, based on Lumped Parameter method, in which appropriate spring and dashpot coefficients are proposed for different subsoil conditions.

AS1170.4 (2007), Earthquake Actions in Australia, does not address the soil-structure interaction effects in seismic design of structures explicitly and consequently structural designers are not able to include those important effects in the analysis and design procedure using the mentioned standard. Therefore, as concluded in the previous section, seismic design of moment resisting building frames resting on relatively soft grounds could not be adequately safe due to amplification of lateral deflections and corresponding inter-storey drifts which possibly change the performance levels of the buildings.

All the reviewed seismic design codes permit the use of alternate methods of design to those prescribed in their seismic requirements with the approval of regularity agency having due jurisdiction. The ground motions in seismic regions such as New Zealand, Japan, China, Indonesia, and some parts of Australia will most probably govern the design of lateral resisting systems of building frames. Thus, well developed seismic design procedures to consider SSI effects in seismic design of building structures are highly required.

2.6 Relationships for Considering SSI Effects in Seismic Design

Several researchers attempted to formulate the effects of the SSI on the seismic response of buildings. Veletsos and Meek (1974) proposed a simple criterion indicating when considering the effects of soil-structure interaction is necessary based on soil shear velocity, natural frequency of fixed base structure, and total height of the structure. The specific objectives of the mentioned contribution were to identify the parameters which best describe the interaction effects and evaluate these effects in order to define the conditions under which they are of sufficient importance to warrant consideration in design.

In addition, Veletsos and Meek (1974) presented a basic equation to determine the ratio of the maximum lateral deflection of the structure in the soil-structure system ($\tilde{\delta}$) to the maximum lateral deflection of fixed base structure (δ) as follows:

$$\frac{\tilde{\delta}}{\delta} = \left(\frac{f}{\tilde{f}}\right)^2 \tag{2.11}$$

where,

$\tilde{f}$ =Natural frequency of soil-structure system; and

f =Natural frequency of fixed base structure.

In spite of the fact that the proposed equation has been extracted from a rigorous analytical procedure, it is not directly suitable for practical purposes. In order to determine the maximum lateral deflection of the structure in the soil-structure system ($\tilde{\delta}$), the natural frequency of fixed base structure (f), the maximum lateral deflection of fixed-base structure (δ), and the natural frequency of soil-structure system ($\tilde{f}$) should be available. The first two parameters can be found directly from analysing the fixed base structure but the third one ($\tilde{f}$) can be determined only after undertaking full dynamic soil-structure interaction analysis and designing the structural sections.

As a result, Equation (2.11) cannot be individually utilised as empirical relationship for determining seismic response of structures under the influence of soil-structure interaction. However, it could be adopted as a basic relationship for further developments.

Khalil et al. (2007), based on their analytical study, presented a criterion which was expressed in terms of soil shear wave velocity *(V_s)*, foundation area *(A)*, flexural rigidity of the building columns including inertial moment (I_c), modulus of elasticity *(E_c)*, storey height *(H)*, number of stories *(N_s)*, and spans in both transversal and longitudinal directions *(N_{bt}, N_{bl})*, as follows:

$$K_{ss} = \frac{N_{bt} \times N_{bl} \times \rho \times V_s^2 \times H^3 \times \sqrt{A}}{N_s \times E_c \times I_c^{0.75}} \tag{2.12}$$

where, K_{ss} is soil-structure relative rigidity and ρ is the soil density.

Khalil et al. (2007) conducted equivalent linear analyses adopting Lumped Parameters method for considering soil-structure interaction effects on elastic seismic behaviour of multi-storey buildings including 1, 3, 5, 7, and 10 storey moment resisting building frames resting on subsoils with various shear wave velocities between 98 m/s and 300 m/s. Based on their study, consideration the soil-structure interaction in a dynamic analysis is essential only when the following criterion exists:

$$Log(K_{ss}) < 1.50 \tag{2.13}$$

In the above mentioned case ignoring the SSI effects could lead to significant misestimation of the seismic response while for higher values, the SSI effects could be neglected. Although the proposed criterion looks comprehensive, practical engineers can use it only after designing the structural sections and the foundation as the relationship comprises foundation area *(A)* and the flexural rigidity of the building columns such as inertial moment (I_c) and modulus of elasticity *(E_c)*. In this case, the user of the criterion is unable to distinguish whether or not considering SSI effect in seismic design of the structure is necessary before finishing the first loop of design process. In addition, the proposed criterion only indicates the necessity of considering soil-structure interaction in seismic design and cannot determine seismic response of the structures. On the other hand, the above mentioned study has been based on equivalent linear analysis and Lumped Parameters method for idealisation of the subsoil and disadvantages and demerits of using those approaches have been described in Section 2.4.3. Practising engineers and engineering companies tend to use reliable and accurate procedures rather than modelling the complex problems themselves and spending hours and hours to solve. On the other hand, as discussed in Section 2.5, most of the national and international seismic design codes either ignore the

soil-structure interaction effects or do not explicitly address all the detrimental influences of SSI in the seismic design. As a result, there is a strong need to develop a simplified but accurate procedure to consider detrimental effects of soil-structure interaction in seismic design of building structures.

In order to respond to this need, in this study, a simplified relationship will be developed assisting designers to determine elastic and inelastic lateral deflections of regular mid-rise moment resisting building frames under the influence of soil-structure interaction utilising analysis results of fixed base structure as well as other basic site and structural characteristics such as height of the structure, bedrock depth, and shear wave velocity of the subsoil.

2.7 Shaking Table Experimental Tests

In this study, adopted numerical approach for dynamic analysis of soil-structure interaction will be verified using shaking table test results conducted at the University of Technology Sydney (UTS) and the effects of soil-structure interaction on seismic response of moment resisting building frames will be monitored and investigated. Shaking table test is an experimental technique used in earthquake engineering to simulate ground motions. Since the emergence of shaking tables in the 1920s, large number of earthquake model tests have been performed. Shaking table tests have been considered as 1g modelling, in which the gravity acceleration of the model and prototype are always the same. Shaking table test is relatively cheap and easy to model complex prototypes, although there is a lack of accuracy due to 1g manner (e.g. low confining pressure of model affects test results especially in sandy soils). It should be noted that, in centrifuge tests by increasing the gravity force via rotating the model, it is possible to accurately model the soil stress- strain condition as exists in prototype. In comparison, although centrifuge test models the stress-strain conditions accurately, it is difficult to build complex prototypes, and due to small size of the model, fewer instruments can be installed (Jakrapiyanun, 2002).

The geotechnical model cannot be directly mounted on shake table because of the requirements of confinement. To model the soil in shaking table tests, a container is required to hold the soil in place. In literature, this container is called Soil Container, Soil Tank, or Shear Stack. During the past few decades, several researchers have carried out shaking table tests on soil-structure systems using various types of soil

containers and structural models as summarised in Table 2.3.

Table 2.3: Past performed shaking table tests on soil-structure systems using various types of soil containers

Container type	References	Comments
Rigid	**Gohl and Finn (1987)** **Yan and Byrne (1989)** **Valsangkar et al. (1991)** **Zen et al. (1992)** **Sato et al. (1995)** **Bathurst et al. (2007)** **Soo Ha et al. (2011)**	*Adopted structural model*: Hollow aluminium tubing, hollow aluminium piles, and retaining wall *Adopted soil model*: Dry Ottawa sand, saturated sand, saturated sand mixed with treated soil
Flexible	**Stanton et al. (1998)** **Richards et al. (1990)** **Kanatani et al. (1995)** **Meymand (1998)** **Maugeri et al. (2000)** **Lu et al. (2004)** **Moss et al. (2010)**	*Adopted structural model*: Steel piles only, wooden shallow foundation, and aluminium piles with SDOF (single Degree of Freedom) steel structure *Adopted soil model*: Dry sand, saturated sand, and reconstituted clayey soil
Laminar	**Jafarzadeh and Yanagisawa (1995)** **Taylor et al. (1995)** **Ishimura et al. (1992)** **Taylor (1997)** **Tao et al. (1998)** **Endo and Komanobe (1995)** **Jakrapiyanun (2002)** **Prasad et al. (2004)** **Pitilakis et al. (2008)** **Chau et al. (2009)** **Tang et al. (2009)** **Turan et al. (2009)** **Chen et al. (2010)** **Lee et al. (2012)**	*Adopted structural model*: Steel piles only, concrete piles only, SDOF (single Degree of Freedom) steel structure on shallow foundation, and SDOF (single Degree of Freedom) steel structure on concrete piles *Adopted soil model*: Dry sand, moist sand, poorly graded river sand, and saturated sand

In many of past experiments, the structure model on top of the soil has not been taken into consideration at all. Some of the tests were only performed on the soil inside the container (e.g. Sato et al., 1995; Kanatani et al., 1995; Taylor, 1997; Prasad et al., 2004; Lee et al 2012) in order to investigate dynamic behaviour of the soil under the influence of earthquake loads, while some others were undertaken on soil-foundation system to observe the dynamic interaction of shallow or pile foundation with the underlying soil (e.g. Stanton et al., 1998; Tao et al., 1998; Richards et al., 1990). In some of the past mentioned experiments, the structural model has been considered but simplified to SDOF (single Degree of Freedom) oscillator (e.g. Meymand, 1998; Ishimura et al., 1992; Jakrapiyanun, 2002; Lu et al., 2004; Pitilakis et al., 2008; Chau et al., 2009) so as to model and investigate dynamic soil-structure interaction. However, by simplifying the structural model, the behaviour of the soil-structure system may not be completely conforming to reality. Thus, in this study, the adopted structural model will simulate most of the structural properties of the real prototype building such as frequency of vibrations, number of stories, and mass. Therefore, this experiment will be a unique experimental shaking table test which considers the structural model in the soil-structure system precisely. As a result, realistic seismic response of a multi-storey frame could be determined experimentally and compared with the numerical modelling results.

Soil containers can be categorised into three main categorise, namely, rigid, flexible, and laminar containers. Rigid containers are the simplest type consisting of no moving parts. According to Jakrapiyanun (2002), studying earth retaining structures such as retaining walls, bridge abutments, and quay walls seems to be appropriate on rigid wall containers as the soil on one side of the earth retaining structure is lower than the other side. Therefore, the soil on the shallower depth is less restricted. The main drawback to rigid containers is distorting the free field boundary conditions. This occurs because firstly the rigid walls cannot move along with soil, and secondly there are excessive energy reflections from their boundaries. In order to provide the free field conditions in this type of container, an extremely large container is required which is not feasible in most cases. Another option to reduce the reflecting energy is to attach energy absorbing layers to the container walls. Steedman and Zeng (1991) concluded that only one third of incident waves could reflect from these kinds of absorbent boundaries. Despite the fact that using absorbent boundaries

decreases the reflection of outward propagating waves back into the model from the boundary walls, those boundaries may cause additional modelling variables like stiffness and friction of the layers (Gohl and Finn, 1987). Valsangkar et al. (1991) employed 25-mm thick Styrofoam as the absorbing layers in their rigid container. The layers were attached to both end walls perpendicular to the shaking direction. Reimer and Meymand (1996) modelled four types of containers and clearly demonstrated the disability of rigid containers in modelling the free field conditions.

Flexible containers allow the modelled soil inside them to move more analogous to the natural conditions of the free field in comparison with rigid containers. In addition, reflection of outward propagating waves back into the model from the walls could be reduced more efficiently. An example for flexible soil containers is a flexible cylindrical soil container shown in Figure 2.7 designed by Meymand (1998). This container is cylindrically shaped (2440 mm (7.5 ft) in diameter and 2130 mm (7 ft) in height). The top ring and base plate were made of steel plates. The top ring was supported by four steel pipes in order to provide the container with full translational and rotational freedom. A rubber membrane was bolted to the top ring and the base plate with compression rings in between. Bands 50 mm (2.0 in) wide were arrayed circumferentially around the exterior of the membrane. Combination of the rubber membrane and bands provided the desired lateral flexibility and radial stiffness (to avoid bulging). In addition, the base plate of the container was roughened by epoxying a high friction coating containing angular crushed gravel pieces onto its surface, and the soil was isolated from the top ring by not filling the container to the top.

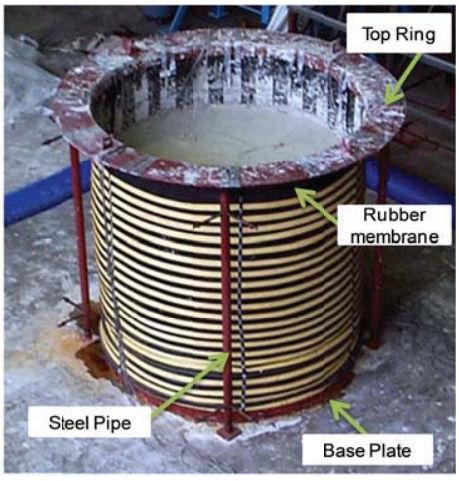

Figure 2.7: Flexible cylindrical soil container (Meymand, 1998)

Gazates (1982) pointed out that laminar soil containers can realistically simulate the free field conditions in comparison with rigid and flexible containers. Several types of inter-layer sliding systems for laminar soil containers have been used over the past few decades such as commercial ball bearings (Ishimura et al., 1992), sliding systems such as Teflon (Chau et al., 2009), and elastic materials such as rubber (Taylor, 1997).

Figure 2.8 illustrates the laminar soil container designed by Taylor (1997). The container had inside dimensions of 5m length, 1m width, and 1.15 m height made of rectangular aluminium frames. Small rubber blocks were inserted between frames with 0.5 m spacing in the longitudinal sides. The noticeable and major points of modelling techniques utilised by Taylor (1997) are as follows:

- As the same tuning stiffness for the container and the soil is required in the desired strain level, and based on the selected maximum strain level for the soil, the natural frequency of the soil was determined. Afterwards, the natural frequency of empty container was fitted to the estimated natural frequency of the soil;
- Sand was glued to the base of the container and end walls to provide frictional contact between the soil and container's base and end walls; and
- The estimated weight of the container was 33% to the soil weight. It is preferable to reduce this portion as much as possible.

By satisfying the above conditions in design of Taylor's laminar soil container, authentic conditions of the free field ground motion could be captured in shaking table tests. Thus, lateral movements of the container in shaking table tests may be almost identical to the free field movements in reality.

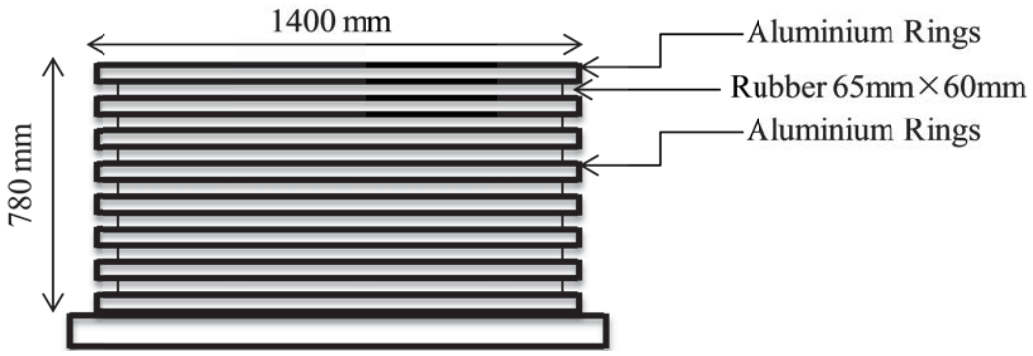

Figure 2.8: Laminar soil container developed by Taylor (1997)

Many researchers (e.g. Gazetas, 1982; Taylor et al., 1995; Pitilakis et al., 2008; Tang et al., 2009) concluded that laminar soil containers are the most advanced and efficient type of the soil containers. Based on the conclusions made by the above mentioned researchers, the merits of adopting laminar soil containers in shaking table tests over the other types of soil containers are as follows:

- Well designed laminar soil containers can better model the free field conditions in comparison with rigid and flexible containers as the lateral deformations in laminar soil containers are almost identical to the free field movements;
- Uniform lateral motion exists in each horizontal plane;
- Lateral motion of the entire depth follows the sinusal shape which represents authentic conditions of the free field ground motion; and
- Most of the recent experimental shaking table tests over the past 10 years (e.g. Jakrapiyanun, 2002; Prasad et al., 2004; Pitilakis et al., 2008; Chau et al. , 2009; Tang et al., 2009; Turan et al., 2009; Chen et al., 2010; Lee et al., 2012) have been carried out using laminar soil containers due its accuracy in modelling the realistic site conditions.

With respect to the above mentioned merits of using laminar soil containers over the other types of containers (flexible and rigid soil containers) and in order to perform rigorous and reliable experimental shaking table tests, a laminar soil container will be employed in this study.

2.8 Summary

In this chapter, a comprehensive literature review has been conducted regarding the effects of soil-structure interaction on the seismic behaviour of building frames and relationships for considering soil-structure interaction effects in seismic design. According to the available literature, soil-structure interaction, particularly for unbraced structures resting on soft soils, creates large lateral displacements and inter-storey drifts which may change the performance level of the buildings. Consequently, the safety and integrity of the unbraced building frames would be endangered.

Based on the available literature, the past researchers performed functional research studies in the field of soil-structure interaction. However, conventional elastic method for structural analysis, which can only predict the performance levels implicitly, was

the structural analysis technique utilised in the past numerical investigations instead of exploiting inelastic method that determines the magnitude of inelastic deformations and distortions directly and accurately. In addition, the past studies have been conducted based on the equivalent linear method which only takes into account the strain-dependent modulus and damping of the subsoil in an average sense, in order to approximate some effects of nonlinearity. Besides, the past studies have been carried out adopting Winkler model or Lumped Parameter approach which are both unable to determine accurate results to realistically depict the dynamic behaviour of the subsoil in the dynamic analysis of soil-structure interaction in comparison to numerical methods. As a result, the outcomes of the past numerical investigations and research studies on seismic behaviour of moment resisting building frames can be significantly improved.

In this research, in order to perform a comprehensive and realistic investigation on the seismic response of moment resisting building frames under the influence of soil-structure interaction, numerical approach using direct method, which could realistically simulate the complex nature of the soil-structure interaction in dynamic analysis, will be utilised. Fully nonlinear method of analysis will be adopted in order to correctly capture the physics associated with dynamic soil-structure interaction problem and to follow the stress-strain relations as required. Moreover, inelastic structural analysis and P-Delta effects will be taken into consideration in order to conduct rigorous dynamic analyses and attain the most accurate outcomes. Besides, structural models, representing the range of mid-rise moment resisting frames, will be selected in conjunction with various soil types from stiff to soft having the properties extracted directly from actual geotechnical studies of some existing projects to ensure the input soil data are completely conforming to reality. Adopted numerical model for dynamic analysis of soil-structure interaction will be verified and validated using shaking table tests and the effects of soil-structure interaction on seismic response of moment resisting building frames will be monitored and investigated. Unlike past shaking table experiments which were performed without the structure or employed simplified SDOF (single Degree of Freedom) oscillators, in this study, the adopted structural model will simulate most of the structural properties of the real prototype building such as frequency of vibrations, number of stories, and mass. Therefore, this experiment will be a unique experimental shaking table test considering the

structural model in the soil-structure system precisely. As a result, realistic seismic response of a multi-storey frame from the experiments could be determined and compared with the numerical modelling results. In addition, in order to perform rigorous and reliable experimental tests, a laminar soil container, which is an appropriate soil container for shaking table tests (its lateral movements in the dynamic tests are almost identical to the free field movements in reality), will be employed.

As AS1170.4 (2007), Earthquake Actions in Australia, does not address the soil-structure interaction effects in seismic design of structures explicitly and most of the renown international seismic design codes (e.g. NZS1170.5, 2007; IBC, 2012; NBCC, 2010) underestimate detrimental effects of soil-structure interaction such as amplification of lateral deflections and corresponding inter-storey drifts and their impact on performance levels of the building, well developed and simplified seismic design procedures to consider those detrimental effects of soil-structure interaction in the seismic design of building structures are strongly required.

In order to respond to this need, in this study, empirical relationships will be developed enabling designers to determine elastic and inelastic lateral deflections of mid-rise moment resisting building frames, similar to the adopted structures in this study, under the influence of soil-structure interaction utilising analysis results of fixed base structure as well as other basic site and structural characteristics. Design engineers may replace the complex and time consuming numerical procedures to determine the actual response of moment resisting building frames under the influence of SSI with the proposed relationships.

CHAPTER THREE

3. NUMERICAL SIMULATION OF SOIL-STRUCTURE INTERACTION

3.1 Soil-Structure System in Direct Method

The governing equations of motion for the structure incorporating foundation interaction and the method of solving these equations are relatively complex. The main reason for this complexity lies in the fact that unlike the ordinary dynamic time history equations of motions (e.g. Equation 5.2 in Chapter 5), the right hand side of the dynamic equation of motion of the soil and structure system (shown in Equation 3.1) consist of a combination of different vectors and matrices of the soil and structure. This combination makes the equation mathematically sophisticated to be solved by conventional methods. Therefore, direct method, the method in which the entire soil-structure system is modelled in a single step, is employed in this study. The soil-structure system simulated using direct method, composed of structure, common nodes, soil foundation system and earthquake induced acceleration at the level of the bedrock, is shown in Figure 3.1.

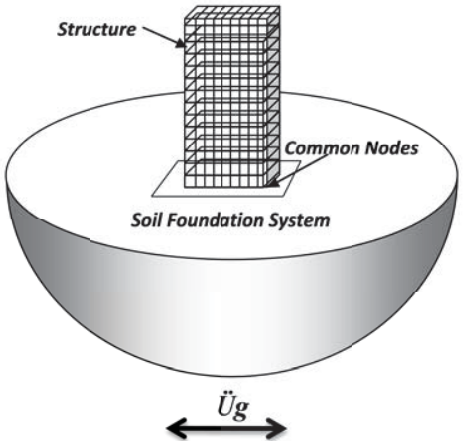

Figure 3.1: Soil-structure system in direct method

The dynamic equation of motion of the soil and structure system can be written as:

$$[M]\{\ddot{u}\} + [C]\{\dot{u}\} + [K]\{u\} = -[M]\{m\}\ddot{u}_g + \{F_v\} \quad (3.1)$$

where, $\{u\}$, $\{\dot{u}\}$, and $\{\ddot{u}\}$ are the nodal displacements, velocities and accelerations with respect to the underlying soil foundation, respectively. [*M*], [*C*] and [*K*] are the mass,

damping, and stiffness matrices of the structure, respectively. It is more appropriate to use the incremental form of Equation (3.1) when plasticity is included, and then the matrix [K] should be the tangential matrix and $\{\ddot{u}_g\}$ is the earthquake induced acceleration at the level of the bedrock. An incremental equation is a form of equation that requires satisfaction of equilibrium at the end of the iteration. Further details about the form and application of incremental equation have been provided by Wolf (1998). For example, if only the horizontal acceleration is considered, then $\{m\}=[1,0,1,0,....1,0]^T$. $\{F_v\}$ is the force vector corresponding to the viscous boundaries. It is nonzero only when there is difference between the motion on the near side of the artificial boundary and the motion in the free field (Wolf, 1998).

3.2 Finite Difference Software, FLAC2D

The use of direct method requires a computer program that can treat the behaviour of both soil and structure with equal rigor simultaneously (Kramer, 1996). Thus, finite difference software, FLAC2D V6.0, is utilised to model the soil-structure system and to solve the equations for the complex geometries and boundary conditions.

FLAC2D (Fast Lagrangian Analysis of Continua) is a two-dimensional explicit finite difference program for engineering mechanics computations. This program can simulate behaviour of different types of structures and materials by elements which can be adjusted to fit the geometry of the model. Each element behaves according to a prescribed constitutive model in response to the applied forces or boundary restraints. The program offers a wide range of capabilities to solve complex problems in mechanics such as inelastic analysis including plastic moment and simulation of hinges for structural systems.

The Finite Difference Method (FDM) is one the earliest numerical modelling techniques that has been employed for the solution of differential equations using initial values and boundary conditions. In FDM, every change of function in the set of equations is directly replaced by an algebraic written terms of the field variables at distinct points in space (Desai and Christian, 1977). In contrast, the Finite Element Method (FEM) has a central requirement that the field quantities (stress, displacement) vary right through each element in a prescribed fashion, using specific functions controlled by defined parameters. The formulation involves the adjustment of these parameters to minimise the error or energy equations.

FLAC uses an “explicit,” time marching method to solve the algebraic equations. The basic formulation for FLAC is for a two-dimensional plane-strain model associated with long structures with invariable cross-sections with the external loads acting in the plane of the cross sections. The dynamic equations of motion are included in the FLAC formulation. In general solution procedure of the dynamic equations of motion, first, FLAC invokes the equations of motion to derive new velocities and displacements from stresses and forces. Then, strain rates are derived from velocities, and new stresses from strain rates (Itasca, 2008).

3.3 Numerical Idealisation of Soil-Structure System

To model soil-structure system in direct method, a novel and enhanced soil-structure model is developed in FLAC2D to simulate various aspects of complex dynamic soil-structure interaction in a realistic and rigorous manner (Figure 3.2). The model treats the behaviour of both soil and structure with equal rigor simultaneously.

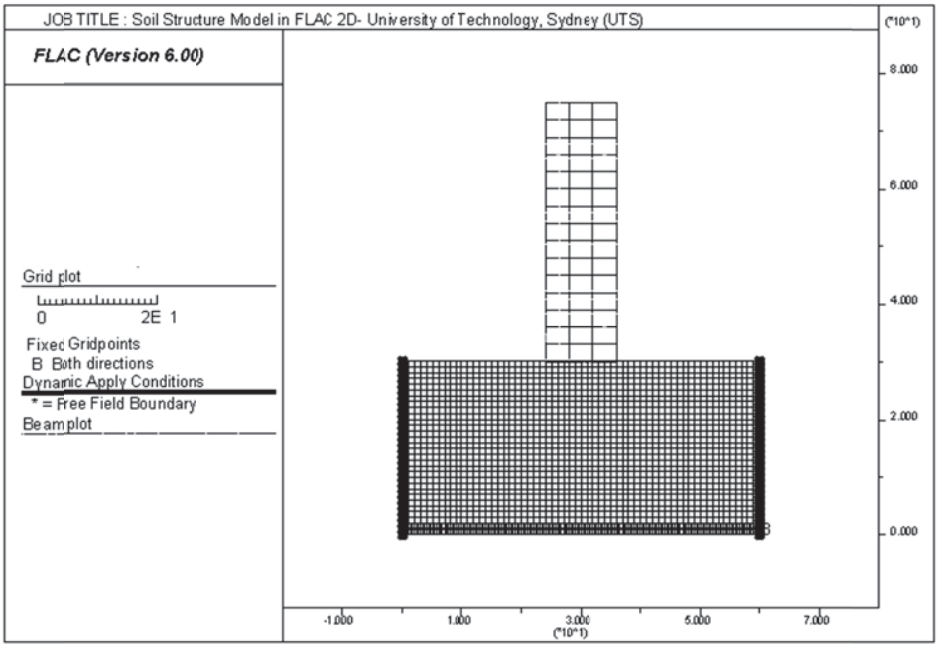

Figure 3.2: Soil-structure model simulated in FLAC2D

The soil-structure model comprises beam structural elements to model the structural components, two dimensional plane-strain quadrilateral elements to model the soil medium, and interface elements to simulate frictional contact between the soil medium and the structure. Rigid boundary condition is assigned to the bedrock and lateral boundaries of the soil medium are assumed to be quiet (viscous) boundaries to avoid reflection of outward propagating waves back into the model. Quiet boundaries are

coupled to the free-field boundaries at the sides of the model to account for the free-field motion which would exist in the absence of the structure. The components of the soil-structure model are illustrated in Figure 3.3. Idealisation of the soil-structure system components and boundary conditions as well as their theoretical principles and assumptions are described in Sections 3.4 - 3.7.

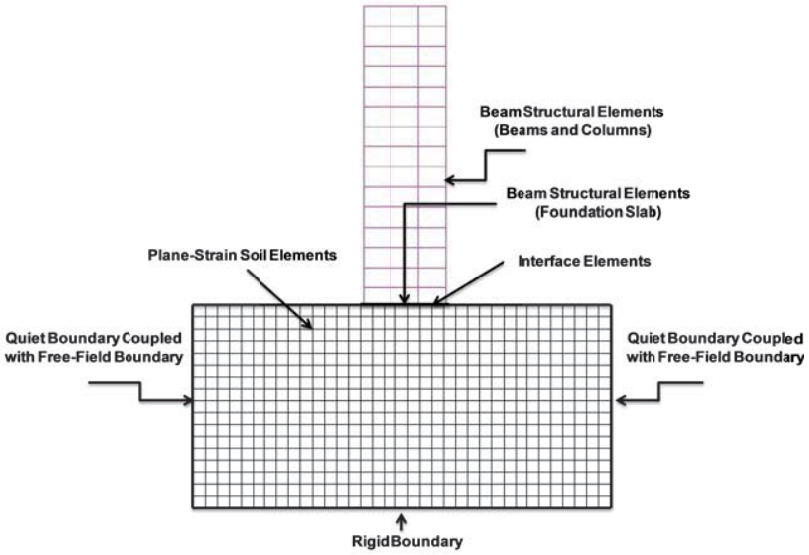

Figure 3.3: Components of the soil-structure model

3.4 Structural Elements

Structural elements of the building frames including beams, columns and foundation slabs are modelled using “Beam Structural Elements (beamSELs)” in the soil-structure model (Figure 3.4). Beam structural elements are two-node, straight, finite elements with six degrees of freedom per node comprising three translational and three rotational components.

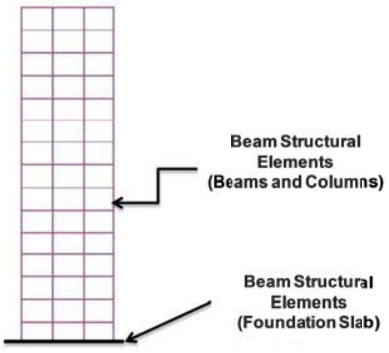

Figure 3.4: Modelling structural elements using beam structural elements

The structural element logic is implemented with explicit-Lagrangian solution procedure. By default, each beamSEL behaves as an isotropic, linearly elastic material with no

failure limit; however, one can specify a limiting plastic moment to model inelastic behaviour of the structure. In inelastic structural analysis, FLAC assumes elastic-perfectly plastic behaviour for beamSELs. In this way, beamSELs behave elastically until they reach the plastic moment and then continue to deform, without inducing additional resistance. Principles of inelastic analysis procedure in FLAC will be described in detail in Section 5.6.2 of Chapter 5.

The full dynamic equations of motion are solved, even for modelling processes that are essentially static. Large displacements, including geometric nonlinearity, can be accommodated by specifying a large-strain solution mode; and the full dynamic response of the system in the time domain can also be obtained with the dynamic-analysis option.

3.4.1 Beam Structural Elements Geometric and Mechanical Properties

Each beam structural element is defined by its geometric and material properties. A beamSEL is assumed to be a straight segment with uniform bisymmetrical cross-sectional properties lying between two nodal points.

Geometric properties for beams, columns, and slab foundations are defined using the following cross sectional parameters:

- A : Cross-sectional area (m^2)
- I_y : Second moment of inertia with respect to y-axis (m^4)

FLAC2D automatically calculates *z*, *y* dimensions for two principal axes of the cross section as well as polar dimension (*r*) for beamSEL cross-section as shown in Figure 3.5 using defined cross sectional parameters, A and I_y.

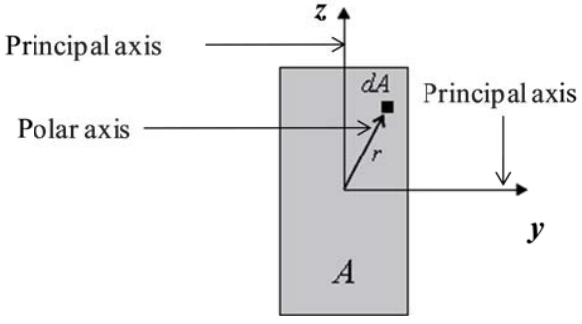

Figure 3.5: General beam structural element cross-section in y-z plane (after Itasca, 2008)

The polar moment of inertia (J), and second moment of inertia with respect to beamSEL *z* axis ($I_{z,}$) are determined afterwards in the beamSEL coordinate system *xyz* by the following integrals:

$$J = \int_A r^2 dA \tag{3.2}$$

$$I_z = \int_A y^2 dA \tag{3.3}$$

Defined mechanical properties and their employed units for beam structural elements are as follows:

- E : Young modulus (Pa)
- ρ : Mass density (kg/m^3)
- v : Poisson's ratio
- M_p *:* Plastic moment capacity ($N.m$)

Plastic moment capacity (M_p) is defined for inelastic structural analysis only. For elastic analysis, the plastic moment capacity value is assumed to be infinite.

3.4.2 Local Systems and Sign Conventions of Beam Structural Element

Beam structural elements have their local coordinate system with 12 active degrees of freedom of the beam element as shown in Figure 3.6.

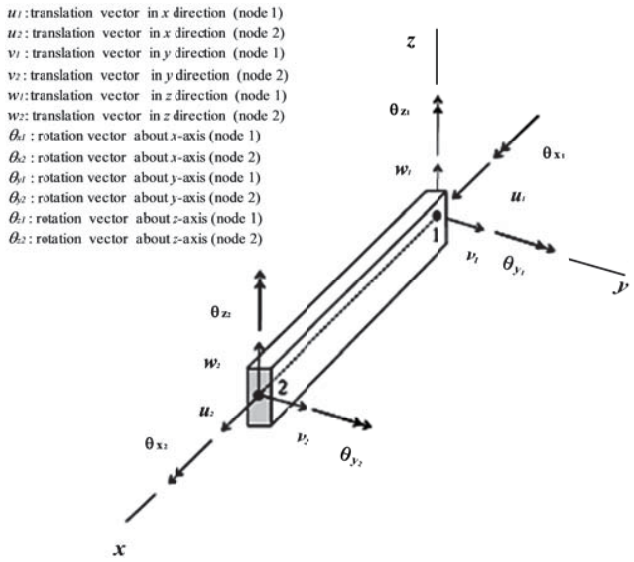

Figure 3.6: Coordinate system of beam structural elements (after Itasca, 2008)

For each generalised displacement (translation and rotation) vector shown in Figure 3.6, corresponding generalised force (force and moment) vector exists. The stiffness matrix of the beam element includes all six degrees of freedom at each node to represent axial, shear and bending actions within the beam structure. This system is utilised to specify both the cross-sectional moments of inertia and applied distributed

loading, and to define the sign convention for force and moment distributions across beamSELs as a single beam (Figure 3.7).

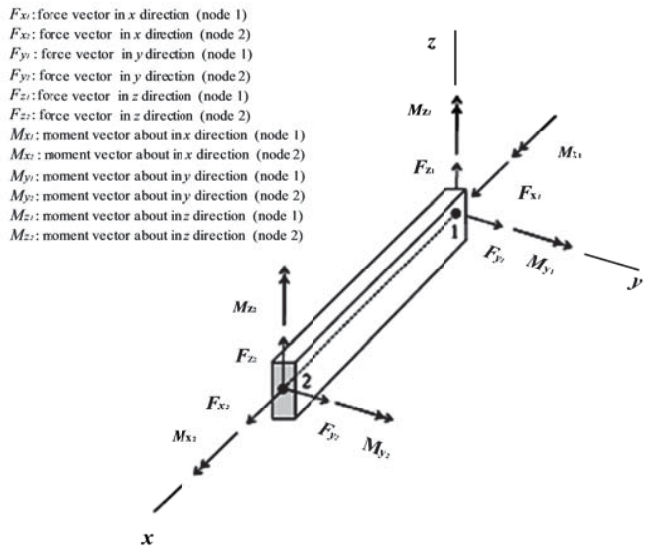

Figure 3.7: Sign convention for forces and moments of beam elements (after Itasca, 2008)

Nodal responses including forces and moments as well as translational and rotational velocities and displacements are computed for each node of beamSEL. Forces and translational velocities are positive in the direction of the positive coordinate axes (either global or node-local) at the node. Positive moments and rotational velocities follow the "right-hand rule": With the thumb pointing in the direction of the positive coordinate axis, the fingers are curled in the positive direction of rotation. The double arrows in Figure 3.7 indicate the direction of the right-hand thumb to define the positive moment and rotation.

3.5 Soil Elements

Soil medium beneath the structure in the soil-structure model is simulated using two dimensional plane-strain grids. The finite difference soil grids composed of quadrilateral elements as shown in Figure 3.8. Quadrilateral elements are four sided elements usually containing four nodes located at the vertices and are bilinear in a rectangular configuration. These elements reveal more information on the stresses compared to the other existing elements. Furthermore quadrilateral elements satisfy equilibrium equation not only in each corner node but also on each face and along all the diagonals of the element. Using quadrilateral elements in FLAC2D substantially reduces the analysis time as the conversion time of this type of element is less than the

other types of the elements. In addition, employing these elements, porous materials can be modelled properly (Itasca, 2008).

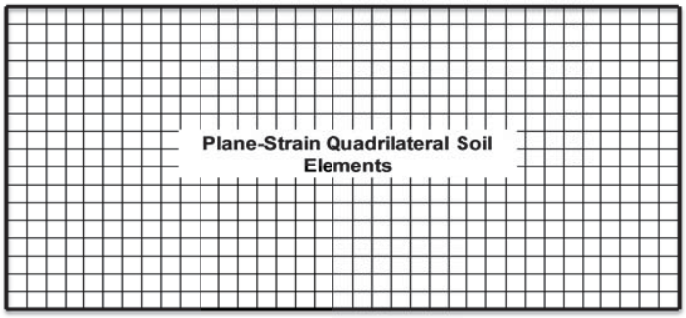

Figure 3.8: Two dimensional plane-strain soil grids consisting of quadrilateral elements

FLAC2D's formulation in finite difference scheme for two dimensional plane-strain soil grids follows the approach of Wilkins (1964). In this scheme, the solid body of soil is divided into a finite difference mesh consisting of quadrilateral elements. Internally, the software subdivides each element into two overlaid sets of constant-strain triangular elements, as shown in Figure 3.9.

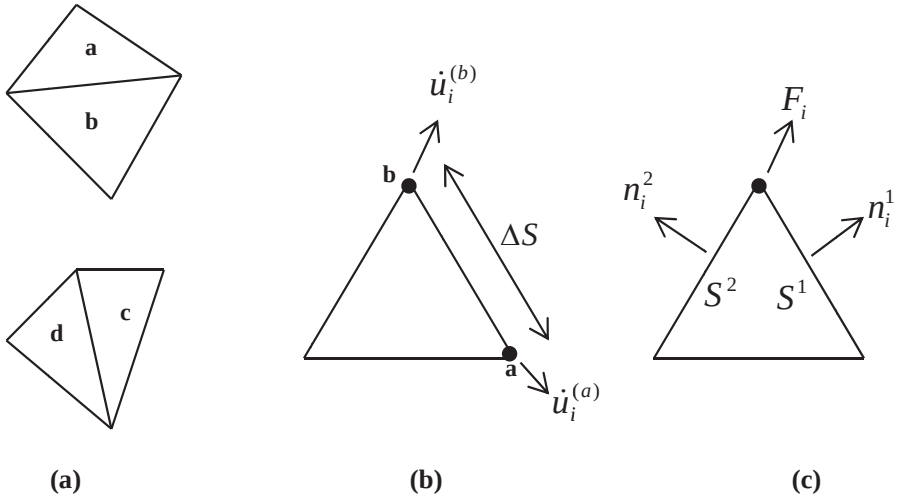

Figure 3.9: (a) Overlaid quadrilateral elements used in soil-structure model; (b) typical triangular element with velocity vectors; (c) nodal force vector (after Malvern, 1969)

The four triangular sub-elements are named a, b, c and d (Figure 3.9). The stress components of each triangle are maintained separately which requires sixteen stress components to be stored for each quadrilateral. It means for each corner of the four triangular sub-elements (totally eight corners), one normal and one shear component need to be stored. The force vector exerted on each node is taken to be the mean of the two force vectors exerted by the two overlaid quadrilaterals. In this way, the response of

the composite element is symmetric, for symmetric loading. If one pair of triangles becomes badly distorted (e.g., if the area of one triangle becomes much smaller than the area of its companion), then the corresponding quadrilateral is not used; only nodal forces from the other (more reasonably shaped) quadrilateral are adopted. If both overlaid sets of triangles are badly distorted, an error message will be issued.

The finite difference equations for the triangular elements (Figure 3.9) are extracted from the generalised form of Gauss' divergence theorem (Malvern, 1969) as follows:

$$\int_s n_i \cdot f \cdot ds = \int_A \frac{\partial f}{\partial x_i} dA \tag{3.4}$$

where, $\int_s$ is the integral around the boundary of a closed surface, n_i is the unit normal to the surface (s), f is a scalar, vector or tensor (for soil modelling it is a vector), x_i are position vectors, ds is an incremental arc length; and $\int_A$ is the integral over the surface area (A).

The average value of the gradient of f over the area A can be calculated as:

$$< \frac{\partial f}{\partial x_i} >= \frac{1}{A} \int_A \frac{\partial f}{\partial x_i} dA \tag{3.5}$$

By substitution of Equation (3.5) into Equation (3.4),

$$< \frac{\partial f}{\partial x_i} >= \frac{1}{A} \int_s n_i \cdot f \cdot ds \tag{3.6}$$

For a triangular sub-element, the finite difference form of Equation (3.6) becomes:

$$< \frac{\partial f}{\partial x_i} >= \frac{1}{A} \sum < f > n_i \cdot \Delta s \tag{3.7}$$

where, Δs is the length of a side of the triangle, and the summation occurs over the three sides of the triangle and the value of $< f >$ is taken to be the average over the sides.

In dynamic formulation, "real" masses are used at grid points rather than the fictitious masses used to improve convergence speed when a static solution is required. Each triangular subzone contributes one-third of its mass (computed from zone density and area) to each of the three associated grid points. The final grid point mass is then divided by two in the case of a quadrilateral zone that contains two overlays.

3.5.1 Soil Elements Constitutive Model and Parameters

The explicit Lagrangian scheme and the mixed-discretization zoning technique exploited in FLAC2D enables users to adopt rigorous geotechnical constitutive models. Two dimensional plane-strain soil quadrilateral elements behave in accordance with a prescribed linear or nonlinear constitutive model in response to applied loads and boundary conditions.

Nonlinear Mohr-Coulomb model has been adopted, in this study, as the soil constitutive model, in the soil-structure model in order to simulate nonlinear behaviour of the soil medium under seismic loading. The adopted Mohr-Coulomb model is a nonlinear elastic-perfectly plastic model that has been employed by many researchers (e.g. Conniff and Kiousis, 2007; Rayhani and EL Naggar, 2008) for modelling dynamic soil-structure interaction to simulate soil behaviour under seismic loads in soil-structure systems. Despite the linear elastic behaviour of conventional Mohr-Coulomb model, variation of shear modulus with shear strain is considered in this study as explained in Section 3.5.3.

Mohr-Coulomb model, in FLAC2D, is explicated in terms of effective stresses based on plane-strain conditions. The failure envelope for this model corresponds to a Mohr-Coulomb criterion (shear yield function) with tension cut off (tensile yield function).

Soil parameters required to be defined for soil elements in conjunction with the Mohr-Coulomb material are as follows:

- Φ : Friction angle (deg)
- C : Cohesion (Pa)
- G : Shear modulus (Pa)
- K : Bulk modulus (Pa)
- ρ : Mass density (kg/m^3)

Table 4.4 in Section 4.5 presents values of the utilised soil parameters in soil-structure model for different soil types.

3.5.2 Soil Damping

According to Roesset et al. (1973), “The most troublesome aspect of analysing soil-structure interaction is defining damping in the system in a useful, meaningful way”. In a homogeneous linear elastic material, stress waves travel indefinitely without change in

the amplitude. This type of behaviour cannot occur in real conditions. The amplitudes of stress waves in real materials, such as soil, attenuate with distance. This attenuation can be attributed to two sources of energy dissipation, one which involves the material through which the waves travel and the other the geometry of the wave propagation problem. However, for specific soils and structures, the operative mechanisms by which the energy is dissipated are not understood sufficiently to allow them to be explicitly modelled. As a result, the effects of the various energy loss mechanisms are usually lumped together and represented by some convenient damping mechanism.

As explained by Das (1983), the most commonly used mechanism for representing energy dissipation is viscous damping which assumes the existence of dissipative forces that are a function of particle velocity. However, for most soils and structures, energy is dissipated hysteretically by yielding or plastic straining of the material.

The type of damping described above is called material damping (intrinsic damping), because the material absorbs the energy of travel during wave propagation. The reduction in energy per unit volume causes the amplitude of the wave to decrease with increasing displacement. However, a different type of damping (reduction in energy per unit volume) can be observed occurring when the energy of the wave is spread over a very large area and thus it dissipates quickly. This type of damping is usually referred to as radiation damping (geometric damping).

Material damping refers to a collection of multiple atomic-level actions, such as interface friction and internal hysteresis, which results in an overall, observable effect. In real materials, part of the elastic energy of a travelling wave is always converted to heat. The conversion is accompanied by decrease in the amplitude of the wave. Viscous damping, by virtue of its mathematical convenience, is often used to present this dissipation of elastic energy. For the purposes of viscoelastic wave propagation, shear behaviour of soils are usually modelled by the stress-strain relationship as follows:

$$\tau = G\gamma + \eta \frac{\partial \gamma}{\partial t} \tag{3.8}$$

where, τ is the shear stress, γ is the shear strain, G is the shear modulus, and η is the viscosity of the material. Thus, the shear stress is the summation of an elastic part (proportional to strain, γ) and a viscous part (proportional to strain rate, $\frac{\partial \gamma}{\partial t}$).

It is currently impractical for typical civil engineering purposes to directly link these atomic actions to system response. Therefore, a material's intrinsic damping is usually approximated using data from one of the several experimental procedures (e.g. resonant column, cyclic triaxial, and spectral analysis of surface waves (SASW) tests) which are different for cohesive and cohesionless soils. It has been observed that material damping of cohesive soils are different from cohesionless due to different atomic-level actions and for each of the mentioned soil categorises, material damping can be extracted from a specific procedure (Wang, 2008).

Since material damping absorbs some of the elastic energy of a stress wave, the specific energy (elastic energy per unit volume) decreases as the wave travels through a material. The reduction of specific energy causes the amplitude of the stress wave to decrease with distance. The specific energy can also decrease by another common mechanism, which can be illustrated by the propagation of stress waves. Dynamic waves produced by an earthquake or other sources distribute in infinite subsoil medium resulting in wave amplitude dissipating in a cylindrical wave front. This dissipation is proportional to $1/\sqrt{r}$ (Figure 3.10); where r is the distance from the source.

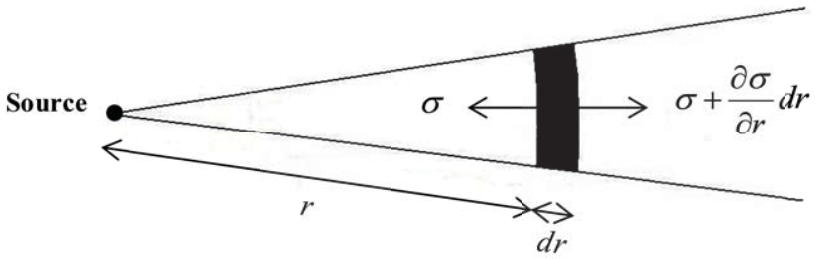

Figure 3.10: Wave amplitude dissipation in soil medium

Equation (3.9) clearly shows that the amplitude of the wave decreases with distance (even though the total elastic energy remains the same).

$$u(r,t) = \frac{1}{r}[f(\upsilon t - r) + g(\upsilon t + r)] \tag{3.9}$$

where, t is elapsed time, υ is $\sqrt{E/\rho}$, and E and ρ are elastic modulus and density of the soil, respectively.

This reduction is of purely geometric origin, resulting from the decrease in the specific energy occurring as the distribution area of the medium increases. Even though elastic energy is conserved, this reduction in amplitude due to spreading of the energy over a greater volume of material is often referred to as radiation damping or geometric damping. For problems in which energy is released from a finite source, ranging from

the large scale case of rupture along an earthquake fault to the smaller-scale of a vibrating foundation, radiation damping could be extremely important. In such cases, the effects of radiation damping often dominate those of material damping.

Ambrosini (2006) pointed out that the damping of soil is an important parameter and must be included in the analysis of soil-structure interaction, especially to determine the maximum top displacement, in which the differences are significant. In addition, he concluded that the reduction of the base shear force and base overturning moment due to the flexibility of the foundation approximately corresponds, 70% to geometric damping and 30% to material damping. For stiff structures having height/width ratios more than one, the rocking motion governs the interaction effect. In this case, especially for low frequency rocking, very little energy is dissipated by the geometric damping of the soil. Thus, the relative importance of the material damping is more pronounced in rocking motion in comparison to translation. The importance of the soil material damping in the displacement response is very significant leading to reduction of the peak displacements as well as the quick reduction of the free vibrations when the earthquake stops.

3.5.3 Soil Shear Modulus

As most soils have curvilinear stress-strain relationships particularly in the small strain rang, as shown in Figure 3.11, the shear modulus is usually described as the secant modulus determined by the extreme points on the hysteresis loop, while the damping factor is proportional to the area inside the hysteresis loop.

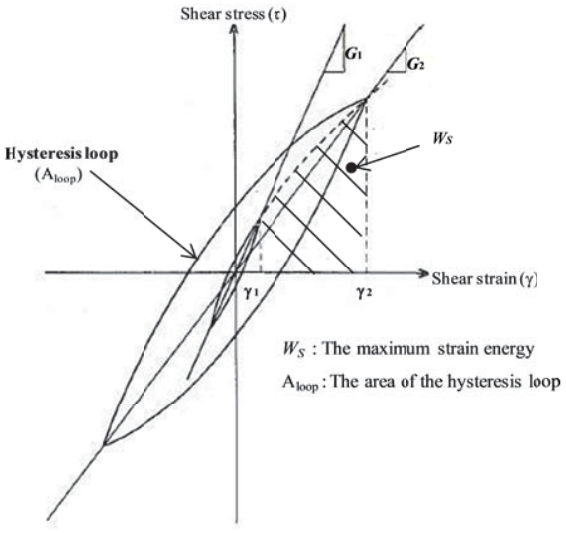

Figure 3.11: Hysteretic stress-strain relationships at different strain amplitudes

Each of these properties depend on the amplitude of the strain for which the hysteresis loop is determined, and therefore both shear modulus and damping factor must be determined as functions of the induced shear strain in the supporting soil.

Two important characteristics of the shape of hysteresis loop are the inclination and the breadth. The inclination of the loop depends on the stiffness of the soil, which can be described at any point during the loading process by the tangent shear modulus. Obviously, tangent shear modulus varies throughout a cycle of loading, but its average value over the entire loop can be approximated by secant shear modulus *G* as follows:

$$G = \frac{\tau_c}{\gamma_c} \tag{3.10}$$

where, τ_c and γ_c are the shear stress and shear strain amplitudes at a defined point, respectively. Thus, *G* describes the general inclination of the hysteresis loop. The breath of the hysteresis loop is related to the area, which can be described by the damping ratio ξ as follows:

$$\xi = \frac{W_D}{4\pi W_S} = \frac{1}{2\pi}\frac{A_{loop}}{G\gamma_c^2} \tag{3.11}$$

where, W_D is the dissipated energy in one hysteresis loop, W_S the maximum strain energy, and A_{loop} the area of the hysteresis loop.

The parameters *G* and ξ are often referred to as equivalent linear material parameters. For certain types of ground response analysis, these are adopted directly to describe the soil behaviour while for nonlinear analysis (hysteretic method) the actual path of the hysteresis loop is required.

As shown in Figure 3.11, the secant shear modulus of the soil element varies with cyclic shear strain amplitude. At low strain amplitudes, the secant shear modulus is high, but it decreases as the shear strain amplitude increases. The locus of points corresponding to the tips of hysteresis loops of various cyclic strain amplitudes is called *backbone (or skeleton)* curve and its slope at the origin represents the largest value of the shear modulus, G_{max}. At greater cyclic strain amplitudes, the modulus ratio G/G_{max} drops to values of less than 1. Thus, characterisation of the stiffness of the soil element requires consideration of both G_{max} and the manner in which the modulus ratio varies with the cyclic shear strain amplitude.

3.5.4 Backbone Curves for Cohesive Soils

Large number of studies (Hardin, 1978; Anderson, 1976; Vucetic and Dobry, 1991; Sun et al., 1998) dealing with relationship between shear modulus ratio (G/G_{max}) and damping ratio with cyclic shear strain (backbone curves) in cohesive soils have been carried out. Sun et al. (1998) represented backbone curves recommended for practical use in seismic site-response evaluations and microzonation. In those curves, relations between G/G_{max} versus cyclic shear strain (Figure 3.12) and damping ratio versus cyclic shear strain (Figure 3.13) for cohesive soils are illustrated.

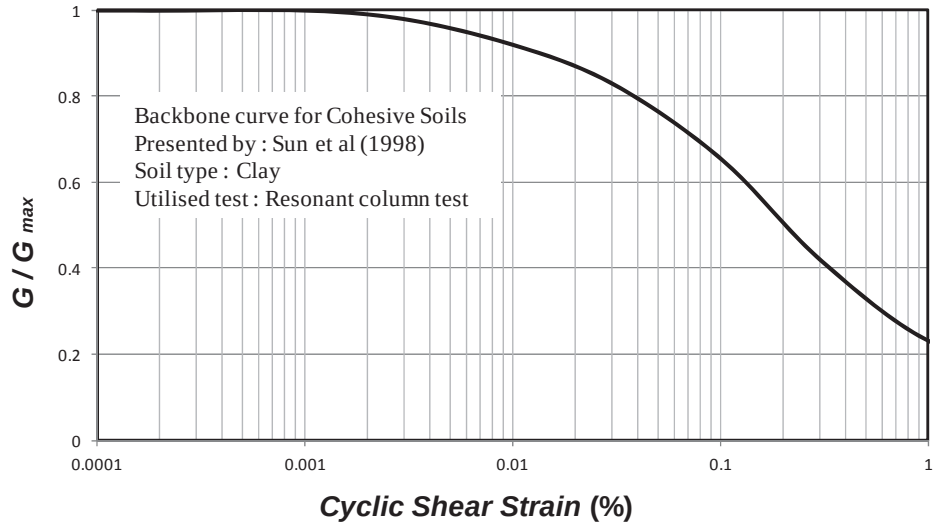

Figure 3.12: Relations between G/G_{max} versus cyclic shear strain for cohesive soils (after Sun et al., 1998)

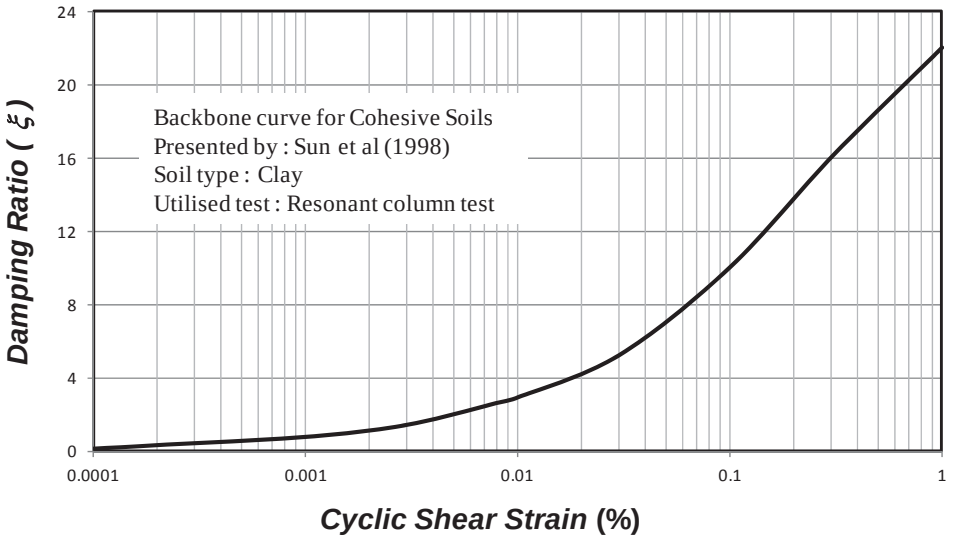

Figure 3.13: Relations between damping versus cyclic shear strain for cohesive soils (after Sun et al., 1998)

Zhang et al. (2005) modified the above mentioned curves based on geologic ages for three categories of soils including Quaternary, Tertiaty and Saprolite soils. Vucetic and Dobry (1991) conducted a study on number of available cyclic loading results and concluded that the soil plasticity index (*PI*) controls the location of the backbone curves for a wide variety of cohesive soils. Sun et al. (1998) backbone curves, employed in this study, take into account the effects of soil plasticity in an average sense, covering common range of soil plasticity indices for cohesive soils. The proposed backbone curves by Sun et al. (1998) can be good representative for soils with Plasticity Indices between 10 to 20, fitting the PI values of the utilised soils in this study (Table 5.3).

3.5.5 Backbone Curves for Cohesionless Soils

Studies carried out by Hardin and Drnevich (1972) and Seed and Idriss (1969) have shown that, while factors such as grain size distribution, degree of saturation, void ratio, lateral earth pressure coefficient, angle of internal friction, and number of stress cycles may have minor effects on the damping ratios of sandy and gravely soils, the main factors affecting the damping ratio are the strain level induced in soil and the soil effective confining pressure. Seed et al. (1986) represented backbone curves for a wide variety of cohesionless soils as illustrated in Figures 3.14 and 3.15. Seed et al. (1986) concluded that damping ratio for gravel is very similar to damping ratio for sand. However, the variation pattern of shear modulus ratio with shear strain shown in Figure 3.14 is generally representative of most sands, but the curve for gravel is a little flatter than the curve for sand. In this study, the average curves (solid lines in Figures 3.14 and 3.15) recommended by Seed et al. (1986) for (G/G_{max} - γ) and (ξ - γ), ignoring the influence of confining pressure for simplicity, have been adopted.

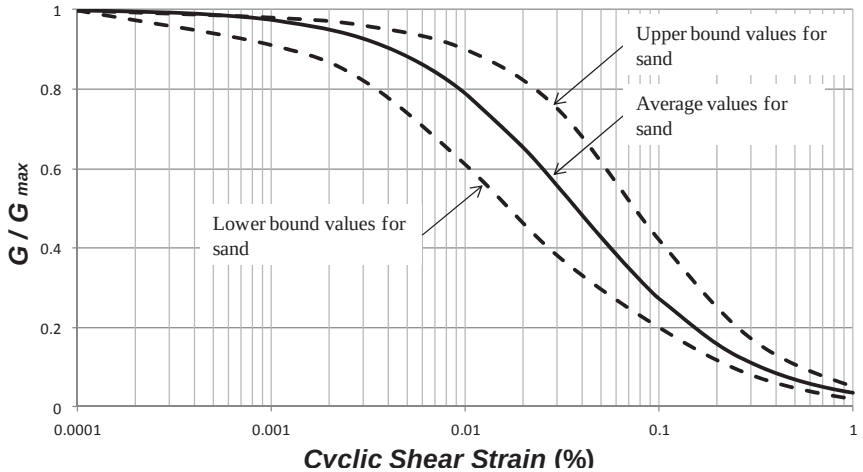

Figure 3.14: Relations between G/G_{max} and cyclic shear strain for cohesionless soils (after Seed et al., 1986)

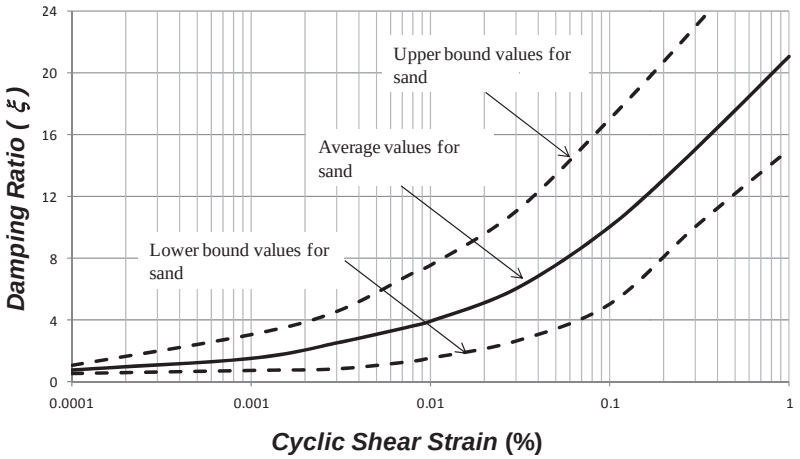

Figure 3.15: Relations between damping ratio and cyclic shear strain for cohesionless soils (after Seed et al, 1986)

3.6 Interface Elements

The foundation facing zone in numerical simulations is separated from the adjacent soil zone by interface elements to simulate frictional contact. The interface between the foundation and soil is represented by normal (k_n) and shear (k_s) springs between two planes contacting each other and is modelled using linear spring system, with the interface shear strength defined by the Mohr–Coulomb failure criterion (Figure 3.16).

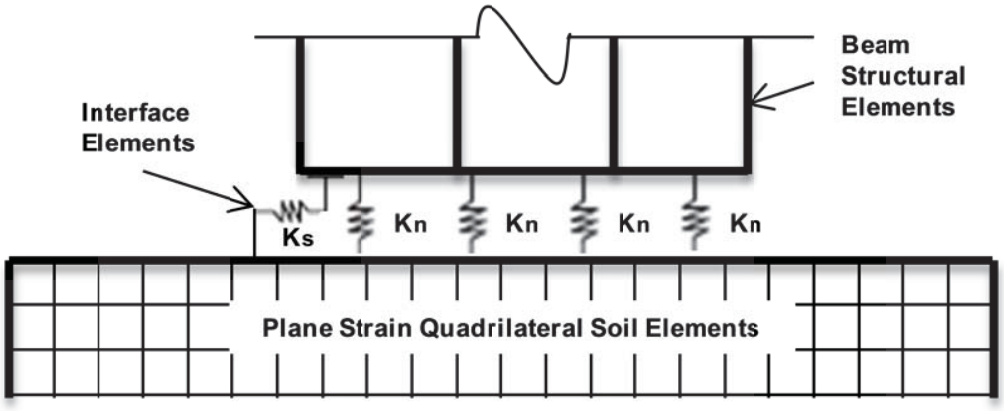

Figure 3.16: Interface elements including normal (k_n) and shear (k_s) springs

The relative interface movement is controlled by interface stiffness values in the normal and tangential directions. Normal and shear spring stiffness values for interface elements of the soil-structure model are set to ten times the equivalent stiffness of the neighbouring zone based on recommended relationship by Rayhani and EL Naggar (2008) and Itasca Consulting Group (2008) for the isotropic soil medium as follows:

$$k_s = k_n = 10\left[\frac{K + \frac{4}{3}G}{\Delta z_{\min}}\right] \tag{3.12}$$

where, K and G are bulk and shear modulus of neighbouring zone, respectively, and $\Delta z_{\min}$ is the smallest width of an adjoining zone in the normal direction. This is a simplifying assumption that has been only used for interface modelling. Since there is no large slip between the soil and foundation, this assumption does not influence the numerical results. The principles and validity of this simplifying assumption have been described by Cundall and Hart (1992). Table 5.5 in Section 5.5 presents employed normal and shear spring stiffness values for interface elements of the soil-structure model for different utilised soil types.

The adopted numerical model in this study employs contact logic which is described by Cundall and Hart (1992) for either side of the interface. The code keeps a list of the grid points (i,j) that lie on each side of any particular surface. Each point is taken in turn and checked for contact with its closest neighbouring point on the opposite side of the interface. During each time-step, the velocity ($\dot{u}_i$) of each grid point is calculated. The incremental displacement for any given time-step is:

$$\Delta u_i = \dot{u}_i \tag{3.13}$$

The incremental relative displacement vector at the contact point is resolved into the normal and shear directions, and total normal and shear forces are determined by

$$F_n^{(t+\Delta t)} = F_n^{(t)} - k_n \Delta u_n^{(t+0.5\Delta t)} L \tag{3.14}$$

$$F_s^{(t+\Delta t)} = F_s^{(t)} - k_s \Delta u_s^{(t+0.5\Delta t)} L \tag{3.15}$$

where,

k_s = Shear spring stiffness;

k_n = Normal spring stiffness;

L = Effective contact length;

F_s = Total shear force;

F_n = Total normal force;

u_s = Incremental relative displacement vector in shear direction;

u_n = Incremental relative displacement vector in normal direction; and

Δt = Time-step.

3.7 Boundary Conditions

Simulation of dynamic soil-structure interaction problems revolves around media which are more appropriate to be modelled as unbounded. Numerical methods, relying on the discretisation of a finite region of space, require that appropriate conditions be enforced at the artificial numerical boundaries. The boundary conditions in the numerical models are prescribed at the boundary of the numerical grids. In the soil-structure model, lateral boundaries of the soil medium are assumed to be quiet boundaries coupled with free-field boundaries, and bedrock boundary condition (bottom of the soil medium grid) is assumed to be rigid boundary. Employed dynamic boundary conditions for soil-structure system are illustrated in Figure 3.17. Detailed explanation of the adopted boundary conditions is provided in the following sections.

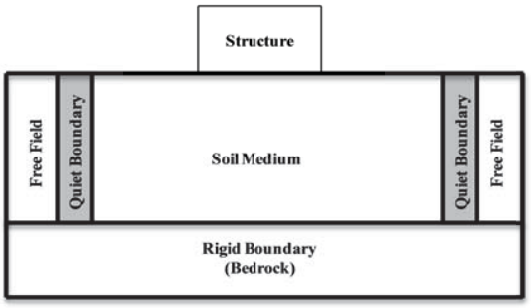

Figure 3.17: Boundary conditions for soil-structure model

3.7.1 Lateral Boundary Conditions

Chopra and Gutierres (1978) suggested that a fixed condition may be assumed at the numerical grid points on the soil side boundaries in the vertical direction while free condition can be assumed in horizontal direction (Figure 3.18). These kinds of boundaries are called preliminary boundaries.

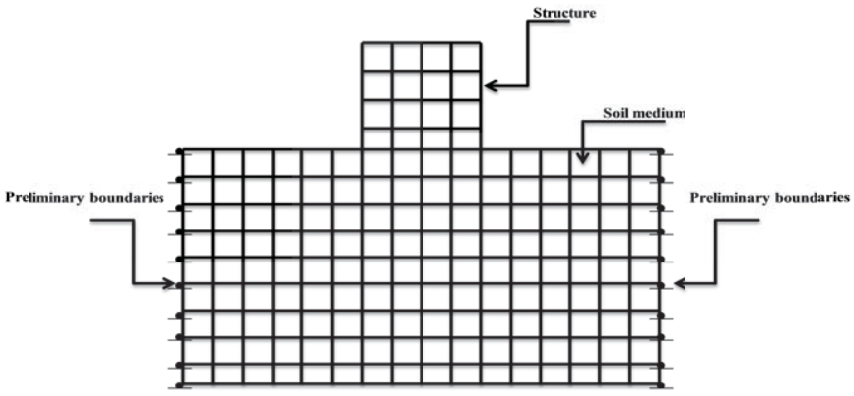

Figure 3.18: Preliminary lateral boundary condition for soil medium (after Chopra and Gutierres, 1978)

In static analyses, preliminary boundaries can be realistically situated at some distance from the centre of the structure. In dynamic problems, however, such boundary conditions could cause the reflection of outward propagating waves back into the model and do not allow the necessary energy radiation. To avoid reflective waves produced by the soil lateral boundaries, Roesset and Ettouney (1977), after a comprehensive study on the performance of different types of soil boundary conditions for dynamic problems, proposed an alternative as the best solution to the problem and introduced quiet (viscous) boundaries.

3.7.1.1 Quiet (Viscous) Boundaries

For lateral boundaries of the soil medium, quiet boundaries (viscous boundaries), proposed and developed by Lysmer and Kuhlemeyer (1969), are utilised in this study. The proposed method is based on utilisation of independent dashpots in the normal and shear directions at the model boundaries. The dashpots provide viscous normal and shear tractions given by:

$$T_n = -\rho.C_P.v_n \tag{3.16}$$

$$T_s = -\rho.C_s.v_s \tag{3.17}$$

where, T_n and T_s are normal and shear tractions at the model boundaries respectively, v_n and v_s are the normal and shear components of the velocity at the boundary, respectively, ρ is the material density, and C_p and C_s are the *p*-wave and *s*-wave velocities, respectively.

3.7.1.2 Free-Field Boundaries

Numerical analysis of the seismic response of surface structures requires the discretisation of a region of the material adjacent to the foundation. The seismic input is normally represented by plane waves propagating upward through the underlying material. Ground responses that are not influenced by the presence of structures are referred to as *free-field motions* (Kramer, 1996). In the current numerical model, the boundary conditions at the sides of the model account for the free-field motion which would exist in the absence of the structure. Free-field boundaries have been simulated using a developed technique in FLAC, involving the execution of a one-dimensional free-field calculation in parallel with the main-grid

analysis. Figure 3.19 shows simulation of lateral boundaries for the soil-structure model in this study.

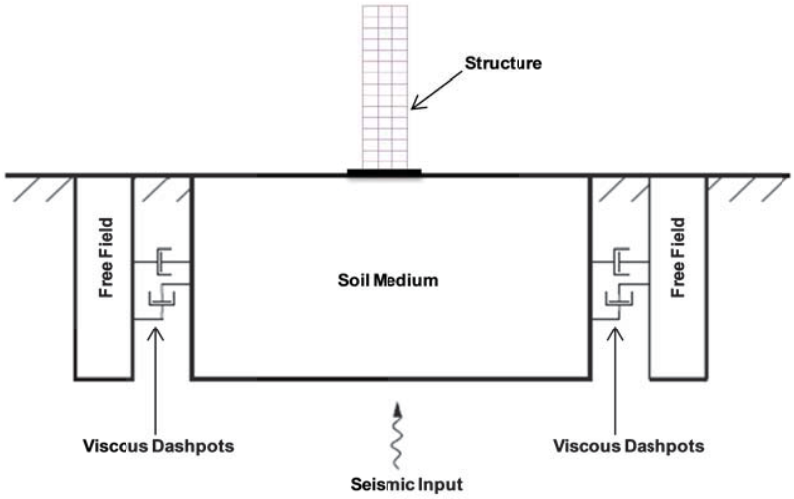

Figure 3.19: Simulating lateral boundary conditions for soil-structure model

As shown in Figure 3.19, the lateral boundaries of the main grid are coupled to the free-field grid simulated by viscous dashpots representing quiet boundaries at the sides of the model, and the unbalanced forces from the free-field grid are applied to the main grid boundary. In order to determine the unbalanced forces from the free-field grid, both conditions applied to the left-hand boundary are expressed in the following equations (similar expressions may be written for the right-hand boundary):

$$F_x = -[\rho C_p (v_x^m - v_x^{ff}) - \sigma_{xx}^{ff}]\Delta S_y \tag{3.18}$$

$$F_y = -[\rho C_s (v_y^m - v_y^{ff}) - \sigma_{xy}^{ff}]\Delta S_y \tag{3.19}$$

where

F_x = unbalanced forces in x direction from the free-field grid;

F_y = unbalanced forces in y direction from the free-field grid;

ΔS_y = mean vertical zone size at boundary grid point;

v_x^m = x-velocity of the grid point in the main grid;

v_y^m = y- velocity of the grid point in the main grid;

v_x^{ff} = x-velocity of the grid point in the free-field grid;

v_y^{ff} = y- velocity of the grid point in the free-field grid;

σ_{xx}^{ff} = mean horizontal free-field stress at the grid point; and

σ_{xy}^{ff} = mean free-field shear stress at the grid point.

Thus, plane waves propagating upward undergo no distortion at the boundary because the free-field grid supplies conditions identical to those in an infinite model. It should be noted that if the main grid is uniform, and there is no surface structure, the lateral dashpots are not exercised because the free-field grid executes the same motion as the main grid.

3.7.2 Bedrock Boundary Condition

There are two possible boundary conditions for simulating the bedrock in a numerical soil-structure model; (i) rigid boundary in which preliminary boundary condition is assigned to the base, and (ii) compliant boundary in which quiet boundary (viscous boundary) is specified along the base of the numerical model. Kocak and Mengi (2000) showed that adopting complaint boundary condition for the bedrock, the effect of the upward-propagating wave train between the bedrock and the soil surface cannot be considered in the dynamic analysis as the entire reflected waves from the surface will be absorbed by the viscous dashpots at the base of the model, while this effect can be captured using rigid boundary condition for the bedrock. Therefore, they concluded that the rigid boundary condition is more appropriate and realistic boundary condition for simulation of the bedrock in dynamic soil-structure analysis. Dutta and Roy (2002), in their critical review on the soil-structure interaction idealisation, concluded the same. In addition, in numerical analyses conducted by other researchers (e.g. Zheng and Takeda, 1995; Koutromanos et al., 2009), boundary condition for the bedrock is assumed to be rigid. With respect to the mentioned previous studies, the simplifying but satisfactory assumption of rigid bedrock boundary condition is adopted in the soil-structure numerical model in this study. In addition, the earthquake acceleration records are directly applied to the grid points along the rigid base of the soil medium mesh in the present study. It should be noted that according to Pitilakis and Terzi (2011), rigid boundary assumption for simulation of the bedrock in soil-structure interaction analysis may not be appropriate when the impedance contrast between the bedrock and the soil medium is substantially high.

3.7.3 Distance between Soil Boundaries

Rayhani and Naggar (2008), after undertaking comprehensive numerical modelling

and centrifuge model tests, concluded that the horizontal distance of the soil lateral boundaries should be at least five times the width of the structure in order to avoid reflection of outward propagating waves back into the model. They also recommended 30 metres as the maximum bedrock depth in the numerical analysis as the most amplification occurs within the first 30 metres of the soil profile, which is in agreement with most of modern seismic codes (e.g. ATC-40, 1996; BSSC, 2003). Those seismic codes evaluate local site effects just based on the properties of the top 30 meters of the soil profile. Thus, in this study, the horizontal distance of the soil lateral boundaries is assumed to be 60 metres (five times the width of the structure which is 12 metres) and the maximum bedrock depth is 30 metres.

3.8 Dynamic Analysis of Soil-Structure Systems

Several attempts have been made in recent years in the development of numerical procedures for assessing the response of supporting soil medium under seismic loading conditions. Successful application of these methods for determining ground seismic response is vitally dependent on the incorporation of the soil properties in the analyses. As a result, substantial effort has been made toward the determination of soil attributes to be used in the numerical procedures.

3.8.1 Numerical Procedures for Dynamic Analysis of Soil-Structure Systems

There are two main numerical procedures for dynamic analysis of soil-structure systems under seismic loads; (i) equivalent-linear method, and (ii) fully nonlinear method. The traditional standard practice for dynamic analysis of soil-structure systems has been based on equivalent-linear method. The fully nonlinear analysis has not been applied as often in practical design due to its complexity. However, practical applications of fully nonlinear analysis have increased in the last decade, as more emphasis is placed on reliable predictions in dynamic analysis of complex soil-structure systems (Byrne et al., 2006). Details of these two methods are explained below.

3.8.1.1 Equivalent Linear Method

The equivalent linear method has been in use for many years to calculate the wave propagation (and response spectra) in soil and rock at sites subjected to seismic excitation. In equivalent-linear method, a linear analysis is carried out with some assumed initial values for damping ratio and shear modulus in various regions of the model. Then the *maximum cyclic shear strain* is recorded for each element and used to

determine the new values for damping and modulus, referring to the backbone curves relating damping ratio and secant modulus to the amplitude of the shear strain. Some empirical scaling factors are usually utilised when relating these strains to the model strains. The new values of damping ratio and shear modulus are then used in the next stage of the numerical analysis. The whole process is repeated several times, until there is no further change in the properties and the structural response. At this stage, "strain-compatible" values of damping and modulus are recorded, and the simulation using these values is deemed to be the best possible prediction of the real behaviour. Rayleigh damping may be used in this method to simulate energy losses in the soil-structure system when subjected to a dynamic loading. Seed and Idriss (1969) described that equivalent-linear method employs linear properties for each element, which remain constant under the influence of seismic excitations. Those values, as explained, are estimated from the mean level of dynamic motion.

Other characteristics of equivalent-linear method are as follows (Seed and Idriss, 1969 and Itasca, 2008):

- The interference and mixing phenomena taking place between different frequency components in a nonlinear material are missing from an equivalent-linear analysis.
- The method does not directly provide information on irreversible displacements and the permanent changes.
- In the case where both shear and compression waves are propagated through a site, the equivalent-linear method typically treats these motions independently.
- Equivalent linear methods cannot be formulated in terms of effective stresses to allow the generation and dissipation of pore pressures during and following earthquake shaking.

3.8.1.2 Fully Nonlinear Method

Fully nonlinear method, adopted in this study, is capable to model nonlinearity in dynamic analysis of soil-structure systems precisely and follows any prescribed nonlinear constitutive relation. In addition, structural geometric nonlinearity (large displacements) can be accommodated precisely in this method. During the solution process, structural materials could behave as isotropic, linearly elastic materials with no failure limit for elastic analysis, or as elasto-plastic materials with specified limiting plastic moment for inelastic structural

analysis to simulate elastic-perfectly plastic behaviour. For the dynamic analysis, the damping of the system in the numerical simulation should be reproduced in magnitude and form, simulating the energy losses in the natural system subjected to the dynamic loading. In soil and rock, natural damping is mainly hysteretic (Gemant and Jackson 1937, and Wegel and Walther 1935). In this study, constant damping has been introduced for the rigid base structure and for simplicity, energy dissipation from the foundation has been ignored. Energy dissipation has been considered for dynamic analysis of soil-structure interaction in this study using hysteretic damping algorithm which is incorporated in this numerical solution allowing the strain-dependent modulus and damping functions to be incorporated directly into the numerical simulation.

Other characteristics of fully nonlinear method are as follows (Byrne et al., 2006 and Itasca, 2008):

- Nonlinear material law, interference and combination of different frequency components can be considered simultaneously.
- Irreversible displacements and other permanent changes can be modelled as required.
- Both shear and compression waves are propagated together in a single simulation, and the material responds to the combined effect of both components. For strong motions, the coupling effects can be very significant. For example, normal stresses may be reduced dynamically, thus causing the shearing strength to be reduced in a frictional material.
- The formulation for the nonlinear material behaviour can be incorporated in terms of effective stresses. Consequently, the generation and dissipation of pore pressures during and following shaking can be modelled.

3.8.1.3 Fully Nonlinear Method vs. Equivalent Linear Method

Byrne et al. (2006) and Beaty and Byrne (2001) reviewed the above mentioned methods and discussed the benefits of the fully nonlinear numerical method over the equivalent-linear method for different practical applications. The equivalent-linear method is not appropriate to be used in dynamic soil-structure interaction analysis as it does not directly capture any nonlinearity effects due to linear solution process. In addition, strain-dependent modulus and damping functions are only taken into account in an average sense, in order to approximate some effects of nonlinearity.

Byrne et al. (2006) concluded that the most appropriate method for dynamic analysis of soil-structure system is fully nonlinear method. The method correctly represents the physics associated with the problem and follows any stress-strain relation in a realistic way. In this method, small strain shear modulus and damping degradation of soil with strain level can be captured precisely in the modelling. Considering the mentioned priorities and capabilities of the fully nonlinear method for the dynamic analysis of soil-structure systems, this method is employed in the dynamic analysis of soil-structure system in this study in order to attain rigorous and more reliable results.

3.8.2 Hysteretic Damping Formulation and Implementation

Modulus degradation curves imply nonlinear stress-strain curves. In case of an ideal soil in which the stress depends only on the strain (not on the number of cycles, or time), an incremental constitutive relation from the degradation curve can be described by the strain-dependent normalised secant modulus (M_s) as follows:

$$M_s = \frac{\bar{\tau}}{\gamma} \tag{3.20}$$

where, $\bar{\tau}$ is the normalised shear stress and γ is the shear strain.

The normalised tangent modulus, M_t, is then obtained as:

$$M_t = \frac{d\bar{\tau}}{d\gamma} = M_s + \gamma \frac{dM_s}{d\gamma} \tag{3.21}$$

The incremental shear modulus in a nonlinear simulation is then given by $G \times M_t$, where, G is the secant shear modulus described in Equation (3.10).

The formulation described above is implemented in FLAC by modifying the strain rate calculation. Therefore, the mean strain rate tensor (averaged over all subzones) is calculated prior to any calls are made to constitutive model functions. At this stage, the hysteretic logic is invoked, returning a modulus multiplier which is passed to any called constitutive model. The model then uses the multiplier M_t to adjust the apparent value of tangent shear modulus of the full zone.

Three built-in tangent modulus functions are available in FLAC to implement hysteretic damping by representing the variation of the shear modulus reduction factor (G/G_{max}) and damping ratio (ξ) with cyclic strain (γ) as follows:

1. *Default Model*: The default hysteresis model is developed by the S-shaped curve of modulus versus logarithm of cyclic strain, representing a cubic equation, with zero slopes at both low and high strains. Thus, the secant modulus (M_s) can be calculated as:

$$M_s = s^2(3 - 2s) \tag{3.22}$$

where,

$$s = \frac{L_2 - L}{L_2 - L_1} \tag{3.23}$$

and L is the logarithmic strain,

$$L = Log_{10}(\gamma) \tag{3.24}$$

The model is defined by two parameters, L_1 and L_2, which are the extreme values of logarithmic strain.

2. *Sigmoidal Models:* These curves are monotonic within the defined range, and have the required asymptotic behaviour. Thus, the functions are well-suited to the purpose of representing modulus degradation curves. These two types of sigmoidal models (Sig3 includes *a*, *b*, and x_0 and Sig4 consists of a, *b*, x_0 and y_0 parameters) are defined as follows:

Sig3 Model

$$M_s = \frac{a}{1 + \exp(-(L - x_0)/b)} \tag{3.25}$$

Sig4 Model

$$M_s = y_0 + \frac{a}{1 + \exp(-(L - x_0)/b)} \tag{3.26}$$

3. *Hardin/Drnevich Models:* The model presented by Hardin and Drnevich (1972), known as Hardin model which is defined by Hardin/Drnevich constant (γ_{ref}) as follows:

$$M_s = \frac{1}{1 + \gamma/\gamma_{ref}} \tag{3.27}$$

Any of the above mentioned models generate backbone curves presented in Sections 3.5.4 and 3.5.5 for sand (Seed et al., 1986) and clay (Sun et al., 1998) adopting the required numerical fitting parameters summarised in Table 3.1.

Table 3.1: Numerical fitting parameters in FLAC for modulus degradation modelling

Data Set	Default	Sig 3	Sig 4	Hardin
Sand	L_1=-3.325 L_2=0.823	a=1.014 b=-0.4792 x_0=-1.249	a=0.9762 b=-0.4393 x_0=-1.285 y_0=0.03154	γ_{ref}=0.06
Clay	L_1=-3.156 L_2=1.904	a=1.017 b=-0.587 x_0=-0.633	a=0.922 b=-0.481 x_0=-0.745 y_0=0.0823	γ_{ref}=0.234

3.9 Summary

In this study, a numerical soil-structure model is developed in direct method using state of the art capabilities of FLAC2D to simulate complex nature of dynamic soil-structure interaction as accurate and realistic as possible.

The soil-structure model employs beam structural elements to model beams, columns and foundation slabs. During analysis process, structural material could behave as an isotropic, linearly elastic material with no failure limit for elastic structural analysis or as an elastic-perfectly plastic material with specified limiting plastic moment for inelastic structural analysis. Therefore, both elastic and plastic (inelastic) structural behaviour can be captured by the model in dynamic analysis. In addition, structural geometric nonlinearity (large displacements) has been accommodated in dynamic analysis.

Two dimensional plane-strain grids composed of quadrilateral elements are utilised to model the soil medium. Nonlinear behaviour of the soil medium has been captured using backbone curves of shear modulus ratio versus shear strain (G/G_{max} - γ) and damping ratio versus shear strain (ξ - γ) adopting Mohr-Coulomb constitutive model.

Employing the backbone curves for simulating nonlinear behaviour of the soil, in this study, fully nonlinear method for analysis of dynamic soil- structure interaction has been employed in order to attain rigorous and reliable results. Fully nonlinear method is capable to precisely model nonlinearity in dynamic analysis of soil-structure systems and follow any prescribed nonlinear constitutive relation. Small strain shear modulus and damping degradation of soil with strain level can be considered in the modelling precisely.

Interface elements represented by normal and shear springs between soil and structure are exploited to simulate frictional contact between two planes contacting each other, with the interface shear strength defined by the Mohr-Coulomb failure criterion. In order to avoid reflection of outward propagating waves back into the model, quiet (viscous) boundaries comprising independent dashpots in the normal and shear directions are placed at the lateral boundaries of the soil medium. The lateral boundaries of the main grid are coupled to the free-field grids by viscous dashpots of quiet boundaries at the sides of the model to simulate the free-field motion which would exist in the absence of the structure. Horizontal distance of the soil lateral boundaries assumed to be 60 metres and maximum bedrock depth is 30 metres. Rigid boundary condition is assigned to the bedrock.

The new developed model is a novel and enhanced numerical soil-structure model as it is capable of capturing structural plasticity (inelastic behaviour) and soil nonlinearity, treating the behaviour of both soil and structure with equal rigor simultaneously. Besides, adopting direct method, which perfectly simulates complex geometries and material properties in numerical methods, the model can perform fully nonlinear time history dynamic analysis to simulate realistic dynamic behaviour of soil and structure under seismic excitations as accurate and realistic as possible. In addition, as the model employs a Multi Degree of Freedom (MDOF) structure, inter-storey drifts can be determined and utilised for investigating the performance levels of the building structures under the influence of dynamic soil-structure interaction.

CHAPTER FOUR

4. EXPERIMANTAL STUDY AND VERIFICATION

4.1 General

Full-scale field tests or scale model tests are essential to study soil-structure system behaviour during earthquakes. Such tests are also required to validate numerical or analytical models. Full-scale field experiments have the advantage of considering realistic site conditions; whereas, the use of scale models on shaking table offers the advantage of simulating complex systems under controlled conditions, and the opportunity to gain insight into the fundamental mechanisms operating in these systems.

In many circumstances, the scale models on shaking table may afford a more economical option than the corresponding full-scale tests. The practice of conducting parametric studies with scale models can be used to augment areas where case histories and prototype tests provide only sparse data. In addition to qualitative interpretation, scale model test results are often used as calibration benchmarks for analytical methods, or to make quantitative predictions of the prototype response. For such applications, it is necessary to have a set of scaling relations which can relate the observations and predictions.

In this chapter, the developed novel and enhanced numerical soil-structure model, described in Chapter 3, is validated and verified by performing shaking table tests to the scale soil-structure model. The dynamic simulation has been carried out on the shaking table located in the civil laboratory of the University of Technology, Sydney (UTS). It should be noted that the UTS shaking table has a uni-axial configuration, allowing for one-dimensional input motions. Table 4.1 summarises the UTS shaking table characteristics.

Table 4.1: UTS shaking table specifications

Size of the Table	3m x 3 m
Maximum Payload	10 tonnes
Overturning Moment	100 kN-m
Maximum Displacement	±100 mm
Maximum Velocity	±550 mm/sec
Maximum Acceleration	±2.5g (no load) or ±0.9g (full load)
Testing Frequency	0.1 – 50 Hz

4.2 Prototype Characteristics

The prototype of the experimental tests is a soil-structure system with dimensional characteristics illustrated in Figure 4.1.

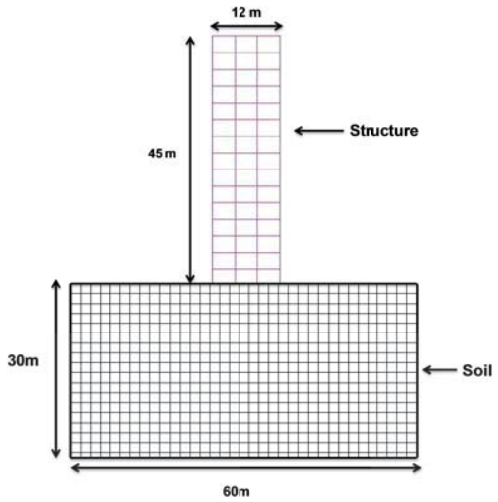

Figure 4.1: Dimensional characteristics of the prototype

The prototype building frame of the soil-structure system is a two dimensional fifteen storey concrete moment resisting frame. The building frame height and width are 45 and 12 metres, respectively and spacing between the frames into the page is 4 metres. The building is resting on a footing which is 4 meters wide and 12 meters long. Natural frequency of the prototype building is 0.384 Hz and its total mass is 953 tonnes. The natural frequency and mass of the prototype building have been determined from the numerical analysis and load values explained in Section 5.6. Soil medium underneath the structure is a clayey soil with shear wave velocity of 200 m/s and unit weight of 14.40 kN/m^3 (soil density of 1470 kg/m^3). As described in Section 3.7.3, the horizontal distance of the soil lateral boundaries and bedrock depth have been selected to be 60 metres (five times the width of the structure) and 30 metres, respectively.

4.3 Scaling Factors for Shaking Table Testing

Scale models can be defined as having geometric, kinematic, or dynamic similarities to the prototype (Langhaar, 1951; Sulaeman, 2010). Geometric similarity defines a model and prototype with homologous physical dimensions. Kinematic similarity refers to a model and prototype with homologous particles at homologous points at homologous times. Dynamic similarity describes a condition where homologous parts of the model and prototype experience homologous net forces. Moncarz and

Krawinkler (1981) explained that scale models meet the requirements of similitude to the prototype to differing degrees, and researchers may apply nomenclature such as “true”, “adequate”, or “distorted” to the model. A true model fulfils all similitude requirements. An adequate model correctly scales the primary features of the problem, with secondary influences allowed to deviate while the prediction equation is not significantly affected. Distorted models refer to those cases in which deviation from similitude requirements distorts the prediction equation, or where compensating distortions in other dimensionless products are introduced to preserve the prediction equation.

In addition, Moncarz and Krawinkler (1981) elucidated that in 1-g scale modelling, where, ρ is density, E is modulus of elasticity, a is acceleration, and g is gravitational acceleration, the dimensionless product a/g (Froude’s number) must be kept equal to unity implying that the ratio of model to prototype specific stiffness (E/ρ) is equal to the geometric scaling factor λ. This is known as “Cauchy condition” which can also be stated in terms of shear wave velocity as follows:

$$\frac{(V_S)_p}{(V_S)_m} = \sqrt{\lambda} \tag{4.1}$$

where, subscripts p and m stand for prototype, and model, respectively, and V_s is shear wave velocity.

In addition, Moncarz and Krawinkler (1981) showed that satisfying the Cauchy condition is a necessary requirement for simultaneous replication of restoring forces, inertial forces, and gravitational forces in a dynamic system.

Iai (1989) derived a comprehensive set of scaling relations for a soil-structure system under dynamic loading and defined the entire problem in terms of geometric, density, and strain scaling factors. This method relates the geometric (λ) and density (λ_ρ) scaling factors, and then derives the strain scaling factor (λ_ε) from shear wave velocity tests on both the model and prototype soil, as presented in Equation (4.2).

$$\lambda_\varepsilon = \left[\frac{\lambda}{(\frac{(V_S)_p}{(V_S)_m})^2} \right] \tag{4.2}$$

Meymand (1998) and Moss et al (2010) explained that no governing equation can be written describing the entire soil-structure system, nor can dimensional analysis or similitude theory be directly applied to this complex system to achieve “true” model similarity. The viable scale modelling approach for application of scale model similitude therefore consists of identifying and successfully modelling the primary forces and processes in the system, while suppressing secondary effects, thereby yielding an “adequate” model.

Several researchers (e.g. Meymand, 1998; Turan et al., 2009, Moss et al., 2010) pointed out that in order to achieve an adequate model for dynamic soil-structure interaction simulation in shaking table tests, Cauchy condition (Equation 4.1), should be satisfied. In addition, the strain scaling factor (λ_ε) should be kept equal to one. It should be noted that when Cauchy condition is satisfied, obviously, the result of substituting the value of $(V_s)_p/(V_s)_m$ from Equation (4.1) into Equation (4.2) is equal to one.

The objective of the scale modelling procedure for this test program is to achieve “dynamic similarity”, where model and prototype experience homologous forces. For this purpose, adopted methodology by Meymand (1998) is the framework for scale model similitude in this study. According to this approach, three principal test conditions establish many of the scaling parameters. The first condition is that testing is conducted in a 1-g environment, which defines model and prototype accelerations to be equal. Secondly, a model with similar density to the prototype is desired, fixing another component of the scaling relations. Thirdly, the test medium is primarily composed of saturated clayey soil, whose undrained stress-strain response is independent of confining pressure, thereby simplifying the constitutive scaling requirements. In addition to the three principal test conditions, Meymand (1998) pointed out that the natural frequency of the prototype should be scaled by an appropriate scaling relation.

By defining scaling conditions for density and acceleration, the mass, length, and time scale factors can all be expressed in terms of the geometric scaling factor (λ), and a complete set of dimensionally correct scaling relations (ratio of prototype to model) can be derived for all variables being studied. The scaling relations for the variables contributing to the primary modes of system response are shown in Table 4.2 (Meymand, 1998; Turan et al., 2009; Moss et al., 2010; Sulaeman, 2010; Lee et al., 2012).

Table 4.2: Scaling relations in terms of geometric scaling factor (λ)

Mass Density	**1**	Acceleration	**1**	Length	**λ**
Force	λ^3	Shear Wave Velocity	$\lambda^{1/2}$	Stress	**λ**
Stiffness	λ^2	Time	$\lambda^{1/2}$	Strain	**1**
Modulus	**λ**	Frequency	$\lambda^{-1/2}$	EI	λ^5

In Table 4.2, the shear wave velocity scaling factor $((V_s)_p/(V_s)_m)$ is equal to $\lambda^{1/2}$. Therefore, Cauchy condition (Equation 4.1) is met in the scaling relations. In addition, strain scaling factor (λ_ε), which can be determined by substituting the value of $(V_s)_p/(V_s)_m$ from Equation (4.1) into Equation (4.2), is kept equal to one. Thus, as mentioned earlier, both requirements for achieving an adequate model for dynamic soil-structure interaction simulation in shaking table tests are satisfied. The application of the scaling relations and development of the soil-structure model components will be discussed in the following sections.

4.3.1 Adopted Geometric Scaling Factor

Adopting an appropriate geometric scaling factor (λ) is one of the important steps in scale modelling on shaking table. Although small scale models could save cost, the precision of the results could be substantially reduced. Therefore, to attain the largest achievable scale model which represents the most accurate results possible, geometric scaling factor (λ) has been selected with respect to the following limitations of the UTS uni-axial shaking table as the design criteria:

- Size of the table : 3m ×3 m
- Maximum payload : 10,000 kg
- Overturning moment : 100 kN-m

Table 4.3 compares the characteristics of the scale model shown in Figure 4.2 for different scaling factors. In this table, the related weight is just accounted for soil inside the tank excluding weights of the container and structure. As previously mentioned, a model with similar density to the prototype is desired satisfying dynamic similarity. As a result, soil unit weight in the model and prototype should be the same and equal to 14.40 kN/m^3. In addition, the ratio between width and length of the soil

container is another variable to be considered. According to the previously designed containers (e.g Gazetas, 1982; Taylor, 1997; Pitilakis et al., 2008; Chau et al., 2009), ratio of 2:3 between width and length of the soil container is deemed to be the most appropriate ratio. Thus, this ratio has been adopted in this study.

Table 4.3: Dimensional characteristics of scale model considering different scaling factors

Geometric Scale factor	B′ (m)	L′ (m)	W′ (m)	D′ (m)	H′ (m)	D′+H′ (m)	Volume (m^3)	Weight (kg)	Overturning Moment (kN.m)
1:1	12	60	36	30	45	75	64800	0.95E+8	1.40E+10
1:10	1.20	6	3.60	3	4.50	7.50	64.80	95256	1400
1:20	0.60	2.40	1.80	1.50	2.25	3.75	8.10	11907	89.50
1:30	0.40	2	1.20	1	1.50	2.50	2.40	3528	17.30
1:40	0.30	1.50	0.90	0.75	1.12	1.87	1.01	1488	5.60
1:50	0.24	1.20	0.72	0.60	0.90	1.50	0.51	762	2.30
1:100	0.12	0.60	0.36	0.30	0.45	0.75	0.06	95	0.15

*For definition of variables refer to Figure 4.2

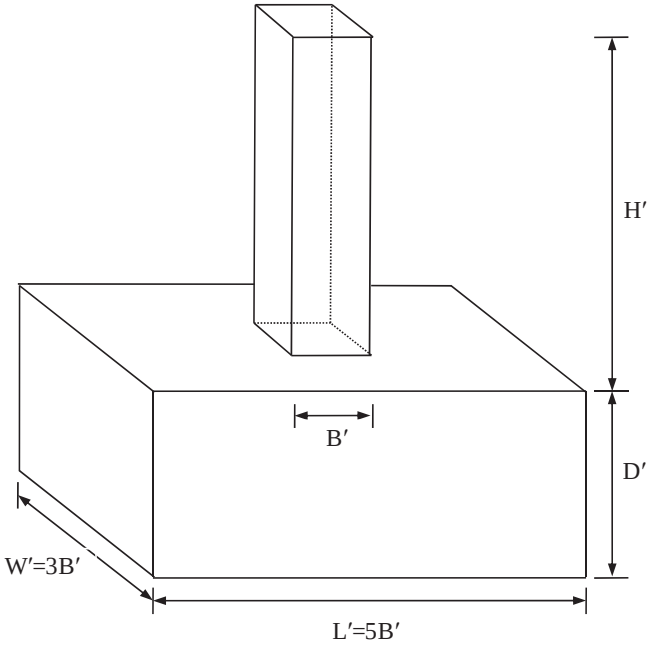

Figure 4.2: Scale model of soil structure interaction problem

Referring to Tables 4.1 and 4.3, with respect to the design criteria, scaling factor of 1:30 provides the largest achievable scale model with rational scales, maximum payload, and overturning moment which meet the facility limitations. Thus, geometric scaling factor (λ) of **1:30** is adopted for experimental shaking table tests on the scale model in this study.

4.4 Structural Model Design and Construction

4.4.1 Characteristics of Structural Model

Employing geometric scaling factor of 1:30 according to Table 4.3, height (*H*), length (*L*), and width (*W*) of the structural model are determined to be, 1.50 m, 0.40 m, and 0.40 m, respectively (Figure 4.3).

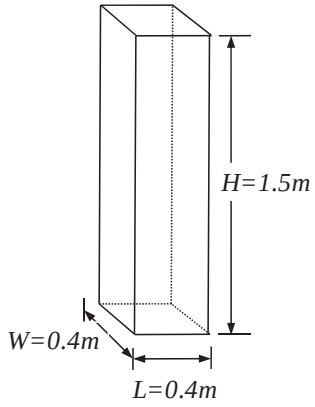

Figure 4.3: Structural model dimensions

Referring to Meymand (1998) principal test conditions, explained in Section 4.3, in order to achieve dynamic similarity, in addition to geometric dimensions, the natural frequency of the prototype should be scaled by an appropriate scaling relation and the density of the model and the prototype should be equal. In this way, prototype structure may be modelled more accurately in shaking table tests. The mentioned two parameters play key roles in the scaling process, and scaling them deemed to be adequate. In addition, steel structural model is constructible and adjustable to the test environment, while concrete structural model could not be constructed with the required dimensions and dynamic properties. Therefore, the concrete structure prototype was scaled into a steel structure model, by scaling the natural frequency and the density of the prototype.

According to Table 4.2, the scaling relationship between natural frequency of the model (f_m) and natural frequency of the prototype (f_p) is:

$$\frac{f_m}{f_p} = \lambda^{-1/2} = 5.480 \tag{4.3}$$

As mentioned in Section 4.2, natural frequency of the prototype structure is f_p = 0.384 Hz. Therefore, the required natural frequency of the structural model (f_m) can be determined as follows:

$$f_m = 5.480 \times f_p = 5.480 \times 0.384 = 2.11 \ Hz$$

The determined natural frequency of the model is conforming with the approximated value of average frequency of the building equal to 2.95 *Hz*, calculated by Equation 6.2(7) of AS 1170.4-2007.

Scaling relationship between density of the model (ρ_m) and density of the prototype (ρ_p), based on Table 4.2, is:

$$\frac{\rho_m}{\rho_p} = 1 \Rightarrow \rho_m = \rho_p \tag{4.4}$$

Density of the prototype structure (ρ_p) can be determined as follows:

$$\rho_p = \frac{m_p}{V_p} = \frac{953{,}000}{45 \times 12 \times 4} = 441 kg/m^3 \tag{4.5}$$

where, m_p is the mass of the prototype structure and V_p is the volume of the prototype structure.

Substituting the density of the prototype structure (ρ_p) from Equation (4.5) into Equation (4.4), the mass of the structural model (m_m) can be estimated as:

$$m_m = \rho_m \times V_m = 441 \ kg/m^3 \times (1.50 \ m \times 0.40 \ m \times 0.40 \ m) = 106 \ kg \tag{4.6}$$

where, V_m is the volume of the structural model.

4.4.2 Design of Structural Model

Based on the discussion in Section 4.4.1, the required characteristics of the structural model is summarised in Table 4.4.

Table 4.4: Characteristics of the structural model

Total Height (m)	Total Length (m)	Total Width (m)	Natural Frequency (Hz)	Total Mass (kg)
1.50	0.40	0.40	2.11	106

Knowing the required characteristics of the structural model, its 3D numerical model has been built in SAP2000 software using two dimensional shell elements to model columns and floors as shown in Figure 4.4. The numerical model consists of fifteen horizontal steel plates as the floors and four vertical steel plates as the columns. Steel plate grade 250, according to AS/NZS 3678-2011 (Structural Steel), with the minimum yield stress of 280 MPa and minimum tensile strength of 410 MPa, has been adopted in the design. The thickness of the steel plates have been determined in design

process after several cycles of trial and error in order to fit the required natural frequency and mass as summarised in Table 4.4.

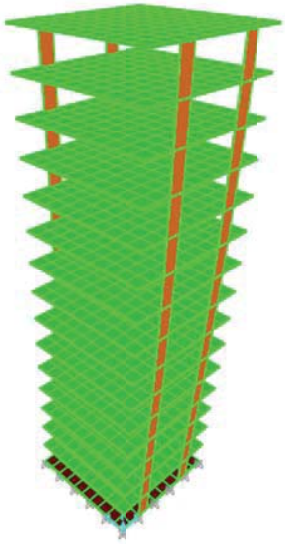

Figure 4.4: 3D numerical model of the structural model in SAP2000

After the numerical modelling and design, construction detail drawings were prepared to reflect the design requirements of the structural model. Construction details of the structural model are illustrated in Figure 4.5.

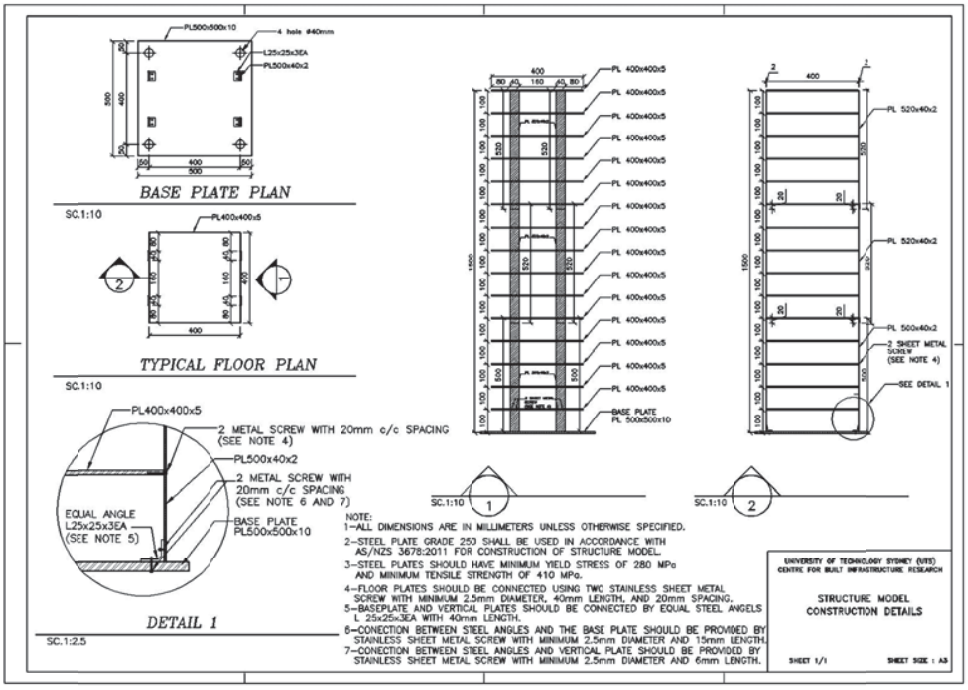

Figure 4.5: Construction detail drawings of the structural model

The numerical results show that the designed structure has the natural frequency of f_m =2.13 *Hz* and the calculated total mass is 105.6 *kg*, which are in good agreement with the requirements in Table 4.4.

4.4.3 Construction of Structural Model

In the construction phase, the detail drawings were passed on to the UTS engineering workshop. At the workshop, the steel plates were cut and drilled according to the drawings (Figure 4.6) and then sent to the UTS civil laboratory to be assembled.

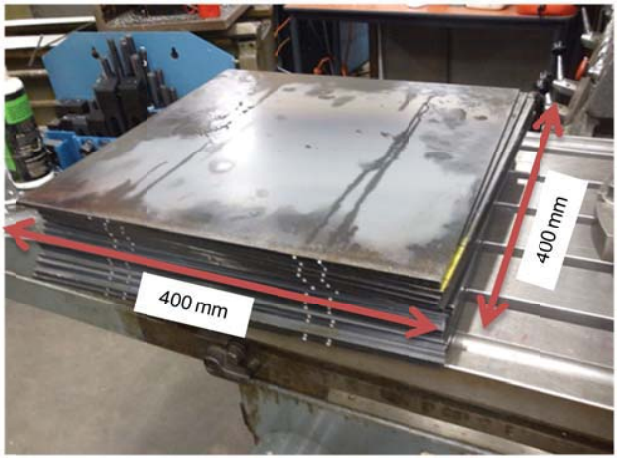

Figure 4.6: Cut and drilled steel plates by the UTS engineering workshop

Afterwards, the steel plates were assembled in order to form the structural model using stainless sheet metal screws with 2.5 mm diameter and 25 mm length. Figures 4.7 and 4.8 show the assembling process of the structural model and completed structural model, respectively.

Figure 4.7: Assembling process of the structural model

Figure 4.8: Completed structural model

The mass of the model (m_m), without the base plate, was measured to be 104 *kg* which matches the required structural mass (Table 4.4). Total measured mass of the structural model considering the mass of the base plate is 115kg.

4.5 Soil Container Design and Construction

4.5.1 Characteristics of Laminar Soil Container

With respect to several merits of using laminar soil containers, discussed in Section 2.7 of the literature review, over the other container types (flexible and rigid soil containers), and in order to carry out precise and reliable experimental shaking table tests, laminar soil container has been adopted in this study.

Referring to Table 4.3, by selecting 1:30 as the geometric scaling factor, the container should have minimum length, width, and depth of 2.0m, 1.20m, and 1.0m, respectively. Allowing a further 10 mm on each side for construction purposes similar

to Prasad et al. (2004), the final length (L^*), width (W^*), and depth (D^*) of the laminar soil container are estimated to be 2.10m, 1.30m, and 1.10m, respectively (Figure 4.9).

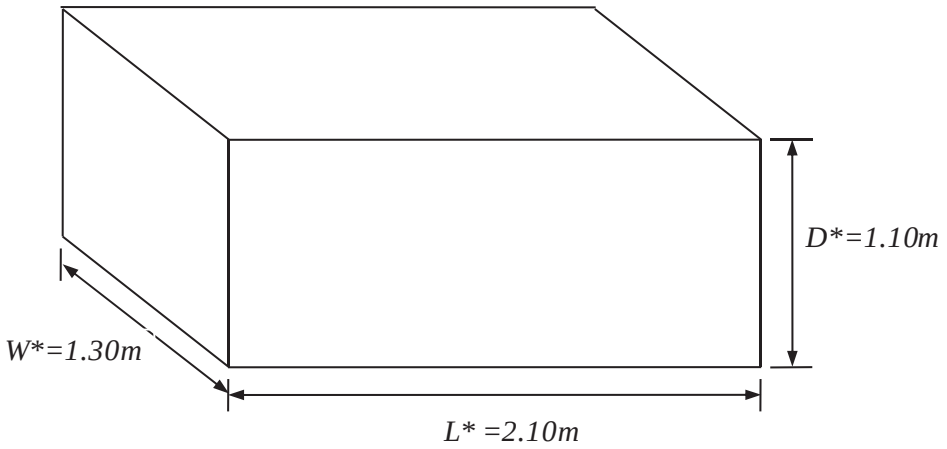

Figure 4.9: Adopted laminar soil container dimensions

In terms of choosing the materials to built the soil container, according to the previous conducted research works (e.g. Ishimura et al., 1992; Taylor, 1997; Jakrapiyanun, 2002; Pitilakis et al., 2008; Chau et al., 2009), aluminium frames and rubber layers were employed in an alternating pattern. Therefore, the laminar soil container consists of a rectangular laminar box made of aluminium rectangular hollow section frames separated by rubber layers. The aluminium frames provide lateral confinement of the soil, while the rubber layers allow the container to deform in a shear beam manner.

4.5.2 Design of Laminar Soil Container

Taylor et al. (1995) stated that the mass and stiffness characteristics of the soil container should be carefully chosen so that the container's natural frequency and mode shapes in horizontal shear are compatible with those of the contained soil.

The primary aims of the design are to ensure that the soil mass controls the overall dynamic response of the soil-container system, and the soil mass is subjected to the simple shear boundary conditions that exist in the idealised prototype system. In this system, horizontal soil strata overlaying rigid bedrock and the lateral boundaries are at infinity. When subjected to horizontal bedrock movements, the soil responds like a shear beam as horizontal shear waves propagate vertically, leading to a sinusoidal lateral displacement profile.

According to Table 4.2, scaling factor between shear wave velocity of the soil model $(V_s)_m$ and shear wave velocity of the prototype soil $(V_s)_p$ can be expressed as follows:

$$\frac{(V_s)_m}{(V_s)_p} = \lambda^{1/2} = 0.182 \tag{4.7}$$

Knowing that the shear wave velocity of the prototype soil $(V_s)_p$ is 200 m/s from Section 4.2, the shear wave velocity of the soil model $(V_s)_m$ can be determined from Equation (4.7):

$$(V_s)_m = 0.182 \times (V_s)_p = 0.182 \times 200 = 36.4 \ m/s$$

According to Kramer (1996), natural frequency of the subsoil (f_s) can be calculated from the following relationship:

$$f_s = \frac{V_s}{4H_s} \tag{4.8}$$

where, V_s is the shear wave velocity of the subsoil and H_s is the bedrock depth.

Thus, the natural frequency of the soil model (f_m) can be determined by substituting the values of the shear wave velocity $(V_s)_m$ and bedrock depth $(H_s)_m$ of the soil model equal to 36.4 m/*s* and 1 m, respectively, in Equation (4.8):

$$f_m = \frac{(V_s)_m}{4(H_s)_m} = \frac{36.4}{4 \times 1} = 9.1Hz$$

With respect to the required dimensions of the soil container, a numerical 3D model of the laminar soil container has been built in SAP2000 software using one dimensional frame elements to model aluminium rectangular hollow section frames and two dimensional shell elements to model rubber layers as shown in Figure 4.10. The numerical model comprises ten aluminium rings and nine rubber layers.

Afterwards, the mass and stiffness characteristics of the soil container have been designed in a way that the container and soil model natural frequencies match. For this purpose, size and mechanical properties of the aluminium rectangular hollow section frames and rubber layers were determined in design process after several cycles of trial and error in a way that the natural frequency of the model soil (f_m=9.1 *Hz*) with the natural frequency of the laminar soil container match together.

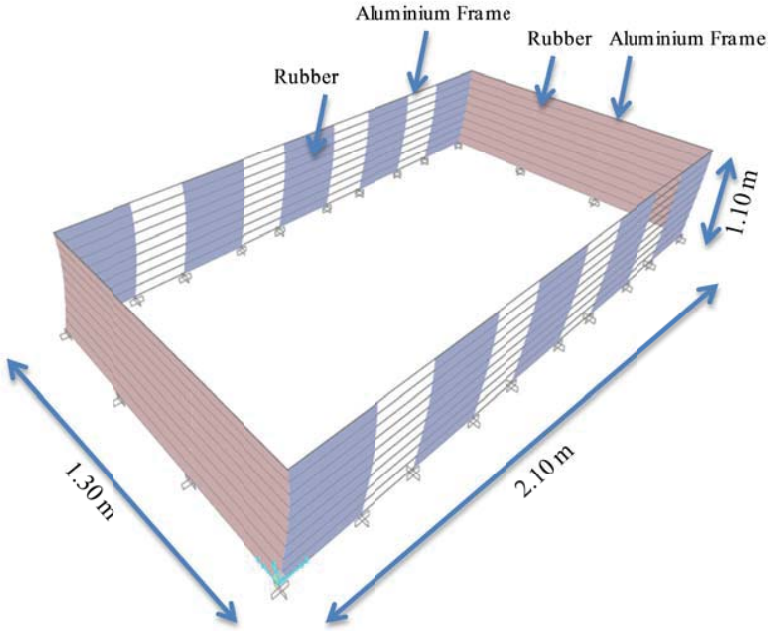

Figure 4.10: 3D numerical model of the laminar soil container in SAP2000

The final arrangement and construction details of the laminar soil container are depicted in the prepared laminar soil container construction detail drawings (Figures 4.11 to 4.14). *In the construction detail drawings, all the dimensions are in millimetres*. Figure 4.11 shows the soil container general plan and the arrangement of the rubber layers. The current arrangement for 40×40 mm flexible rubbers in plan, were proposed in the design in order to provide low elastic stiffness and low natural frequency for the container. It also reduces the problem of the container being too stiff relative to the soil at high shear strains.

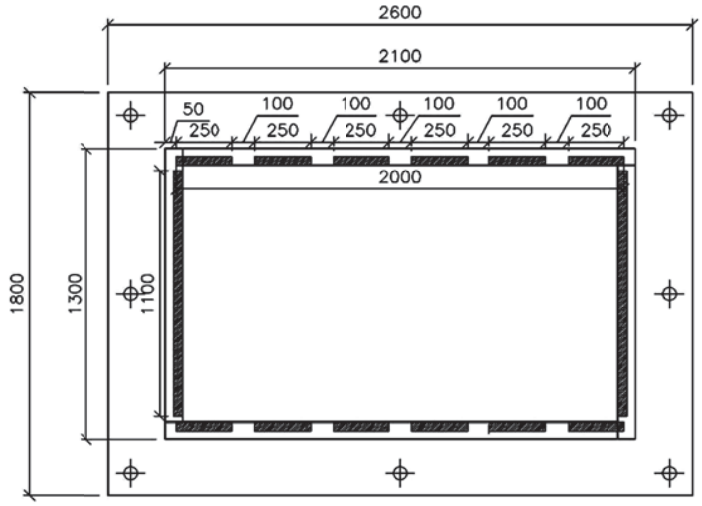

Figure 4.11: Laminar soil container general plan

Base plate of the container is a timber hardwood plate with eight 40 mm diameter holes. The container can be fixed and secured on the shaking table using eight M38 bolts passing through the provided holes as shown in Figure 4.12. In addition, six horizontal timber plates (PL1800×50×25 mm) have been utilised underneath the timber base plate as the stiffeners to increase the bending capacity of the base plate and ease the transportation of the container (Figure 4.12).

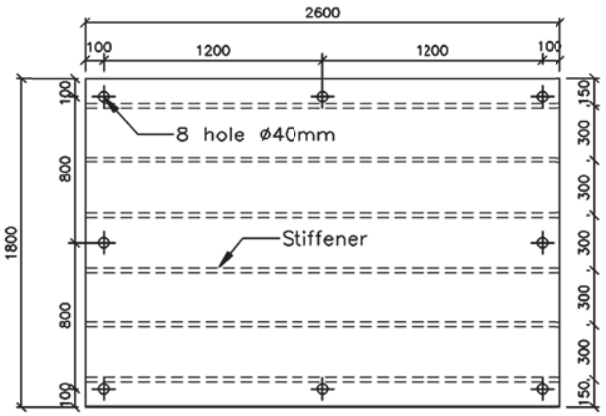

Figure 4.12: Construction detail drawing of the hardwood timber base plate

The first aluminium ring resting on the base plate, with length and width of 2.10 m and 1.30 m, respectively, is called the base frame. This base frame is fixed to the timber base plate with twelve M20 bolts grade 4.6, according to AS/NZS 3678-2011, with minimum length of 80 mm (Figure 4.13). In this way, connection between the timber base plate and the rest of the container is provided. The capacities of all the utilised bolt connections of the container were checked for tension and shear in accordance with AS/NZS 3678-2011.

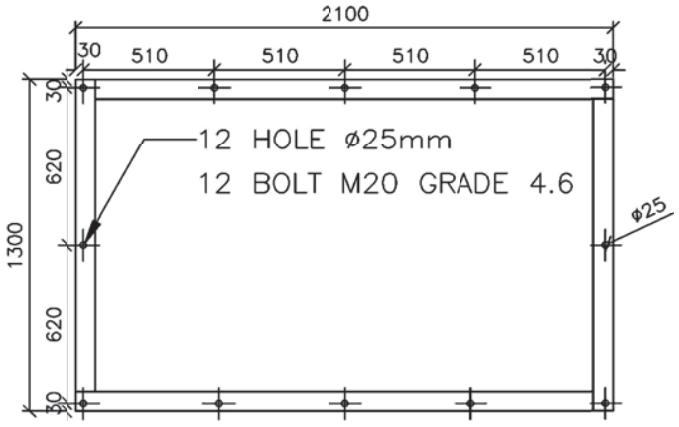

Figure 4.13: Construction detail drawing of the aluminium base frame

Connections between aluminium rectangular hollow section frames and rubbers are provided using strong Megapoxy 69 glue. Megapoxy 69 is a clear non-sag gel type

epoxy structural adhesive for bonding metals to metals, metals to concrete and masonry, assembly of granite and marble fabrications, and many other civil engineering applications requiring superior bond strengths. Figure 4.14 illustrates the utilised aluminium frame sections, rubber sizes, long section of the container, and connection details between different components of the container.

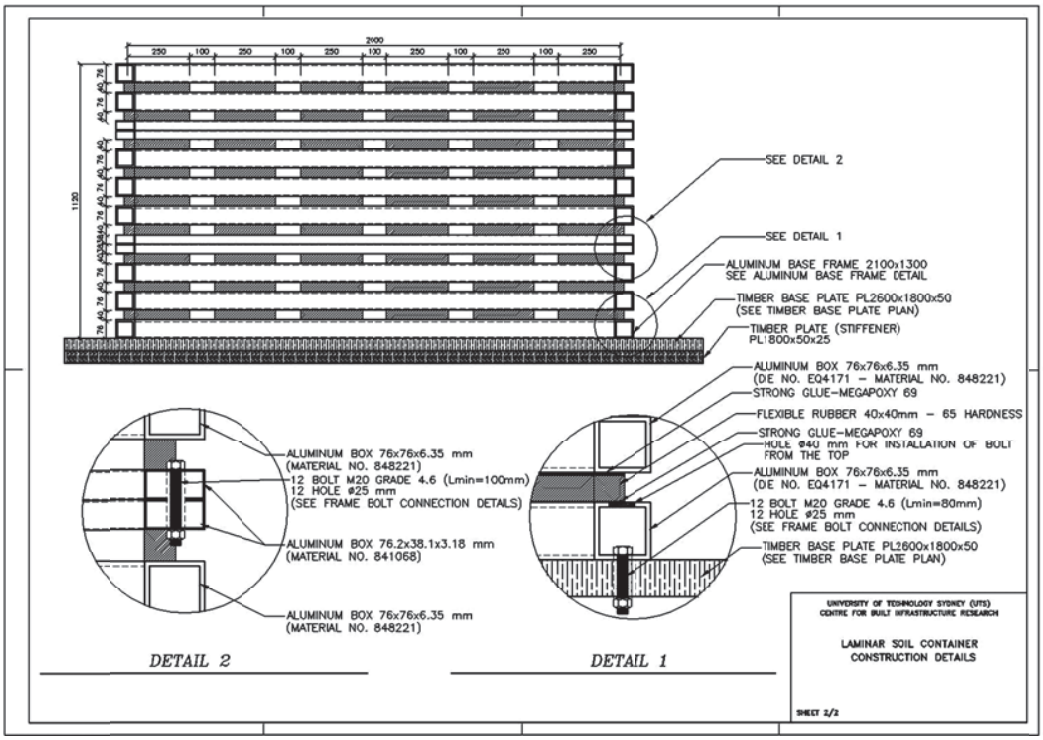

Figure 4.14: Construction detail drawing of the connections

4.5.3 Construction of Laminar Soil Container

As the first step, aluminium rectangular hollow sections were cut and drilled according to the drawings (Figure 4.15).

Figure 4.15: Cutting and drilling aluminium sections at the UTS structures laboratory

Then, cut and drilled aluminium sections were welded so as to form the required aluminium rectangular frames for the laminar soil container construction (Figure 4.16).

(a) **(b)**

Figure 4.16: (a) Cut and drilled aluminium sections; (b) ready to use welded rectangular aluminium frames

Using hardwood timber plates, according to construction detail drawing of the base plate (Figure 4.12), timber base plate was constructed at the civil laboratory utilising slim diameter hardwood nails (Figure 4.17a). Then, the prepared base frame was placed on top of the timber base plate and used as the pattern for drilling the holes which are required for connecting the base plat to the base frame (Figure 4.17b).

(a) **(b)**

Figure 4.17: (a) Construction of timber base plate at the structures laboratory; (b) drilling required holes on the timber base plate

Afterwards, M20 grade 4.6 bolts were passed through the holes and fastened to provide a fix connection between the base plate and the base frame (Figure 4.17b).

At the next step, rubbers were placed and glued on top of the base frame according to the general plan as shown in Figure 4.18 using Megapoxy 69 glue.

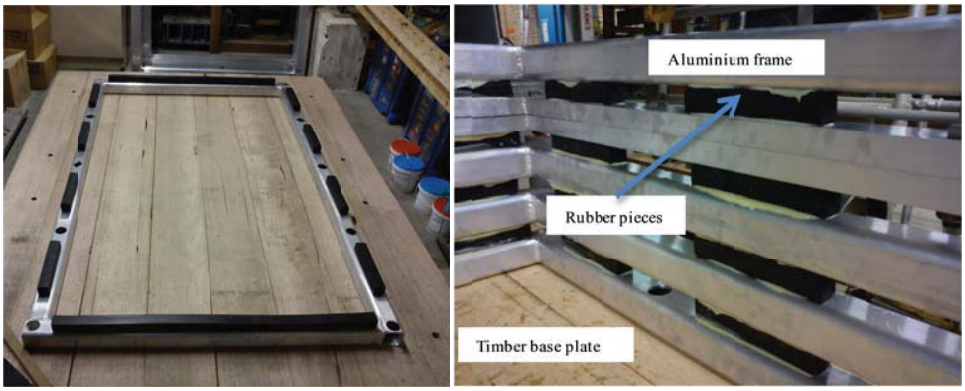

(a) **(b)**

Figure 4.18: (a) Bolted connection between the base plate and base frame; (b) soil container walls consisting of glued aluminium frames and rubbers

By gluing aluminium rectangular frames and rubbers in a successive manner, the walls of the container have been built up (Figure 4.18b) until the wall construction is completed (Figure 4.19).

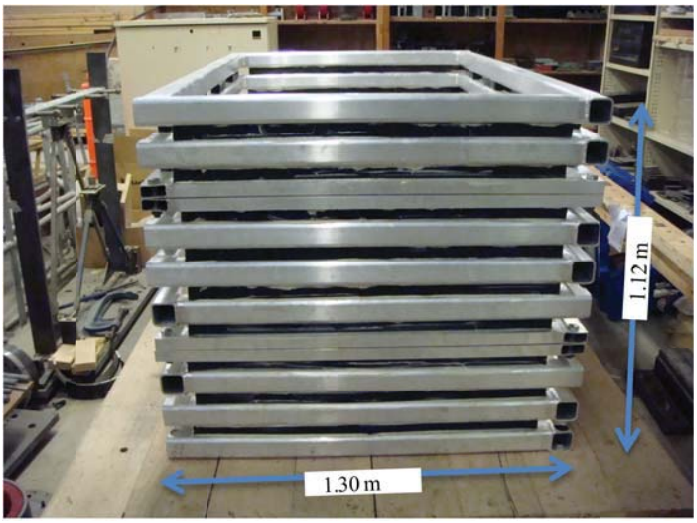

Figure 4.19: Laminar soil container view after completion of the walls

4.6 Soil Mix Design

4.6.1 Characteristics of Soil Model

Meymand (1998), Moss et al. (2010), and Sulaeman (2010) pointed out that the parameters describing dynamic soil properties in soil-structure interaction phenomenon are shear wave velocity, density, modulus degradation, damping, and stress-strain response.

These parameters are discrete and nonlinear, and are functions of the loading rate, the number of cycles, and strain reversals. When the unit weight of the soil model is considered to be equal to the unit weight of the prototype soil, as explained in Section 4.3, then one scaling condition can be determined. Meymand (1998) explained that "the nonlinear stress-strain and modulus degradation and damping curves are not directly modelled from a prototype case, but rather the method of implied prototypes is used to consider whether the scale model properties for these parameters are reasonable. This leaves shear modulus (or shear wave velocity) as the principal soil modelling criterion". Shear modulus (or shear wave velocity) has been considered as the principal soil modelling criterion by several other studies (e.g. Turan et al., 2009; Sulaeman, 2010; Lee et al., 2012) as well.

As explained in Section 4.5.2, with respect to the value of the shear wave velocity of the prototype soil $(V_s)_p$ equal to 200 m/s, the required shear wave velocity of the soil model $(V_s)_m$ was determined from Equation (4.7). Therefore, in order to achieve dynamic similarity, the soil model should have the shear wave velocity $(V_s)_m$ and unit weight $(\gamma_s)_m$ of 36.4 m/s and 14.4 kN/m^3, respectively.

Meymand (1998), Turan et al. (2009), and Moss et al. (2010) adopted synthetic clay mixture reporting that a reconstituted soil would not be able to satisfy the competing scale modelling criterion of shear wave velocity with enough bearing capacity for the foundation in shaking table tests while synthetic clay mix provides adequate undrained shear strength to mobilise the required shallow foundation bearing capacity underneath the structural model meeting the scale modelling criterion of shear wave velocity. If the underneath soil does not provide enough bearing capacity for the structural model foundation, the underneath soil may experience failure or excessive settlements while testing process is being undertaken. In addition, Meymand (1998) and Moss et al. (2010) pointed out that employing a reconstituted soil is deemed impractical in shaking table tests due to the large size of the test container and the very long time that would be required for consolidation in a 1-g environment.

Thus, in this study, a synthetic clay mixture, which meets the contending scale modelling criterion of shear wave velocity with adequate bearing capacity for the foundation, was adopted as the soil medium for the shaking table testing process.

4.6.2 Development of Soil Mix

In order to develop the synthetic clay mixture, in this study, the following materials were used:

- Q38 kaolinite clay;
- ActiveBond 23 bentonite;
- Class F fly ash;
- Lime; and
- Water.

Q38 kaolinite clay is a dry milled kaolin China clay of a white-cream colour. Kaolinite is formed by the breakdown of feldspar, which is induced by water and carbon dioxide and is often formed by the alteration of aluminium silicate minerals in a warm and humid environment (Craig, 2000; Murray, 1999). The kaolinite samples had an average liquid limit and plastic limit of 50% and 30%, respectively.

ActiveBond 23 bentonite is a pure form of bentonite, which is plastic, impermeable, having a high absorbing and swelling capacity and is high viscous when suspended in water (Churchman, 2000). The bentonite samples acquired average liquid limit and plastic limit of 340% and 55%, respectively.

The burning of hard, old anthracite and bituminous coal typically produces Class F fly ash. This fly ash is pozzolanic in nature, and contains less than 20% lime (CaO). Possessing pozzolanic properties, the glassy silica and alumina of Class F fly ash requires a cementing agent, such as Portland cement, quicklime, or hydrated lime, with the presence of water in order to react and produce cementitious compounds (Siddique, 2002).

Combination of (4 class F fly ash): (1 quick lime) was utilised in the mix. According to Wartman (1996), this combination acts as a chemically reactive material when mixed with the kaolinite-bentonite clay. The chemical reactivity is attributed to the high calcium oxide content of the fly ash. When mixed with the clay, the combination causes rapid cation exchange to occur on the clay minerals leading to a substantial reduction in plasticity. The cation exchange causes the double layer around the clay mineral to shrink resulting in an increase in stiffness and by association, shear wave velocity. Figure 4.20, shows the different dry components of the soil mix in three different containers.

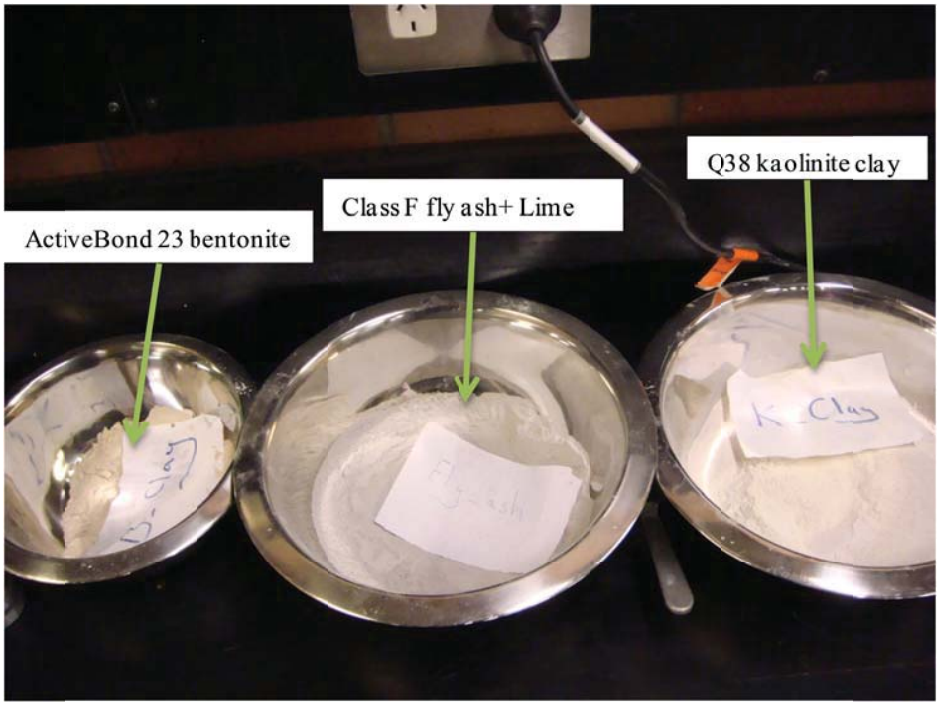

Figure 4.20: Different dry components of the soil mix

To find the most appropriate mix for the test program, three different mixes, including Mix A, Mix B, and Mix C were developed and examined in the UTS soils laboratory. The proportion of different mix components for the three mixes are summarised in Table 4.5.

Table 4.5: Proportion of different components for the examined mixtures

Mix Components	Mix A	Mix B	Mix C
Q38 kaolinite clay	67.5 %	60 %	60 %
ActiveBond 23 bentonite	22.5 %	20 %	20 %
Class F fly ash+ Lime	10 %	20%	20%
Water *	100%	100%	120%

* % of the dry mix.

Mix A, which is the closest mix to the proposed mix by Meymand (1998), has higher percentages of kaolinite and bentinite, lower percentage of class F fly ash and lime, and the same percentage of water content comparing to Mix B. Mix B and C have the same dry component percentages, but the water content which is expected to provide the key elements of mixability and workability for shake table model testing was increased by 20% in Mix C in comparison to Mix B in order to achieve better mixibility and workability for the mix.

Each proposed mix was prepared three times to control repeatability of the test and each time three cylindrical test specimens of size D=50 mm and h=100 mm were taken (Figure 4.21a). During the mixing procedure, first dry kaolinite and bentonite were added to the mixing container and mixed in dry condition using spatula. Then, fly ash and lime, which had been combined separately, added to the dry mix and completely mixed using spatula in order to form a homogenous dry mix. Afterwards, water was added in a slow and successive manner while the whole components were being mixed inside the mixing container. Alternating hand and mechanical mixing was introduced to ensure a homogenous mix for all samples. The resulting mixtures were of reasonable workability for placement into the moulds; particularly, Mix C had the highest workability among the other mixtures. In an effort to minimise entrapped air and to provide compaction, the mixture was placed into the mould in several layers and worked into the mould with palette knives (Figure 4.21b).

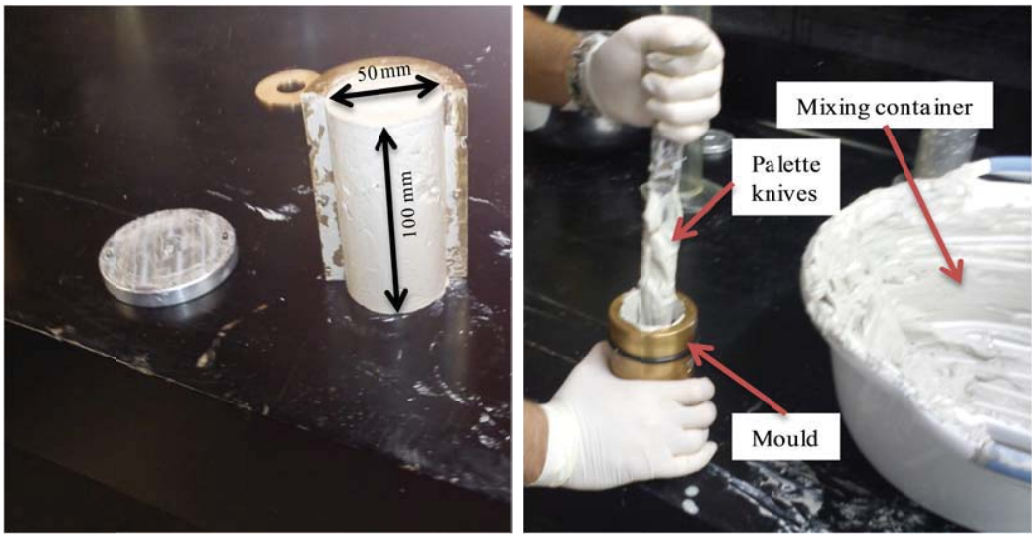

(a) **(b)**

Figure 4.21: (a) Soil mix cylindrical test specimen; (b) placing the mixtures into the mould with palette knives

It should be noted that in order to seal the specimens, plastic sheets were wrapped around the final specimens to minimise moisture loss and assist the cation exchange process. Afterwards, all specimens were stored in an identical controlled ambient environment of 25^{o}C and after one day of cure age, the specimens were de-moulded to be prepared for shear wave velocity measurement at different cure ages by performing bender element tests. The elapsed time from specimen preparation to testing is termed “cure age”.

The bender element test is a non-destructive test that has gained popularity in the laboratory determination of small strain shear modulus. Bender elements are essentially a pair of piezoelectric transducers (top cap at the top and support pedestal at the bottom) and two porous plates (Figure 4.22).

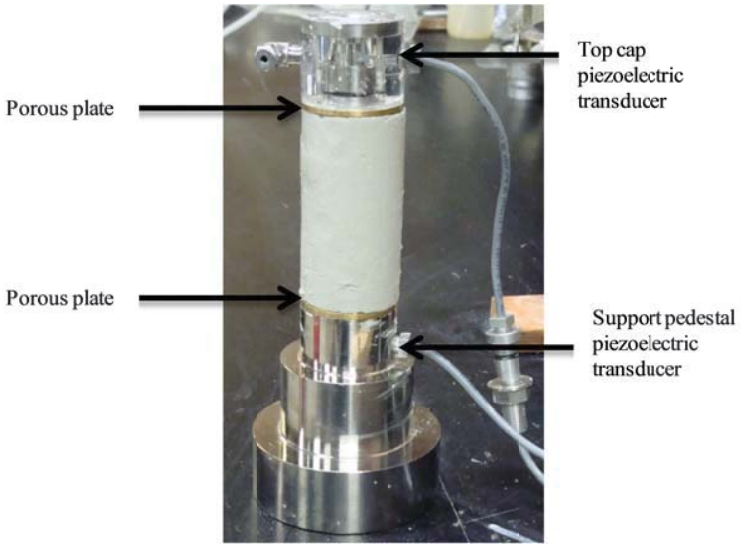

Figure 4.22: Bender element piezoelectric transducers

When a bender element is deformed, the lattice distorts the dipole moment of the crystal and a voltage is generated. Conversely applying a voltage potential causes a bender element to deform. Hence bender elements can be used as either shear wave or compressional wave sources or receivers. Bender elements couple well with the soil, and mechanically similar bender elements operate in the same frequency range and are therefore "tuned" to each other. The bender element systems connect directly into a master control box (Figure 4.23) which, in turn connects to a PC running bender elements control software.

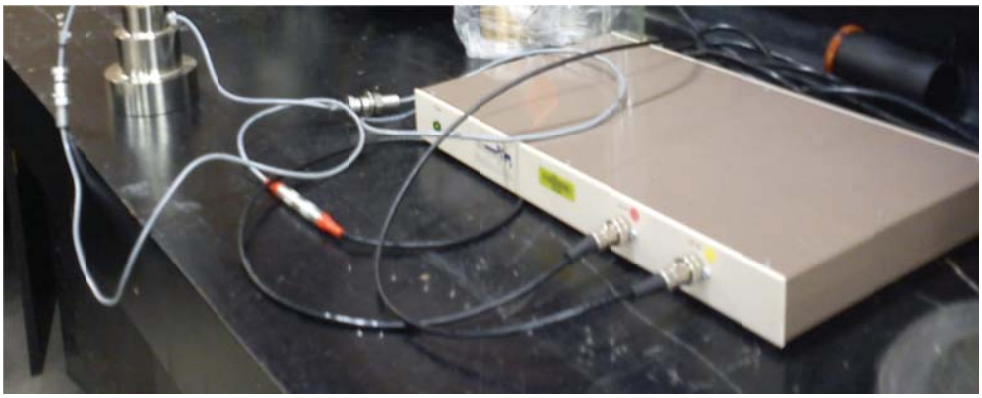

Figure 4.23: Master control box of bender element system

The employed bender element system in this study, located at the UTS soils laboratory, is manufactured to allow both shear wave (S) and compressional wave (P) testing to be performed. It allows the following source signal types to be used:

- Sine wave
- Square wave
- User defined

The standard wave types (sinusoid and square) can be controlled using the following parameters:

- Amplitude
- Period
- Repeat time (0 to 60 seconds)

In addition, the system acquires the following technical specifications:

- Data acquisition speed: 2,000,000 sample/second
- Resolution of data acquisition (bits) : 16 bit
- Connectivity to control box : USB
- Available gain ranges for data acquisition : from 10 to 500

To perform bender element tests, the soil specimens were placed between bender elements (Figure 4.24), and shear wave velocity of each soil specimen was obtained at different cure ages by measuring the time required for the wave to travel between two bender elements using PC running bender element control software (Figure 4.25). It should be noted that the propagated shear wave type was sin wave with amplitude of 10 V (volt) and period of 1 second.

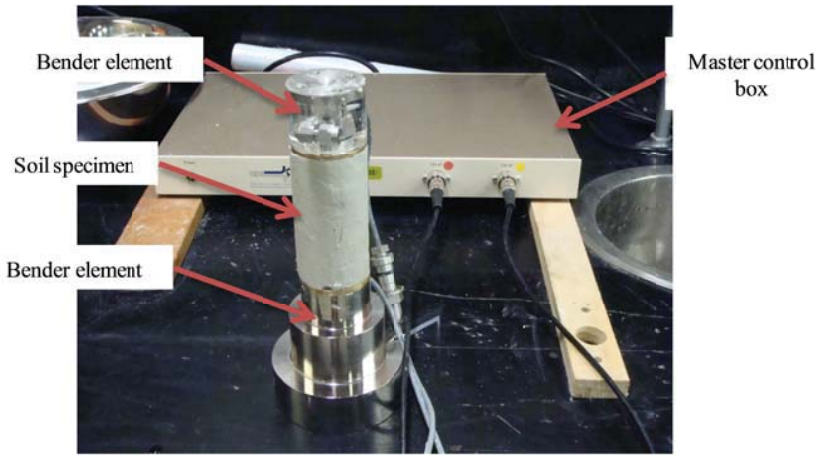

Figure 4.24: Soil specimen placed between bender elements

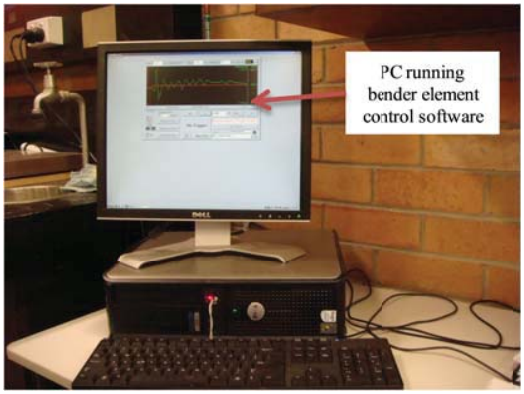

Figure 4.25: PC running bender element control software

The above mentioned test procedure has been repeated for nine soil specimens taken from mixes A, B, and C, respectively, over 14 successive days. Figure 4.26 illustrates the extracted average shear wave velocities versus cure ages for the three different mixes over the period of two weeks.

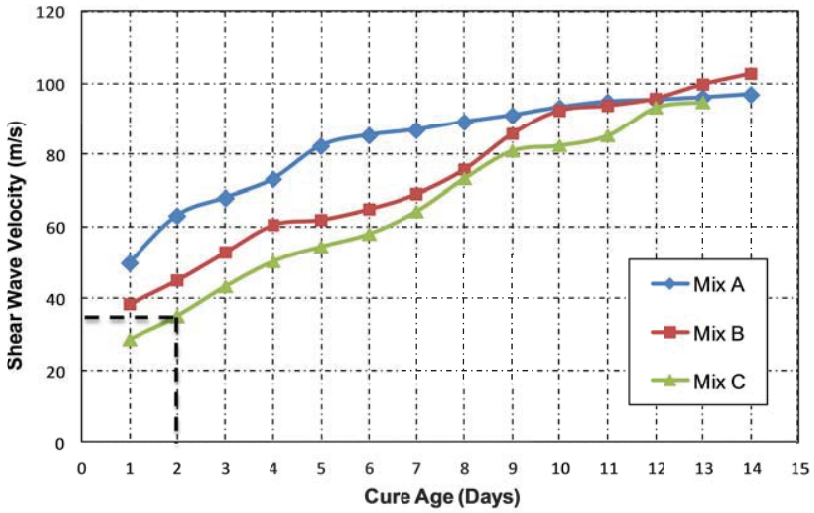

Figure 4.26: Shear wave velocities versus cure age for the examined mixes

Observing the obtained shear wave velocity values in Figure 4.26, it is understood that shear wave velocity values of the three mixes increase by the cure age. It means the examined soil mixes gain stiffness and consequently shear wave velocity increase over the cure age as expected (e.g. Wartman, 1996; Riemer, et al., 1998; Meymand, 1998; Moss et al., 2010). In addition, it is noted that only Mix C produces the required shear wave velocity $(V_s)_m$ of 36 m/s for the soil model on the second day of its cure age while the other two mixes are unable to produce such a low shear wave velocity as required. Therefore, Mix C has been selected as the appropriate mix for shaking table tests in this study. However, further checks regarding the bearing capacity and density of the material is required as

explained below. It should be noted that the proposed soil mix (Mix C) acquires the properties of cemented soil that can be found in nature or treated soil. According to Horpibulsuk et al. (2010), behaviour of cemented soils can be very similar to over consolidated soils. Thus, shear modulus degradation and damping of the adopted soil mix may be similar to over consolidated soils as represented in Figures 3.14 and 3.15.

4.6.3 Properties of the Selected Soil Mix

As mentioned in Section 4.6.2, the shear wave velocity of Mix C on the second day of the cure age matches the targeted value of the soil shear wave velocity. If the soil density during the same cure age is equal to prototype soil density, both criteria to achieve dynamic similarity between the model and the prototype soil are met. Therefore, Mix C has been reproduced at the UTS soils laboratory and the standard method of soil particle density determination was performed on the second day of the cure age according to AS 1289.3.5.1-2006 (Methods of testing soils for engineering purposes). Accordingly, soil density in the second day of the cure age (ρ_s) was determined to be 1450 kg/m^3 which is almost equal to the prototype soil density (1470 kg/m^3). Thus, shear wave velocity and soil density values of Mix C on the second day of the cure age satisfy the mentioned dynamic similarity requirements. In addition, as mentioned earlier, the soil model undrained shear strength is supposed to be adequate to satisfy the required shallow foundation bearing capacity underneath the structural model. In order to check the undrained shear capacity, three cylindrical test specimens of size D=100 mm and h=200 mm were taken and sealed (Figure 4.27a) from Mix C with the mixing and moulding process described in Section 4.6.2. Then, on the second day of the samples cure age, Unconfined Compression tests (UC) were performed on the three soil specimens in accordance with AS5101.4-2008 (Method 4: unconfined compressive strength of compacted materials) in order to determine soil shear strength. Figure 4.27b depicts a failed specimen after undertaking the test. The average undrained shear strength (C_u) of Mix C on the second day of the cure age, resulting from three examined specimens, was 1.57 kPa. According to the carried out foundation calculations, by adopting this value of undrained shear strength, the soil mix will provide enough bearing capacity with acceptable factor of safety under the structural model on the second day of the cure age to avoid any failure or excessive settlement underneath the structure (q_{ult} = 5.14 C_u, FoS > 2.0). Eventually, the selected soil mix (Mix C) on the second day of the cure age is expected to have the properties summarised in Table 4.6.

Table 4.6: Properties of the selected soil mix on the second day of cure age

Shear wave velocity $\mathbf{V_s}$ (m/s)	Undrained shear strength $\mathbf{C_u}$ (kPa)	Soil Density ρ (kg/m^3)
36	1.57	1450

(a) **(b)**

Figure 4.27: (a) Sealed soil Mix C cylindrical test specimen of size D=100 mm and h=200 mm; (b) failed soil specimen after performing Unconfined Compression test

4.7 Scaling of Adopted Earthquake Acceleration Records

Four earthquake acceleration records including Kobe, 1995 (Figure 4.28a), Northridge, 1994 (Figure 4.29a), El Centro, 1940 (Figure 4.30a), and Hachinohe, 1968 (Figure 4.31a) have been adopted for the shaking table tests. The first two earthquakes are near field ground motions and the latter two are far field motions. These earthquakes have been chosen by the International Association for Structural Control and Monitoring for benchmark seismic studies (Karamodin and Kazemi, 2008). Details of the adopted earthquake records will be discussed in Section 5.3.2. According to Table 4.2, as determined by Equation (4.3), scaling relationship between natural frequency of the model (f_m) and natural frequency of the prototype (f_p) is 5.48 while scaling relations between the model and prototype accelerations is 1.0, meaning the earthquake magnitude remains the same as the prototype based on the first principle of "dynamic similarity" which defines model and prototype accelerations to be equal (Table 4.2).

Therefore, for scaling the earthquake records, it is required to reduce the time steps of the original records by a factor of 5.48. As a result, the original time steps of Kobe, Northridge, and El Centro earthquake acceleration records were shifted from 0.02 to 0.00365, while for Hachinohe earthquake record, the original time steps of 0.01 shifted to 0.001825. The scaled acceleration records of the four adopted earthquakes are illustrated in Figures 4.28 to 4.31.

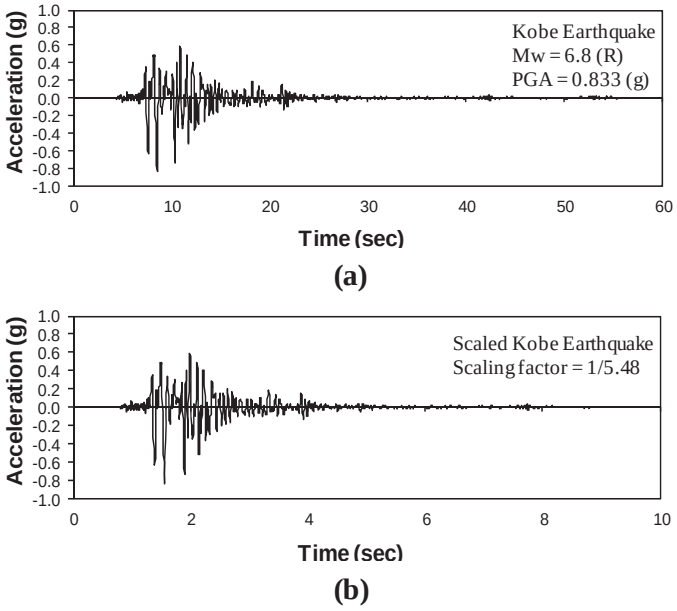

Figure 4.28: Kobe earthquake (1995); (a) original record; (b) scaled record

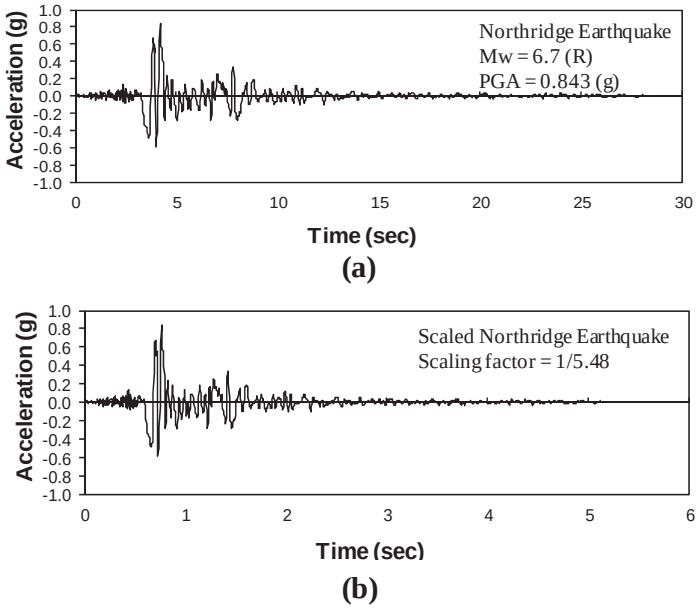

Figure 4.29: Northridge earthquake (1994); (a) original record; (b) scaled record

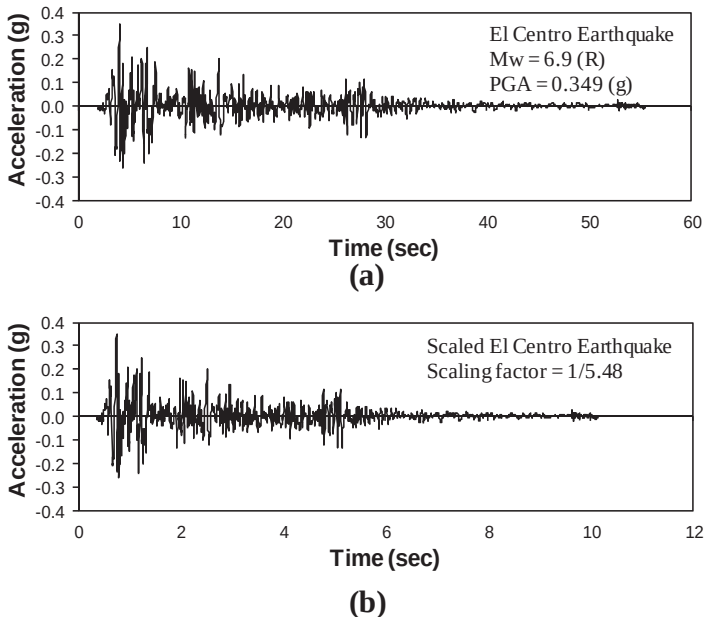

Figure 4.30: El Centro earthquake (1940); (a) original record; (b) scaled record

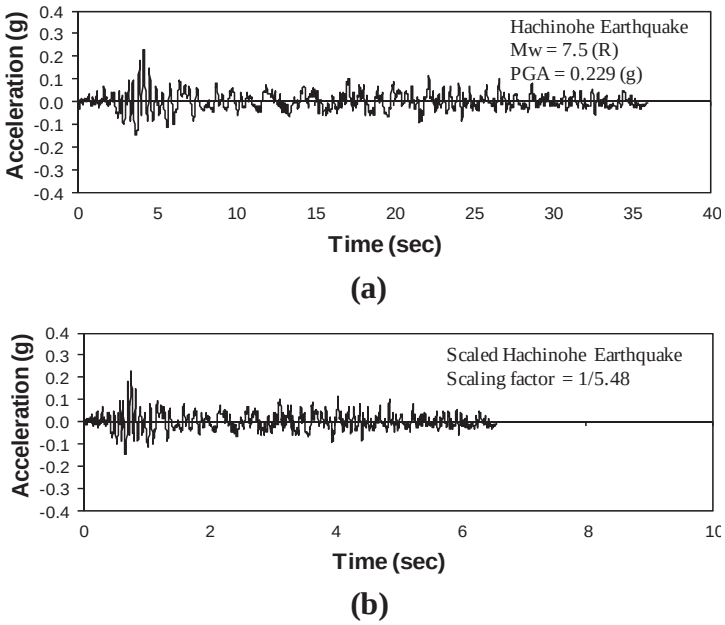

Figure 4.31: Hachinohe earthquake (1968); (a) original record; (b) scaled record

4.8 Instrumentation and Data Acquisition System

Two different classes of measuring instruments were utilised in the current shaking table test programme, namely, displacement transducers (Figure 4.32a) and accelerometers (Figure 4.32b) in order to measure structural deformations and accelerations, respectively.

(a)

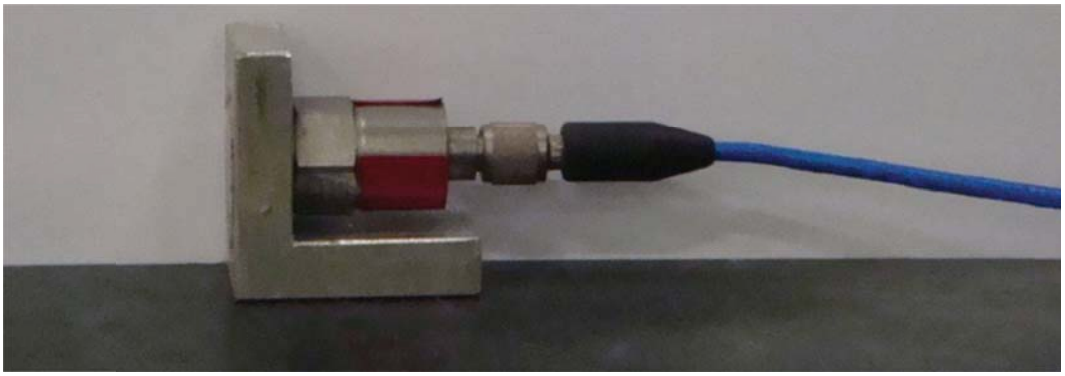

(b)

Figure 4.32: Utilised measuring instruments in the shaking table tests; (a) displacement transducer; (b) accelerometer

The utilised measuring instruments possess the following specifications:

- Displacement transducers
  - Model : GH Rod-style position sensor
  - Digital pulse accuracy : ± 0.005 mm
  - Update times : less than 1 ms
  - Repeatability : ± 0.001%
  - Operating temperature range : -40 to +80 ºC
- Accelerometer
  - Model : PCB triaxial accelerometer
  - Frequency range : ± 5%
  - Measurement range : ± 490 m/s-2
  - Measurement accuracy : ± 0.006 m/s-2
  - Operating temperature : -54 to +121 ºC

The instruments were directly connected to a data acquisition system managed by the integrated software package, which is run on a desktop computer and interfaces with the

MTS (MTS System Corp.) shaking table control system. Each displacement transducer and accelerometer was individually calibrated before installation to ensure high accuracy. An online calibration check was performed just before each shaking table test through the data acquisition system, thereby identifying any malfunctioning or miswired sensors. With the calibration routine embedded in the data acquisition system, the acquired data was automatically transformed into engineering units.

4.9 Shaking Table Tests on Fixed Base Structural Model

Tests were carried out on the constructed structural model, described in Section 4.4, as a *fixed base model* (structure directly fixed on top of the shaking table) in order to:

- Ensure the structural model possesses targeted natural frequency;
- Determine the damping ratio of the structural model; and
- Obtain seismic response of fixed base model under the influence of the four scaled earthquake records, explained in Section 4.7, to verify the numerical model.

To achieve the above, constructed structural model was fixed and secured on the UTS shaking table as shown in Figure 4.33.

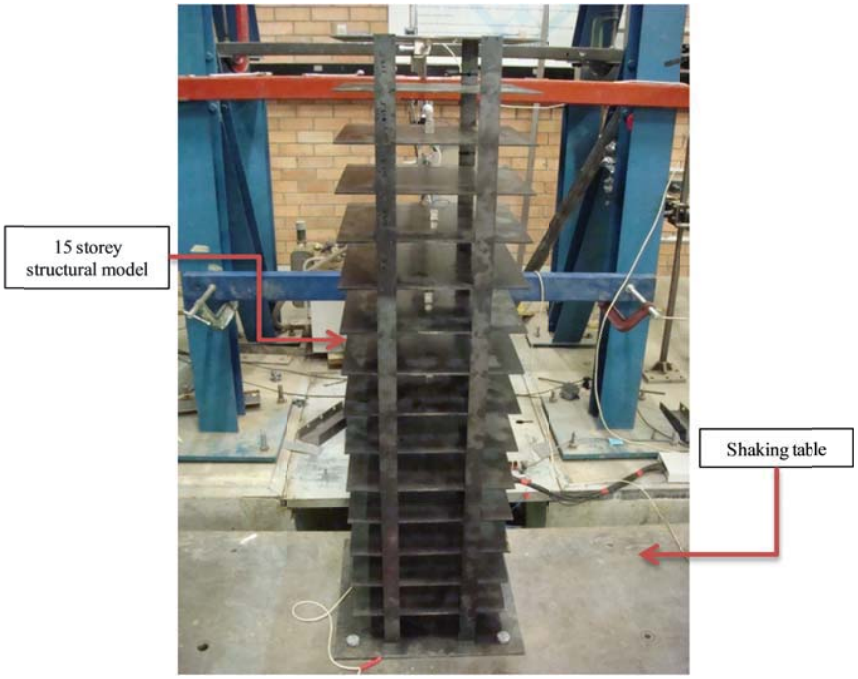

Figure 4.33: Fixed base structural model secured on the UTS shaking table

After securing the structural model on the shaking table, instrumentations including displacement transducers and accelerometers were installed on the structure in order to monitor the behaviour of the structure and to primarily measure structural lateral displacements. It should be noted that in addition to the displacement transducers installed at levels 3, 5, 7, 11, 13, and 15, eight accelerometers were installed at levels 3, 5, 7, 9, 11, 13, and 15 so as to check the consistency of the recorded displacements. Displacement, acceleration and velocity in time domain are closely related to each other. If the measured parameter is acceleration, displacement can be found through a double integration in time domain. Therefore, displacements of the various levels were determined by integrating the corresponding accelerations, measured by the accelerometers, in time domain and checked against the recorded displacements to ensure the consistency and accuracy of the obtained records. Figure 4.34 illustrates the final arrangement of the displacement transducers and accelerometers at different levels of the structural model.

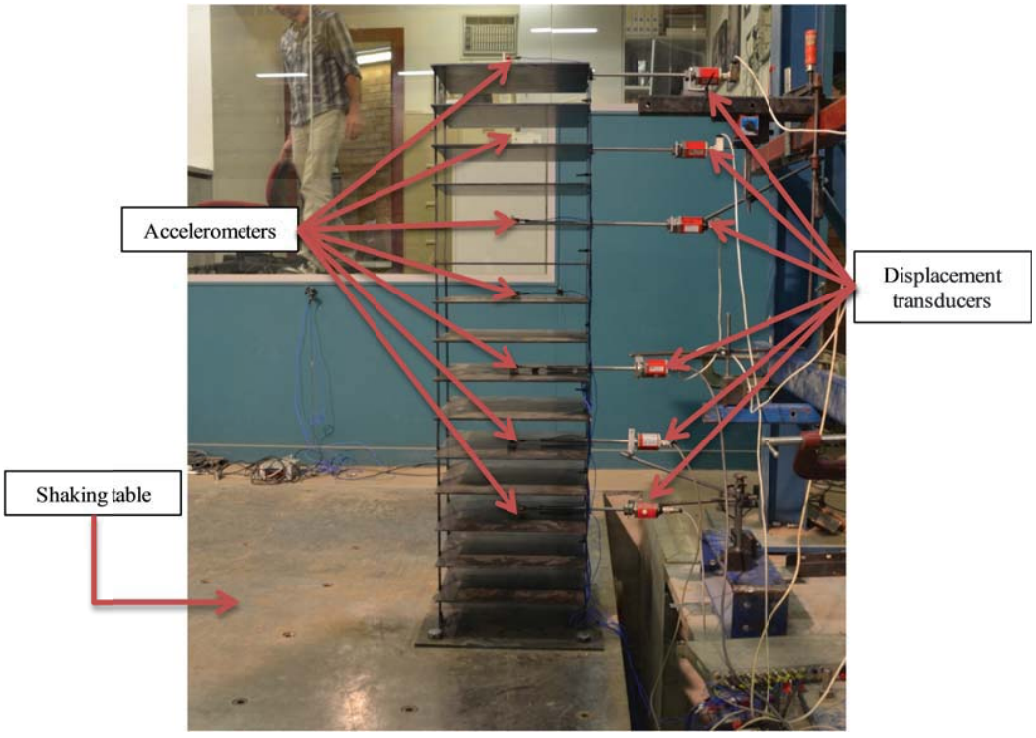

Figure 4.34: Final arrangement of the measuring instruments

4.9.1 Shaking Table Tests Procedure

Initially, Sine Sweep test was performed on the structural model to determine the natural frequency of the model. Sine Sweep test involves a logarithmic frequency

sweep holding a specified acceleration constant at the base of the structure. For the current Sin Sweep test, frequency of the shaking table has increased from 0.1 Hz to 50 Hz. The first resonance between the shaking table and structural model frequencies showed the fundamental natural frequency of the model. The test was repeated three times to ensure the determined natural frequency is adequately accurate. The resulting natural frequency of the constructed structural model obtained from sin sweep test results was 2.19 Hz which is in a very good agreement with the desired natural frequency of structural model (Table 4.4). Therefore, the constructed structural model, with the natural frequency (f_m) of 2.19 Hz and the total mass (m_m) of 104 kg, possesses the required characteristics as summarised in Table 4.4, to meet the dynamic similarity criteria.

After ensuring adequacy of the structural model characteristics, shaking table tests were performed by applying scaled earthquake acceleration records of Kobe, 1995 (Figure 4.28b), Northridge, 1994 (Figure 4.29b), El Centro, 1940 (Figure 4.30b), and Hachinohe, 1968 (Figure 4.31b) to the fixed base structural model.

4.9.2 Determining Structural Damping Ratio

The estimated value of the structural damping ratio of the constructed structural model has been determined from the free vibration lateral displacement records of the structural model using the following Taylor series expansion (Roy et al., 2006):

$$\frac{U_n}{U_{n+m}} = e^{2\pi m\xi} = 1 + \sum_{n=1}^{\infty} \frac{(2\pi m\zeta)^n}{n!} = 1 + 2\pi m\xi + \frac{(2\pi m\xi)^2}{2!} + \ldots \qquad (4.9)$$

where, ξ is the structural damping ratio and U_n and U_{n+m} are two positive peaks of the free vibration response of the structure which are *m* cycles apart.

Substituting the values of U_n and U_{n+m} for the two positive peaks of the free vibration lateral displacement records in Equation (4.9), which are 10 cycles apart, and repeating the whole process several times, the estimated structural damping ratio (ξ) is 1.1%.

4.9.3 Fixed base Model Test Results

The results of the performed shaking table tests under the influence of four scaled earthquake acceleration records in terms of maximum lateral deflections are determined and presented in Figures 4.35 to 4.38. In determination of the lateral deflections, the movement of the shaking table has been subtracted from storey

movements. Therefore, all the records are in comparison to the base movements. It should be noted that for the sake of accuracy and consistency, the recorded displacements using displacement transducers, verified against the calculated displacements from accelerometer records, are presented.

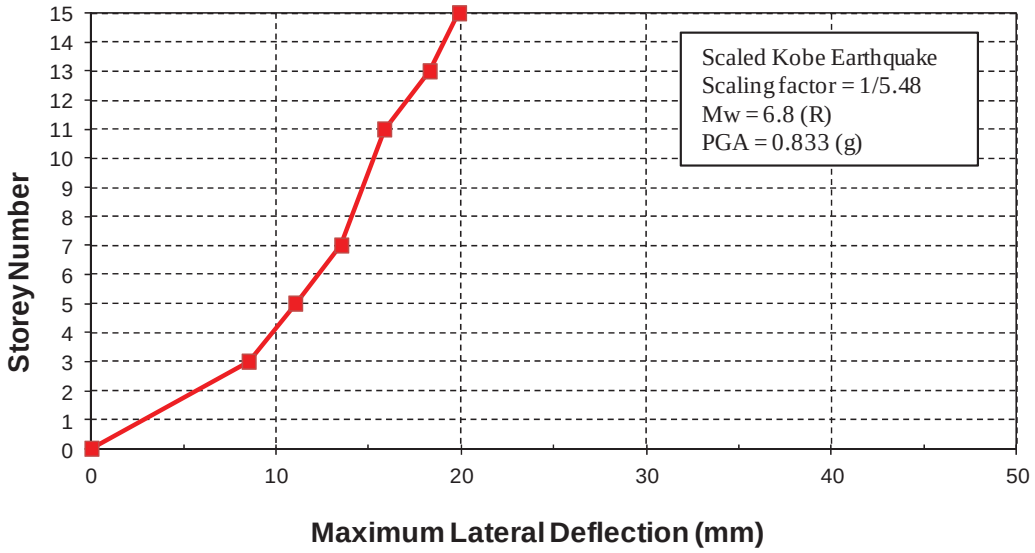

Figure 4.35: Recorded maximum lateral deflections of fixed base 15 storey structural model under the influence of scaled Kobe (1995) earthquake

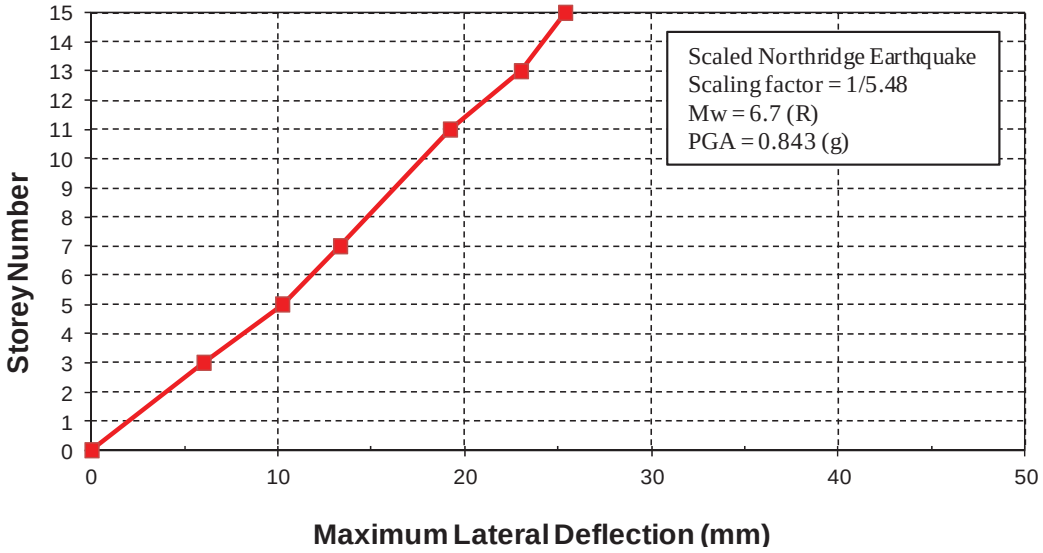

Figure 4.36: Recorded maximum lateral deflections of fixed base 15 storey structural model under the influence of scaled Northridge (1994) earthquake

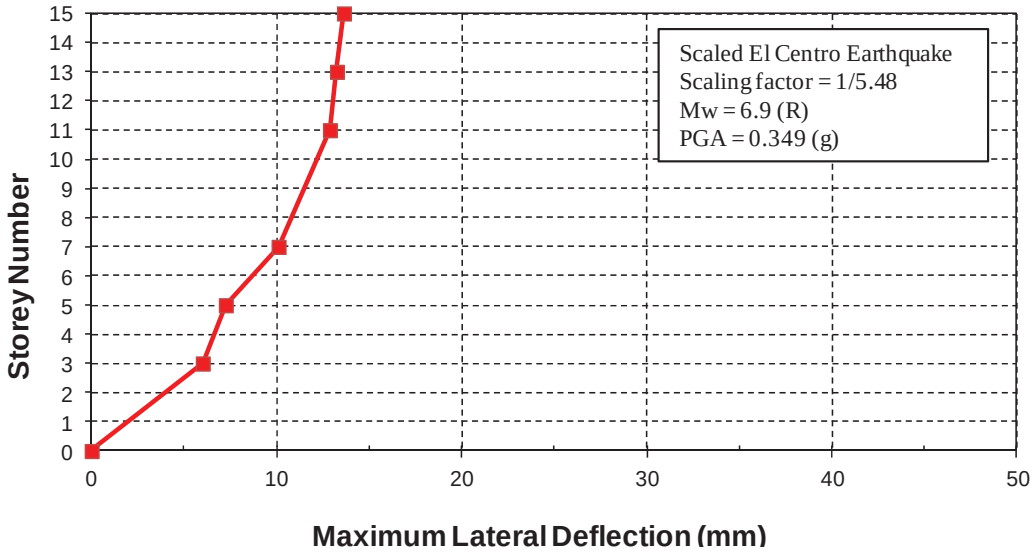

Figure 4.37: Recorded maximum lateral deflections of fixed base 15 storey structural model under the influence of scaled El Centro (1940) earthquake

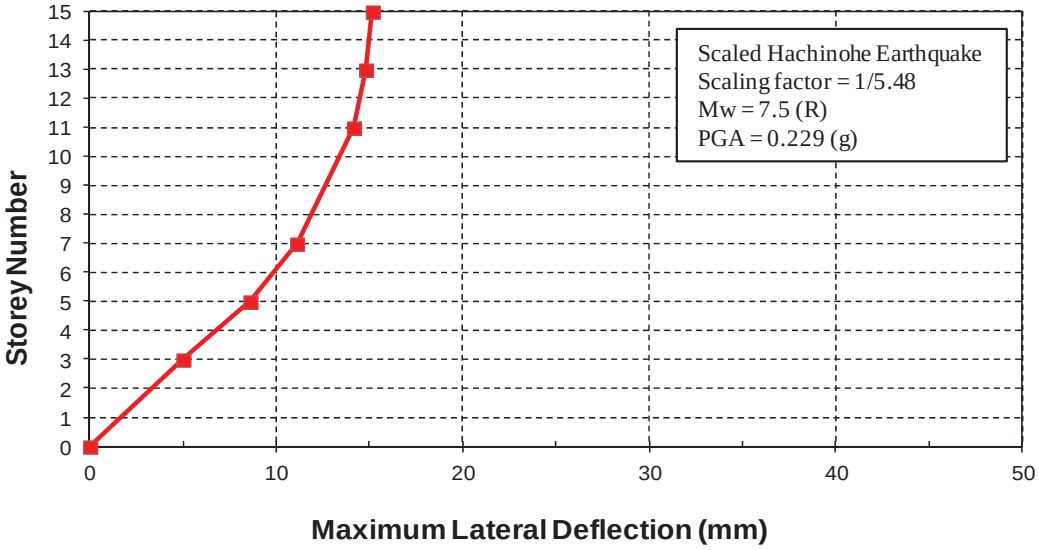

Figure 4.38: Recorded maximum lateral deflections of fixed base 15 storey structural model under the influence of scaled Hachinohe (1968) earthquake

4.10 Shaking Table Tests on Soil-Structure Model

The ultimate purpose of this phase of the shaking table tests, as the main phase of the experimental investigations, is to verify and validate the new developed numerical soil-structure model, described in Chapter 3, by carrying out shaking table tests on the scale soil-structure model of the soil-structure system prototype, discussed in Section 4.1.

4.10.1 Test Preparations and Setup

The first step in setting up the main phase of the shaking table tests, was securing the constructed laminar soil container, explained in Section 4.5, on the UTS shaking table. For this purpose, the soil container was placed at the designated location, then fixed and secured on the shaking table using eight M38 bolts passing through the provided holes. The internal surface of the soil container then was covered and sealed with two layers of black plastic sheeting.

Similar to Gohl and Finn, (1987) and Valsangkar et al. (1991), 25mm thick absorbing layers of Polystyrene foam sheets have been installed at the end walls of the soil container to simulate viscous boundaries in the free field condition. The thick layers of Polystyrene minimise reflection of outward propagating waves back into the model and allow the necessary energy radiation. In addition, a layer of well graded gravelly soil particles were glued to the bottom of the soil container so as to simulate frictional contact between the soil and the bedrock. This layer provides friction between the timber base plate, as the bedrock, and the in-situ soil mix and does not allow the soil mix to slip over the base plate. Various components of the laminar soil container are shown in Figure 4.39.

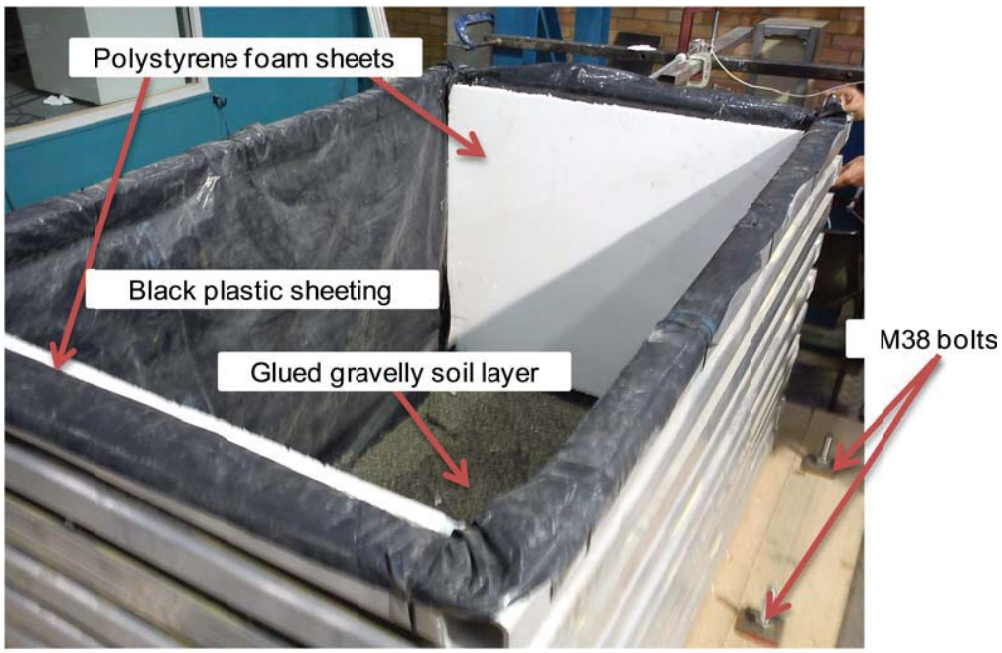

Figure 4.39: Various components of the secured laminar soil container on the shaking table

Afterwards, Sine Sweep test was undertaken on the empty laminar soil container to estimate the natural frequency of the container. After three times repeating the test,

the natural frequency of the container was found to be 10 Hz. The difference between the obtained natural frequency of the container and the natural frequency of the soil, calculated during original design of the laminar soil container in Section 4.5.2 (equal to 9.1 Hz) is approximately 10% which is acceptable. Therefore, the constructed laminar soil container, with the natural frequency (f_m) of 10 Hz, is deemed to be appropriate for the tests.

As explained in Section 4.6.2, the selected soil mix obtains the required stiffness and consequently the shear wave velocity after two days of curing. As a result, the time schedule of the testing process is highly intensive and time sensitive. Therefore, soil mixing and placement should be carried out in one day in order to produce a homogenous soil mix and after two days of curing, the final tests are to be performed.

With respect to what has been discussed above, after determining the natural frequency of the laminar soil container on the shaking table, all the components of the soil mix including kaolinite, bentonite, fly ash, lime, and water as well as two mixers were moved near the shaking table (Figure 4.40a). Then, two cubic metres of the soil mix was produced and placed into the laminar soil container (Figure 4.40b). During the soil mixing process, ten cylindrical soil samples of *D*=50 mm and *h*=100 mm were taken from the soil mix for quality control of the mix.

(a) **(b)**

Figure 4.40: (a) Placing the mix components and mixer near the shaking table; (b) producing and placing the soil mix into the soil container

The entire mixing process and filling the laminar soil container were completed in one day. Figure 4.41 shows the finished surface of the soil mix inside the soil container after completing the filling and mixing processes. Then, the soil mix inside the container was left to be cured for two days while the surface of the soil container was covered and sealed.

Figure 4.41: Finished surface of the level soil inside the soil container

On the second day, the structural model was lifted up (Figure 4.42a) and placed on the designated location, exactly in the middle of the soil surface (Figure 4.42b). After securing the structural model on top of the soil, no excessive settlement or failure was observed underneath the base plate, indicating that the shear strength of the soil mix was adequate to carry the weight of the structural model, as expected and examined in Section 4.6.3.

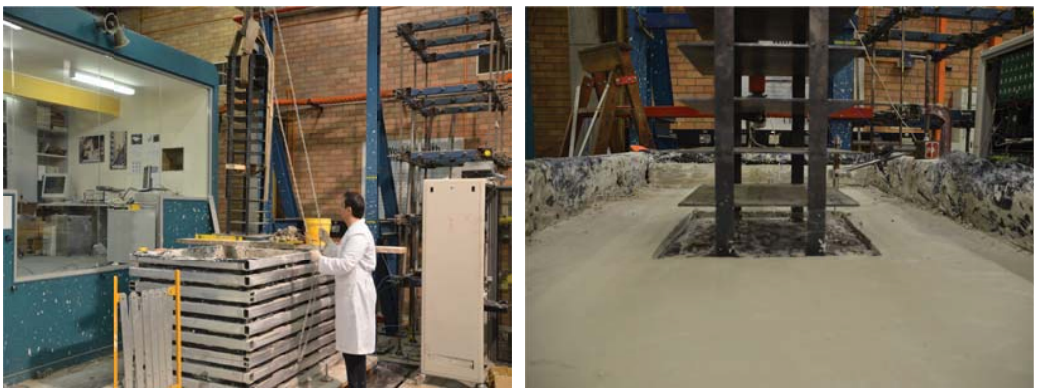

(a) **(b)**

Figure 4.42: (a) Placing the structural model on top of the soil mix; (b) final arrangement of the level structural model on top of the soil

Instrumentation of the structure in the soil-structure system has been similar to the fixed base structure, as explained in Section 4.9 (Figure 4.43a). In addition, vertical displacement transducers were placed on the level base plate of the structure (simulating the foundation) to determine the vertical displacements of the structure during the testing process (Figure 4.43b).

(a) **(b)**

Figure 4.43: (a) Installing the displacement transducers on the structural model; (b) vertical displacement transducer installed at the level of the base plate

Figure 4.44 shows the final setup of the displacement transducers and accelerometers at different levels of the structural model in the soil-structure model on the shaking table.

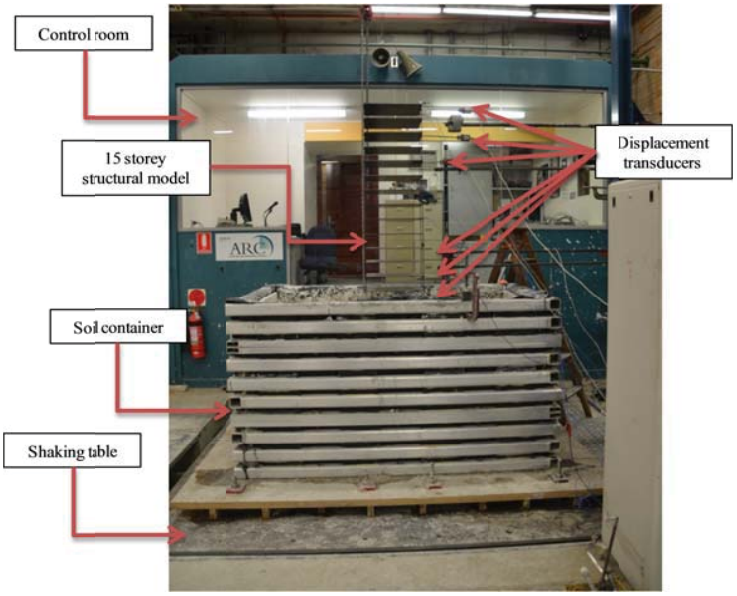

Figure 4.44: Final setup of the measuring instruments of the soil-structure model

4.10.2 Shaking Table Tests on Flexible Base Model

Before applying the scaled earthquake acceleration records to the flexible base model (soil-structure model), Sine Sweep test was carried out in order to estimate the natural frequency of the flexible base model. During the Sin Sweep test, frequency of the shaking table was raised from 0.1 Hz to 50 Hz to obtain the natural frequency of the soil-structure model. The obtained natural frequency of the soil-structure model from the performed Sin Sweep test was estimated to be 1.60 Hz. It can be noted that as expected, natural frequency of the soil-structure model is considerably smaller than the natural frequency of the fixed base

structural model, previously was determined to be 2.19 Hz. Afterwards, shaking table tests were undertaken by applying scaled earthquake acceleration records of Kobe, 1995 (Figure 4.28b), Northridge, 1994 (Figure 4.29b), El-Centro, 1940 (Figure 4.30b), and Hachinohe, 1968 (Figure 4.31b) to the flexible base model, with the final setup as shown in Figure 4.44.

4.10.3 Flexible Base Model Test Results

The results of the carried out shaking table tests under the influence of four scaled earthquake acceleration records in terms of the maximum lateral deflections of various storey of the structure are illustrated in Figures 4.45 to 4.48. Figure 4.49 illustrates an example of experimental time-history displacement results for fixed base and flexible base models under the influence of Kobe earthquake (1995). In addition, the maximum vertical displacements of the base plate have been obtained from the vertical displacement transducers installed at the level of the base plate for each earthquake record, respectively, and summarised in Table 4.7. It should be noted that the lateral deflections of the structural model under the influence of two different earthquakes with the same magnitude such as Kobe (1995) and Northridge (1994) could be totally different (as shown in Figures 4.45 and 4.46 due to the difference in the spectral displacement response (S_d). Base on the response spectra of Northridge (1994) and Kobe (1995) earthquakes, for the same value of the natural period of the system, the spectral displacement response (S_d) of Northridge (1994) is more than Kobe (1995). Thus, the lateral structural deflections under the influence of Northridge (1994) are larger than the lateral displacements under the influence of Kobe (1995).

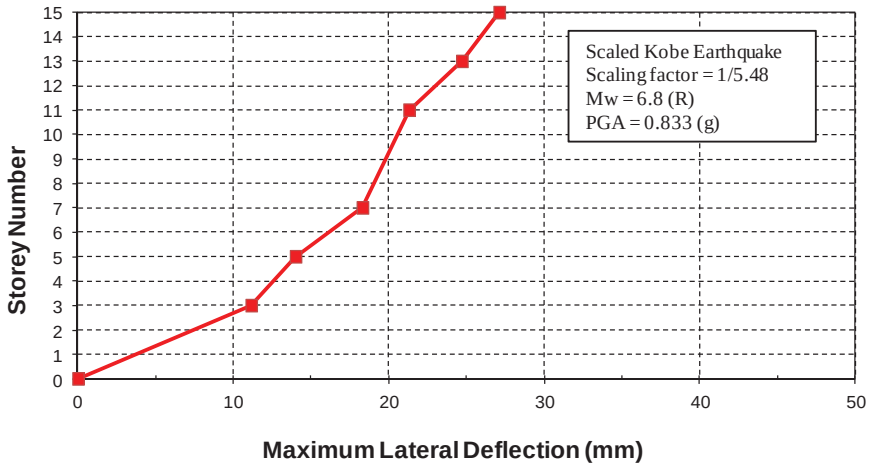

Figure 4.45: Recorded maximum lateral deflections of flexible base model under the influence of scaled Kobe (1995) earthquake

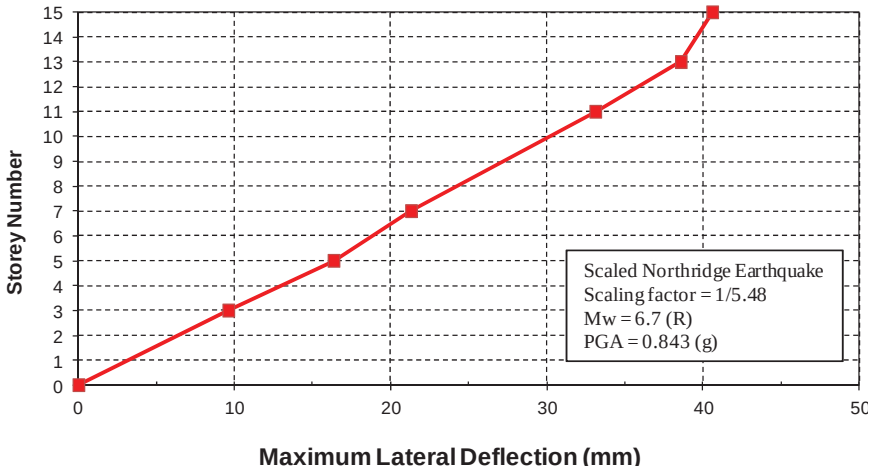

Figure 4.46: Recorded maximum lateral deflections of flexible base model under the influence of scaled Northridge (1994) earthquake

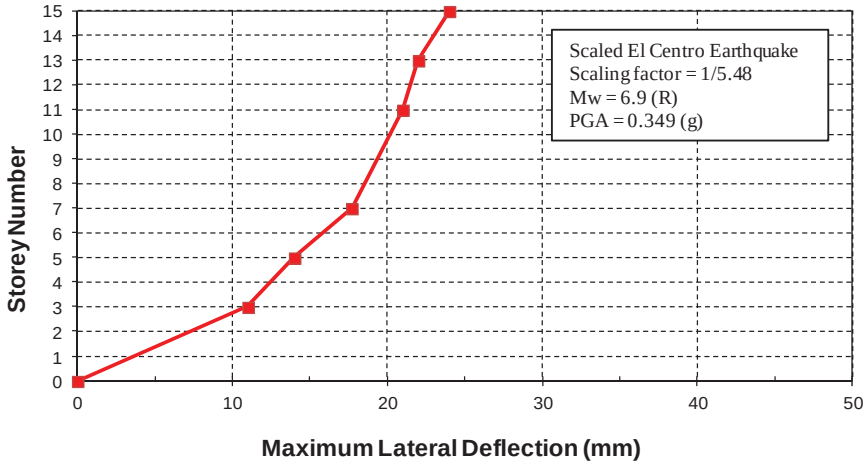

Figure 4.47: Recorded maximum lateral deflections of flexible base model under the influence of scaled El Centro (1940) earthquake

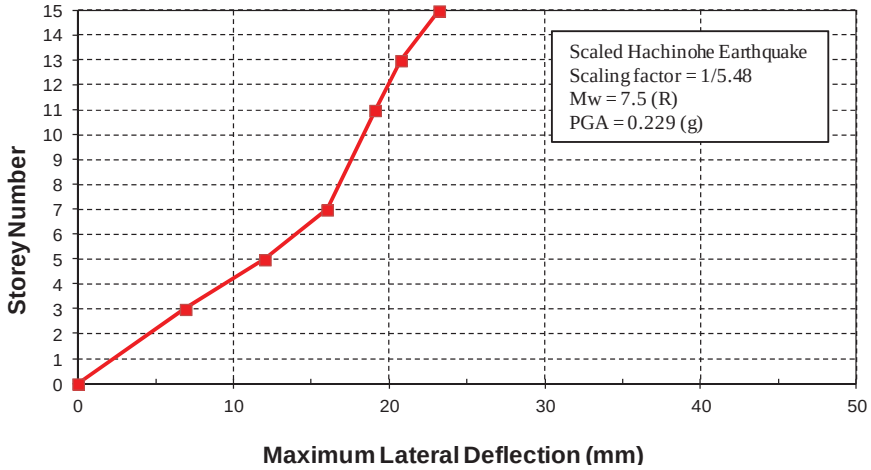

Figure 4.48: Recorded maximum lateral deflections of flexible base model under the influence of scaled Hachinohe (1968) earthquake

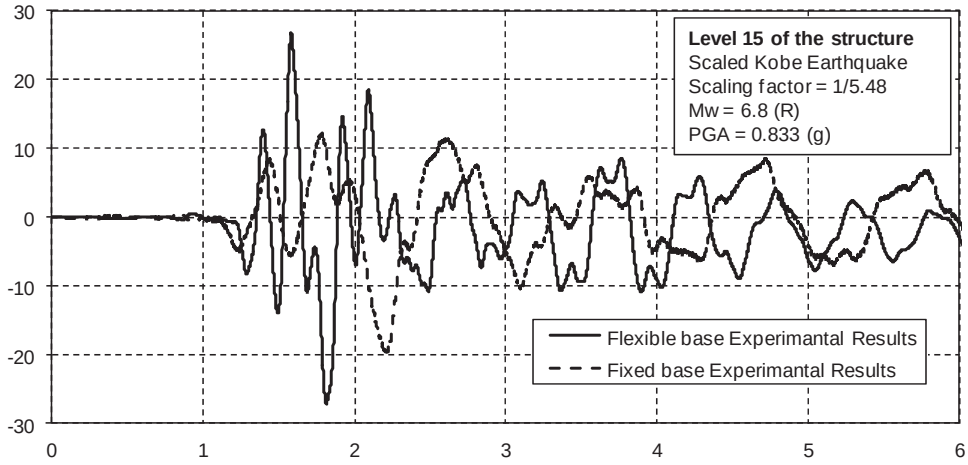

Figure 4.49: Sample experimental time-history displacement results for fixed base and flexible base models under the influence of Kobe earthquake (1995) at level 15

Table 4.7: Maximum vertical displacements of the base plate

Scaled Earthquake Acceleration Record	Maximum Vertical Displacement	Rocking Angle of the Foundation
Kobe (1995)	2.54 mm	0.58º
Northridge (1994)	1.32 mm	0.30º
El-Centro (1940)	1.98 mm	0.45º
Hachinohe (1968)	1.47 mm	0.33º

4.11 Verification of Numerical Models Using Shaking Table Test Results

As explained earlier, the main goal of undertaking shaking table tests, in this study, is to validate the novel and enhanced numerical soil-structure model, developed in Chapter 3, by comparing the numerical and experimental results. Verification of the numerical soil-structure model has been carried out in two stages. The numerical model of the constructed structural model, shown in Figure 4.8, was built in FLAC2D using dimensions of the physical model. After building the geometry of the structural model, the required structural parameters including cross-sectional area of the beams (A_b), moment of inertia of the beams (I_b), cross-sectional area of the columns (A_c), moment of inertia of the columns (I_c), cross-sectional area of the foundation slab (A_s), moment of inertia of the foundation slab (I_s), modulus of elasticity of steel (E), density (ρ), and structural damping ratio (ξ), summarised in Table 4.8, were extracted from the construction detail drawings and specifications and adopted in the numerical simulation of the structure in FLAC2D. Figure 4.50 illustrates the created model that numerically

defines the geometry, properties, and loading of the physical fixed base model in FLAC2D.

Table 4.8: Adopted parameters for numerical simulation of the structural model

A_b (m^2)	I_b (m^4)	A_c (m^2)	I_c (m^4)	A_s (m^2)	I_s (m^4)	E (kPa)	ρ (kg/m^3)	ξ (%)
0.002	4.16E-9	1.6E-4	5.33E-11	0.005	4.16E-8	2.0E8	7850	1.1

The simulated soil-structure model in FLAC2D is shown in Figure 4.51. Summarised structural characteristics in Table 4.8 have been adopted to simulate the structural part of the model.

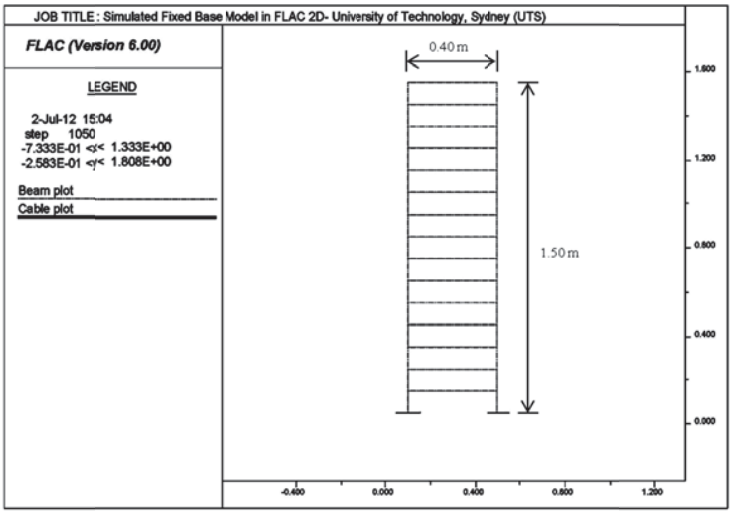

Figure 4.50: Simulated numerical fixed base model in FLAC2D

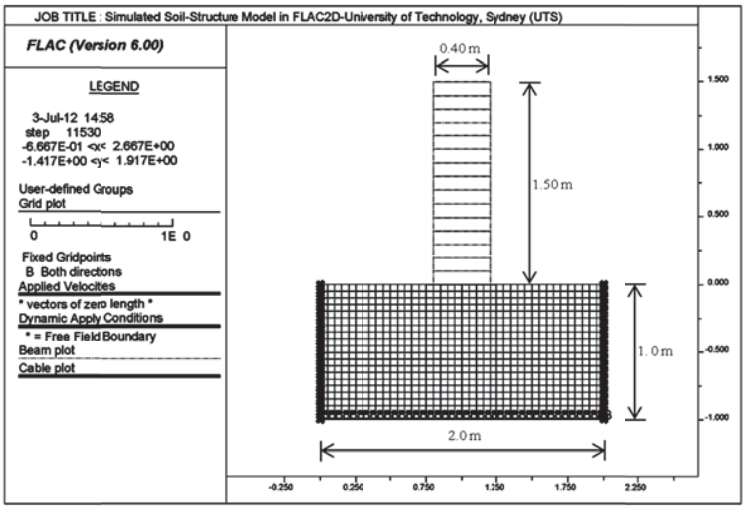

Figure 4.51: Simulated numerical flexible base model in FLAC2D

As reported in Section 4.10.4, ten cylindrical soil specimens of size D=50 mm and h=100 mm were successively taken from the soil mix, during the soil mixing process. In order to adopt the most accurate soil parameters in simulation of the physical soil-structure model (Figure 4.44), shear wave velocity (V_s) and soil density (ρ) of the samples in the second day of curing were determined by performing bender element and density tests on the UTS soils laboratory. The average results of the ten specimens indicated that the values of shear wave velocity (V_s) and soil density (ρ) were 35.5 m/s and 1450 kg/m^3, respectively. These results have been in very good agreement and conformity to the initial laboratory test results, summarised in Table 4.6. The adopted soil properties in the numerical simulation of the flexible base model consist of shear strength (S_u), shear wave velocity (V_s), low strain shear modulus (G_{max}), bulk modulus (K), and density (ρ), summarised in Table 4.9.

In addition, normal spring stiffness (k_n) and shear spring stiffness (k_s) for the interface elements of the flexible base model were calculated based on Equation 3.12 of Chapter 3 and the values are reported in Table 4.9.

Table 4.9: Adopted soil parameters in numerical simulation of flexible base model

Parameters	S_u (kPa)	V_s (m/s)	G_{max} (kPa)	K (kPa)	ρ (kg/m^3)	k_n (kPa/m)	k_s (kPa/m)
Values	1.57	35.5	1830	90760	1450	3.7E7	3.7E7

After creating fixed base and flexible base numerical models in FLAC2D (Figures 4.50 and 4.51), fully nonlinear time history dynamic analyses, described in Section 3.8.4.2, were carried out on both fixed base and flexible base models under the influence of four scaled earthquake acceleration records including Kobe, 1995 (Figure 4.28b), Northridge, 1994 (Figure 4.29b), El-Centro, 1940 (Figure 4.30b), and Hachinohe, 1968 (Figure 4.31b). Geometric nonlinearity of the structures, capturing P-Delta effects, has been accommodated by specifying large-strain solution mode in FLAC2D software in the structural analyses of fixed base and flexible base models. In addition, running the analysis in large strain mode reduces the analysis time and increases the accuracy of the analysis in determination of the deformations. The built-in tangent-modulus function

model presented by Hardin and Drnevich (1972) for clay (Table 3.1), with the value of γ_{ref} = 0.234, was adopted in the dynamic analysis of flexible base model to take into account hysteretic damping in the analyses. In this way, nonlinear behaviour of the subsoil has been considered in the dynamic analysis.

Afterwards, the numerical results of the fully nonlinear time history dynamic analyses under the influence of the four mentioned scaled earthquake acceleration records in terms of the maximum lateral deflections and the maximum vertical displacements of the base plate were determined for both fixed base and flexible base models from FLAC2D displacement history records for each scaled earthquake.

Then, derived results of the numerical fixed base and flexible base models were compared with the experimental results of the shaking table tests, performed on the fixed base model (Figures 4.35 to 4.38) and the flexible base model (Figures 4.45 to 4.48).

The numerical predictions and experimental values of the maximum lateral displacements of the fixed base and the flexible base models are presented and compared in Figures 4.52 to 4.55. Average values of the numerical predictions and experimental values of the maximum lateral displacements of fixed base and flexible base models were determined and compared in Figure 4.56. In addition, the predicted and measured vertical displacements of the base plate are summarised and compared in Table 4.10.

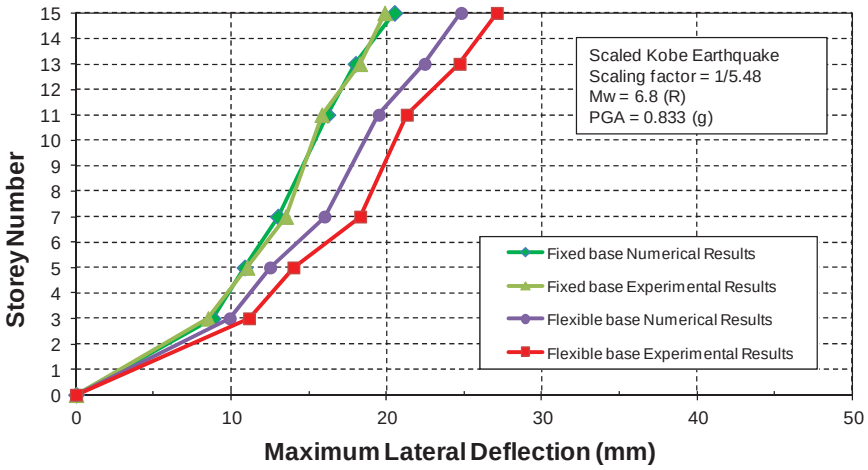

Figure 4.52: Numerical and experimental maximum lateral displacements of fixed base and flexible base models under the influence of scaled Kobe (1995) earthquake

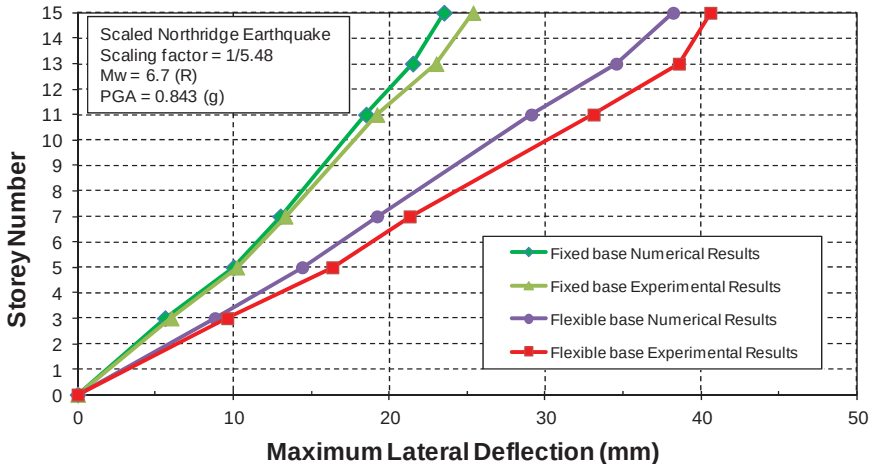

Figure 4.53: Numerical and experimental maximum lateral displacements of fixed base and flexible base models under the influence of scaled Northridge (1994) earthquake

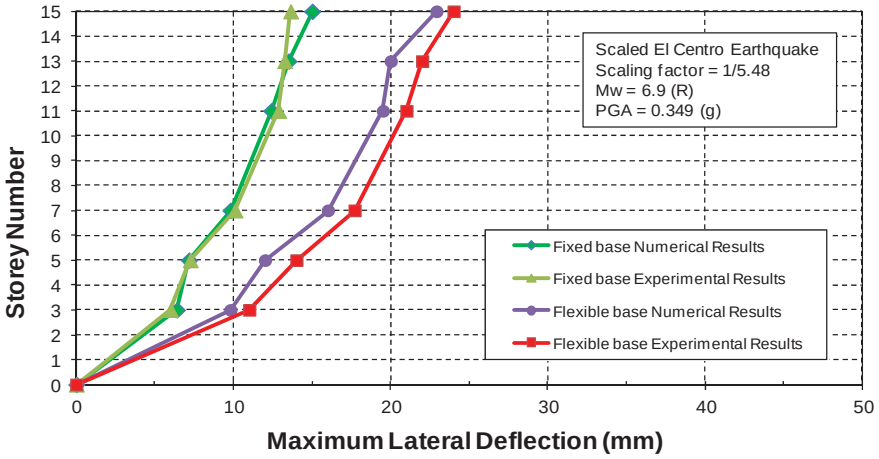

Figure 4.54: Numerical and experimental maximum lateral displacements of fixed base and flexible base models under the influence of scaled El Centro (1940) earthquake

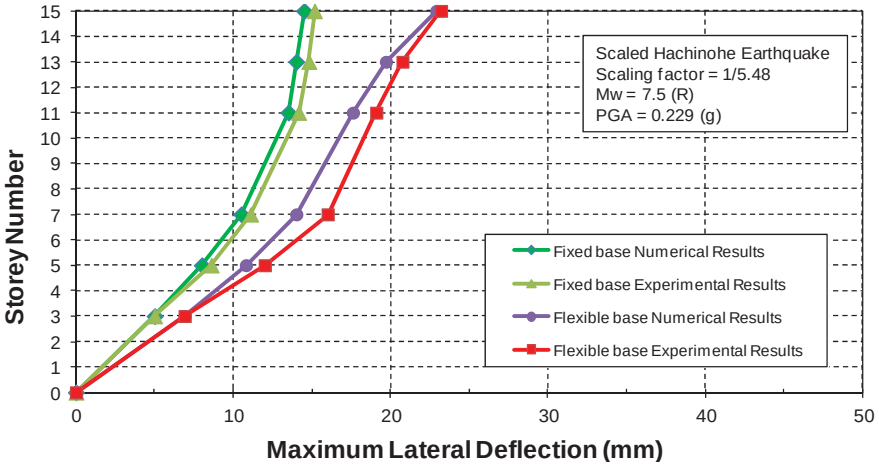

Figure 4.55: Numerical and experimental maximum lateral displacements of fixed base and flexible base models under the influence of scaled Hachinohe (1968) earthquake

Comparing the predicted and observed values of the maximum lateral displacements of fixed base and flexible base models under the influence of the four mentioned scaled earthquake acceleration records (Figures 4.52 to 4.55), the accuracy of the numerical fixed base and flexible base model is examined. Accordingly, it becomes apparent that the trend and the values of the numerical seismic response, predicted by the fixed base numerical model as well as the new developed numerical soil-structure model, are in a good agreement and consistent with the experimental shaking table test results.

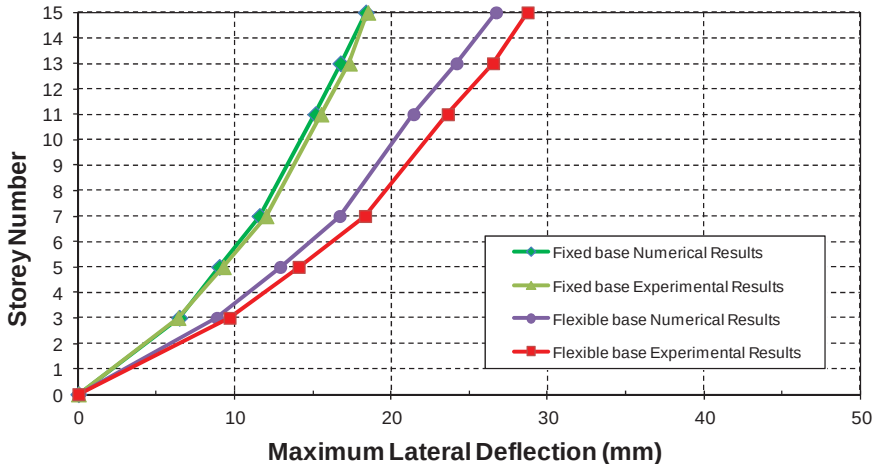

Figure 4.56: Average values of the numerical predictions and experimental values of the maximum lateral displacements of fixed base and flexible base models

Based on the experimental average values of maximum lateral deflections of fixed base and flexible base models (Figure 4.56), lateral deflections of flexible base models have increased by 55% in comparison to fixed base model. According to Kramer (1996), relative lateral structural displacements under the influence of soil-structure interaction consist of rocking component and distortion component. Any change in the displacements is an outcome of changes in these components. In this particular case, considering the maximum foundation rotation values summarised in Table 4.10 and maximum lateral displacements reported in Figure 4.56, it is noted that approximately 55% of the maximum lateral deflections of the flexible base model (Figure 4.56) were due to the rocking component, while 45% took place due to the distortion component. For example, under the influence of Northridge (1994) earthquake, maximum lateral deflection at the top of the fixed base model was measured to be 25.3 mm due to distortion component, while maximum lateral deflection at the top of the flexible base model was 40.6 mm which 22.5 mm of that value was due to rocking component and 18.1 mm took place due to distortion component.

Table 4.10: Numerical and experimental maximum vertical displacements and rotations

	Maximum Vertical Displacement		Maximum Foundation Rotation	
Scaled Earthquake	Numerical Prediction	Experimental Measurement	Numerical Prediction	Experimental Measurement
Kobe	2.33 mm	2.54 mm	0.54º	0.58º
Northridge	1.22 mm	1.32 mm	0.28º	0.30º
El-Centro	1.85 mm	1.98 mm	0.42º	0.45º
Hachinohe	1.40 mm	1.47 mm	0.32º	0.33º

As shown in Figure 4.57, due to amplification of the experimental average values of maximum lateral deflections of fixed base and flexible base models (Figure 4.56), performance level of the structural model may change significantly from life safe to near collapse level. Such a considerable change in the performance level of the model is extremely dangerous and safety threatening. Thus, in the examined experimental investigation, dynamic soil-structure interaction has profound effects on seismic response of the structural model resting on relatively soft soil.

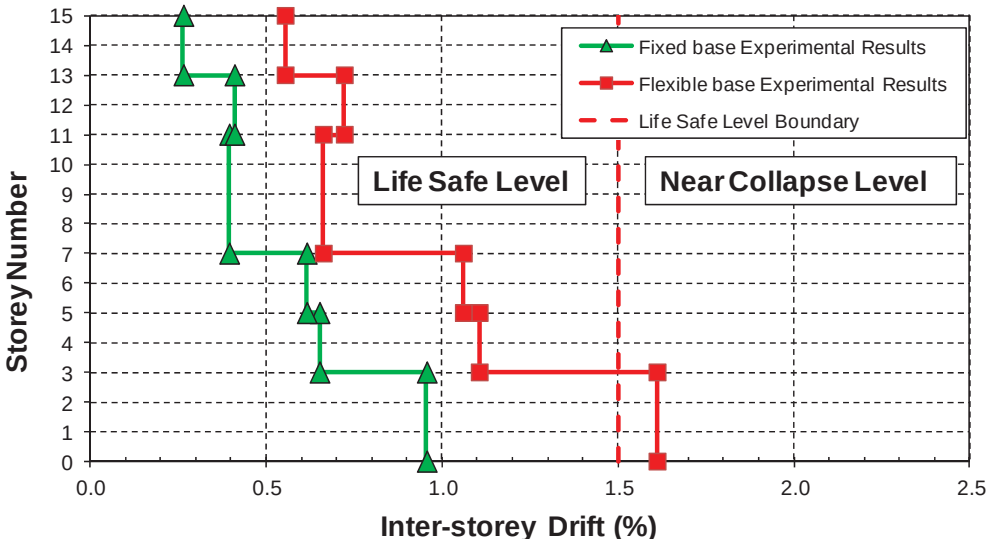

Figure 4.57: Average experimental inter-storey drifts of fixed base and flexible base models

Reviewing the average maximum lateral deflections (Figure 4.56) and maximum vertical displacements and rotations (Table 4.10), it becomes apparent that the numerical predictions and laboratory measurements are in a good agreement (less than 10% difference). Therefore, the numerical soil-structure model can replicate the behaviour of real soil-structure system with acceptable accuracy.

The observed discrepancy between the numerical predictions and laboratory observations could be due to the variation of soil properties such as shear wave velocity and shear modulus with depth occurring during mixing and placement process. In addition, energy absorption at the bolted connection of the base in the physical laboratory model which cannot be captured by rigid base assumption of the numerical model may be another reason for the observed discrepancy.

4.12 Summary

In this Chapter, a prototype soil-structure system including a building frame 45 m high and 12 m wide resting on a clayey soil with shear wave velocity of 200 m/s and unit weight of 14.40 kN/m^3 has been selected and scaled using geometric scaling factor of 1:30. The building frame was modelled with a 15 storey steel structural model, 1.50 m in height and 0.40 m in width while for modelling soil medium, a synthetic clay mixture consisting of kaolinite, bentonite, class F fly ash, lime, and water was adopted after conducting required tests such as bender element tests and Unconfined Compression tests (UC) to determine the shear wave velocity and the shear strength of the soil, respectively. The selected soil model was placed into a laminar soil container, designed and constructed to realistically simulate the free field conditions in shaking table tests. After placing the soil mix into the laminar soil container and elapsing two days of cure age, the 15 storey structural model was lifted up and located on top of the soil surface in the laminar soil container and the set up was instrumented to monitor the structural performance.

Afterwards, shaking table tests were performed on fixed base model (structure directly mounted on the shaking table) and flexible base model (soil-structure model) by applying scaled earthquake acceleration records of Kobe (1995), Northridge (1994), El Centro (1940), and Hachinohe (1968). The results of the carried out shaking table tests under the influence of four scaled earthquake acceleration records in terms of lateral displacements were measured and compared. Based on the experimental average values of maximum lateral deflections of fixed base and flexible base models, lateral deflections of the flexible base model have noticeably increased in comparison to the fixed base model. As a result, performance level of the structural model may change extensively from life safe to near collapse level which is very dangerous and safety threatening. Thus, dynamic

soil-structure interaction plays a significant role in seismic behaviour of examined building frame resting on relatively soft soils.

Then, fixed base and soil-structure numerical models were created in FLAC2D and fully nonlinear time history dynamic analyses under the influence of four mentioned scaled earthquakes were carried out to the numerical models. The predicted results in terms of maximum lateral deflections and maximum vertical displacements were obtained. The predicted results from numerical models were compared with the experimental results of the shaking table tests. Evidently, the numerical predictions and laboratory measurements are in a good agreement. Thus, the numerical soil-structure model can replicate the behaviour of real soil-structure system with acceptable accuracy. It is concluded that the proposed numerical soil-structure model is a valid and qualified method of simulation with sufficient accuracy which can be employed for further numerical dynamic soil-structure interaction investigations.

CHAPTER FIVE

5. NUMERICAL PARAMETRIC STUDY

5.1 Introduction

Performance-based engineering (PBE) is a technique for seismic evaluation and design using performance level prediction for safety and risk assessment. Over the past few years, application of performance-based seismic design concepts has been promoted and developed. The development of this approach has been a natural outgrowth of the evaluation and upgrade process for existing buildings. Performance objectives are expressed as an acceptable level of damage, typically categorised as one of several performance levels. Performance levels describe the state of structures after being subjected to a certain hazard level and are classified as: *fully operational*, *operational*, *life safe*, *near collapse*, or *collapse* (Vision 2000, 1995; FEMA 273, 1997). Overall lateral deflection, ductility demand, and inter-storey drifts are the most commonly used damage parameters. The above mentioned five qualitative performance levels are related to the corresponding quantitative maximum inter-storey drifts of: *0·2%*, *0·5%*, *1·5%*, *2·5%*, and *>2·5%*, respectively.

Practising civil engineers usually use inelastic analysis methods for the seismic evaluation and design of existing and new buildings. The main objective of inelastic seismic analysis is to estimate more precise prediction of the expected behaviour of the structure against probable future earthquakes. Since structural damage implies inelastic behaviour, traditional design and analysis procedures based on elastic method can only predict the performance level implicitly. By contrast, the objective of inelastic method is to estimate the magnitude of inelastic deformations and distortions directly and accurately (ATC-40, 1996). In this research, fully nonlinear time history dynamic analysis is carried out based on elastic and inelastic analysis and design procedures. As a result, the main differences between structural response predictions from two methods for mid-rise moment resisting frames under the influence of soil-structure interaction can be elucidated. In this chapter, a comprehensive parametric study on elastic and inelastic response of regular mid-rise moment resisting building frames under the influence of soil-structure interaction is conduced. To achieve this goal, three types of mid-rise moment resisting building frames, including 5, 10, and 15 storey buildings are selected in conjunction with three soil types

with the shear wave velocities less than 600m/s, representing soil classes C_e, D_e, and E_e according to Australian Standards, having three bedrock depths of 10, 20, and 30 metres.

5.2 Characteristics of Adopted Structure Models

According to Chandler et al. (2010), "Mid-rise buildings are aggregation of dwelling buildings ranging from 5 to 15 stories". With respect to this definition, in order to cover this range, three structural models consisting of 5, 10, and 15 story models, representing conventional types of regular mid-rise reinforced concrete moment resiting building frames have been selected in this study as per specifications summarised in Table 5.1. It can be noted that, the selected span width conforms to architectural norms and construction practices of the conventional buildings in mega cities.

Table 5.1: Dimensional characteristics of the studied frames

Reference Name (Code)	Number of Stories	Number of Bays	Story Height (m)	Bay Width (m)	Total Height (m)	Total Width (m)	Spacing of the frames into the page (m)
S5	5	3	3	4	15	12	4
S10	10	3	3	4	30	12	4
S15	15	3	3	4	45	12	4

For the structural concrete utilised in this analysis and design, specified compressive strength (f_c') and mass density (ρ) are assumed to be 32*MPa* and 2400 kg/m^3, respectively. The modulus of elasticity of concrete (E) was calculated according to clause 3.1.2.a of AS3600:2009 (Australian Standard for Concrete Structures) as follows:

$$E = (\rho)^{1.5} \times (0.043\sqrt{f_c'}) \tag{5.1}$$

where, unit of E is in *MPa*, unit of ρ is in kg/m^3, and unit of f_c' is in *MPa*.

5.3 Nonlinear Time-History Dynamic Analysis

Nonlinear time-history dynamic analysis is carried out in this study in order to determine elastic and inelastic dynamic response of structure models. Time-history analysis is a step-by-step analysis of the dynamic response of a structure to a specified loading that varies with time. The dynamic equilibrium equations to be solved can be presented as:

$$M\ddot{u}(t) + C\dot{u}(t) + Ku(t) = r(t) \tag{5.2}$$

where, M, C, and K are the mass, damping and stiffness matrices, respectively; $u(t)$, $\dot{u}(t)$, and $\ddot{u}(t)$ are the displacements, velocities and accelerations of the structure,

respectively, and *r(t)* is the applied load to the structure. Where the applied load includes ground acceleration, the displacements, velocities, and accelerations are relative to this ground motion. It should be noted that any number of time-history load cases can be defined in this procedure.

In nonlinear time-history analysis, the stiffness, damping, and load all depend upon the displacements, velocities, and time. This requires an iterative solution to the equations of motion. The nonlinear analysis internally solves the equations of motion at each output time step and at each load function time step, just as for linear analysis. In addition, a maximum sub step size smaller than the output time step is specified in order to reduce the amount of nonlinear iteration. In addition, the non-linear properties of the structure are considered as part of a time domain analysis. This approach is the most rigorous, and is required by some building codes for appropriate design (e.g. ATC-40, 1996; BSSC, 2003).

5.3.1 Geometric Nonlinearity and P-Delta Effects in Time-History Analysis

When the load acting on a structure and the resulting deflections are small enough, the load-deflection relationship for the structure is linear. This permits the numerical software form the equilibrium equations using the original (undeformed) geometry of the structure. Strictly speaking, the equilibrium equations should actually refer to the geometry of the deformed structure. When a structure undergoes geometric nonlinearity (in particular, large strains and rotations), the common linear engineering stress and strain measures no longer apply, and the equilibrium equations must be written for the deformed geometry.

As all equilibrium equations are written in the deformed configuration of the structure, this may require a large amount of iteration; Newton-Raphson iterations are usually most effective. Although large displacement and large rotation effects are modelled, all strains are assumed to be small. This means that if the position or orientation of an element changes during the analysis, the effect on the structure in the analysis accounts for P-Delta.

The P-Delta effect refers specifically to the nonlinear geometric effect of a large tensile or compressive direct stress upon transverse bending and shear behaviour. A compressive stress tends to make a structural member more flexible in transverse bending and shear, whereas a tensile stress tends to stiffen the member against

transverse deformation. This option is particularly useful for considering the effects of gravity loads upon the lateral stiffness of building structures. The basic concepts behind the P- Delta effect are illustrated in the following example. Consider a cantilever beam subjected to an axial load P and a transverse tip load F as shown in Figure 5.1.

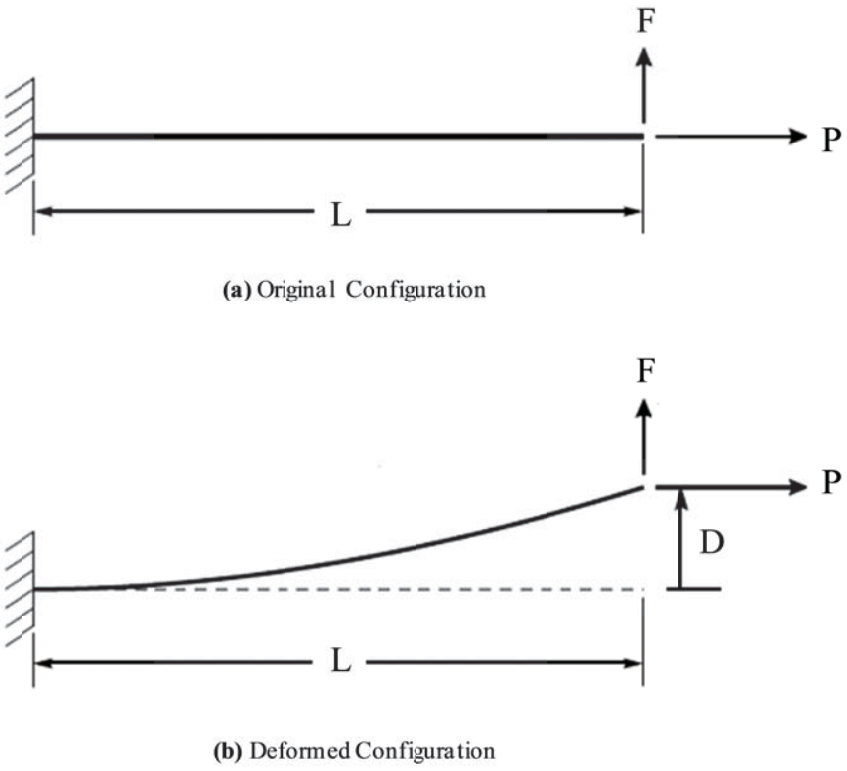

Figure 5.1: Configurations of the cantilever beam; (a) original configuration; (b) deformed configuration

The internal axial force throughout the member is equal to *P* in the original configuration. When equilibrium is examined in the original configuration (using the undeformed geometry), the moment at the base is $M = FL$, and decreases linearly to zero at the loaded end. When, equilibrium is considered in the deformed configuration, there is an additional moment caused by the axial force *P* acting on the transverse tip displacement (*D*). The moment no longer varies linearly along the length and the variation depends on the deflected shape and the moment at the base is now $M = FL - PD$.

Once a nonlinear analysis is performed, the final stiffness matrix can be used for subsequent linear analyses. Any geometric nonlinearity considered in the nonlinear analysis will affect the linear results. In particular, this can be used to include

relatively constant P-Delta effects in buildings or the tension-stiffening effects in cable structures into a series of superposable linear analyses.

FLAC2D software has a specific mode called "*Large Strain mode*" to capture structural geometric nonlinearities in dynamic analysis. Running nonlinear time-history analysis in large-strain mode enables the FLAC2D model to capture structural geometric nonlinearity and P-Delta effects accurately by updating the structural matrix. Thus, in order to take the mentioned effects into account, all the structural dynamic analyses in this study have been performed in large-strain mode.

5.3.2 Utilised Ground Motions in Time History Analyses

In order to perform a comprehensive investigation on seismic response of structure models, two near field earthquake acceleration records including Kobe, 1995 (Figure 5.2) and Northridge, 1994 (Figure 5.3) and two far field earthquake acceleration records comprising El-Centro, 1940 (Figure 5.4) and Hachinohe, 1968 (Figure 5.5) are selected and utilised in time-history analysis. These earthquakes have been chosen by the International Association for Structural Control and Monitoring for benchmark seismic studies (Karamodin and Kazemi, 2008).

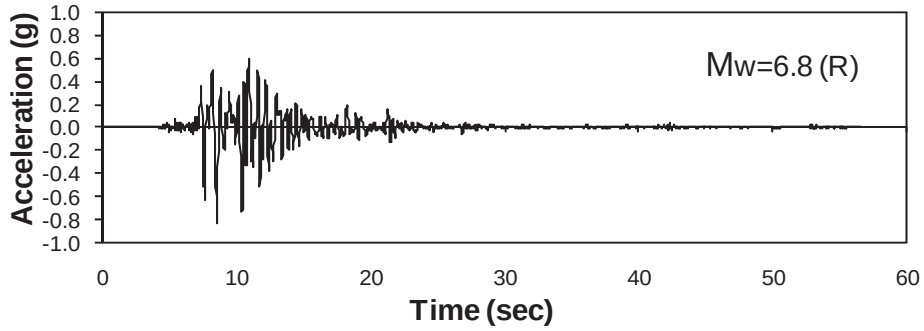

Figure 5.2: Near field acceleration record of Kobe earthquake (1995)

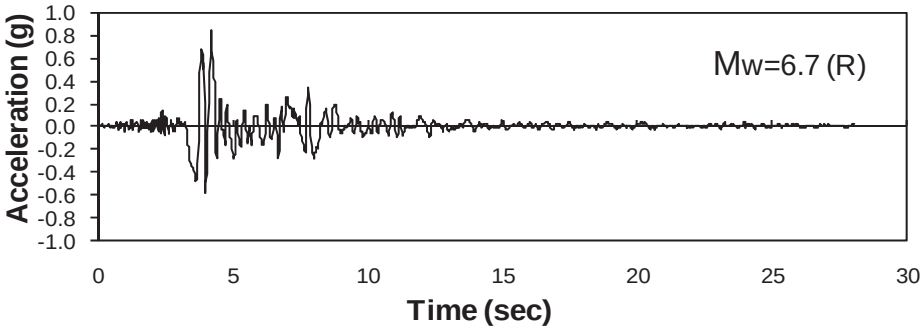

Figure 5.3: Near field acceleration record of Northridge earthquake (1994)

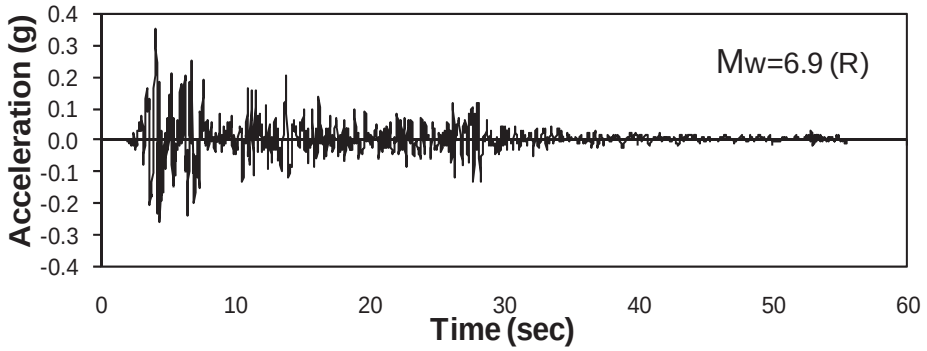

Figure 5.4: Far field acceleration record of El-Centro earthquake (1940)

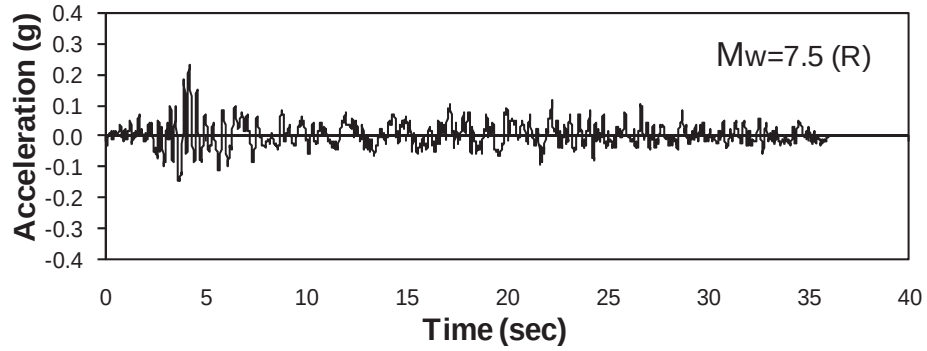

Figure 5.5: Far field acceleration record of Hachinohe earthquake (1968)

The characteristics of the earthquake ground motions are summarised in Table 5.2.

Table 5.2: Utilised Earthquake ground motions

Earthquake	Country	Year	PGA (g)	Mw (R)	T (S) Duration	Type	Hypocentral Distance (km)	Reference
Northridge	USA	1994	0.843	6.7	30.0	Near field	9.2	PEER (2012)
Kobe	Japan	1995	0.833	6.8	56.0	Near field	7.4	PEER (2012)
El Centro	USA	1940	0.349	6.9	56.5	Far field	15.69	PEER (2012)
Hachinohe	Japan	1968	0.229	7.5	36.0	Far field	14.1	PEER (2012)

5.4 Geotechnical Characteristics of employed Subsoils

When shear wave velocity of the supporting soil is less than 600 m/s, effects of dynamic soil-structure interaction on seismic response of structural systems, particularly for moment resisting building frames, are significant (e.g. Veletsos and Meek 1974; Galal and Naimi 2008). Thus, in this research, three soil types with the shear wave velocity less that 600m/s comprising one cohesionless and two cohesive soils, representing classes C_e, D_e and E_e, according to AS 1170.4 have been utilised. Characteristics of the utilised soils are shown in Table 5.3. The subsoil properties have been extracted from

actual in-situ and laboratory tests (Rahvar 2005, 2006a, 2006b). Therefore, these parameters have merit over the assumed parameters which may not be completely conforming to reality. It is assumed that water table is below the bedrock level.

Table 5.3: Geotechnical characteristics of the adopted soils in this study

Soil Type (AS1170)	Shear wave velocity Vs (m/s)	Unified classification (USCS)	Maximum shear modulus G_{max} (kPa)	Poisson's Ratio	Soil density ρ (kg/m^3)	c' (kPa)	ϕ' (degree)	Plastic Index (PI)	Reference
C_e	600	GM	623,409	0.28	1730	5	40	-	Rahvar (2005)
D_e	320	CL	177,304	0.39	1730	20	19	20	Rahvar (2006a)
E_e	150	CL	33,100	0.40	1470	20	12	15	Rahvar (2006b)

5.5 Utilised Soil and Interface Parameters in FLAC Soil-Structure Model

The shear wave velocity values, shown in Table 5.3, have been obtained from down-hole test, which is a low strain in-situ test. This test generates a cyclic shear strain of about 10^{-4} percent where the resulting shear modulus is called G_{max}. In the event of an earthquake, the cyclic shear strain amplitude increases and the shear strain modulus and damping ratio which both vary with the cyclic shear strain amplitude, change relatively. Damping and tangent module are selected to be appropriate to the level of excitation at each point in time and space which is called hysteretic damping algorithm.

As mentioned earlier, fully nonlinear method adopts hysteretic damping algorithm which captures the hysteresis curves and energy-absorbing characteristics of the real soil. Small strain shear modulus and damping degradation of the soil with strain level can be considered in the modelling precisely. In the soil-structure model, the built-in tangent modulus function presented by Hardin and Drnevich (1972), known as Hardin model is employed as the model provides reliable fits to backbone curves represented by Seed et al. (1986) for sand and Sun et al. (1998) for clay in order to implement hysteretic damping to the model (Figures 5.6 and 5.7). Adopted model in FLAC2D generates backbone curves represented by Seed et al. (1986) for sand and Sun et al. (1998) for clay, adopting γ_{ref} = 0.06 (Figure 5.6) and γ_{ref} = 0.234 (Figure 5.7) for sand and clay as numerical fitting parameters, respectively. Further details of the method to simulate the backbone curves have been explained in Section 3.8.2 (Chapter 3).

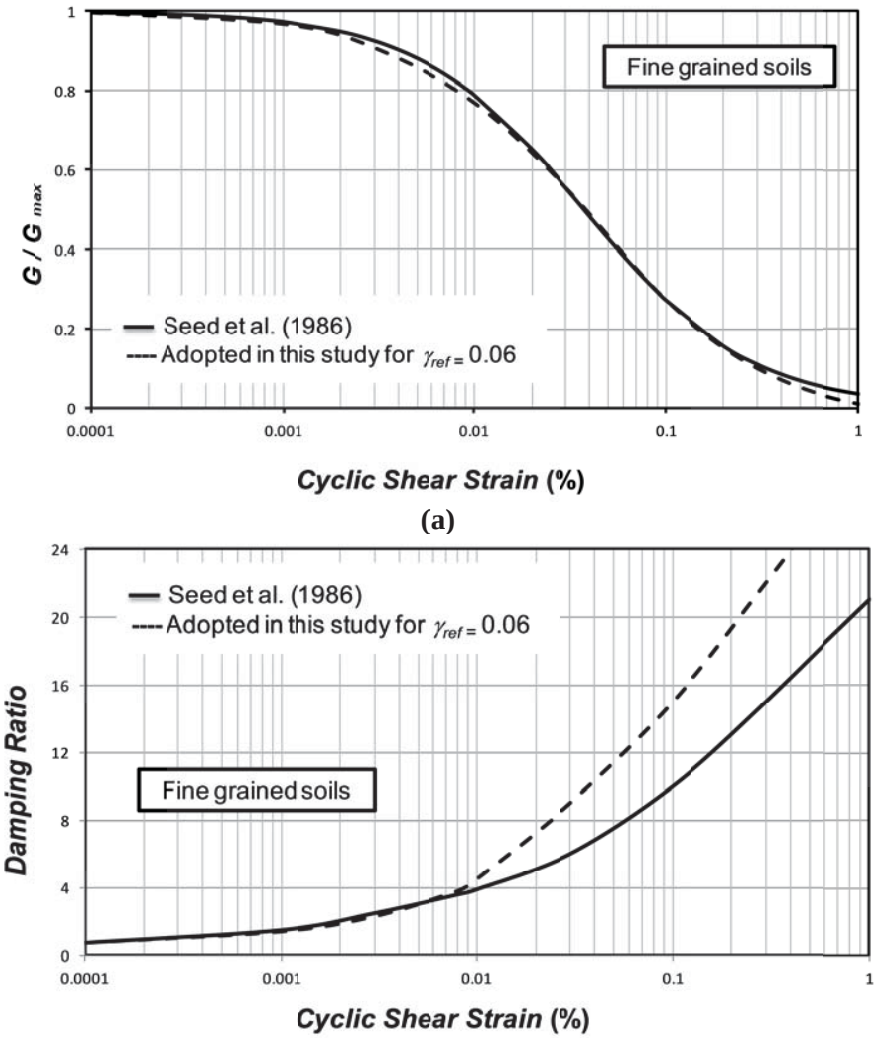

Figure 5.6: Adopted fitting curves for clay in this study; (a) Relations between G/G_{max} versus shear strain; (b) Relations between material damping ratio versus shear strain

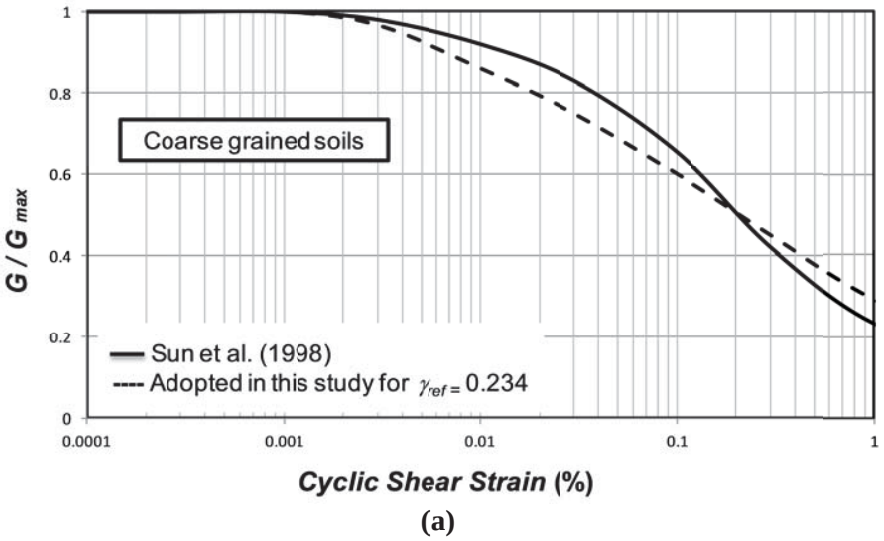

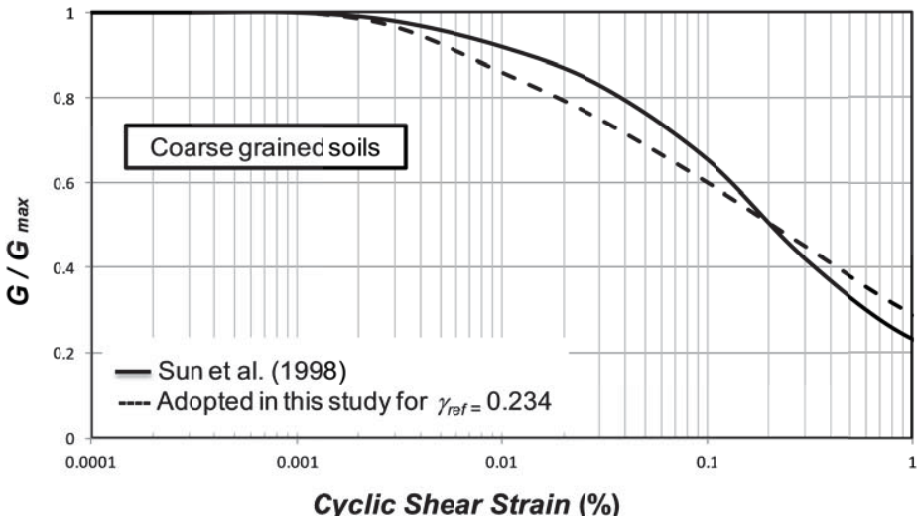

(b)

Figure 5.7: Adopted fitting curves for sand in this study; (a) Relations between G/G_{max} versus cyclic shear strain; (b) Relations between material damping ratio versus cyclic shear strain

In order to model the interface elements, the normal and shear spring stiffness values for the three mentioned soil types have been determined according to Equation (3.12) in Section 3.6. In this way, the load transfer between the concrete foundation and the soil is simulated. Details of the interface modelling have been described in Section 3.6 (Chapter 3). Utilised normal (k_n) and shear (k_s) spring stiffness values are shown in Table 5.4.

Table 5.4: Utilised soil interface parameters

Soil Type (AS1170)	k_n *(kPa/m)*	k_s *(kPa/m)*
C_e	2.0E7	2.0E7
D_e	9.8E6	9.8E6
E_e	2.0E6	2.0E6

5.6 Structural Section Design of the Models Using SAP2000

In this study, structural sections of the models are designed based on both conventional elastic method, and inelastic method assuming elastic-perfectly plastic behaviour for the structural members. For this purpose, structural members of 5, 10, and 15 storey models (Table 5.1) are simulated, analysed, and designed using SAP2000 V14 software.

SAP2000 V14, the latest and most powerful version of the well- known SAP series of structural analysis programs, is a finite element program which performs static,

dynamic, linear, nonlinear, elastic, and inelastic analyses of structural systems. Advanced analytical techniques allow for step-by-step large deformation analysis, dynamic seismic analysis, Eigen and Ritz analyses based on stiffness of nonlinear cases, material nonlinear analysis, multi-layered nonlinear shell element, buckling analysis, progressive collapse analysis, energy methods for drift control, velocity-dependent dampers, base isolators, support plasticity and nonlinear segmental construction analysis. Nonlinear analyses can be static or time history, with options for direct integration nonlinear time history dynamic analysis. Furthermore, SAP2000 features powerful and completely integrated modules for design of both steel and reinforced concrete structures following most major design codes (e.g. ACI 318 and AS3600). The program provides the user with options to create, modify, analyse and design structural models, all from within the same user interface. In addition, the program is capable of performing initial member sizing and design optimisation. In this progress, the checks are made for each user specified (or program defaulted) load combination and at several user controlled stations along the length of the element. Maximum demand/capacity ratios are then reported and used for design optimisation. These features make SAP2000 the state of the art in structural analysis program (Computers and Structures, Inc., 2009). The following general steps are required to analyse and design a structure using SAP2000:

i. Create or modify a model that numerically defines the geometry, properties, and loading;
ii. Perform an analysis of the model;
iii. Review the results of the analysis;
iv. Perform, check, and optimise the design of the structure.

This is usually an iterative process that may involve several cycles of the above sequence of steps.

5.6.1 Elastic Structural Design of the Models

SAP2000 provides options to design different types of moment resisting frames as required for regular and seismic designs. For regular design, the frame should be identified as Ordinary. For Seismic design, the frame has to be identified as either Intermediate (moderately ductile) or Special (fully ductile) moment resisting frame.

For elastic structural design of the building models, the structural type of three models consisting of 5, 10, and 15 storey frames assumed to be intermediate moment-resiting

frames (moderately ductile) with the following factors for the elastic analysis according to AS 1170.4 (Earthquake action in Australia):

Structural Ductility Factor (μ) = 3.0

Performance Factor (S_p) = 0.67

The structural models are simulated in SAP2000 to reflect the geometries and properties of models S5 (5 storey), S10 (10 storey), and S15 (15 storey) as described in Section 5.2. Then gravity loads including permanent (dead) and imposed (live) actions are determined and applied to the structural models, in accordance with AS/NZS1170.1-2002 (Permanent, imposed and other actions). The values of permanent action (dead load) and imposed action (live load) are determined as uniform distributed loads over the floors according to AS/NZS1170.1-2002, considering the spacing of the frames being 4 metres as reported below:

Permanent Action (G) = 6 kPa

Imposed Action (Q) = 2 kPa

Then, nonlinear time-history dynamic analyses under the influence of four earthquake ground motions shown in Figures 5.2 to 5.5 and Table 5.2 are performed on S5, S10, and S15 models. In the dynamic analyses, geometric nonlinearity and P-Delta effects are considered according to AS3600-2009. In addition, cracked sections for the reinforced concrete sections are taken into consideration by multiplying cracked section coefficients by stiffness values of the structural members (*EI*) according to ACI318-2002. Based on this standard, cracked section coefficients are 0.35 and 0.7 for beams and columns, respectively.

After finalising the dynamic analyses, concrete sections of three models (S5, S10, and S15) were designed according to AS3600-2009 (Australian Standard for Concrete Structures). The following design load combinations are considered for concrete design of the structural members subjected to Permanent (G), Imposed (Q), and Earthquake (E_u) actions according to AS/NZS1170.0-2002 (Australian Standard for structural design actions):

- Load Combination 1= 1.35G
- Load Combination 2= 1.2 G+1.5Q
- Load Combination 3=G+0.4Q±Eu

In the concrete design procedure, capacity of each structural member against the maximum factored axial force and bending moments obtained from each load combination results in capacity ratio giving an indication of the stress condition of a structural member with respect to the capacity of the member. In this design, capacity ratio of the structural members has been in the range of 0.85 to 0.95 (all less than 1.0). In addition, shear capacity of the designed members are checked according to Section 8.2 of AS3600-2009 (Australian Standard for Concrete Structures).

After strength design of the structural sections, inter-storey drifts of the models are checked in a way that performance levels of the designed models stay in *life safe* level by limiting the maximum inter-storey drifts to 1.5% of the storey height for each level. Inter-storey drifts for each two adjacent stories can be determined according to AS 1170.4 as follows:

$$drift = [(d_{(i+1)e} - d_{ie}) \times (\mu / S_p)] / h \tag{5.3}$$

where, $d_{(i+1)e}$ is deflection at the *i+1* level determined by elastic analysis, d_{ie} is deflection at the *i* level determined by elastic analysis, μ is Structural Ductility Factor, S_p is Performance Factor, and *h* is the storey height.

Considering 3 metres storey height, and adopted values for μ and S_p, the following form of Equation (5.3) is utilised as a criterion to keep performance levels of the designed structure models in life safe level:

$$drift = [(d_{(i+1)e} - d_{ie}) \times (3/0.67)] / 3000 \leq 1.5\% \tag{5.4}$$

where, $d_{(i+1)e}$ and d_{ie} are measured in mm. Therefore, the final form of the equation could be written as follows:

$$(d_{(i+1)e} - d_{ie}) \leq 10\,mm \tag{5.5}$$

Eventually, concrete section design for models S5, S10, and S15 is finalised in a way that the maximum elastic inter-storey drifts in all the models are less than 10 mm. In the final selection of the beam and column sections, constructability and norms have been considered. Figure 5.8 summarises the concrete sections designed for the adopted frames based on elastic structural design method.

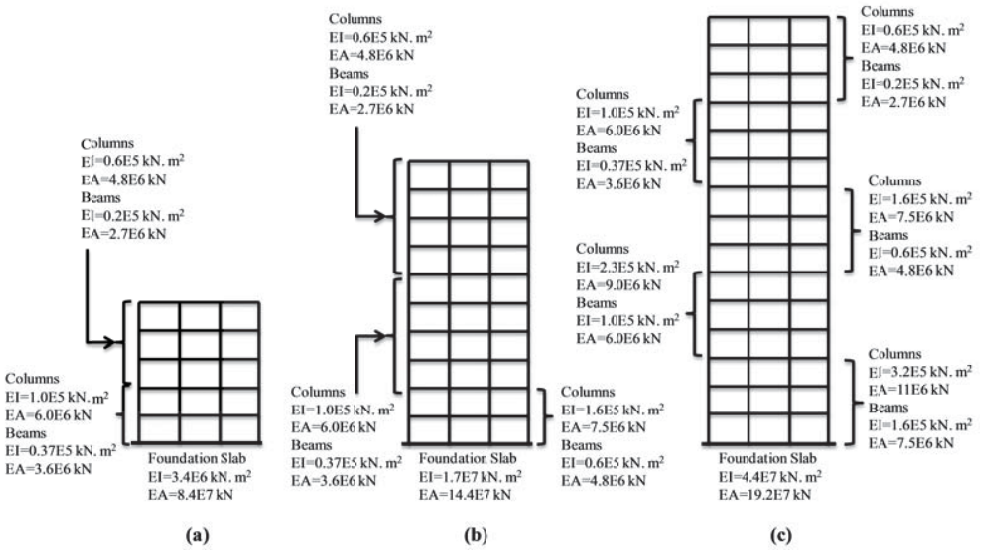

Figure 5.8: Concrete sections designed for the adopted frames based on elastic design method; (a) 5 storey model (S5); (b) 10 storey model (S10); (c) 15 storey model (S15)

5.6.2 Inelastic Structural Design of the Models

Inelastic seismic analysis and design method is employed in this study to directly estimate the performance level of the structural systems. This method is rapid and provides a rational approach for the analysis of the structure. Furthermore, it provides a cost effective design since the sections required by this method are generally smaller in size than those required by elastic method. The plastic moment can be introduced to determine the plastic behaviour of the column and beam elements.

The generic process of inelastic analysis is similar to conventional elastic procedure described in Section 5.6.1. The primary difference is that the properties of the components of the model include plastic moment in addition to the initial elastic properties. These are normally based on approximations derived from test results on individual components or theoretical analyses (ATC-40, 1996).

In this study, inelastic bending is simulated in structural elements by specifying a limiting plastic moment. When the plastic moment is specified, the value may be calculated by considering a flexural structural member of width b and height h with yield stress σ_y. If the member is composed of a material that behaves in an elastic-perfectly plastic manner (Figure 5.8), the plastic resisting moments (M^P) for rectangular sections can be computed as follows:

$$M^p = \sigma_y \left(\frac{bh^2}{4}\right) \tag{5.6}$$

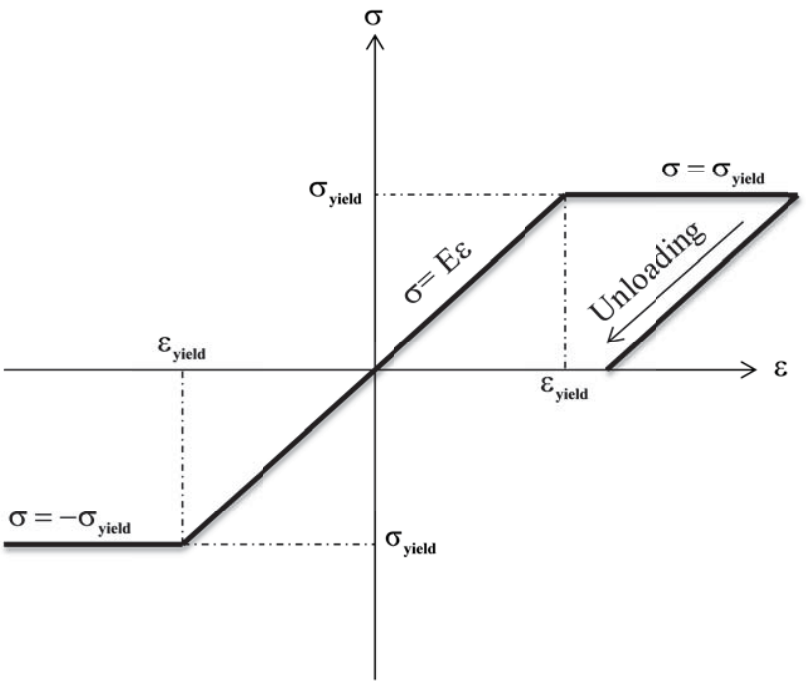

Figure 5.9: Elastic-perfectly plastic behaviour of structural elements

Present formulations adopted in this study for inelastic analysis and design assume that structural elements behave elastically until reaching the defined plastic moment. The section at which the plastic moment (M^P) is reached can continue to deform, without inducing additional resistance.

For inelastic structural design of the building models, in addition to the design procedure described in Section 5.6.1, plastic resisting moments, (M^P), for each concrete section of models S5 (5 storey), S10 (10 storey), and S15 (15 storey) have been determined according to Equation (5.6) and assigned to the sections considering the yield stress of concrete material (σ_y) equal to the compressive strength of concrete (f_c') according to Shing and Tanabe (2001).

Structural members are designed in accordance with AS3600-2009 (Australian Standard for Concrete Structures) in a way that performance levels of the designed models stay in *life safe* level by limiting the maximum inelastic inter-storey drifts to 1.5%. In order to determine inelastic inter-storey drifts for each two adjacent stories, maximum lateral deflections of each storey is derived from SAP2000 deflection history records. Using the maximum storey deflections, inelastic inter-storey drifts have been determined using the following equation based on AS 1170.4:

$$drift = (d_{i+1} - d_i)/h \tag{5.7}$$

where, d_{i+1} is deflection at *(i+1)* level, d_i is deflection at *(i)* level, and h is the storey height. In practical designs, it is often assumed that the storey deflection is equal to the horizontal displacement of the nodes on the level which may be due to translation, rotation, and distortion.

Considering 3 metres storey height and 1.5% maximum inter-storey drift, following form of Equation (5.7) is employed as a criterion to keep performance levels of the designed structure models in the life safe level:

$$drift = [(d_{i+1} - d_i)/3000 \leq 1.5\% \tag{5.8}$$

where, d_{i+1} and d_i measure in mm. Therefore, the final form of the equation could be written as follows:

$$(d_{i+1} - d_i) \leq 45\,mm \tag{5.9}$$

Finally, inelastic concrete section design for models S5, S10, and S15 is finalised in a way that maximum inelastic inter-storey drifts in all the models are less than 45 mm. In the final selection of the beam and column sections, constructability and norms have been considered. Figure 5.10 summarises the concrete sections designed for the adopted frames based on elastic structural design method.

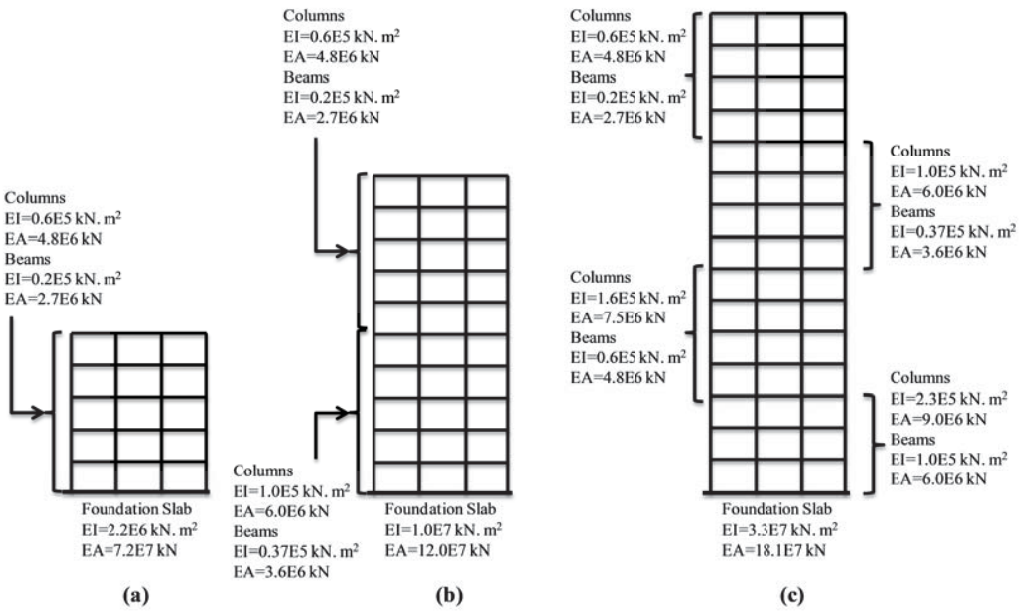

Figure 5.10: Concrete sections designed for the adopted frames based on inelastic design method; (a) 5 storey model (S5); (b) 10 storey model (S10); (c) 15 storey model (S15)

5.7 Determining Seismic Response of the Models Considering Dynamic Soil-Structure Interaction

In this study, fully nonlinear time history dynamic analysis method is adopted to simulate dynamic soil-structure interaction using FLAC2D (Version 6.0) in order to determine elastic and inelastic seismic response of the studied concrete moment resisting building frames subjected to earthquake loading. Dynamic analyses are carried out for structural models S5 (5 storey), S10 (10 storey), and S15 (15 storey) with structural characteristics described in Sections 5.2 and 5.6 in conjunction with three soil types representing soil classes C_e, D_e and E_e with geotechnical properties presented in Sections 5.4 and 5.5 for two different systems: (i) fixed base structure on the rigid ground (Figure 5.11a), and (ii) flexible base structure considering subsoil using direct method of soil-structure interaction analysis (Figure 5.11b) using new developed soil-structure model discussed in Chapter 3. Dynamic analyses for fixed base and flexible base cases have been performed based on both conventional elastic analysis procedure, described in Section 5.6.1, and inelastic analysis method, discussed in Section 5.6.2, assuming elastic-perfectly plastic behaviour for the structural members.

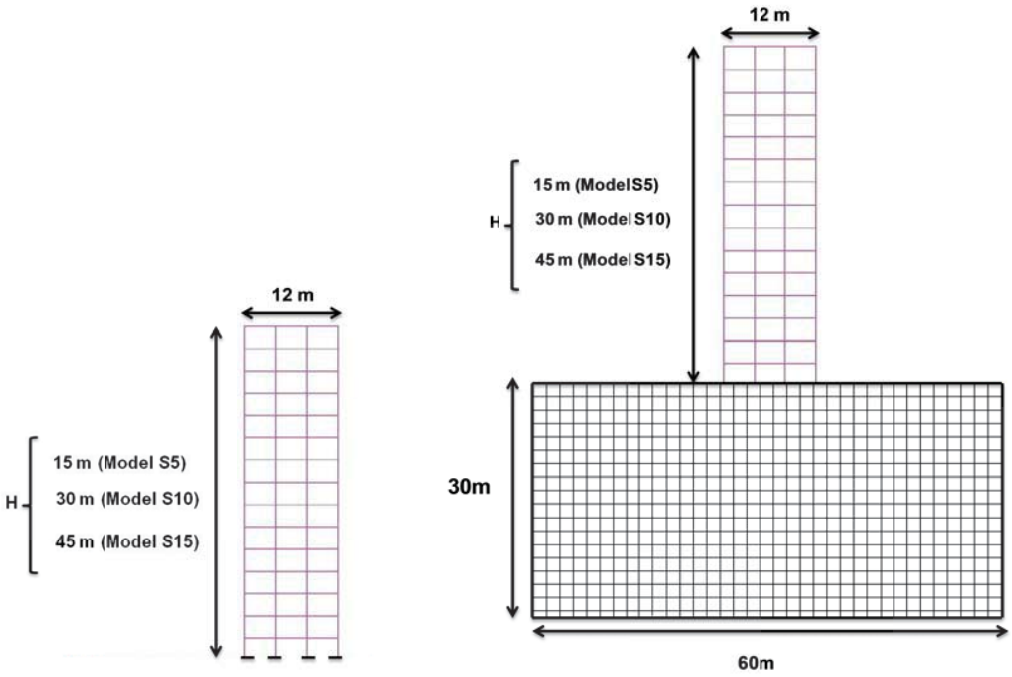

Figure 5.11: Numerical Models; (a) fixed base model; (b) flexible base model

As a summary, the following aspects have been incorporated in the elastic and inelastic dynamic time-history analyses in this study:

- Nonlinear behaviour of the subsoil is considered adopting Hardin model to implement backbone curves represented by Seed et al. (1986) for coarse grained soils and Sun et al. (1998) for fine grained soils in the fully nonlinear dynamic analyses (Section 5.4)
- Geometric nonlinearity of the structures capturing P-Delta effects is accommodated by specifying large-strain solution mode in FLAC software.
- Cracked sections for the reinforced concrete sections are taken into account by multiplying moment of inertial of the uncracked sections (I_g) by cracked section coefficients ($0.35I_g$ for beams and $0.70I_g$ for columns) according to Section 10.11.1 of ACI318.2002.

Presented earthquake ground motions in Table 5.2 including Kobe, 1995 (Figure 5.2) and Northridge, 1994 (Figure 5.3) El-Centro, 1940 (Figure 5.4) and Hachinohe, 1968 (Figure 5.5) were applied to both systems. In the case of modelling soil and structure simultaneously using direct method (flexible base model), the earthquake records are applied to the combination of soil and structure directly at the bedrock level, while for modelling the structure as the fixed base (without soil), the earthquake records are applied to the fixed base of the structural models.

As discussed in Section 3.7.3, in this study, the horizontal distance of the soil lateral boundaries is assumed to be 60 metres (five times the width of the structure which is 12 metres) and the maximum bedrock depth is 30 metres. In order to observe the effects of bedrock depth variations on seismic response of the studied structural models, the above mentioned procedure is carried out for structural models resting on soil classes C_e, D_e and E_e with bedrock depths of 10 m, 20 m, and 30 m.

5.8 Results and Discussions

The results of elastic and inelastic analyses in terms of base shears, lateral deflections, and inter-storey drifts under the influence of four earthquake ground motions including Kobe, 1995 (Figure 5.2) and Northridge, 1994 (Figure 5.3) El-Centro, 1940 (Figure 5.4) and Hachinohe, 1968 (Figure 5.5) are derived from FLAC2D history records for fixed base and flexible base models resting on three different soil types, having three bedrock depths of 10 m, 20 m, and 30 m. The mentioned results are presented in Appendix A.

In order to have a comprehensive comparison between the results and illustrate a clear conclusion about the effects of structural height variations, subsoil stiffness, and bedrock depth variations on elastic and inelastic seismic response of moment resisting frames under the influence of dynamic soil-structure interaction, average values of the elastic and inelastic base shears, maximum lateral deflections, and inter-storey drifts under the influence of four mentioned earthquake records (Table 5.2) are determined and compared.

To ease the discussion of the obtained results, in this study, the structures which are analysed and designed based on elastic procedure are named “elastic analysis case”. The term of “inelastic analysis case” is used to refer to the structures analysed and designed according to inelastic method.

Average base shear ratios of flexible base models ($\tilde{V}$) to fixed base models (V) for elastic and inelastic analysis cases under the applied earthquakes are summarised in Tables 5.5 and 5.6 and average values of maximum elastic and inelastic lateral deflection ratios of flexible base models to fixed base models ($\tilde{\delta}/\delta$) at the top of the structure models under the applied earthquakes are tabulated in Tables 5.7 and 5.8, respectively. Elastic inter-storey drifts (Figures 5.16 to 5.19) are determined from the corresponding average values of elastic storey deflections (Figures 5.12 to 5.15) for each two adjacent stories using Equation (5.3) while inelastic inter-storey drifts (Figures 5.24 to 5.27) are calculated from the corresponding average values of inelastic storey deflections (Figures 5.20 to 5.23) for each two adjacent stories based on Equation (5.7).

Table 5.5: Elastic base shear ratios of flexible base to fixed base models ($\tilde{V}$ /V)

Soil Classification	Soil Class C_e			Soil Class D_e			Soil Class E_e		
Bedrock Depth	H=30 (m)	H=20 (m)	H=10 (m)	H=30 (m)	H=20 (m)	H=10 (m)	H=30 (m)	H=20 (m)	H=10 (m)
Model S5	0.94	0.98	1.00	0.76	0.93	0.99	0.55	0.77	0.98
Model S10	0.92	0.93	1.00	0.62	0.83	0.99	0.43	0.61	0.95
Model S15	0.92	0.95	0.99	0.58	0.72	0.98	0.33	0.53	0.83

Note : $\tilde{V}$ = base shear of flexible base model; V = base shear of fixed base model

Table 5.6: Inelastic base shear ratios of flexible base to fixed base models ($\tilde{V}$ /V)

Soil Classification	Soil Class C_e			Soil Class D_e			Soil Class E_e		
Bedrock Depth	H=30 (m)	H=20 (m)	H=10 (m)	H=30 (m)	H=20 (m)	H=10 (m)	H=30 (m)	H=20 (m)	H=10 (m)
Model S5	0.98	1.00	1.00	0.79	0.95	1.0	0.62	0.84	0.99
Model S10	0.95	1.00	1.00	0.76	0.88	1.0	0.52	0.68	0.97
Model S15	0.95	0.99	1.00	0.71	0.80	0.94	0.42	0.56	0.88

Note : $\tilde{V}$ = base shear of flexible base model; V = base shear of fixed base model

Table 5.7: Maximum elastic lateral deflection ratios of flexible base models to fixed base models ($\tilde{\delta}/\delta$)

Soil Classification	Soil Class C_e			Soil Class D_e			Soil Class E_e		
Bedrock Depth	H=30 (m)	H=20 (m)	H=10 (m)	H=30 (m)	H=20 (m)	H=10 (m)	H=30 (m)	H=20 (m)	H=10 (m)
Model S5	1.01	1.01	1.00	1.03	1.01	1.01	1.11	1.07	1.04
Model S10	1.03	1.02	1.01	1.10	1.06	1.03	1.40	1.27	1.14
Model S15	1.07	1.04	1.02	1.19	1.13	1.07	1.89	1.60	1.30

Note : $\tilde{\delta}$ = maximum lateral deflection of flexible base model; δ = maximum lateral deflection of fixed base model

Table 5.8: Maximum inelastic lateral deflection ratios of flexible base models to fixed base models ($\tilde{\delta}/\delta$)

Soil Classification	Soil Class C_e			Soil Class D_e			Soil Class E_e		
Bedrock Depth	H=30 (m)	H=20 (m)	H=10 (m)	H=30 (m)	H=20 (m)	H=10 (m)	H=30 (m)	H=20 (m)	H=10 (m)
Model S5	1.00	1.00	1.00	1.02	1.00	1.00	1.07	1.05	1.02
Model S10	1.02	1.01	1.00	1.07	1.05	1.03	1.31	1.21	1.11
Model S15	1.04	1.03	1.01	1.15	1.10	1.05	1.67	1.45	1.23

Note : $\tilde{\delta}$ = maximum lateral deflection of flexible base model; δ = maximum lateral deflection of fixed base model

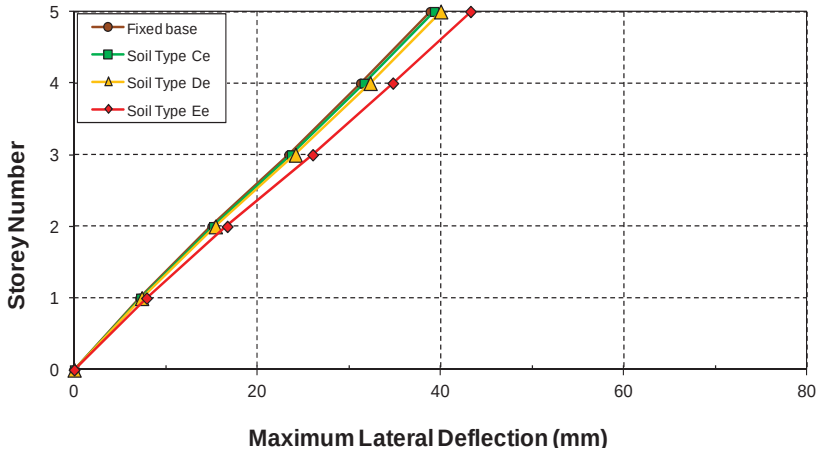

(a)

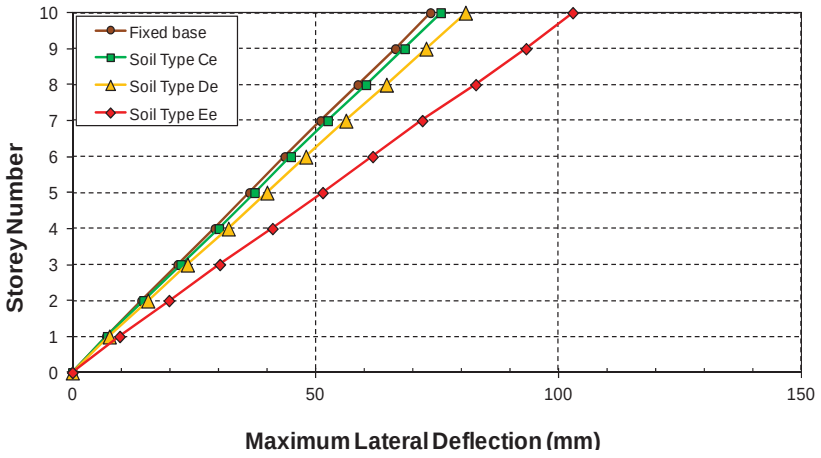

(b)

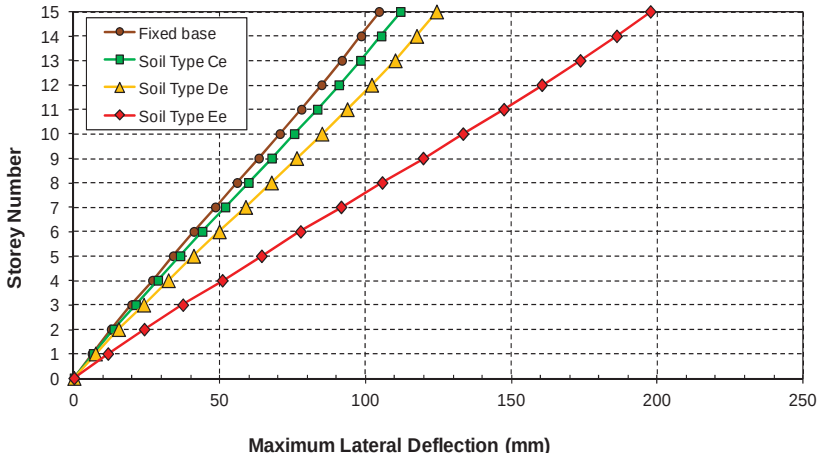

(c)

Figure 5.12: Elastic storey deflections of the adopted structural models resting on soil classes C_e, D_e, and E_e with bedrock depth of 30 metres; (a) model S5; (b) model S10; (c) model S15

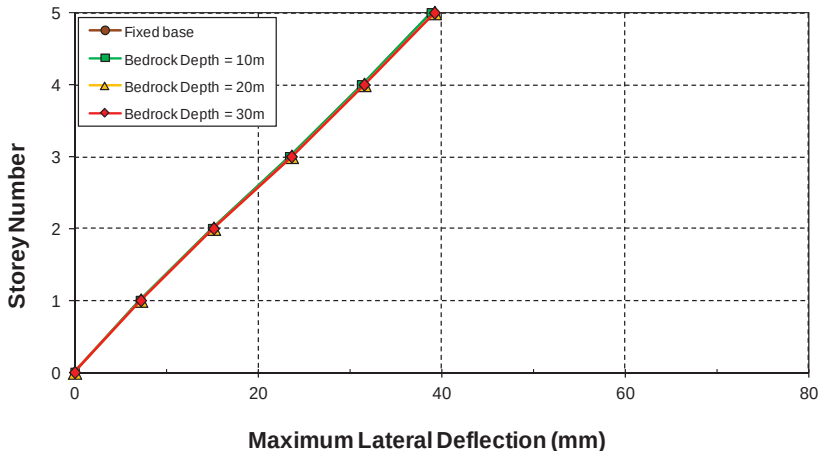

(a)

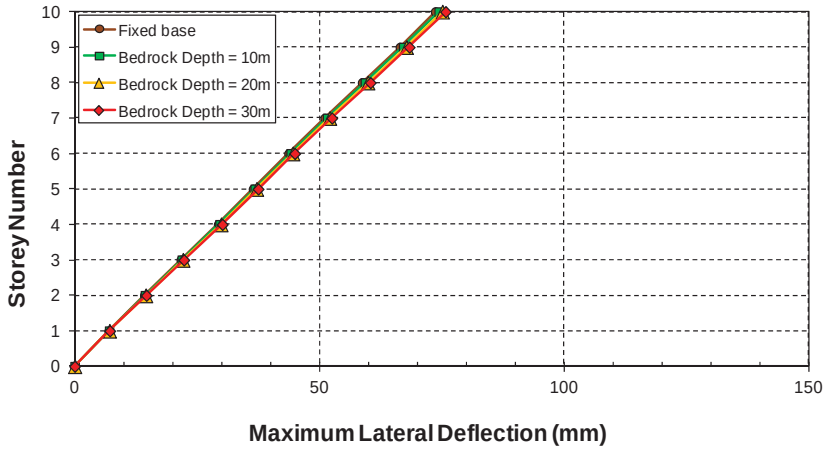

(b)

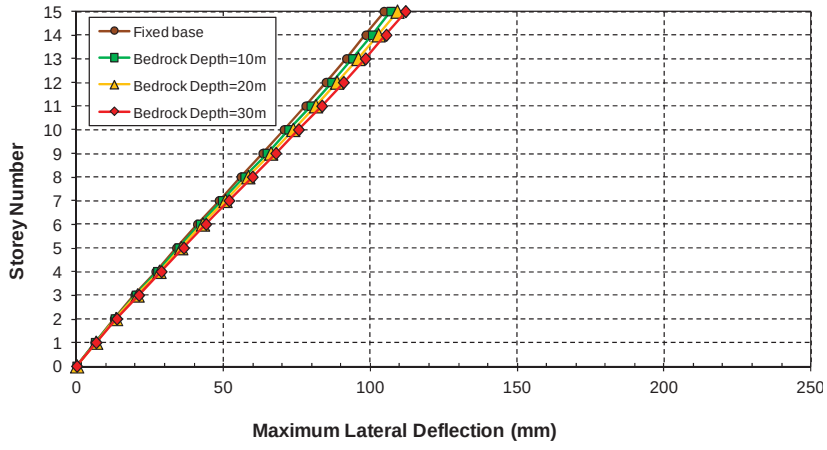

(c)

Figure 5.13: Elastic storey deflections of the adopted structural models resting on soil class C_e with variable bedrock depths; (a) model S5; (b) model S10; (c) model S15

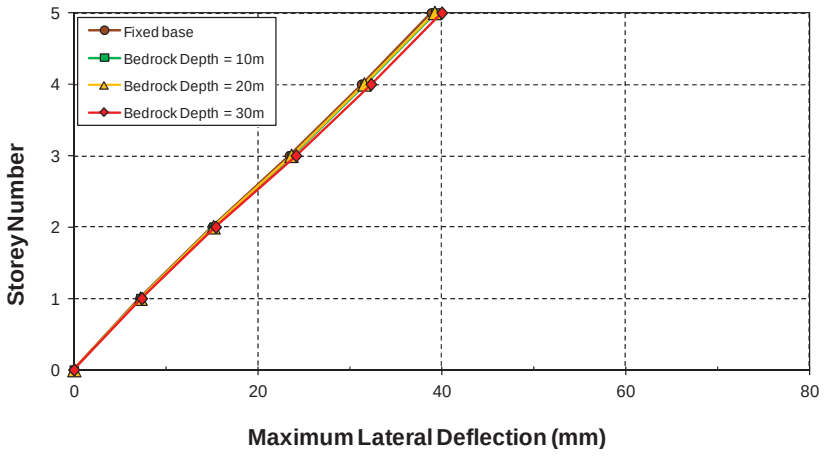

(a)

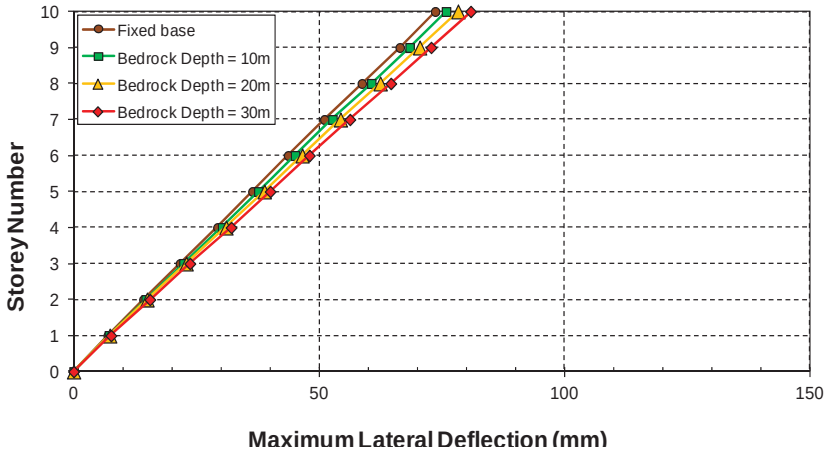

(b)

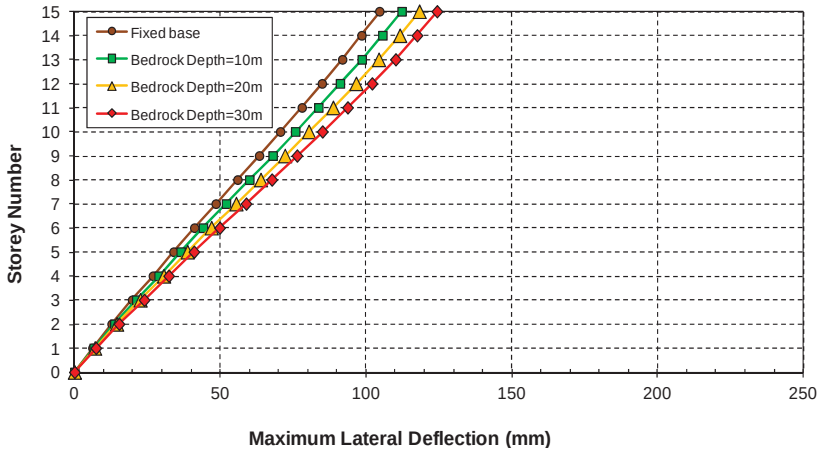

(c)

Figure 5.14: Elastic storey deflections of the adopted structural models resting on soil class D_e with variable bedrock depths; (a) model S5; (b) model S10; (c) model S15

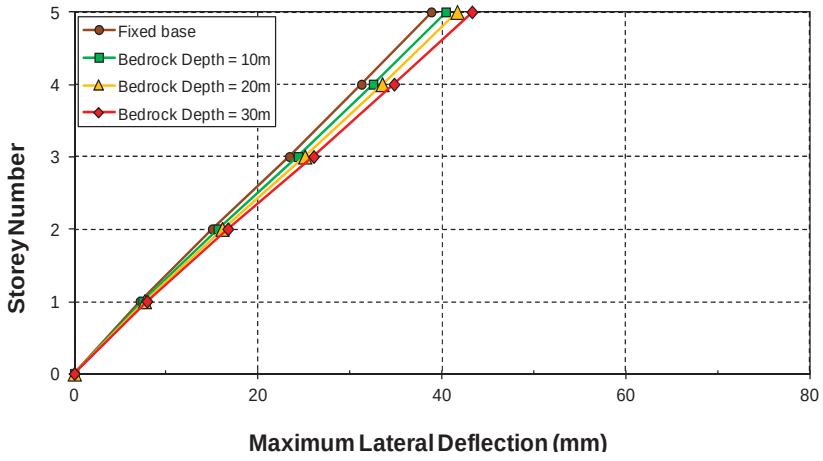

(a)

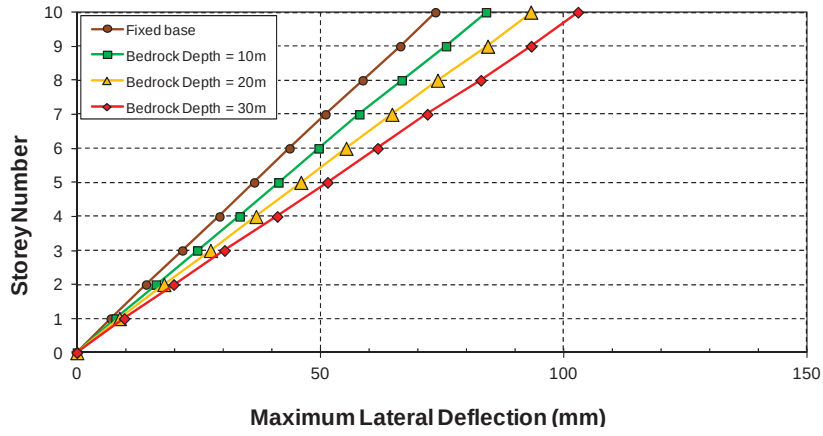

(b)

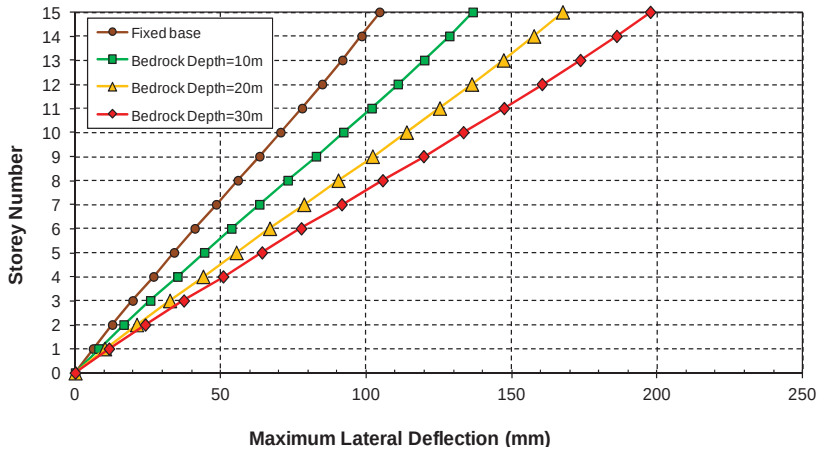

(c)

Figure 5.15: Elastic storey deflections of the adopted structural models resting on soil class E_e with variable bedrock depths; (a) model S5; (b) model S10; (c) model S15

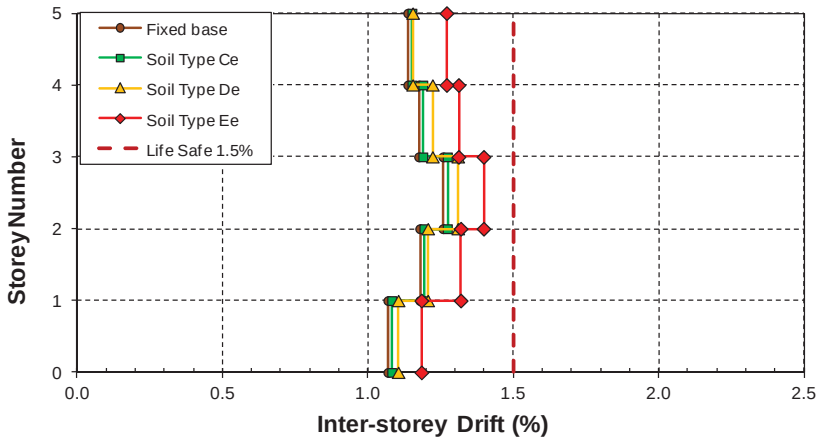

(a)

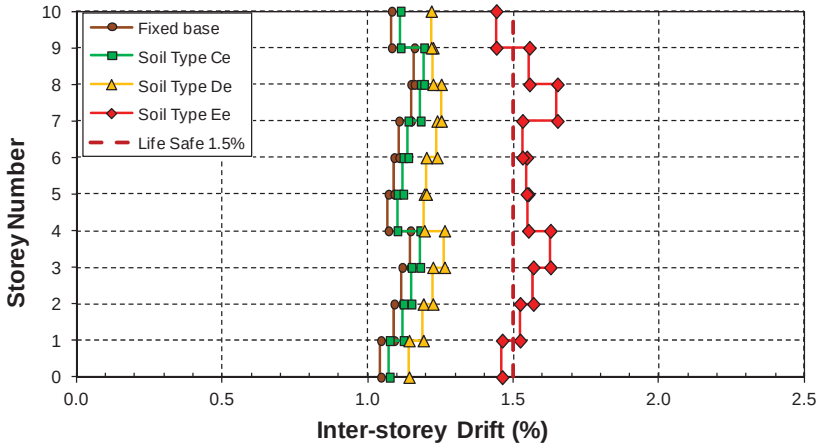

(b)

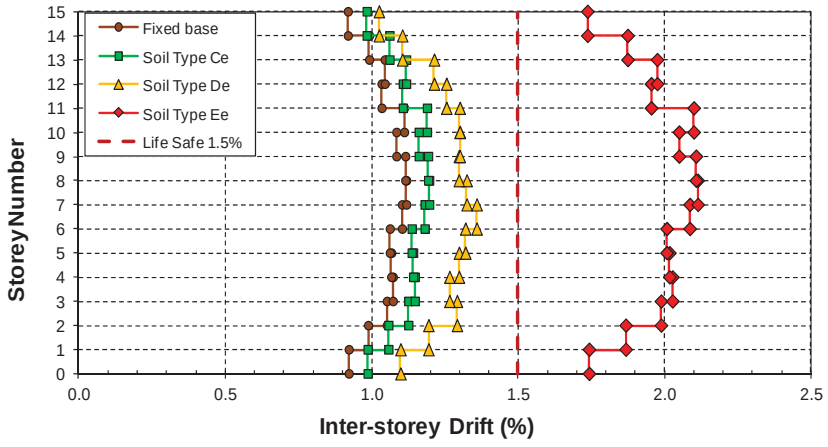

(c)

Figure 5.16: Elastic inter-storey drifts of the adopted structural models resting on soil class C_e, D_e, and E_e with bedrock depth of 30 metres; (a) model S5; (b) model S10; (c) model S15

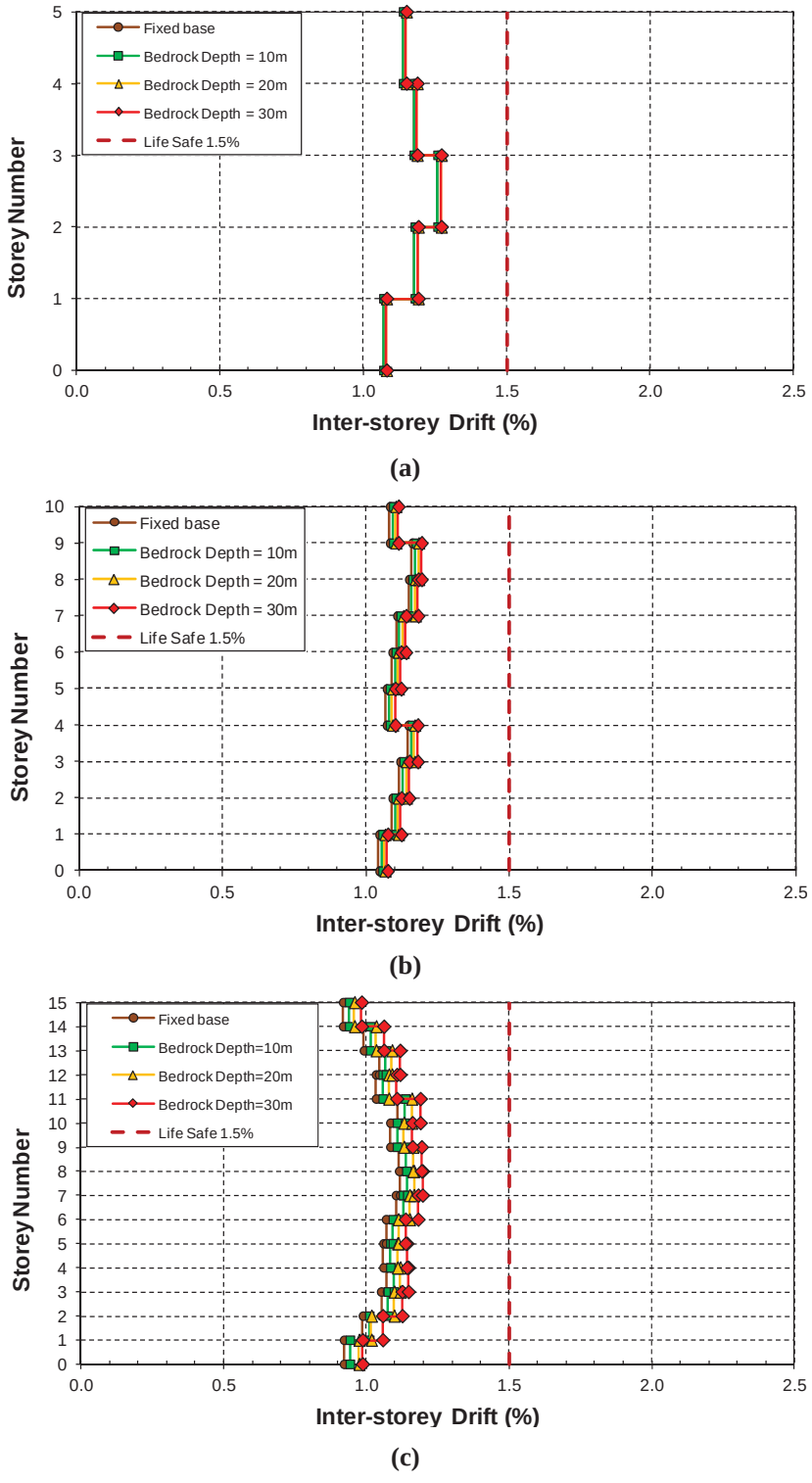

Figure 5.17: Elastic inter-storey drifts of the adopted structural models resting on soil class C_e with variable bedrock depths; (a) model S5; (b) model S10; (c) model S15

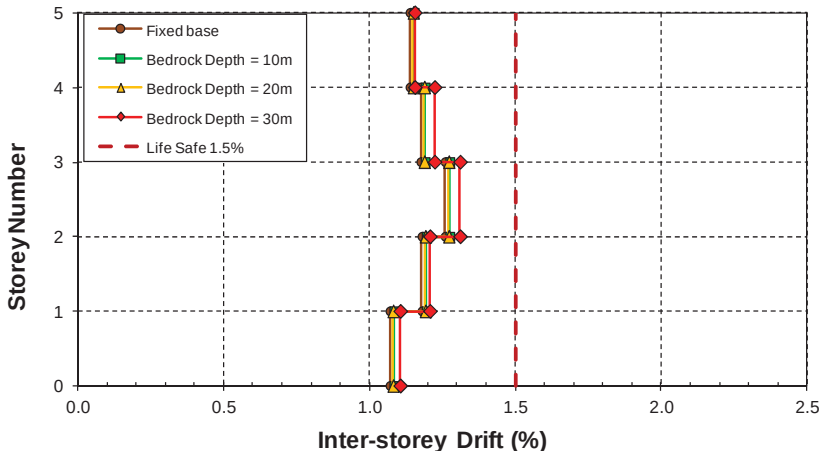

(a)

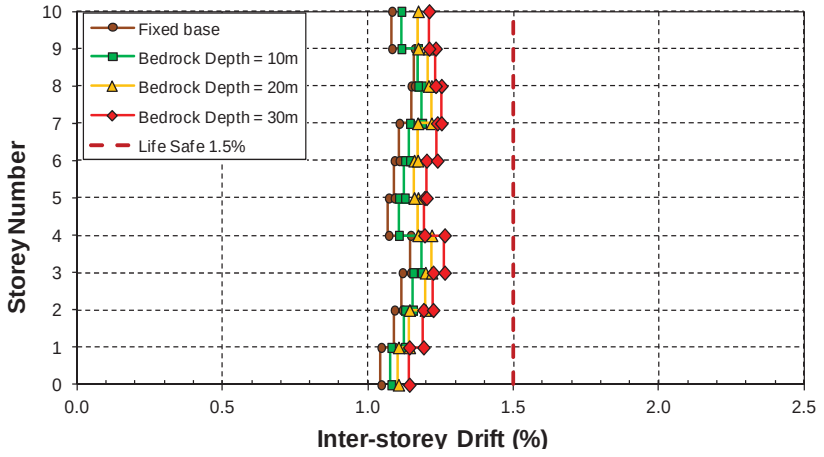

(b)

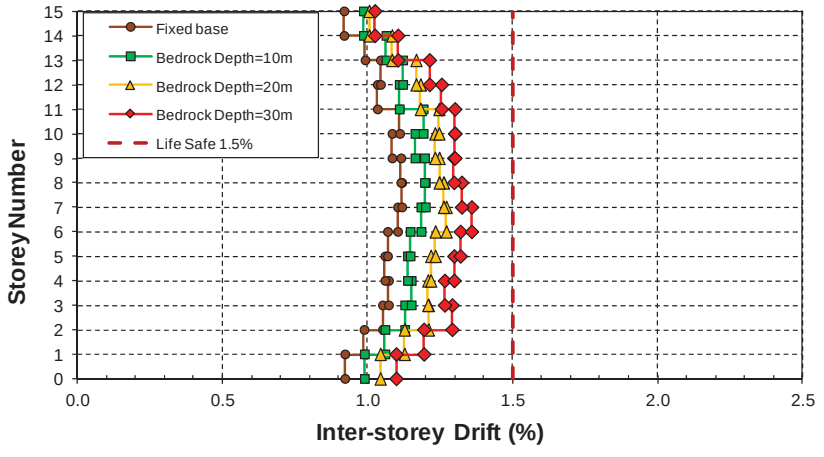

(c)

Figure 5.18: Elastic inter-storey drifts of the adopted structural models resting on soil class D_e with variable bedrock depths; (a) model S5; (b) model S10; (c) model S15

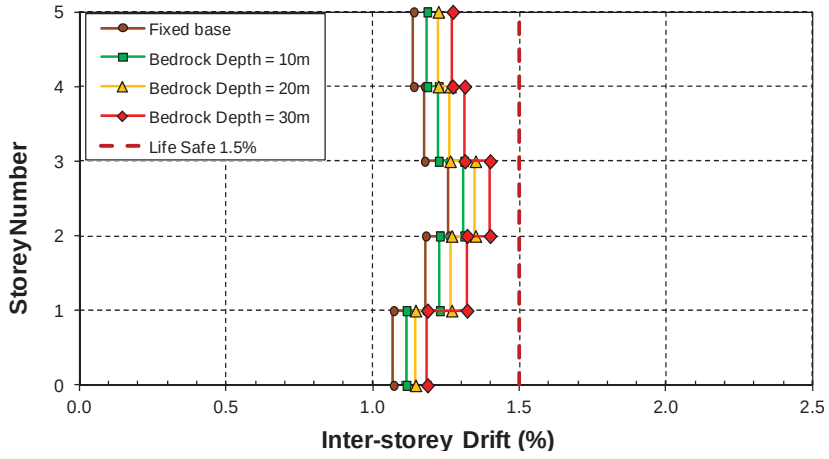

(a)

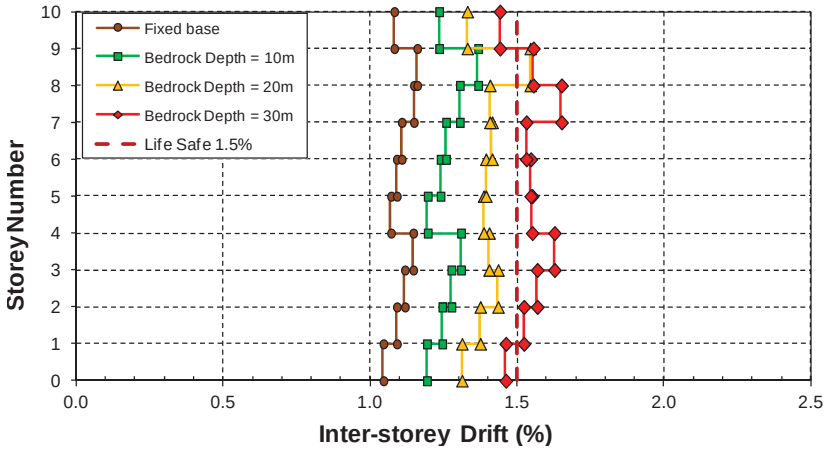

(b)

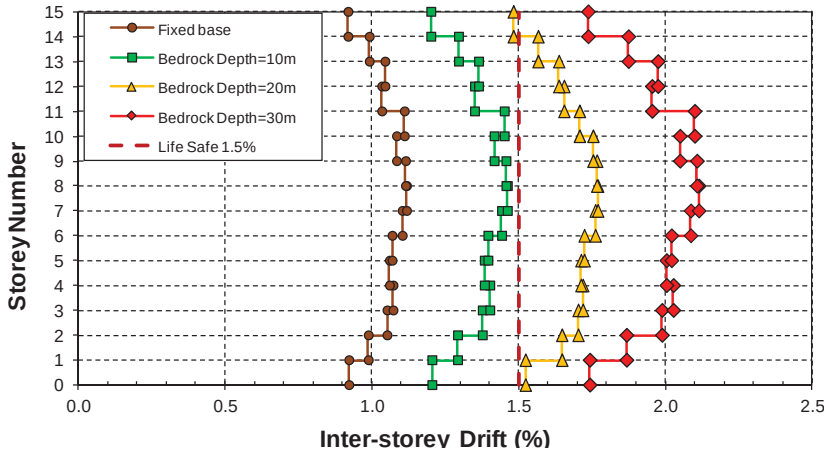

(c)

Figure 5.19: Elastic inter-storey drifts of the adopted structural models resting on soil class E_e with variable bedrock depths; (a) model S5; (b) model S10; (c) model S15

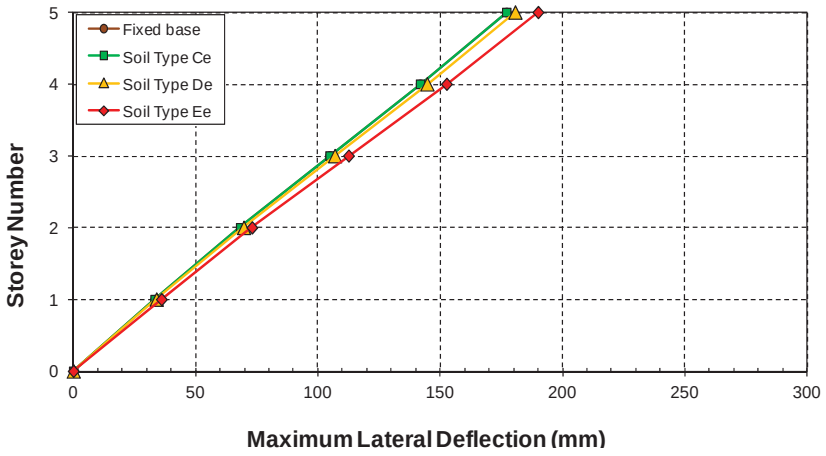

(a)

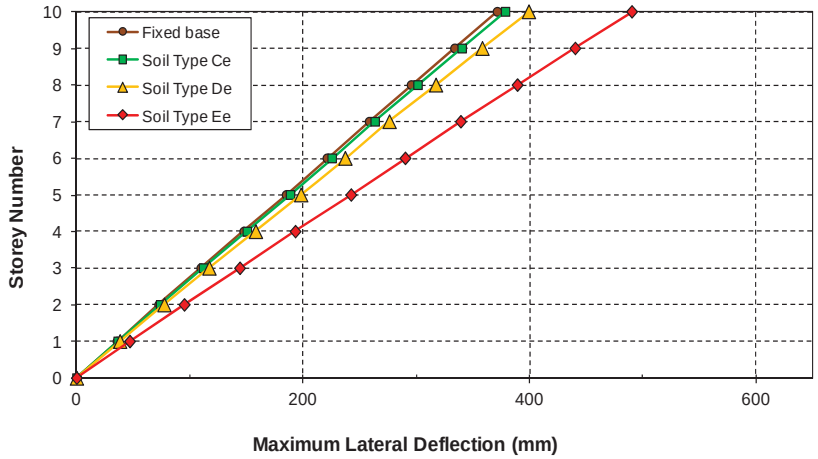

(b)

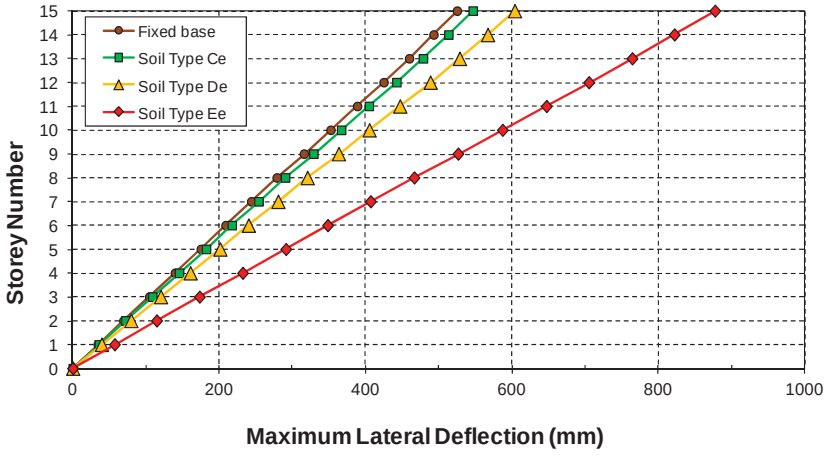

(c)

Figure 5.20: Inelastic storey deflections of the adopted structural models resting on soil classes C_e, D_e, and E_e with bedrock depth of 30 metres; (a) model S5; (b) model S10; (c) model S15

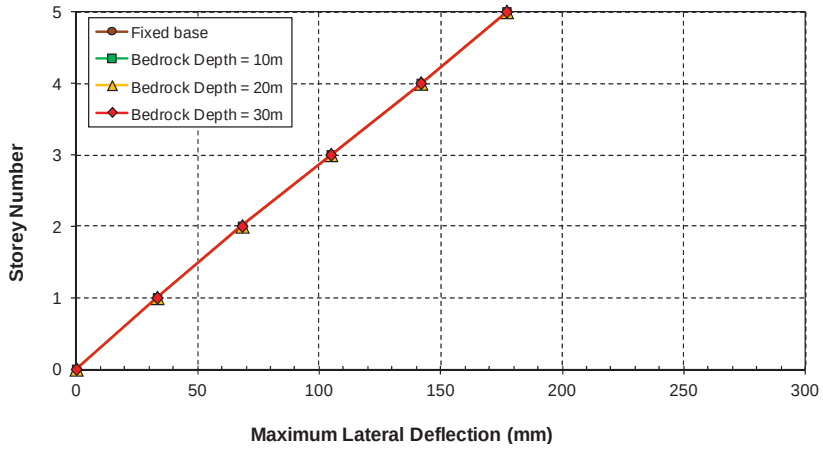

(a)

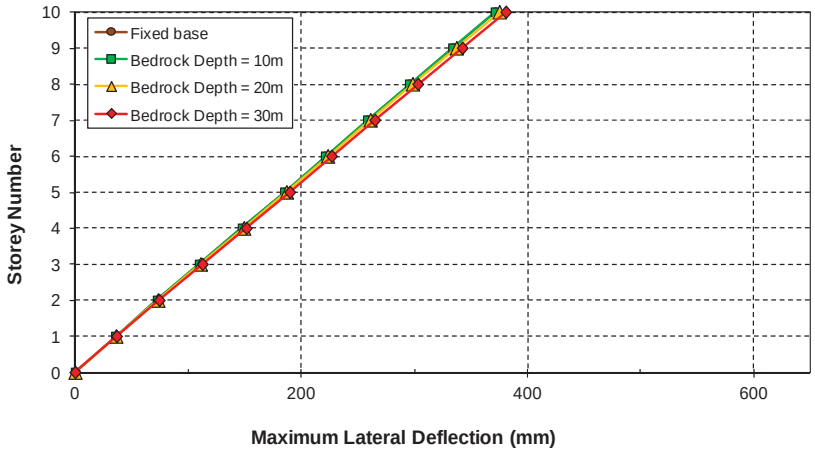

(b)

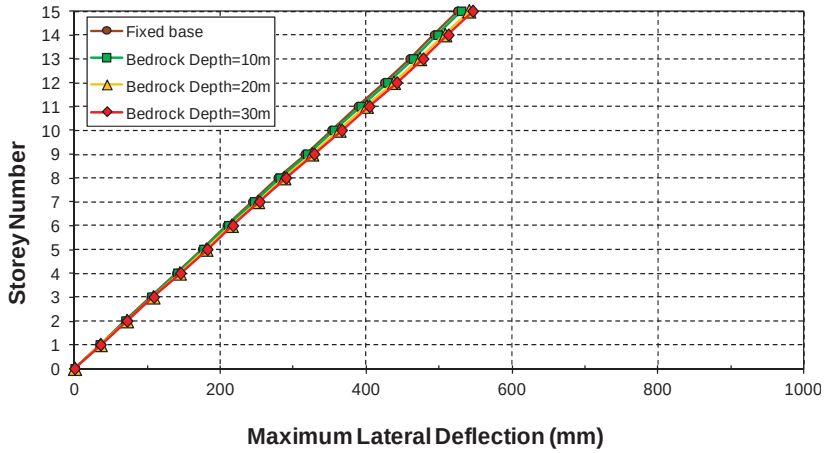

(c)

Figure 5.21: Inelastic storey deflections of the adopted structural models resting on soil class C_e with variable bedrock depths; (a) model S5; (b) model S10; (c) model S15

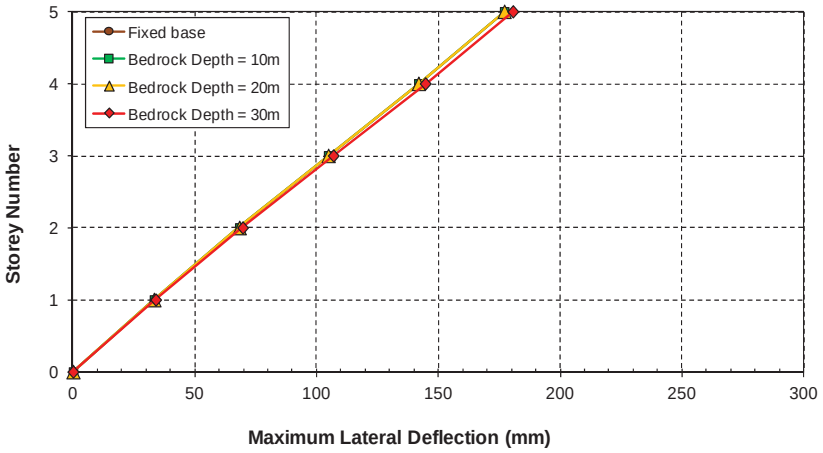

(a)

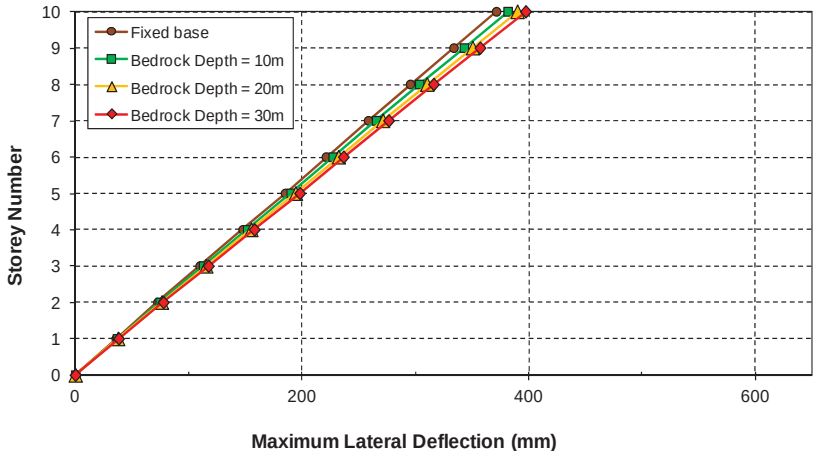

(b)

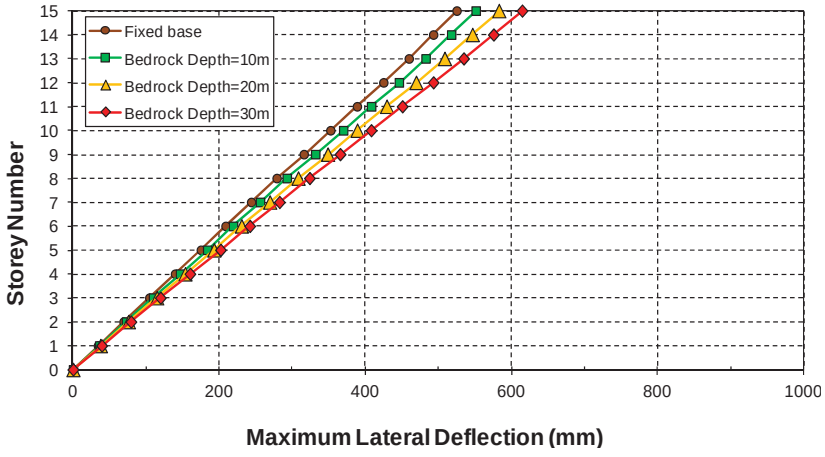

(c)

Figure 5.22: Inelastic storey deflections of the adopted structural models resting on soil class D_e with variable bedrock depths; (a) model S5; (b) model S10; (c) model S15

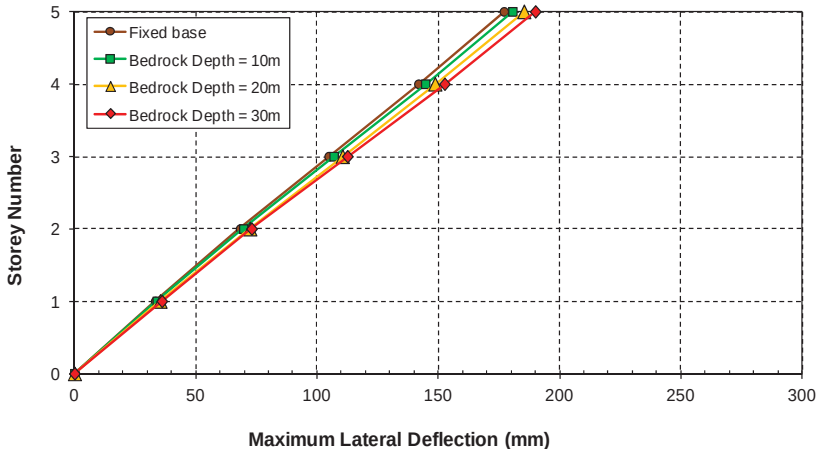

(a)

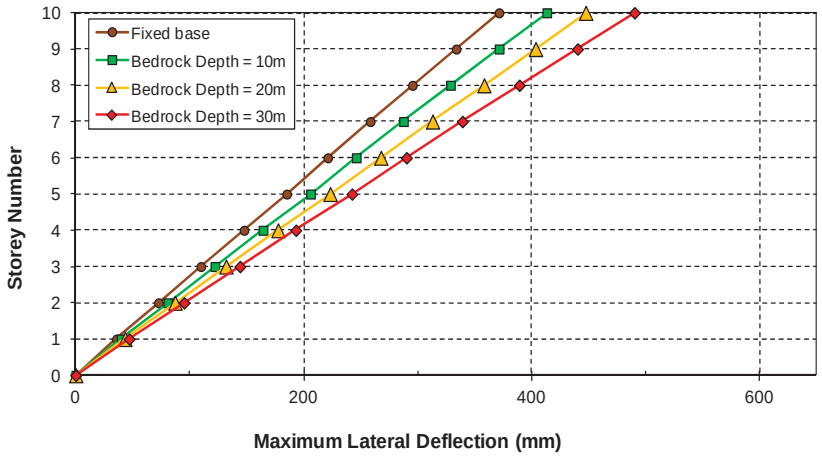

(b)

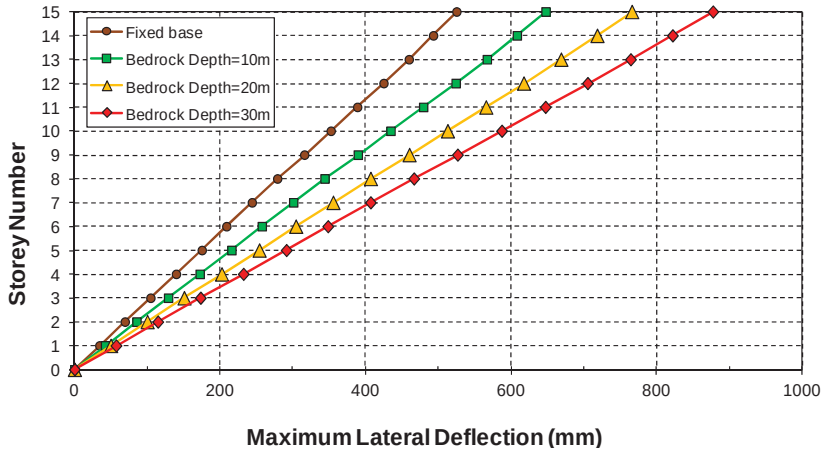

(c)

Figure 5.23: Inelastic storey deflections of the adopted structural models resting on soil class E_e with variable bedrock depths; (a) model S5; (b) model S10; (c) model S15

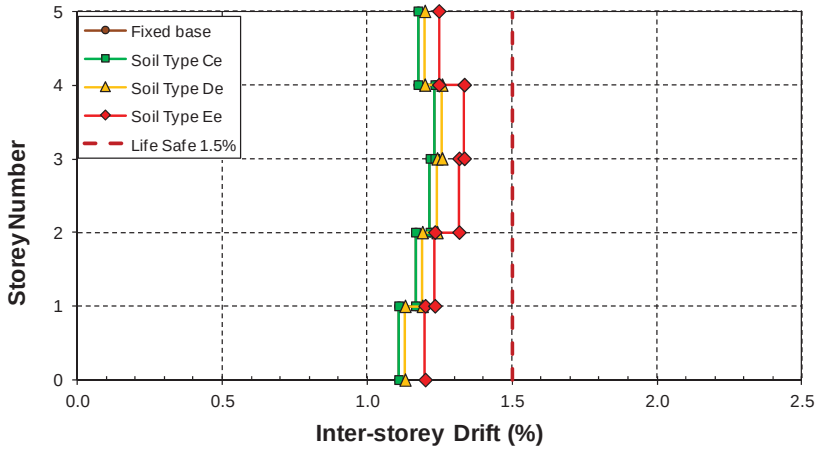

(a)

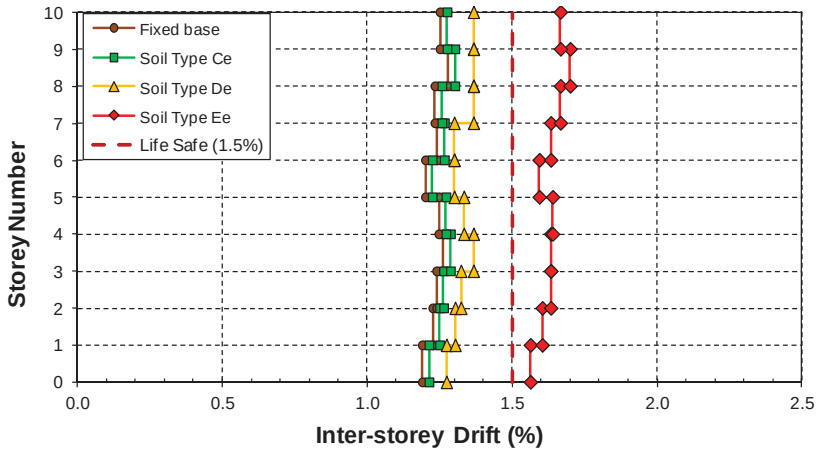

(b)

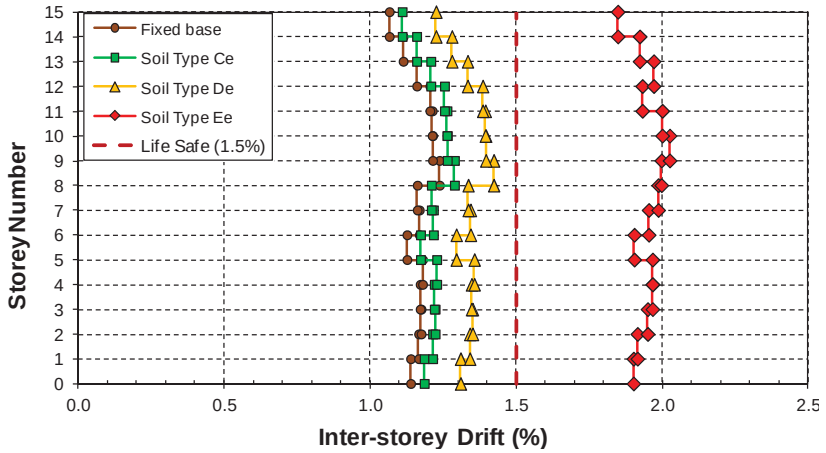

(c)

Figure 5.24: Inelastic inter-storey drifts of the adopted structural models resting on soil classes C_e, D_e, and E_e with bedrock depth of 30 metres; (a) model S5; (b) model S10; (c) model S15

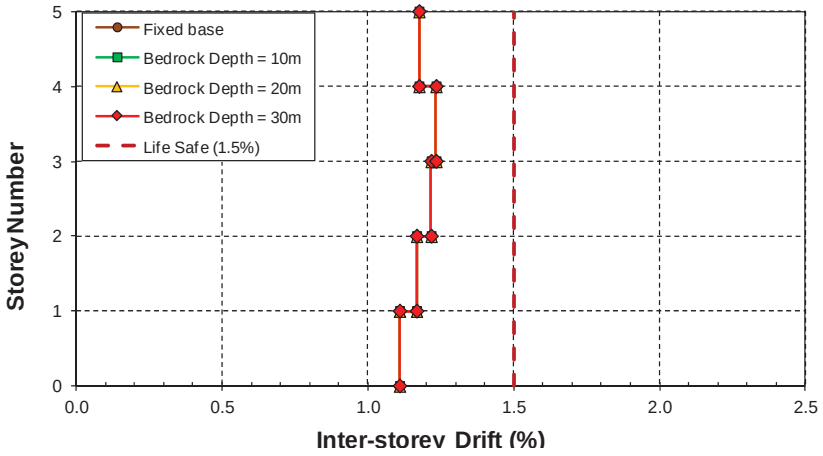

(a)

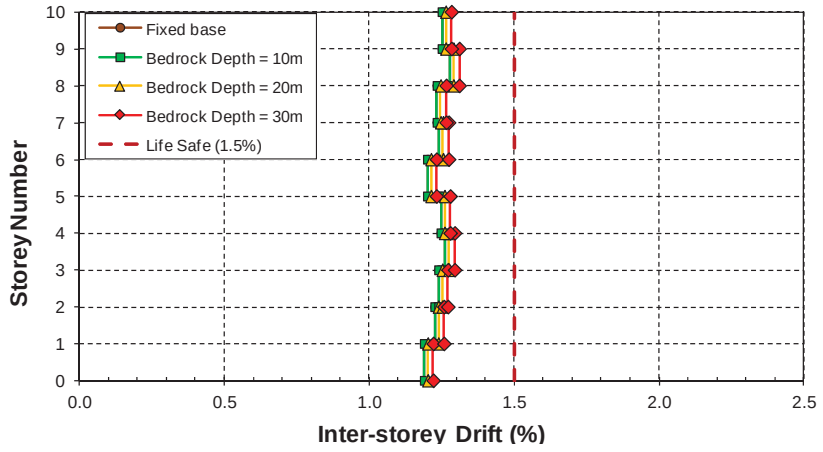

(b)

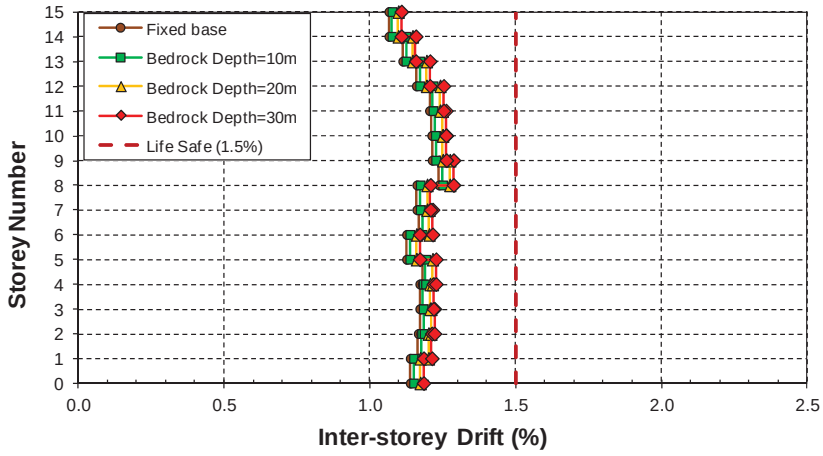

(c)

Figure 5.25: Inelastic inter-storey drifts of the adopted structural models resting on soil class C_e with variable bedrock depths; (a) model S5; (b) model S10; (c) model S15

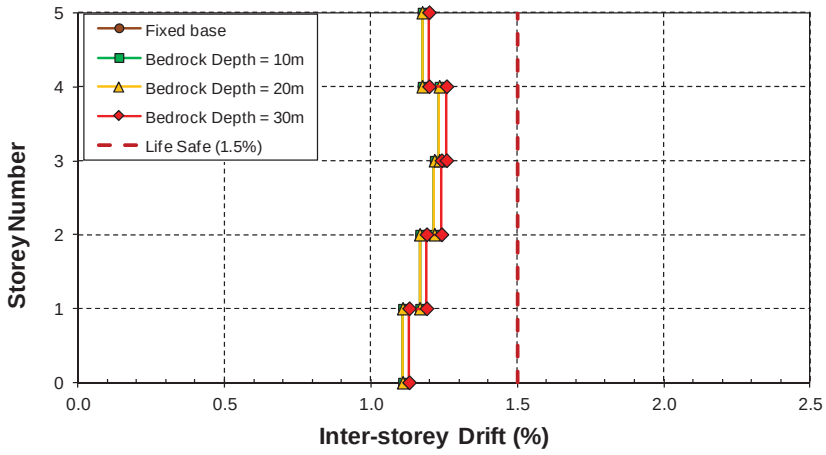

(a)

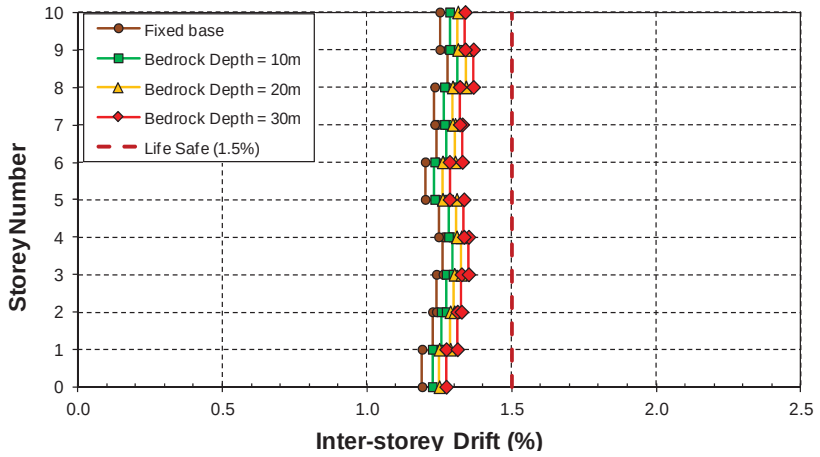

(b)

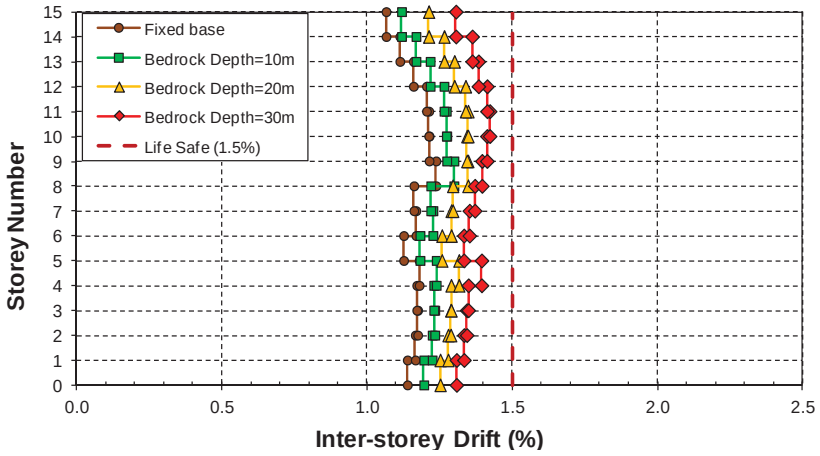

(c)

Figure 5.26: Inelastic inter-storey drifts of the adopted structural models resting on soil class D_e with variable bedrock depths; (a) model S5; (b) model S10; (c) model S15

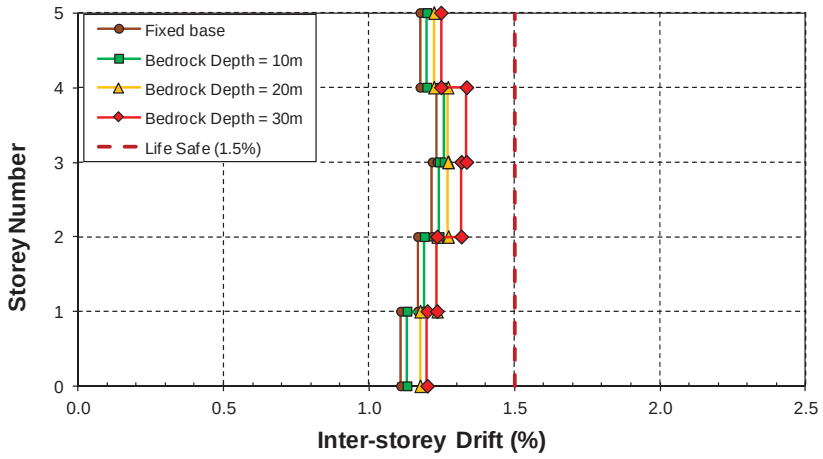

(a)

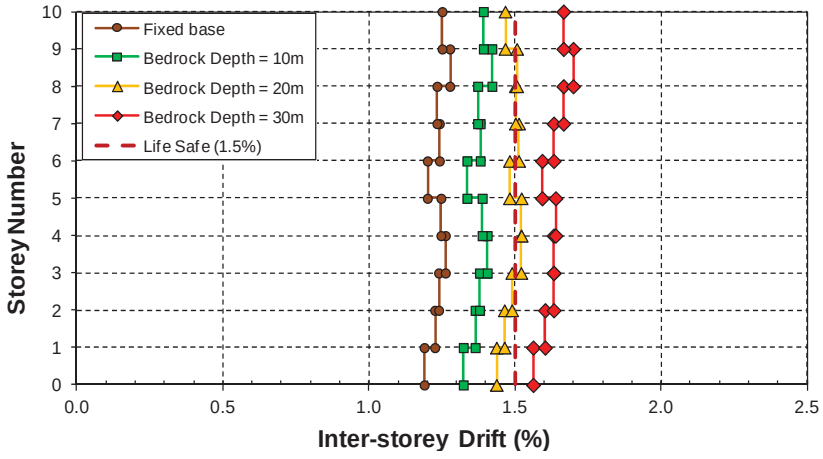

(b)

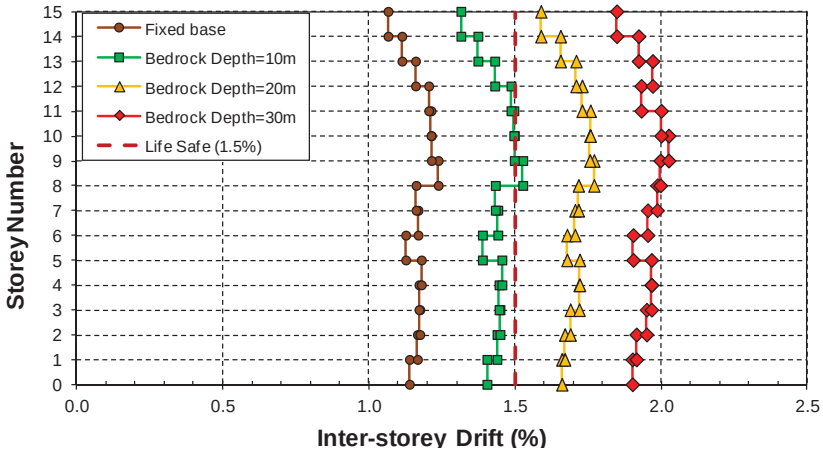

(c)

Figure 5.27: Inelastic inter-storey drifts of the adopted structural models resting on soil class E_e with variable bedrock depths; (a) model S5; (b) model S10; (c) model S15

5.8.2 Base Shear

According to base shear ratios of flexible base models ($\tilde{V}$) to fixed base models (V) for elastic and inelastic cases, summarised in Tables 5.6 and 5.7, it is observed that the base shear ratios ($\tilde{V}$ /V) in all the studied models are less than one for both elastic and inelastic analysis cases. However, these ratios are fairly higher and closer to unity for inelastic analysis case in comparison with elastic analysis case. Thus, *base shear of the structures modelled with soil as flexible base are always less than base shear of structures modelled as fixed base.* These results have good conformity to Section 5.6.2 of BSSC (2003) regulations as in this section reduction of base shear due to SSI is predicted. In general, by decreasing shear wave velocity (V_s) and shear modulus (G_{max}), base shear of flexible base models decrease relatively.

Considering the effects of SSI, the spectral acceleration decreases considerably due to lengthening of the natural period. As a result, such increase in the natural period substantially changes the response spectral acceleration (Sa). This concept has been numerically investigated and proved in this study. In the case of adopted mid-rise moment resisting building frames resting on soft soil deposits, natural period lies in the long period region of the acceleration response spectrum curve due to the natural period lengthening for the studied structural models. Evidently, the spectral acceleration response (Sa) tends to decrease, leading to the reduction of the base shears of the flexible models in comparison to the fixed base models. In addition, it is observed that, by decreasing the bedrock depths from 30 m to 10 m, the base shear ratios ($\tilde{V}$ /V) increase. This ratio is very close to unity for the models on soil class C_e, nevertheless, by reducing the shear wave velocity (V_s) and shear modulus (G_{max}) of the subsoil in soil classes D_e and E_e, and increasing bedrock depths for both elastic and inelastic analysis cases, the base shear ratio ($\tilde{V}$ /V) decreases. This ratio is slightly higher in inelastic analysis cases in comparison with elastic analysis cases. In inelastic case, as the lateral distortions are more than elastic case due to appearing plastic hinges within the structure. Therefore, more shear stress will be accommodated between the structural levels leading to more base shear. Thus, base shear ratios for inelastic analysis cases are always more than base shear ratios of elastic analysis cases.

5.8.3 Lateral Deflections and Inter-storey Drifts

Comparing the maximum lateral deflection ratios ($\tilde{\delta}/\delta$) for elastic analysis case (Table 5.8) and inelastic analysis case (Table 5.9) as well as storey deflections and inter-storey drifts of fixed base and flexible base models resting on soil classes C_e, D_e, and E_e

with bedrock depth of 30m for elastic analysis case (Figures 5.12 and 5.16) and inelastic analysis case (Figures 5.20 and 5.24) respectively, it becomes apparent that elastic lateral deflections and corresponding inter-storey drifts of flexible base models resting on soil class C_e have increased only by 1%, 3%, and 7% in comparison with fixed base S5, S10, and S15 models, respectively. For inelastic analysis case, lateral deflections and corresponding inter-storey drifts of flexible base models resting on the same soil class have been amplified by 2% and 4% in comparison with fixed-base models for models S10 and S15, respectively, while model S5 experiences insignificant changes in the lateral deflections and inter-storey drifts. Overall, inter-storey drifts of the flexible base models resting on soil class C_e do not differ much from that of the fixed-base model for both analysis cases. Thus, performance level of studied mid-rise moment resisting building frames resting on soil class C_e remains in life safe level and soil-structure interaction effects can be neglected in both elastic and inelastic analysis cases. However, lateral deflections and inter-storey drifts of flexible base models resting on soil class D_e increase by 3%, 10%, and 19% in elastic case and 2%, 7%, and 15% in inelastic case, respectively, in comparison with fixed base S5, S10, and S15 models. Those increments, for models S10 and S15 are potentially safety threatening as they may change the performance level of the mentioned building frames from life safe to near collapse.

For the models on soil class E_e (V_s=150m/s), lateral deflections and inter-storey drifts of flexible base models have increased by 11%, 40%, and 89% in elastic case and 7%, 31%, and 67% in inelastic case in comparison with fixed base S5, S10, and S15 models, respectively. Performance levels of S10 and S15 models change from life safe to near collapse level as shown in Figures 5.11 to 5.12 for elastic case and Figures 5.22 to 5.23 for inelastic case. Such a significant change in the inter-storey drifts and subsequently performance levels of 10 and 15 storey models resting on soil class E_e is absolutely dangerous and safety threatening for both elastic and inelastic analysis cases. Thus, it can be concluded that as shear wave velocity (V_s) and shear modulus (G_{max}) of the subsoil decrease, the maximum lateral deflections and consequently, the corresponding inter-storey-drifts of mid-rise moment resisting building frames increase significantly.

It can be noted that by decreasing the shear wave velocity and consequently stiffness of the

subsoil, the difference between the vibration period of the flexible and the fixed base models increase for both elastic and inelastic analysis cases. Thus, the effects of soil-structure interaction for soil classes D_e and E_e (particularly E_e) are quite significant. However, the vibration periods of fixed base and flexible base models for relatively rigid grounds such as soil class C_e are very similar. Thus, the effects of soil-structure interaction are negligible. Taking SSI effects into account, the spectral displacement (S_d), increases considerably due to lengthening of the natural period. Therefore, such increase in the natural period dominantly alters the response of the building frames under the seismic excitation. The above mentioned concept has been investigated and proved in this study. In the case of adopted mid-rise moment resisting building frames resting on soft soil deposits, natural period lies in the long period region of the response spectrum curve due to the natural period lengthening for such systems. Hence, the displacement response (S_d) tends to increase, and eventually performance level of the structures may change from life safe to near collapse or total collapse.

Generally, by decreasing the dynamic properties of the subsoil such as shear wave velocity and shear modulus, base shear ratios decrease while lateral deflections and inter-storey drifts of the moment resisting building frames increase relatively. In brief, the conventional elastic and inelastic design procedure excluding SSI is not adequate to guarantee the structural safety for moment resisting building frames resting on soil classes D_e and E_e.

Observing the effects of bedrock depth variations on the maximum lateral deflection ratios (Tables 5.8 and 5.9), elastic storey deflections (Figures 5.13 to 5.15) and corresponding inter-storey drifts (Figures 5.17 to 5.19) of the models resting on soil classes C_e, D_e, and E_e as well as inelastic storey deflections (Figures 5.21 to 5.23) and corresponding inter-storey drifts (Figures 5.25 to 5.27) of the models resting on soil classes C_e, D_e, and E_e, respectively, it is evident that as the bedrock depth varies from 30m to 10 m, the increments in the lateral deflections and corresponding inter-storey drifts of flexible base models resting on soil class C_e reduces for both elastic and inelastic analysis cases. For the models resting on soil class D_e, it is observed that elastic and inelastic lateral deflections and corresponding inter-storey drifts of models S5, S10, and S15 with 10 m of soil depth underneath as well as models S5 and S10 with 20m bedrock depth do not differ much from fixed base models. Thus, the amplification of lateral deflections and inter-storey drifts due to SSI effects for those models are negligible while

for model S15 with 20m bedrock depth, lateral deflections and inter-storey drifts noticeably increase in comparison with fixed base model. Distinctly, for models S10 and S15 resting on soil class E_e the maximum lateral deflections and inter-storey drifts of flexible base models in comparison with fixed base models increase substantially in both elastic and inelastic analysis cases. Obviously, performance level of these building frames may change from life safe to near collapse when SSI is considered in the analysis, which is dangerous and safety threatening.

It is noticeable that by increasing the bedrock depth, the natural period of the subsoil increases and consequently the difference between the period of vibration in two cases (i.e. structures modelled on flexible soils and structures modelled as fixed base) increase. Thus, the effects of dynamic soil-structure interaction for deeper bedrock depths are more considerable. In the case of deeper bedrock, natural period lies in the long period region of the response spectrum curve due to the natural period lengthening for such systems. Consequently, the displacement response tends to increase and the performance level of the structures may be changed from life safe to near collapse or even total collapse. From the above observations, it can be concluded that considering soil-structure interaction effects in seismic design of mid-rise moment resisting building frames resting on soil classes D_e and E_e is essential, particularly for:

- 10 storey building frames or higher resting on more than 20 metres of soil class D_e; and
- Building frames higher than 5 storey resting on soil class E_e irrespective of the bedrock depth.

Thus, the conventional elastic and inelastic design procedures excluding SSI may not be adequate to guarantee the structural safety of mid rise moment resisting building frames resting on soft soil deposits.

5.9 Summary

In this chapter, in order to have a comprehensive comparison between the results and draw a clear conclusion about the effects of structural height, subsoil stiffness, and bedrock depth on elastic and inelastic seismic response of regular mid-rise moment resisting building frames under the influence of soil-structure interaction, numerical investigations have been performed utilising 5, 10, and 15 storey structural models resting on soil classes C_e (V_s=600m/s), D_e (V_s=320m/s), and E_e (V_s=150m/s), having

three bedrock depths of 10 m, 20 m, and 30 m. The structural sections of the structural models have been designed based on both elastic method, and inelastic procedure considering elastic-perfectly plastic behaviour of structural elements.

According to the results, it is observed that base shear of the structures modelled with soil as flexible base are generally less than the base shear of the structures modelled as fixed base for both elastic and inelastic cases. In addition, it is observed that lateral deflections and corresponding inter-storey drifts of flexible base models resting on soil class C_e do not differ much from fixed base models for both elastic and inelastic analysis cases. Thus, performance level of regular mid-rise moment resisting building frames resting on soil class C_e remains in life safe level and soil-structure interaction effects are insignificant in both elastic and inelastic analysis cases. However, lateral deflections and inter-storey drifts of flexible base models resting on soil classes D_e and E_e (in particular for 10 storey building frames or higher resting on more than 20 metres of soil class D_e and building frames higher than 5 storey resting on soil class E_e irrespective of the bedrock depth) significantly increase in comparison with fixed base models. In general, as shear wave velocity (V_s) and shear modulus (G_{max}) of the subsoil decrease or bedrock depth (h_s) increases, the base shear of flexible base models in comparison with fixed base models decrease while lateral deflections and consequently, corresponding inter-storey drifts increase relatively. The amplification of lateral deflections and corresponding inter-storey drifts is more significant in elastic analysis case, with the range of amplification factors ranging from 1.01 to 1.89, in comparison to inelastic analysis case, with the amplification factors ranging from 1.00 to 1.67.

The amplification of the lateral deflections and corresponding inter-storey drifts of flexible base models resting on soil classes D_e and E_e can change the performance level of the structures from life safe to near collapse or total collapse which is absolutely dangerous and safety threatening for both elastic and inelastic analysis cases. As a result, soil-structure interaction has considerable effects on the elastic and inelastic seismic response of regular mid-rise moment resisting building frames resting on soil classes D_e and E_e. It can be concluded that the conventional elastic and inelastic design procedures excluding SSI may not be adequate to guarantee the structural safety of mid-rise moment resisting building frames resting on soft soil deposits. Evidently, while conducting full soil-structure interaction analysis, effects of soil thickness and shear wave velocity should be carefully considered.

CHAPTER SIX

6. SIMPLIFIED DESIGN PROCEDURE FOR PRACTICAL APPLICATIONS

6.1 Introduction

As discussed in details in the previous chapter, considering soil-structure interaction effects in seismic design of mid-rise moment resisting building frames resting on soil classes D_e and E_e, is essential, particularly for 10 storey building frames or higher resting on more than 20 metres of soil class D_e and building frames higher than 5 storey resting on soil class E_e irrespective of the bedrock depth. Thus the conventional elastic and inelastic design procedures excluding SSI may not be adequate to guarantee the structural safety of mid-rise moment resisting building frames resting on soft soil deposits. It was also recommended to practising engineers and engineering companies working in regions located in high earthquake risk zones, to consider dynamic soil-structure interaction effects in the analysis and design of mid-rise moment resisting building frames resting on soft soils to ensure safety of the design.

With respect to what has been concluded above, this question may immediately arise as to is it necessary for design engineers to follow the entire numerical procedure, described in this study, to determine the actual response of building frames under the influence of SSI? It is obvious that going through the whole numerical procedure could be complicated and time consuming. On the other hand, practising engineers and engineering companies tend to use simple but accurate procedures rather than modelling the complex problems which could be time consuming. As a result, there is a strong need to develop a simplified but accurate procedure for practical purposes in order to evaluate seismic response of building structures considering detrimental effects of soil-structure interaction.

In order to respond to this need, in this chapter, an empirical relationship, based on the results of parametric study reported in Chapter 5, is developed enabling designers to determine lateral deflections of the building frames under the influence of soil-structure interaction utilising fixed base results as well as other basic site and structural characteristics.

As elucidated in Chapter 5, base shear of the structures modelled with soil as flexible base are less than the base shear of structures modelled as fixed base. Therefore, base shear reduction due to SSI is deemed to be conservative and could be ignored in the design procedure contributing to safer design. However, lateral deflection amplification due to SSI has detrimental effects on performance and safety of building frames and must be taken into account in any design procedure.

6.2 Developing Initial Form of the Empirical Relationship

In order to present an empirical relationship to determine the elastic and inelastic lateral deflection amplifications due to SSI with respect to other basic site and structural characteristics, a relationship between $\tilde{\delta}/\delta$ and system parameters employed in this study (Chapter 5) is required to be developed.

Veletsos and Meek (1974) presented the following basic equation for ($\tilde{\delta}/\delta$):

$$\frac{\tilde{\delta}}{\delta} = (\frac{f}{\tilde{f}})^2 \tag{6.1}$$

where,

$\tilde{\delta}$ =Maximum lateral deflection of the structure in soil-structure system;

δ= Maximum lateral deflection of fixed base structure;

$\tilde{f}$ =Natural frequency of soil-structure system; and

f =Natural frequency of fixed base structure.

In addition, BSSC (2003) expressed the ratio of the natural frequency of the soil-structure system ($\tilde{f}$) to the natural frequency of the fixed base structure (f) by the following expression:

$$\frac{\tilde{f}}{f} = \frac{1}{\sqrt{[1+\frac{k}{k_x}(1+\frac{k_x}{k_\theta}\frac{h^2}{r^2})}} \tag{6.2}$$

where,

k=Stiffness of the structure;

k_x = Lateral stiffness of the subsoil foundation;

k_θ = Rocking stiffness of the subsoil foundation;

r = Radius of the foundation base (equal to B/2 where B is foundation width); and

h= Height of the structure.

The ratio of the natural frequency of the fixed base structure (f) to the natural frequency of the soil-structure system ($\tilde{f}$) in Equation (6.1) can be substituted from Equation (6.2) as follows:

$$\frac{\tilde{\delta}}{\delta} = 1 + \frac{k}{k_x} + \frac{kh^2}{k_\theta r^2} \tag{6.3}$$

According to Wolf (1994), the values of lateral stiffness (k_x) and rocking stiffness (k_θ) of the subsoil foundation can be determined using the following equations:

$$k_x = \frac{8Gr}{2-\nu} \tag{6.4}$$

$$k_\theta = \frac{8Gr^{3\backslash}}{3(1-\nu)} \tag{6.5}$$

where,

ν =Poisson's ratio of the subsoil; and

G = Shear modulus of the subsoil which is related to the soil density (ρ) and shear wave velocity of the subsoil (V_s) using:

$$G = \rho V_s^2 \tag{6.6}$$

By replacing shear modulus (G) in Equations (6.4) and (6.5) by Equation (6.6) below are obtained:

$$k_x = \frac{8\rho V_s^2 r}{2-\nu} \tag{6.7}$$

$$k_\theta = \frac{8\rho V_s^2 r^{3\backslash}}{3(1-\nu)} \tag{6.8}$$

Substituting the values of lateral stiffness (k_x) and rocking stiffness (k_θ) into Equation (6.3) leads to Equation (6.9):

$$\frac{\tilde{\delta}}{\delta} = 1 + \frac{(2-\nu)k}{8\rho r V_s^2} + \frac{3(1-\nu)kh^2}{8\rho r^5 V_s^2} \tag{6.9}$$

With respect to Equation (6.9), the initial form of the simplified relationship between ($\tilde{\delta}/\delta$) and site and structural characteristics can be assumed as:

$$\frac{\tilde{\delta}}{\delta} = 1 + \frac{\alpha E_{str}}{\rho V_s^2} + \frac{\beta (h/B)^2 E_{str}}{\rho V_s^2} \tag{6.10}$$

where, h is the height of the structure, B is the foundation width, ρ is the soil density, V_s is the shear wave velocity of the subsoil, E_{str} is the modulus of elasticity of the structural material, and, α and β are model parameters.

On the other hand, as Veletsos and Meek (1974) relationship is based on elastic half space theory, the effect of bedrock depth variation was not captured by their relationship. As described in Section 5.8.3, by increasing the bedrock depth, lateral deflections of soil-structure system (flexible base model) increase, relatively. Thus, ($\tilde{\delta}/\delta$) can be presented as:

$$\frac{\tilde{\delta}}{\delta} = f(h_s / B) \tag{6.11}$$

where, h_s is the bedrock depth.

Thus, by comparing Equations (6.10) and (6.11), the initial form of the simplified empirical relationship, relating ($\tilde{\delta}/\delta$) to site and structural characteristics may have the following form:

$$\frac{\tilde{\delta}}{\delta} = 1 + \frac{\alpha E_{str}}{\rho V_s^2} + \frac{(h/B)^2 (h_s/B)^{\gamma} E_{str}}{\lambda \rho V_s^2} \tag{6.12}$$

where, α, γ, and λ are model parameters.

6.3 Proposed Simplified Design Procedure

In order to find the model parameters in Equation (6.12), for both elastic and inelastic analysis cases, the lateral deflection ratio ($\tilde{\delta}/\delta$), corresponding to three different types of soils (C_e, D_e, and E_e), having three bedrock depths of 10, 20, and 30 metres, summarised in Tables 5.7 and 5.8, were employed.

Then, two correlations were developed using regression analysis in order to find the best fit between Equation (6.12) and the numerical data summarised in Tables 5.7 and 5.8 for elastic and inelastic analyses, respectively.

For elastic analysis case, the model parameters for the best developed correlation in regression analysis with coefficient of determination R^2=0.99, are:

$\alpha = 0, \gamma = 1$ and $\lambda = 33800$

Figure 6.1 presents the results of regression analysis to find the best fit to the numerical predictions for elastic analysis case.

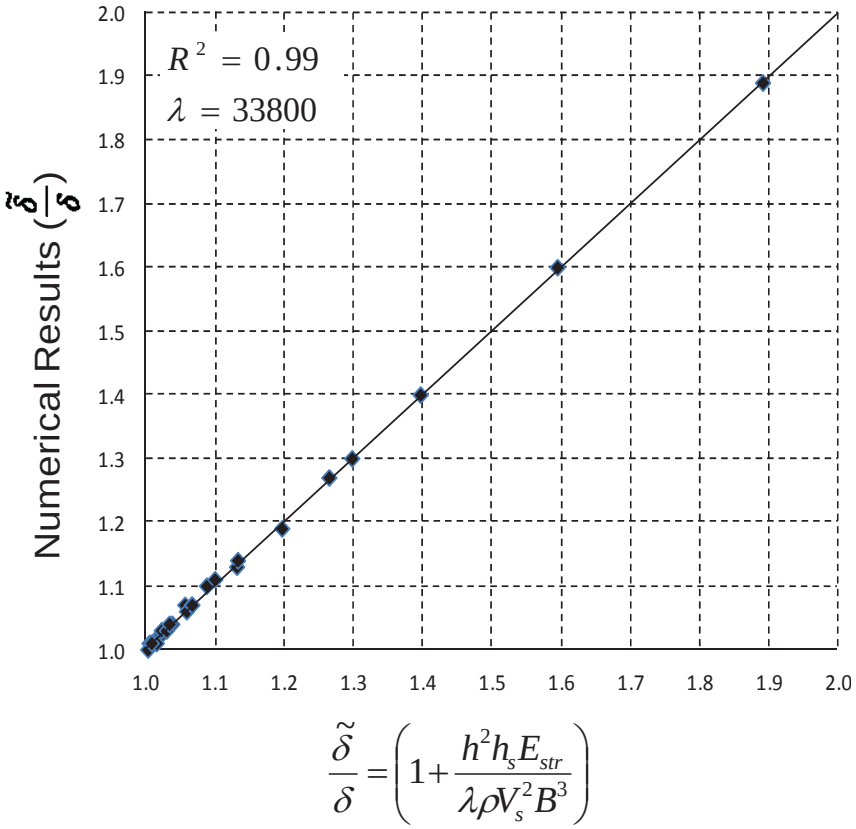

Figure 6.1: Results of regression analysis to find the best fit to the numerical predictions of maximum lateral deflections for elastic analysis case

Similar procedure has been followed for inelastic analysis case. Accordingly, the model parameters for the best correlation in regression analysis with coefficient of determination R^2=0.98 are as follows:

$\alpha = 0, \gamma = 1$ and $\lambda = 44700$

Figure 6.2 presents the results of regression analysis to find the best fit to the numerical predictions for inelastic analysis case.

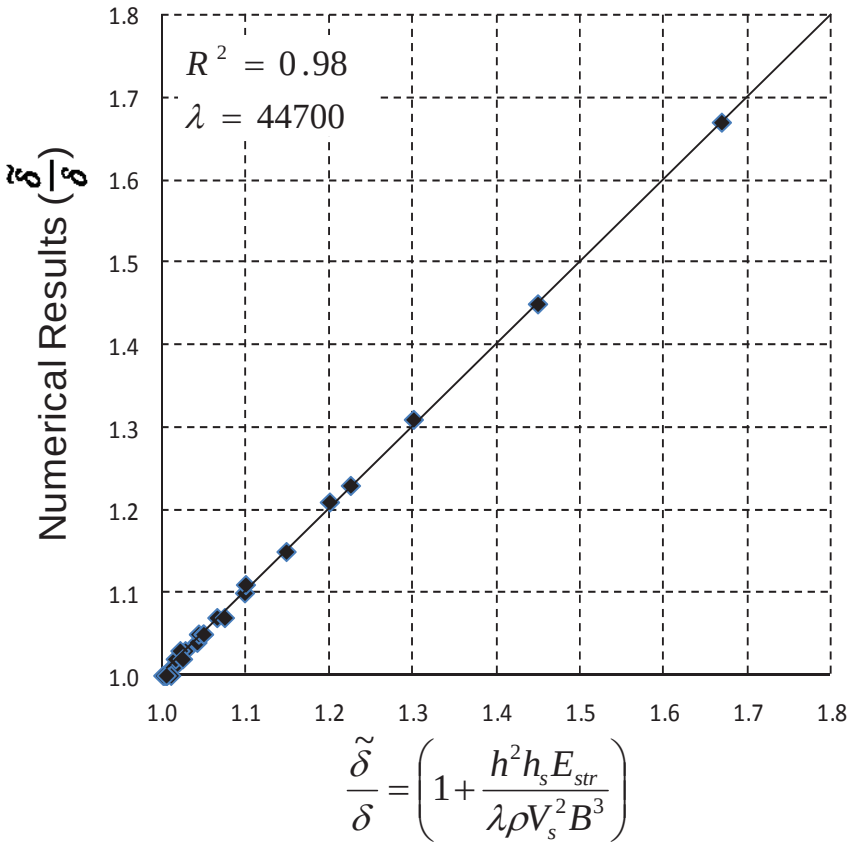

Figure 6.2: Results of regression analysis to find the best fit to the numerical predictions of maximum lateral deflections for inelastic analysis case

Thus Equations (6.12) can be simplified in a general form as shown in Equation (6.13):

$$\tilde{\delta} = \delta\left(1 + \frac{h^2 h_s E_{str}}{\lambda \rho V_s^2 B^3}\right) \tag{6.13}$$

where, λ is Analysis Type Factor ($\lambda = 33800$ for elastic analysis and $\lambda = 44700$ for inelastic analysis), $\tilde{\delta}$ is the maximum lateral deflection of the structure under the influence of SSI, and δ is the maximum lateral deflection of the fixed base structure (without SSI effects).

Equation (6.14) only shows the relationship between the maximum lateral deflection of the structure under the influence of SSI ($\tilde{\delta}$) and the maximum lateral deflection of the fixed base structure (δ). However, lateral storey deflections cannot be extracted directly

from the relationship. In order to adopt the relationship in practical engineering problems, Equation (6.13) is required to include storey deflections to enable design engineers to determine inter-storey drifts and check the performance levels of the structures. Thus, lateral storey deflections for each level of the structure under influence of SSI ($\tilde{d}_i$) as well as lateral storey deflections for each level of the structure for the fixed base structure (d_i) are obtained from the numerical results of elastic and inelastic analysis cases. Then, regression analyses have been performed to find the best fit between the numerical predictions of ($\tilde{d}_i / d_i$) and the right hand side of Equation (6.13) for elastic and inelastic analysis cases, respectively.

Figures 6.3 and 6.4 present the results of regression analyses to find the best fit to the numerical predictions of lateral storey deflections for elastic and inelastic analysis cases, respectively.

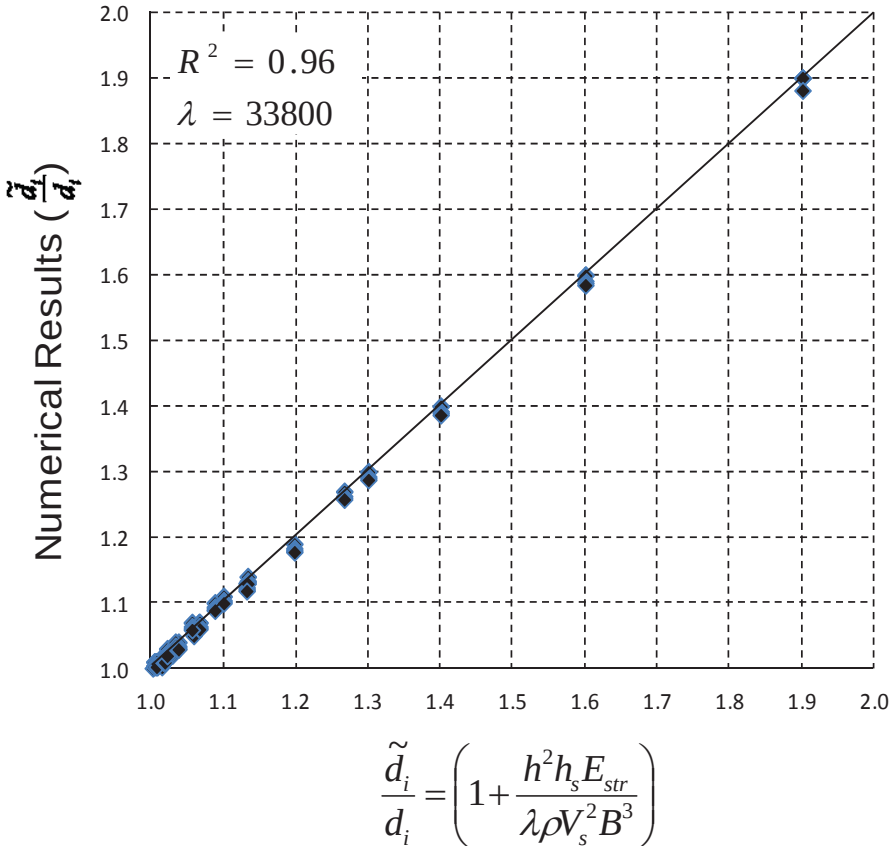

Figure 6.3: Results of regression analysis to find the best fit to the numerical predictions of lateral storey deflections for elastic analysis case

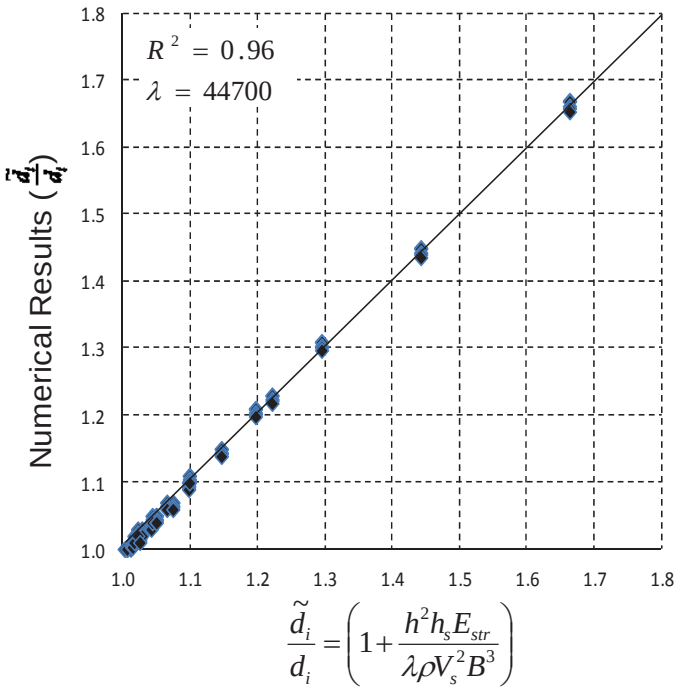

Figure 6.4: Results of regression analysis to find the best fit to the numerical predictions of lateral storey deflections for inelastic analysis case

According to the presented results, the best correlations in regression analyses with coefficient of determination R^2=0.96, adopting $\lambda = 33800$ and $\lambda = 44700$ for elastic and inelastic analysis cases, respectively, are similar to the best fits of maximum lateral deflections.

As a result, in order to determine the lateral storey deflections under the influence of SSI, Equation (6.14) can be presented:

$$\tilde{d}_i = d_i\left(1 + \frac{h^2 h_s E_{str}}{\lambda \rho V_s^2 B^3}\right) \tag{6.14}$$

where, $\tilde{d}_i$ is the lateral storey deflection at *(i)* level under the influence of SSI and d_i is the lateral storey deflection at *(i)* level for the fixed base structure (without SSI effects). For practical purposes, the maximum lateral deflections for each storey under the influence of SSI can be extracted from Equation (6.14). Then, inter-storey drifts under the influence of soil-structure interaction for each two adjacent stories can be determined and checked against the limiting value of 1.5% for life safe performance level. Thus, detrimental effects of soil-structure interaction may be more accurately taken into account in the seismic design of mid-rise moment resisting building frames to ensure the design is safe and reliable. The simplified procedure described in this section can be employed for practical purposes by

structural engineers and engineering companies, as a reliable and accurate method of considering SSI effect in the seismic design procedure. It should be noted that the proposed simplified design procedure can only be used in seismic design of regular mid-rise moment resisting building frames resting on shallow foundations with no embedment depth. This design procedure does not cover irregular and high-rise buildings as well as building structures resting on pile foundations. In addition, as Sun et al. (1998) backbone curves have been employed in this study, which take into account the effects of soil plasticity in an average sense. It should be noted that parameters such as relative density, Plasticity Index, and confining pressure can influence the soil shear wave velocity and shear modulus degradation curve. Thus, further research on effects of Plasticity Index and confining pressure variation on seismic response of regular mid-rise building frames would be helpful.

6.4 Worked Example

In order to use Equation (6.14) for practical purposes, structural engineers should first determine the maximum lateral deflections for each level (d_i) from dynamic analysis of the fixed based model. Then, by having d_i values for each level and determining the site and structural characteristics including the shear wave velocity of the subsoil (V_s), the bedrock depth (h_s), the height of the structure *(h)*, the foundation width (*B*), the soil density (ρ), the modulus of elasticity of the structural material (E_{str}), and appropriate analysis type factor (λ), the lateral storey deflections for each level under the influence of SSI ($\tilde{d}_i$) can be estimated from Equation (6.14).

In this section, as a worked example of using the proposed simplified design procedure, a 15 storey intermediate moment resisting building frame 45 m high and 12 m wide (h=45 m and B=12 m) with structural ductility factor (μ) of 3 and performance factor (S_p) of 0.67 has been selected and modelled in FLAC2D adopting soil density (ρ) of 1470 kg/m^3 and modulus of elasticity of the structural material (E_{str}) of 28600 *MPa*. Dynamic analysis is performed on the fixed base model adopting conventional elastic analysis procedure (λ=33800), applying Northridge, 1994 (Figure 5.3) earthquake ground motion. The results of dynamic analysis in terms of maximum lateral deflections for each storey are derived from FLAC2D history record and presented in Figures 6.5 and 6.6 as the fixed base results. The fixed base results represent the lateral storey deflections at level *i* for the fixed base structure (d_i) in Equation (6.14). Having d_i values for each storey as well as the height of the structure *(h)*, the foundation width (*B*), the soil density

(ρ), the modulus of elasticity of the structural material (E_{str}), and analysis type factor (λ), the lateral storey deflection at level *i* under the influence of SSI ($\tilde{d}_i$) are determined for each storey using Equation (6.14) for the following cases:

- Variable shear wave velocities for the subsoil adopting soil classes C_e, D_e, and E_e (Figure 6.5) assuming the bedrock depth of 30 m; and
- Variable bedrock depths including h_s=10 m, 20 m, and 30 m adopting shear wave velocity of the subsoil equal to 150 m/s (Figure 6.6).

Figures 6.5 and 6.6 illustrate the calculated lateral storey deflections at each level under the influence of SSI ($\tilde{d}_i$), obtained from Equation (6.14) for two mentioned cases.

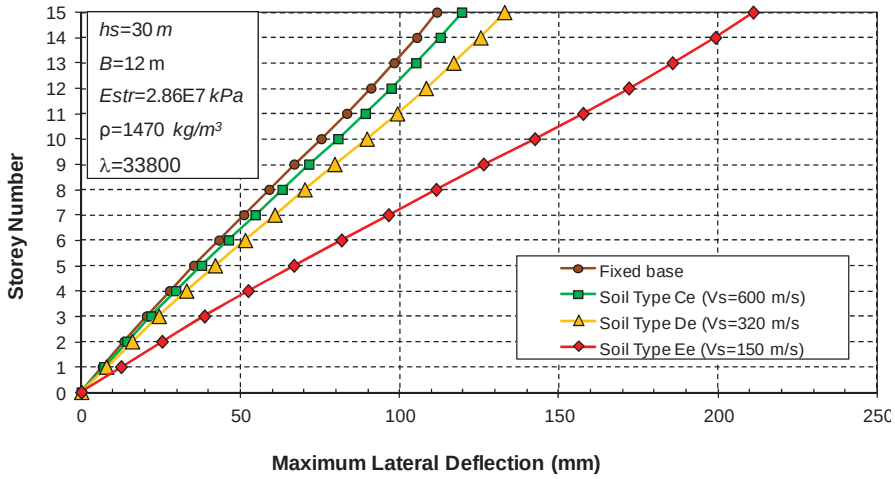

Figure 6.5: Determined lateral storey deflections at each level for 15 storey building resting on soil classes C_e, D_e, and E_e

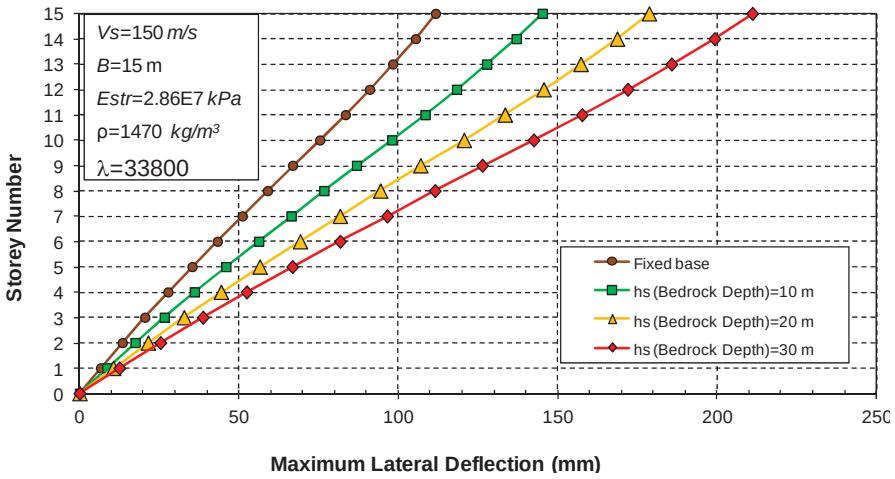

Figure 6.6: Determined lateral storey deflections at each level for 15 storey building resting on soil class E_e with variable bedrock depths

Having the lateral storey deflections, the corresponding inter-storey drifts under the influence of soil-structure interaction for each two adjacent stories have been determined (Figures 6.7 and 6.8) using Equation (5.3) in Chapter 5. It is now possible to check the inter-storey drifts of the building frame against the limiting value of 1.5% for life safe performance level.

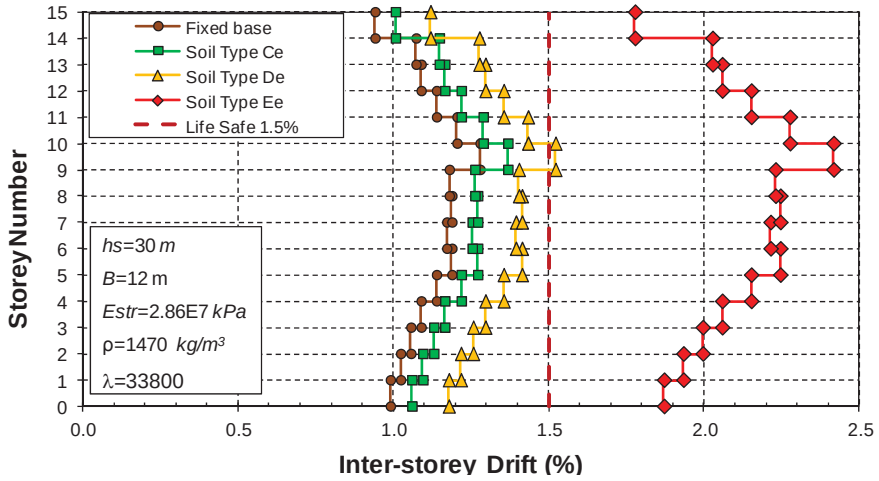

Figure 6.7: Inter-storey drifts for 15 storey building resting on soil classes C_e, De, and E_e

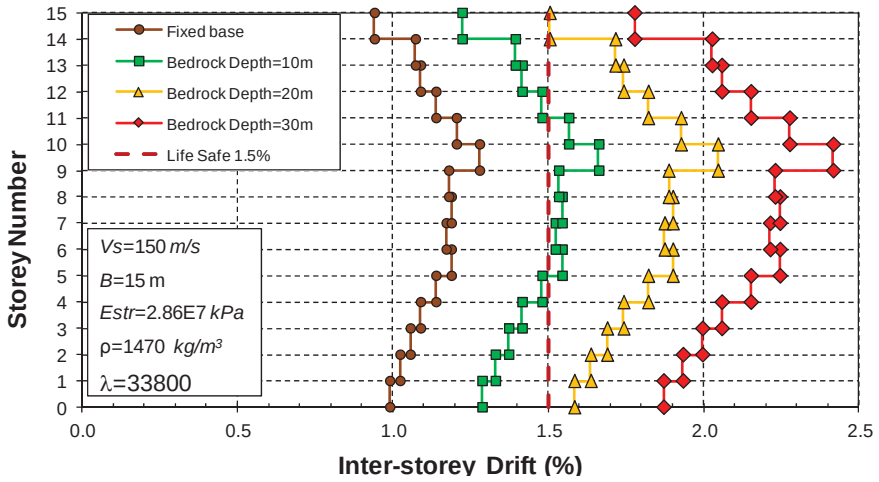

Figure 6.8: Inter-storey drifts for 15 storey building resting on soil class E_e with variable bedrock depths

Inter-storey drifts, shown in Figures 6.7 and 6.8, clearly illustrate that by reducing the shear wave velocity of the subsoil or increasing the bedrock depth, performance level of the 15 storey moment resisting building frame changes from life safe to near collapse level when SSI is considered in the analysis, which is dangerous and safety threatening.

In addition, comparing the calculated inter-storey drifts (Figures 6.7 and 6.8) with the results of numerical analyses (Figures 5.16c and 5.19c), it is noted that numerical and calculated results are in a good agreement. Therefore, the proposed simplified method can reproduce the results of numerical analysis with acceptable accuracy. Using the proposed simplified method, it can be ensured that performance levels of the mid-rise moment resisting building frames under the influence of SSI remain in life safe level, and the seismic design is safe and reliable.

6.5 Summary

In this chapter, in order to consider the amplification of lateral deflections and corresponding inter-storey drifts under the influence of soil-structure interaction in seismic design of regular mid-rise moment resisting building frames, a simplified design procedure has been proposed. The proposed design procedure enables structural engineers to extract the maximum lateral deflections for each storey under the influence of SSI from Equation (6.14) in this chapter by having the lateral storey deflections at *(i)* level for the fixed base structure (d_i), the shear wave velocity of the subsoil (V_s), the bedrock depth (h_s), the storey height *(h)*, the foundation width (B), the soil density (ρ), the modulus of elasticity of the structural material (E_{str}), and analysis type factor (λ) for elastic or inelastic structural analysis. Then, inter-storey drifts under the influence of soil-structure interaction for each two adjacent stories can be determined and checked against the limiting value of 1.5% for life safe performance level. Thus, detrimental effects of soil-structure interaction can be captured more precisely in the seismic design procedure of regular mid-rise moment resisting building frames to ensure the design safety and reliability. The proposed simplified procedure can be employed for practical purposes by structural engineers and engineering companies, as a reliable and accurate method of considering SSI effect in the seismic design procedure. The proposed simplified design procedure can only be employed in seismic design of regular mid-rise moment resisting building frames resting on shallow foundations with no embedment depth and does not cover irregular and high-rise buildings as well as building structures resting on pile foundations.

CHAPTER SEVEN

7. CONCLUSIONS AND RECOMMENDATIONS

7.1 Conclusions

The importance of SSI both for static and dynamic loads has been well established and the related literature covers at least 30 years of computational and analytical approaches to solve soil–structure interaction problems. Since 1990s, great effort has been made for substituting the classical methods of design by the new ones based on the concept of performance-based seismic design. Furthermore, the necessity of estimating the vulnerability of existing structures and assessing reliable methods for their retrofit have greatly attracted the attention of engineering community in most seismic zones throughout the world. Furthermore, the ground motions in seismic regions in Asia-Pacific such as New Zealand, Indonesia, and some parts of Australia will most probably govern the design of lateral resisting systems of the buildings. Thus, there is a strong need to develop design tools to evaluate seismic response of structures considering the foundation flexibility and subsoil conditions.

In this thesis, an enhanced numerical soil-structure model has been developed and proposed to capture structural plasticity and soil nonlinearity simultaneously, treating the behaviour of soil and structure with equal rigor. The soil-structure model employs beam structural elements to model beams, columns and foundation slabs. The structural elements are capable of capturing both elastic and inelastic structural behaviour as well as structural geometric nonlinearity (large displacements) in dynamic analysis. The soil medium consists of two dimensional plane-strain quadrilateral elements. Nonlinear behaviour of the soil medium has been captured using backbone curves of shear modulus ratio versus shear strain (G/G_{max} - γ) and damping ratio versus shear strain (ξ - γ) adopting Mohr-Coulomb constitutive model. Adopting direct method of analysis, the numerical model can perform fully nonlinear time history dynamic analysis to simulate realistic dynamic behaviour of soil and structure under seismic excitations accurately. Fully nonlinear method precisely follows any prescribed nonlinear constitutive relation and adopts hysteretic damping algorithm enabling strain-dependent modulus (G/G_{max} - γ) and damping functions (ξ - γ) to be

incorporated directly in the analysis to capture the hysteresis curves and energy-absorbing characteristics of real soil. Interface elements represented by normal and shear springs between soil and structure are utilised to simulate frictional contact between two planes contacting each other, with the interface shear strength defined by the Mohr-Coulomb failure criterion. In order to avoid reflection of outward propagating waves back into the model, quiet (viscous) boundaries comprising independent dashpots in the normal and shear directions are placed at the lateral boundaries of the soil medium. The lateral boundaries of the main grid are coupled to the free-field grids by viscous dashpots of quiet boundaries at the sides of the model to simulate the free-field motion which would exist in the absence of the structure. Horizontal distance of the soil lateral boundaries assumed to be 60 metres and the maximum bedrock depth is 30 metres. Rigid boundary condition is assigned to the bedrock. Since the adopted numerical soil-structure model is a Multi Degree of Freedom (MDOF) structure, inter-storey drifts can be estimated and employed to investigate the performance levels of the building structures under the influence of dynamic soil-structure interaction.

In the experimental investigation, performed in the UTS civil laboratories, a soil-structure model has been employed with geometric scaling factor of 1:30. Unlike past shaking table experiments which were performed without the structure or employed simplified SDOF (single Degree of Freedom) oscillators, the adopted soil-structure model is a Multi Degree of Freedom (MDOF) structure simulating most of the structural properties of the real prototype building such as frequency of vibrations, number of stories, and mass. Therefore, this experiment is a unique experimental shaking table test considering the structural model in the soil-structure system precisely. The adopted soil model is a clay mixture consisting of kaolinite, bentonite, class F fly ash, lime, and water with its properties extracted after conducting the required tests such as bender element tests and Unconfined Compression tests (UC) to determine the shear wave velocity and the shear strength of the soil, respectively. In addition, in order to perform rigorous and reliable experimental tests, laminar soil container, which is an advanced and suitable soil container for shaking table tests and its lateral movements in the dynamic tests are almost identical to the free field movements in reality, was employed. Experimental shaking table tests were performed on the soil-structure model under the influence of

four scaled earthquake acceleration records and the results were measured. Then, the maximum structural lateral and vertical displacements predicted by the numerical soil-structure model were determined and compared with the experimental results. Comparing the predicted and observed values of lateral and vertical structural displacements, it is understood that the numerical predictions and laboratory measurements are in a good agreement. Therefore, the numerical soil-structure model can replicate the behaviour of real soil-structure system with acceptable accuracy. Thus, it is concluded that the proposed numerical soil-structure model is a valid and qualified method of simulation with sufficient accuracy which can be employed for further dynamic soil-structure interaction numerical investigations. In addition, according to the experimental results, it is noted that the lateral deflections of flexible base model have evidently amplified in comparison to the fixed base model. As a result, performance level of the structural model may change extensively (e.g. from life safe to near collapse level), which may be extremely dangerous and safety threatening. Thus, it is experimentally observed that dynamic soil-structure interaction plays a significant role in seismic behaviour of moment resisting building frame resting on relatively soft soils.

In order to have a clear and comprehensible conclusion regarding the effects of structural height, subsoil stiffness, and bedrock depth on elastic and inelastic seismic response of regular mid-rise moment resisting building frames under the influence of SSI, a comprehensive numerical investigation has been conducted. In this study, 5 10, and 15 storey structural models resting on soil classes C_e (V_s=600*m/s*), D_e (V_s=320*m/s*), and E_e (V_s=150*m/s*), having three bedrock depths of 10 m, 20 m, and 30 m were adopted. According to the results, it is observed that the base shear of the structures modelled with soil as flexible base are generally less than the base shear of the structures modelled as fixed base for both elastic and inelastic cases. In addition, it is realised that the lateral deflections and corresponding inter-storey drifts of flexible base models resting on soil class C_e do not differ much from fixed base models for both elastic and inelastic analysis cases. Thus, performance level of regular mid-rise moment resisting building frames resting on soil class C_e remains in life safe level and soil-structure interaction effects are insignificant in both elastic and inelastic analysis cases. However, lateral deflections and inter-storey drifts of flexible base models resting on soil classes D_e and E_e (in particular for 10 storey

building frames or higher resting on more than 20 metres of soil class D_e and building frames higher than 5 storey resting on soil class E_e irrespective of the bedrock depth) extensively increase in comparison with fixed base models. In general, as shear wave velocity (V_s) and shear modulus (G_{max}) of the subsoil decrease or bedrock depth (h_s) increases, the base shear of flexible base models in comparison with fixed base models decrease, while lateral deflections and corresponding inter-storey drifts increase relatively. The amplification of the lateral deflections and corresponding inter-storey drifts of flexible base models resting on soil classes D_e and E_e can change the performance level of the structures from life safe to near collapse or total collapse which is absolutely dangerous and safety threatening for both elastic and inelastic analysis cases. As a result, soil-structure interaction has significant effects on elastic and inelastic seismic responses of regular mid-rise moment resisting building frames resting on soil classes D_e and E_e. It can be concluded that the conventional elastic and inelastic design procedures excluding SSI may not be adequate to guarantee the structural safety of regular mid-rise moment resisting building frames resting on soft soil deposits.

Based on the numerical investigation results, a simplified design procedure has been proposed in this thesis. The simplified design procedure determines amplification of lateral deflections and corresponding inter-storey drifts under the influence of soil-structure interaction in seismic design of regular mid-rise moment resisting building frames. Based on the proposed simplified design procedure, the maximum lateral deflections for each storey under the influence of SSI can be extracted from Equation (6.14) in Chapter 6 of this thesis. Then, inter-storey drifts under the influence of soil-structure interaction for each two adjacent stories can be determined and checked against the limiting value of 1.5% for life safe performance level. As a result, detrimental effects of soil-structure interaction can be captured more precisely in the seismic design procedure of regular mid-rise moment resisting building frames to ensure the design safety and reliability. The proposed simplified procedure can be employed for practical purposes by structural engineers and engineering companies, as a reliable and accurate method of considering SSI effect in the seismic design procedure.

7.2 Recommendations and Future Works

Since the purpose of this research work was to focus on determining the seismic response of regular mid-rise moment resisting building frames resting on various soil types, further numerical and experimental studies and some refinements are recommended to make this research work more comprehensive for practical applications. Future research work may be carried out in the following areas:

1. Conduct the numerical and experimental investigations, adopted in this study, to determine seismic response of regular *high-rise* moment resisting building frames resting on various soil types under the influence of SSI. In this way, the proposed simplified design procedure covers wider range of seismic problems in engineering practice.
2. Extend the numerical model as well as physical shaking table model to consider pile foundations underneath including floating piles and end bearing piles with different section properties and arrangements. In this case, determining seismic response of structures resting on very soft soils (V_s<150*m/s*) under the influence of SSI would be achievable and the boundaries of the proposed simplified procedure could be extended.
3. Extend the numerical model to consider the structural elements as solid elements. As a result, the structural member connections can be simulated and the effects of SSI on seismic design of different types of structural connections can be investigated.
4. Perform the numerical parametric study, presented in this thesis, to determine the effects of structural material strength variation on seismic design of building frames under the influence of SSI. Therefore, a wider range of construction materials e.g. structural steel, timber, composite, and pre-stressed concrete can be taken into consideration in the numerical investigations.
5. Carry out the numerical parametric study to determine the effects of foundation embedment depth, layered soils, Plasticity Index and confining pressure variation on seismic response of building frames considering SSI. Thus, broader range of soil and foundation characteristics can be examined and investigated in the numerical parametric study.

REFERENCES

ACI318-2008, *Building Code Requirements for Structural Concrete*, American Concrete Institute, Detroit, Michigan.

Adam, M, Chouw, N & Estoff, O. 2005, 'Significance of Soft Local Site in Altering the No-Uniform Ground Motions and the Building Response', *Al-Azhar University Engineering Journal*, vol. 8, no. 1, pp. 154-169.

Alavi, B. & Krawinkler, H. 2004, 'Behaviour of Moment Resisting Frame Structures Subjected to Near-fault Ground Motions', *Earthquake Engineering and Structural Dynamics*, vol. 33, no. 6, pp. 687-706.

Anderson, D.G. & Richart, F.E. 1976, 'Effects of Straining on Shear Modulus of Clays', *Journal of Geotechnical Engineering*, vol. 102, no. 9, pp. 975-987.

Ambrosini, R.D. 2006, 'Material Damping vs. Radiation Damping in Soil–Structure Interaction Analysis', *Computers and Geotechnics*, vol. 33, no. 2, pp. 86–92.

AS/NZS1170.01-2002, *Structural Design Actions - Part 0: General Principles*, Australian Standards, Sydney.

AS/NZS1170.1-2002, *Structural Design Actions - Part 1: Permanent, imposed and other actions*, Australian Standards, Sydney.

AS/NZS 3678-2011, *Structural Steel - Hot-rolled plates, floor plates and slabs*, Australian Standards, Sydney.

AS1170.4-2007, *Structural Design Actions - Part 4: Earthquake Actions in Australia*, Australian Standards, Sydney.

AS 1289.3.5.1-2006, *Methods of testing soils for engineering purposes, Determination of the soil particle density of a soil-standard method*, Australian Standards, Sydney.

AS3600-2009, *Concrete Structure*s, Australian Standards, Sydney.

AS5101.4-2008, *Methods for preparation and testing of stabilised materials, Method 4: unconfined compressive strength of compacted materials*, Australian Standards, Sydney.

ATC-40-1996, *Seismic Evaluation and Retrofit of Concrete Buildings*, Volume 1, Applied Technology Council, Redwood City, CA.

Azarbakht, A. & Ashtiany, M.Gh. 2008, 'Influence of the Soil-Structure Interaction on the Design of Steel-Braced Building Foundation', *2008 Seismic Engineering: Commemorating the 1908 Messina and Reggio Calabria Earthquake, Conference AIP Conference Proceedings*, vol. 1020, pp. 595-601.

Baker, A.L.1957, *Raft Foundations*, 3th edn, Concrete Publications Ltd, London.

Balenda, T. & Heidebrecht, A.C. 1986, 'Influence of Different Sites on Seismic Base Shear of Buildings', *Earthquake Engineering & Structural Dynamics*, vol. 14, no. 4, pp. 623-642.

Bathurst, R.J, Keshavarz, A., Zarnani, S. & Take. W. 2007, 'A Simple Displacement Model for Response Analysis of EPS Geofoam Seismic Buffers', *Soil Dynamics and Earthquake Engineering*, vol. 27, no.4, pp. 344-353.

Beaty, M.H., & Byrne, P.M. 2001, 'Observations on the San Fernando Dams', *In Proceedings of 4th International Conference on Recent Advances in Geotechnical Earthquake Engineering and Soil Dynamics*, San Diego, California, March 26-31, University of Missouri-Rolla, pp. 339-347.

Borja, R.I., Wu, W.H., Amies, A.P. & Smith, H.A. 1994, 'Nonlinear Lateral, Rocking and Torsional Vibration of Rigid Foundations', *Journal of Geotechnical Engineering*, vol. 120, no. 3, pp. 491-513.

Bowles, J.E. 1996, *Foundation Analysis and Design*, McGraw-Hill International Editions, 5th edn, Civil Engineering Series.

Brown, C.B., Laurent, J.M. & Tilton. J.R. 1977, 'Beam-plate System on Winkler Foundation', *Journal of the Engineering Mechanics*, vol. 103, no. 4, pp. 589-600.

Bray, J.D. & Dashti, S. 2012, 'Liquefaction-Induced Building Movements', *2nd International Conference on Performance-Based Design in Earthquake Geotechnical Engineering*, Taormina, Italy, May 2012.

Brebbia, C.A., Telles, J. C.F. & Wrobel, L.C. 1984, 'Boundary Element Techniques', Springer-Verlag.

BSSC-2003, *The 2003 NEHRP Recommended Provisions For New Buildings And Other Structures*, FEMA 450, Federal Emergency Management Agency, Washington, DC.

Byrne, P.M., Naesgaard, E. & Seid-Karbasi, M. 2006, 'Analysis and Design of Earth Structures to Resist Seismic Soil Liquefaction', *59th Canadian Geotechnical Conference & 7th Joint CGS/IAH-CNC Groundwater Specialty Conference*, Vancouver, Canada, October 2006, pp. 1-24.

Byrne, P.M., & Wijewickreme, D. 2006, 'Liquefaction Resistance and Post-Liquefaction Response of Soils for Seismic Design of Buildings in Greater Vancouver, *59th Canadian Geotechnical Conference & 7th Joint CGS/IAH-CNC Groundwater Specialty Conference*, Vancouver, Canada, October 2006, pp. 1267-1278.

Chandler, R., Clancy, J., Dixon, D., Goody, J. & Wooding, G. 2010, *Building Type Basics for Housing*, John Wiley & Sons, Inc. Hoboken, New Jersey.

Carbonari, S., Dezi, F. & Leoni, G. 2012, 'Nonlinear Seismic Behaviour of Wall-frame Dual Systems Accounting for Soil–Structure Interaction', *Earthquake Engineering and Structural Dynamics*, DOI: 10.1002/eqe.1195.

Carr, A.J. 2008, *Soil-Structure Interaction*, Advanced nonlinear seismic structural analysis notes, Pavia.

Chau, K.T., Shen, C.Y. & Gou, X. 2009, 'Nonlinear Seismic Soil-Pile-Structure Interactions: Shaking Table Tests and FEM Analyses', *Soil Dynamics and Earthquake Engineering*, vol. 29, no. 29, pp. 300-310.

Chen, J., Shi, X. & Li, J. 2010, 'Shaking Table Test of Utility Tunnel under Non-uniform Earthquake Wave Excitation', *Soil Dynamics and Earthquake Engineering*, vol. 30, no. 11, pp. 1400-1416.

Chopra, A.K. & Gutierres, J.A. 1973, *Earthquake Analysis of Multistorey Buildings Including Foundation Interaction*, ReportNo.EERC73-13, University of California, Berkeley.

Chopra, A.K. & Gutierres, J.A. 1978, 'A Substructure Method for Earthquake Analysis of structures Including Structure-Soil Interaction', *Earthquake Engineering & Structural Dynamics*, vol. 6, no. 1, pp. 51-69.

Churchman, G.J., Askary, M., Peter, P., Wright, M., Raven M.D. & Self P.G. 2002, 'Geotechnical Properties Indicating Environmental Uses for an Unusual Australian Bentonite', *Applied Clay Science*, vol. 20, no. 4, pp. 199-209.

Computers and Structures, Inc. 2009, *CSI Analysis Reference Manual for SAP2000*, Berkeley, California, USA.

Conniff, D.E, & Kiousis, P.D. 2007, 'Elasto-plastic Medium for Foundation Settlements and Monotonic Soil–Structure Interaction under Combined Loadings', *Journal for Numerical and Analytical Methods in Geomechanics*, vol. 31, no. 6, pp. 789-807.

Craig, H. 2000, *Soil Mechanics*, Chapman and Hall, London.

Cundall, P.A. 1976, 'Explicit Finite Difference Methods in Geomechanics', *Proceedings of the EF Conference on Numerical Methods in Geomechanics, Blacksburg*, Virginia, 1976), pp. 132-150.

Cundall, P.A. & Hart, R.D. 1992, 'Numerical Modeling of Discontinua', *Engineering Computations*, vol. 9, no. 2, pp. 101-113.

Cundall, P.A., Hansteen, H., Lacasse, S. & Selnes, P.B. 1980, *NESSI – Soil Structure Interaction Program for Dynamic and Static Problems*, Norwegian Geotechnical Institute, Report 51508-9, December 1980.

Das, B.M. 1983, *Fundamental of Soil Dynamic*, Elsevier Science Publishing Co., Inc. ISBN 0-444-00705-9.

Detournay, C. & Hart, R. 1999, *FLAC and Numerical Modelling in Geomechanics, A.A. Balkema*, Rotterdam, Netherland, ISBN 90-5809-074-4

Desai, C.S. & Christian, J.T. 1977, *Numerical Methods in Geomechanics*, McGraw-Hill, New York.

Desai, C.S., Abel, J.F. 1987, *Introduction to the finite Element Method: A Numerical Method for Engineering Analysis*, CBS Publishers and Distributors.

Desai, C.S., Phan, H.V. & Perumpral, J.V. 1982, 'Mechanics of Three Dimensional Soil–Structure Interaction', *Journal of Engineering Mechanics*, vol. 108, no. 5, pp. 731-47.

DIN EN 1998-5, 2010-2012, *Eurocode 8: Design of structures for earthquake resistance - Part 5: Foundations, retaining structures and geotechnical aspects*, European Committee for Standardisation.

Dutta, C.H. & Roy, R. 2002, 'A Critical Review on Idealization and Modelling for Interaction Aamong Soil–Foundation–Structure System', *Computers and Structures*, vol. 80, no. 3, pp. 1579-1594.

Dutta, C.H., Bhattacharya, K. & Roy, R. 2004, 'Response of Low-rise Buildings under Seismic Ground Excitation Incorporating Soil-Structure Interaction', *Soil Dynamic and Earthquake Engineering*, vol. 24, no. 9, pp. 893-914.

Endo, O. & Komanobe, K. 1995, 'Single and Multi Directional Shaking Table Tests on Sand Liquefaction', *Proceedings of the First International Conference on Earthquake Geotechnical Engineering*, IS-Tokyo, pp. 675-680.

El Ganainy, H. & El Naggar, M.H. 2009, 'Seismic Performance of Three-dimensional Frame Structures with Underground Stories', *Soil Dynamics and Earthquake Engineering*, vol. 29, no. 9, pp. 1249-1261.

FEMA 273-1997, *NEHRP Guidelines for the Seismic Rehabilitation of Buildings*, prepared by the Applied Technology Council for FEMA, Federal Emergency Management Agency , Washington, D.C.

Filonenko, B.M. 1940, *Some Approximate Theories of Elastic Foundation*, Uchenyie Zapiski Moskovskogo Gosudarstvennogo University, Mekhanica.

Galal, K. & Naimi, M. 2008, 'Effect of conditions on the Response of Reinforced Concrete Tall Structures to Near Fault Earthquakes', *The Structural Design of Tall and Special Buildings*, vol. 17, no. 5, pp. 541-562.

Gazetas, G. 1982, 'Vibrational Characteristics of Soil Deposits with Variable Wave Velocity', *International Journal for Numerical and Analytical Methods in Geomechanics*, vol. 6, no. 1, pp. 1-20.

Gazetas, G. 1991, *Foundation Vibrations*, *Foundation Engineering Handbook*, 2nd edn, H.Y. Fang, Ed., Van Nostrand Reinholds, Chapter 15, pp. 553-593.

Gazetas, G. & Mylonakis, G. 1998, 'Seismic Soil-Structure Interaction: New Evidence and Emerging Issues', *Geotechnical Special Publication 75, Geotechnical Earthquake Engineering and Soil Dynamics III*, American Society of Civil Engineers, Reston, Virginia, pp. 1119-1174.

Gemant, A. & Jackson,W. 1937, 'The Measurement of Internal Friction in Some Solid Dielectric Materials', *The London, Edinburgh, and Dublin Philosophical Magazine & Journal of Science*, vol. 22, no. 1, pp. 960-983.

Ghosh, S. & Wilson, E.L. 1969, *Analysis of Axi-symmetric Structures under Arbitrary Loading*, EERC Report No. 69-10, University of California, Berkeley.

Gohl, W.B. & Finn, W.D.L. 1987, 'Seismic Response of Single Piles in Shaking Table Studies', *Proceedings of the Fifth Canadian Conference Earthquake Engineering*, p. 435-444.

Gouasmia1, A. & Djeghaba, K. 2010, 'Direct Approach to Seismic Soil-Structure Interaction Analysis-Building Group Case', *Engineering Structures and Technologies*, vol. 2, no. 1, pp. 22–30

Gulkan, P. 1991, 'Consistent Lumped Parameter Models for Unbounded Soil physical Representation', *Earthquake Engineering and Structural Dynamic*s, vol. 20, no. 1, pp.11-32.

Hadjian, A.H. 1998, 'Dependency of Soil-Structure Interaction Damping on Structure Slenderness', *Proceedings of the 6th U.S Conference on Earthquake Engineering*, EEIR.

Hall, J.R., Kissenpfennig, J.F. & Rizzo, P.C. 1976, 'Discussion on the Paper of Soil-Structure Interaction Analysis for Seismic Response', *Journal of Geotechnical Engineering*, vol. 6, no. 3, pp. 102.

Hardin, B.O. & Drnevich, V.P. 1972, 'Shear Modulus and Damping in Soils: Design Equations and Curves', *Journal of* Soil Mechanics *and Foundation*, vol.7, no. 8, pp. 667-692.

Hardin, B.O. 1978, 'The nature of stress-strain behaviour for soils', *Proceedings of the ASCE Geotechnical Engineering Division specialty conference*, June 19-21, Pasadena, CA, pp. 3-90.

Harris, H.G. & Sabnis, G.M. 1999, *Structural Modeling and Experimental Techniques*, 2nd edn, Boca Raton, CRC Press.

Hashiguchi, K. & Okayasu, T. 2000, 'Time-dependent Elasto-plastic Constitutive Equation Based on the Sub loading Surface Model and its Applications to Soils', *Soils and Foundations*, vol. 40, no. 4, pp. 19-36.

Horpibulsuk, S., Lie, M.D., Liyanapathirana, D.S. & Suebsuk, J. 2010, 'Behaviour of cemented clay simulated via the theoretical framework of the structured Cam Clay model', *Computers and Geomechanics*, vol. 37, no.1-2, pp.1-9.

Horvath, J.S. 1993, 'Beam-Column-Analogy Model for Soil-Structure Interaction Analysis', *Journal of Geotechnical Engineering-ASCE*, vol. 119, no. 2, pp. 358-64.

Hosseinzadeh N.A. & Nateghi, F. 2004, 'Shake table study of soil structure interaction effects on seismic response of single and adjacent buildings', *Proceedings of the13th World Conference on Earthquake Engineering*, Vancouver, B.C., Canada, Paper No.1918.

Hetenyi, M. 1946, *Beams on Elastic Foundations*, University of Michigan Press, Ann Arbor.

IBC 2012, *International Building Code*, International Code Council (ICC).

Iai, S. 1989, 'Similitude for Shaking Table Tests on Soil-Structure-Fluid Model in 1g Gravitational Field', *Soils and Foundations*, vol. 29, no. 1, pp. 105-118.

Ishimura, K., Ohtsuki, A., Yoloyama, K. & Koyanagi, Y. 1992, 'Sway-rocking Model for Simulating Nonlinear Response of Sandy Deposit with Structure', *Proceedings of the Tenth World Conference on Earthquake Engineering*, pp. 1897-1903.

Itasca Consulting Group Inc. 2008, *FLAC2D: Fast Lagrangian Analysis of Continua*, version 6.0, User's manual, Minneapolis.

Itoh, T. 1973, 'Damped Vibration Mode Superposition Method for Dynamic Response Analysis', *Earthquake Engineering and structural Dynamics*, vol. 2, no. 6, pp. 47-57.

Iwan, W.D., Huang, C.T., & Guyader, A.C. 2000, 'Important Features of the Response of Inelastic Structures to Near-field Ground Motion', *Proceedings of the Twelfth World Conference on Earthquake Engineering*, New Zealand Society for Earthquake Engineering, New Zealand, Paper No. 1740.

Jafarzadeh, F. & Yanagisawa, E. 1995, 'Settlement of Sand Models under Unidirectional Shaking', *Proceedings of the First International Conference on Earthquake Geotechnical Engineering*, IS-Tokyo, pp. 693-698.

Jahromi, H.Z. 2009, 'Partitioned Analysis of Nonlinear Soil-Structure Interaction', PhD thesis in Civil Engineering, University of London, London.

Jakrapiyanun, W. 2002, 'Physical Modeling of Dynamics Soil-Foundation-Structure-Interaction Using a Laminar Container', PhD thesis, University of California, San Diego.

Jennings, P.C. & Bielak, J. 1973, 'Dynamics of Buildings–soil Interaction', *Bulletin of the Seismological Society of America*, vol. 63, pp. 9-48.

Kanatani, M., Nishi, K. & Touma, J. 1995, 'Large Shake Table Tests on Saturated Sand layer and Numerical Simulation by Nonlinear Analysis Method', *Proceedings of the First International Conference on Earthquake Geotechnical Engineering*, IS-Tokyo. pp. 705-710.

Karamodin, A.K. & Kazemi, H.H. 2008, 'Semi-active Control of Structures Using Neuro-Predictive Algorithm for MR Dampers', *Structural Control and Health Monitoring*, vol. 17, no. 3, pp. 237-253.

Katsikadelis, J. 2002, *Boundary Elements Theory and Applications*, Elsevier, Oxford.

Kerr, A.D. 1965, 'A Study of a New Foundation Model', *Acta Mechanica*, vol. 12, no. 2, pp. 135-47.

Khalil, L., Sadek, M. & Shahrour, I. 2007, 'Influence of the Soil–Structure Interaction on the Fundamental Period of Buildings', *Earthquake Engineering and Structural Dynamics*, vol. 36, no. 15, pp. 2445-2453.

Kline, S. 1965, *Similitude and Approximation Theory*, McGraw-Hill, New York.

Kobayashi, H., Seo, K. & Midorikawa, S. 1986, 'Estimated Strong Ground Motions in the Mexico City Earthquake', *The Mexico Earthquakes 1985, Factors Involved and Lessons Learned, Proceedings of the International Conference*, Camino Real Hotel, Mexico City, Mexico, pp. 97-111.

Kocak, S. & Mengi, Y. 2000, 'A Simple Soil-structure Interaction Model', *Applied Mathematical Modelling*, vol. 24, no. 8-9, pp. 607-635.

Koutromanos, I.A., Maniatakis, Ch.A. & Spyrakos, C.C. 2009, 'Soil-Structure Interaction Effects on Base-isolated Buildings Founded on Soil Stratum', *Engineering Structures*, vol. 31, no. 3, pp. 729-737.

Kramer, S.L. 1996, *Geotechnical Earthquake Engineering*, Prentice Hall civil engineering and engineering mechanics series, ISBN 0-13-374943-6.

Kramrisch, F. & Rogers, P. 1961, 'Simplified Design of Combined Footings', *Journal of the Soil Mechanics*, vol. 87, no. 5, vol. 19-44.

Krawinkler, H., Medina, R. & Alavi, B. 2003, 'Seismic Drift and Ductility Demands and Their Dependence on Ground Motions', *Engineering Structures*, vol. 25, no. 5, pp. 637-653.

Kuhlemeyer, R.L. & Lysmer, J. 1973, 'Finite Element Method Accuracy for Wave Propagation Problems', *Journal of the Soil mechanics and foundations Division, ASCE*, vol. 99(SM5), pp. 421-427.

Kumar, S. & Prakash, SH. 1998, 'Effect of Soil Nonlinearity on Natural Frequency Response of Structures', *Proceedings of the 6th U.S Conference on Earthquake Engineering*, EEIR.

Kunar, R.R., Beresford, P.J. & Cundall, P.A. 1977, 'A Tested Soil-Structure Model for Surface Structures', *Proceedings of the Symposium on Soil-Structure Interaction*, Meerut, India, pp. 137-144.

Kutan, M. & Elmas, M. 2001, 'Non-Linear Seismic Soil-Structure Interaction Analysis Based on the Substructure Method in the Time Domain', *Turkish Journal of Engineering & Environmental Sciences*, vol. 25, no. 6, pp. 617-626.

Langhaar, H. 1951, *Dimensional Analysis and Theory of Models*, John Wiley & Sons Inc., New York.

Lee, CH., Wei, Y. & Huo, Y. 2012, 'Boundary Effects of a Laminar Container in Centrifuge Shaking Table Tests', *Soil Dynamics and Earthquake Engineering*, vol. 34, no. 1, pp. 37-51.

Liao, W.I., Loh, CH. & Wan, S. 2001, 'Earthquake Responses of RC Moment Frames Subjected to Near Fault Ground Motions', *Structural Design of Tall Buildings*, vol. 10, no. 4, pp. 219-229.

Liua, M.Y., Chiangb, W.J, Hwangb, J.H. & Chub, C.R. 2008, 'Wind-induced Vibration of High-rise Building with Tuned Mass Damper Including Soil-Structure Interaction', *Journal of Wind Engineering and Industrial Aerodynamics*, vol. 96, no. 7, pp. 1092-1102.

Lu, J., Elgamal, A., Yan, L., Law, K.H. & Conte, J.P. 2011, 'Large-Scale Numerical Modeling in Geotechnical Earthquake Engineering', *International Journal of Geomechanics*, vol. 11, no. 6, pp. 490-503.

Lu, X., Li, P., Chen, Y. & Chen B. 2004, 'Shaking Table Model Testing on Dynamic Soil-Structure Interaction System', *Proceedings of the 13th World Conference on Earthquake Engineering Vancouver*, B.C., Canada, August 1-6, 2004, Paper No. 3231.

Luco, J.E. 1980, 'Soil–Structure Interaction and Identification of Structural Models, *Proceedings of the 2nd ASCE Conference on Civil Engineering and Nuclear power*, vol. 2, no. 10, pp. 1-31.

Lysmer, J. 1965, 'Vertical Motions of Rigid Footings', PhD thesis in civil engineering, University of Michigan, Ann Arbor.

Lysmer, J. & Kuhlemeyer, R.L. 1969, 'Finite Dynamic Model for Infinite Media', *Journal of the Engineering Mechanics Division, ASCE*, vol. 95, no. 6, pp. 859-877.

Lysmer, J., and Waas, G. 1972, 'Shear Waves in Plane Infinite Structures', *Journal of the Engineering Mechanics Division, ASCE,* vol. 98(EM1), pp. 85-105.

Maheshwari, B.K. & Sarkar, R. 2011, 'Seismic Behavior of Soil-Pile-Structure Interaction in Liquefiable Soils: Parametric Study', *International Journal of Geomechanics*, vol. 11, no. 4, pp. 336-347.

Malvern, L. E. 1969, *Introduction in Mechanics of a Continuous Medium*, Englewood Cliffs, Prentice Hall, New Jersey.

Massumi, A. & Tabatabaiefar, H.R. 2008, 'A Criterion for Considering Soil-Structure Interaction Effects in Seismic Design of Ductile RC-MRFs According to Iranian Codes', *Proceedings of the 14th World Conference on Earthquake Engineering (14WCEE)*, Beijing, China.

Maugeri, M., Musumeci, G. Novita, D. & Taylor, C.A. 2000, 'Shaking Table Test of Failure of a Shallow Foundation Subjected to An Eccentric Load', *Soil Dynamics and Earthquake Engineering*, vol. 20, no. 5-8, pp. 435-444.

Meymand, P.J. 1998, 'Shaking Table Scale Model Tests of Nonlinear Soil-Pile-Superstructure Interaction in Soft Clay', PhD thesis in Civil Engineering, University of California, Berkeley.

Meymand, P.J., Riemer, M. & Seed, R.B. 2000, 'Large Scale Shaking Table Tests of Seismic Soil-Pile Interaction in Soft Clay', *Proceeding of the 12th world Congress on Earthquake Engineering*, Paper no. 0915.

Mirhashemian1, P., Khaji, N. & Shakib, H. 2009, 'Soil-Structure Interaction (SSI) Analysis Using a Hybrid Spectral Element/Finite Element (SE/FE) Approach', *Journal of Seismology and Earthquake Engineering*, vol. 11, no. 2, pp. 83-95.

Moncarz, P. & Krawinkler, H. 1981, *Theory and Application of Experimental Model Analysis in Earthquake Engineering*, Report No. 50, John Blume Earthquake Engineering Ctr., Stanford Univ.

Moss, R.E.S., Crosariol, V. & Kuo, S. 2010, 'Shake Table Testing to Quantify Seismic Soil-Structure Interaction of Underground Structures', *Proceedings of the 5th International Conference on Recent Advances in Geotechnical Earthquake Engineering and Soil Dynamics*, May 24-29, San Diego, Paper No. 1.27b.

Murray, H.H. 1999, 'Applied Clay Mineralogy Today and Tomorrow', *Clay Minerals*, vol. 34, no. 1, pp. 39-49.

Nateghi, F., Rezaei, A. & Behnamfar, F. 2006, 'Structure-Soil-Structure Effects on nonlinear Dynamic Response of Tall Buildings', *Proceedings of the First European Conference on Earthquake Engineering and Seismology*, Geneva, Switzerland, September 2006, Paper No. 206.

NBC 2010, *National Building Code of Canada (NBC)*, NRC Institute for Research in Construction, Canada.

Necettina, A. & Celebi, E. 2005, 'An Efficient Seismic Analysis Procedure for Torisionally Coupled Multistorey Building Including Soil-Structure Interaction', *Turkish Journal of Engineering*, vol. 29, no. 3, pp. 143-157.

Noda, T., Fernado, G. & Asaoka, A. 2000, 'Delayed Failure in Soft Clay Foundations', *Soils and Foundations*, vol. 40, no. 1, pp. 85-97.

Novak, M. 1972, 'Coupled Horizontal and Rocking Vibration of Embedded Footings', *Canadian Geotechnical*, vol. 9, no. 4, pp. 477-497.

Novak, M. 1973, *Vibration of Embedded Footing and Structures*, ASCE National Meeting, session No, 10, Soil & Rock Dynamics, San Francisco, preprint No.2029, P.25.

Novak, M. and Beredugo, Y.O. 1972, 'Vertical Vibration of Embedded Footings', *Journal of the Soil mechanics and foundations Division, ASCE*, vol. 98, no. 2, pp. 1291-1310.

NBCC 2010, *National Building Code of Canada*, National Research Council of Canada, Institute for Research in Construction, Ottawa, Ontario.

NZS1170.5-2007, *Structural Design Actions - Part 5: Earthquake Actions-New Zealand*, New Zealand Standards, Wellington.

PEER 2012, *PEER Ground Motion Database*, Pacific Earthquake Engineering Research Centre, University of California, Berkeley, CA.

Pitilakis, D., Dietz, M., Wood, D.M., Clouteau, D. & Modaressi, A., 2008, 'Numerical Simulation of Dynamic Soil-Structure Interaction in Shaking Table Testing', *Soil Dynamics and Earthquake Engineering*, vol. 28, pp. 453-467.

Pitilakis, K. & Terzi, V. 2011, *'Experimental and theoretical SFSI studies in a model structure in Euroseistest*', Chapter 7 at the book Special Topics in Advances in Earthquake Geotechnical Engineering, Book Series: Geotechnical, Geological and Earthquake Engineering, Editors: Mohamed Sakr & Atilla Ansal, Springer Science & Business Media B.V.

Popov, E.P. 1951, 'Successive Approximation for Beams on Elastic Foundations', *Trans ASCE*, vol. 116, no. 2, pp. 1083-108.

Prasad, S., Towhata, I., Chandradhara, G. & Nanjundaswamy, P. 2004, 'Shaking Table Tests in Earthquake Geotechnical Engineering', *Current science*, vol. 87, no. 10, pp. 1398-1404.

Rahvar 2005, *Geotechnical and Geophysical Investigations and Foundation Design Report of Musalla Construction Site in Tehran*, P. O. Rahvar Pty Ltd., vol. 1, Tehran, pp. 1-64.

Rahvar 2006a, *Geotechnical Investigations and Foundation Design Report of Kooh-e-Noor Commercial Building*, P. O. Rahvar Pty Ltd., Final Report, Tehran, Iran, pp. 1-69.

Rahvar 2006b, *Geotechnical Investigations and Foundation Design Report of Mahshahr Train Station*, P. O. Rahvar Pty Ltd., Iran Railways Authority, Mahshahr, Iran, pp. 1-42.

Rayhani, M.H. & El Naggar, M.H. 2008, 'Numerical Modelling of Seismic Response of Rigid Foundation on Soft Soil', *International Journal of Geomechanics, ASCE*, vol. 8, no. 6, pp. 336-346.

Riemer, M., Gookin, W., Bray, J. & Wartman, J. 1998, 'Using Reflected Waves to Measure Small Strain Dynamic Properties', *Proceedings of the 5th Caltrans Seismic Research Workshop*, Sacramento, pp. 16-18.

Richards, J.R., Elms, D.G. & Budhu, M. 1990, 'Dynamic Fluidization of Soils', *Journal of Geotechnical Engineering*, vol. 116, no. 5, pp. 740-759.

Roesset, J.M. & Ettouney, M.M. 1977, 'Transmitting Boundaries: A Comparison', *International Journal of Numerical and Analytical Methods in Geomechanics*, vol. 1, no. 2, pp. 151-176.

Roesset, J.M., Whitman, R.V. & Dobry, R. 1973, 'Modal Analysis for Structures with Foundation Interaction', *Journal of the Structural Division, ASCE*, vol. 99, no. 4, pp. 399-416.

Roy, R., Craige, J.R. & Kurdila, A.J. 2006, *Fundamentals of Structural Dynamics*, 2nd edn, John Wiley & Sons Inc, New Jersey.

Tabatabaiefar, H.R. & Massumi, A. 2010, 'A Simplified Method to Determine Seismic Responses of Reinforced Concrete Moment Resisting Building Frames under Influence of Soil–Structure Interaction', *Soil Dynamics and Earthquake Engineering*, vol. 30, no. 11, pp. 1259-1267.

Tang, L., Ling, X., Xu, P., Gao, X. & Wang, D. 2009, 'Shake Table Test of Soil-Pile Groups-bridge Structure Interaction in Liquefiable Ground', *Earthquake Engineering and Engineering Vibration*, vol. 9, no. 1, pp. 1-12.

Tao, X., Kagawa, T., Minowa, C. & Abe, A. 1998, 'Verification of Dynamic Soil-Pile Interaction', *Proceedings of Geotechnical Special Publication No. 75, ASCE*, pp. 1199-1210.

Tavakoli, H.R., Naeej, M. & Salari. A. 2011, 'Response of RC Structures Subjected to Near Fault and Far Fault Earthquake Motions Considering Soil-Structure

Interaction', *International Journal of Civil and Structural Engineering*, vol. 1, no. 4, pp. 881-896.

Taylor, C.A. 1997, *Large Scale Shaking Tests of Geotechnical Structures*, Earthquake Engineering Research Centre, University of Bristol.

Taylor, C.A., Dar, A.R. & Crewe, A. J. 1995, 'Shaking Table Modelling of Seismic Geotechnical Problems', *Proceedings of the 10th European Conference on Earthquake Engineers*, Vienna, Austria, pp. 441-446.

Ter-Martirosyan, Z.G. 1992, 'Rheological Parameters of Soils and Design of Foundations', Oxford and IBH Publishing Company Limited, Shahpur Jat, New Delhi.

Turan, A., Hinchberger,S. & El Naggar, H. 2009, 'Design and Commissioning of a Laminar Soil Container for Use on Small Shaking Tables', *Soil Dynamics and Earthquake Engineering*, vol. 29, no. 2, pp. 404-414.

Safak, E. 1995, 'Detection and Identification of Soil–Structure Interaction in Buildings from Vibration Recordings', *Journal of Structural Engineering. ASCE*, vol. 121, no. 3, pp. 889-906.

Sato, H., Tanaka, Y., Kanatani, M., Tamari, Y. & Sugisawa, M. 1995, 'An Experimental and Numerical Study on the Behaviour of Improved Grounds', *Proceeding of the 1st International Conference on Earthquake Geotechnical Engineering*, IS-Tokyo, pp. 767-772.

Seed, H.B., & Idriss, I.M. 1969, 'Influence of Soil Conditions on Ground Motion During Earthquakes', *Journal of the Soil mechanics and foundations Division, ASCE*, vol. 95, no. 2, pp. 99-137.

Seed, H.B. & Lysmer, J. 1975, 'Soil–Structure Interaction Analysis for Seismic Response', Journal *of Geotechnical Engineering Division, ASCE*, vol. 101, no. 5, pp. 439-457.

Seed, H.B., Wong, R., Idriss, I.M. & Tokimatsu, K. 1986, 'Moduli and Damping Factors for Dynamic Analysis of Cohesionless Soil', *Journal of Geotechnical Engineering*, vol. 112, no. 11, pp. 1016-1032.

Shing, B.P. & Tanabe, T. 2001, *Modeling of inelastic behavior of RC structures under seismic loads*, Reston, VA, American Society of Civil Engineers.

Siddique, R. 2002, 'Effect of Fine Aggregate Replacement with Class F Fly Ash on the Mechanical Properties of Concrete', *Cement and Concrete Research*, vol. 33, no. 4, pp. 539-547.

Sivakumaran, K.S. 1990, 'Seismic Analysis of Mono-symmetric Multi-storey Buildings Including Foundation Interaction', *Journal of computers and Structures*, vol. 36 no. 1, pp. 99-107.

Sivakumaran, K.S. & Balendra, T. 1994, 'Seismic Analysis of Asymmetric Multi-storey Buildings Including Foundation Interaction and P-Δ Effects', *Engineering Structures*, vol. 16, no. 8, pp. 609-624.

Soo Ha, I., Olson, S.M., Seo, M. & Kim, M. 2011, 'Evaluation of Re-liquefaction Resistance Using Shaking Table Tests', *Soil Dynamics and Earthquake Engineering*, vol. 31, no. 4, pp. 682-691.

Stanton, J.F., Banerjee, S. & Hasayen, I. 1998, *Shaking Table Tests on Piles*, Final report, Research Project Y-2811, Task 26, Prepared for Washington State Transportation Communication.

Steedman, R.S. & Zeng, X. 1991, 'Physical Modelling of Earthquake Excitation for Geotechnical Engineering', *Proceedings of the 6th Canadian Conference Earthquake Engineering*, pp. 285-295.

Stewart, J.P., Seed, R.B. & Fenves, G.L. 1998, *Empirical Evaluation of Inertial* Soil–*Structure Interaction Effects*, PEER-1998/07, Pacific Earthquake Engineering Research Centre, University of California, Berkeley.

Stewart, J.P., Fenves, G.L. & Seed, R.B. 1999, 'Seismic Soil-Structure Interaction in Buildings: Analytical Aspects', *Journal of* Geotechnical *and* Geoenvironmental Engineering, *ASCE*, vol. 125, no. 1, pp. 26-37.

Sulaeman, A. 2010, 'The Use of Lightweight Concrete Piles for Deep Foundation on Soft Soils', PhD thesis in Civil Engineering, University of Tun Hussein Onn, Malaysia.

Sun, J.I., Golesorkhi, R. & Seed, B. 1998, *Dynamic Module and Damping Ratios for Cohesive Soils*, Earthquake Engineering Research Centre, Report No. UCB/EERC-88/15, University of California, Berkeley.

Valsangkar, A.J., Dawe, J.L. & Mita, K.A. 1991, 'Shake Table Studies of Seismic Response of Single Partially Supported Piles', *Proceeding of the 6th Canadian Conference Earthquake Engineering*, pp. 327-334.

Varun. 2010, 'A Non-linear Dynamic Macro-element for Soil-Structure Interaction Analysis of Piles in Liquefiable Sites', PhD thesis in Civil Engineering, Georgia Institute of Technology, Georgia.

Veletsos, A.S. & Meek, J.W. 1974, 'Dynamic Behaviour of Building-Foundation System', *Journal of Earthquake Engineering and Structural Dynamics*, vol. 3, no. 2, pp. 121-38.

Veletsos, A.S. & Prasad, A.M. 1989, 'Seismic Interaction of Structures and Soils: Stochastic Approach', *Journal of Structural Engineering, ASCE*, vol. 115, no. 4, pp. 935-956,

Vesic, A.B. 1961, 'Bending on Beams Resting on Isotropic Elastic Solid', *Journal of Engineering Mechanics Division, ASCE,* vol. 2, no. 87, pp. 35-53.

Viladkar, M.N., Godbole, P.N. & Garg, S.K. 1997, *Boundary Simulation for Dynamic Soil-Structure Interaction Problems*, ISBN 90 54 10 8878.

Vucetic, M. & Dobry, R. 1991, 'Effects of Soil Plasticity on Cyclic Response', *Journal of Geotechnical Engineering*, vol. 117, no. 1, pp. 89-107.

Wang, J. 2008, 'Modelling the Effects of Intrinsic Damping in Soil-Structure Interaction', Biennial Geotechnical Seminar Conference, pp. 1-8.

Wartman, J. 1996, 'A Laboratory Study of the Effects of Fly Ash on the Geotechnical Properties of Soft Clay', MEng thesis, University of California, Berkeley.

Wegel, R.L. & Walther, H. 1935, 'Internal Dissipation in Solids for Small Cyclic Strains', *Journal of Applied Physics*, vol. 6, no. 4, pp. 141-157.

Wilkins, M.L. 1964, 'Fundamental Methods in Hydrodynamics', *Methods in Computational Physics*, vol. 3, no. 1, pp. 211-263.

Wolf, J. 1985, *Dynamic Soil Structure Interaction*, Prentice Hall Co, New Jersey.

Wolf, J. 1994, *Foundation Vibration Analysis Using Simple Physical Models*, Prentice Hall Co, New Jersey.

Wolf, J. 1998, *Soil-Structure Interaction Analysis in Time Domain*, Prentice Hall Co, New Jersey.

Wolf, J.P. & Deeks, A.J. 2004, *Foundation Vibration Analysis: A Strength-of-Materials Approach*, Elsevier: Oxford, UK.

Yan, L. & Byrne, P.M. 1989, 'Application of Hydraulic Gradient Similitude Method to Small-scale Footing Tests on Sand', *Canadian Geotechnical Journal*, vol. 26, no. 2, pp. 246–259.

Yang, X.M., Chen, Y. & Yang, B.P. 2008, 'Three-Dimension Dynamic Soil-Structure Interaction Analysis Using the Substructure Method in the Time Domain', *Proceedings of the 14th World Conference on Earthquake Engineering*, October 12-17, 2008, Beijing, China.

Zen, K., Yamazaki, H., Toriihara, M. & Mori, T. 1992, 'Shaking Table Test on Liquefaction of Artificially Cemented Sands', *Proceedings of the 10th World Conference on Earthquake Engineering*, Madrid, Spain, pp. 1417-1420.

Zheng, J. & Takeda, T. 1995, 'Effects of Soil-Structure Interaction on Seismic Response of PC Cable-stayed Bridge', *Soil Dynamics and Earthquake Engineering*, vol. 14, no. 6, pp. 427–437.

APPENDIX A

Elastic and inelastic analyses results under the influence of Northridge (1994), Kobe (1995), El-Centro (1940), and Hachinohe (1968) earthquake ground motions

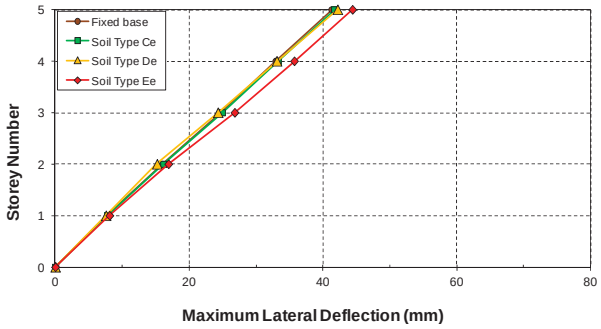

(a)

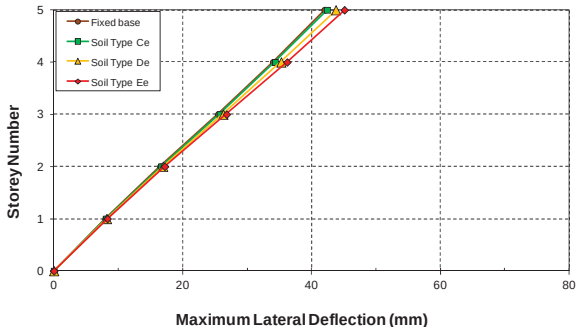

(b)

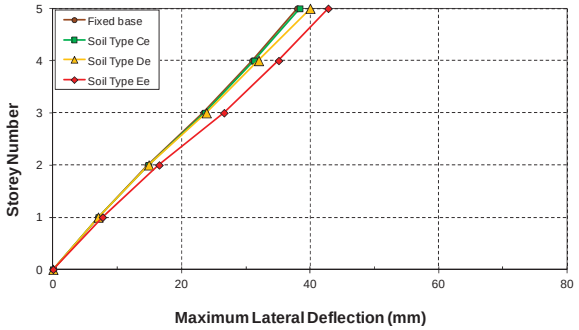

(c)

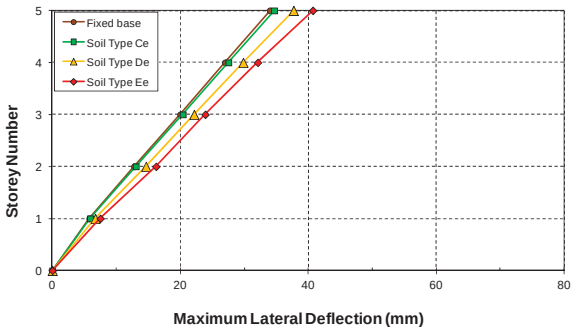

(d)

Figure A.1: Elastic storey deflections of model S5 resting on soil classes C_e, D_e, and E_e with bedrock depth of 30 metres; (a) Northridge (1994); (b) Kobe (1995); (c) El-Centro (1940); (d) Hachinohe (1968)

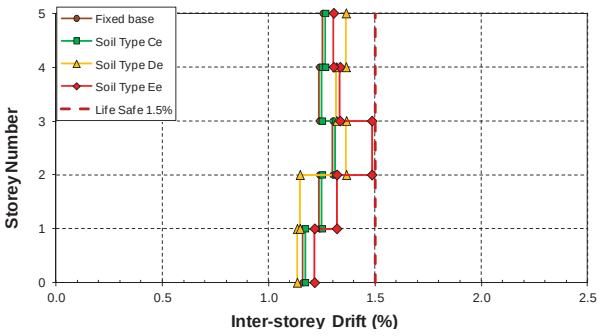

(a)

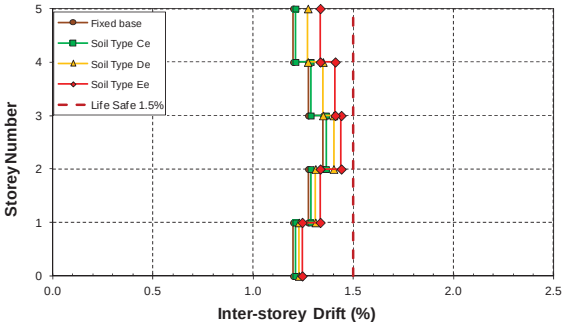

(b)

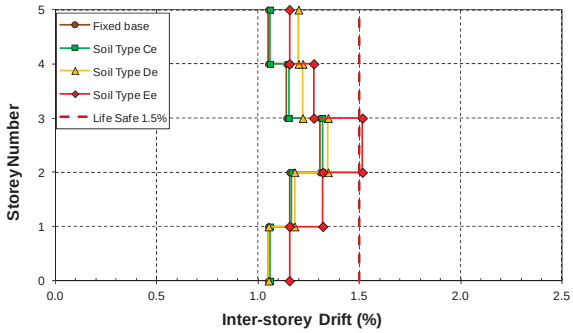

(c)

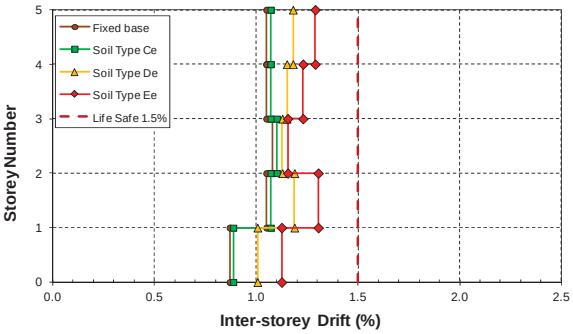

(d)

Figure A.2: Elastic inter-storey drifts of model S5 resting on soil classes C_e, D_e, and E_e with bedrock depth of 30 metres; (a) Northridge (1994); (b) Kobe (1995); (c) El-Centro (1940); (d) Hachinohe (1968)

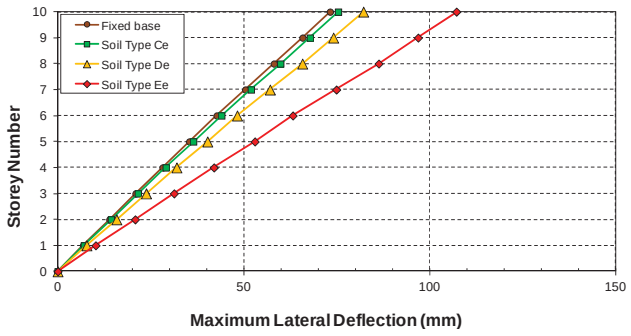

(a)

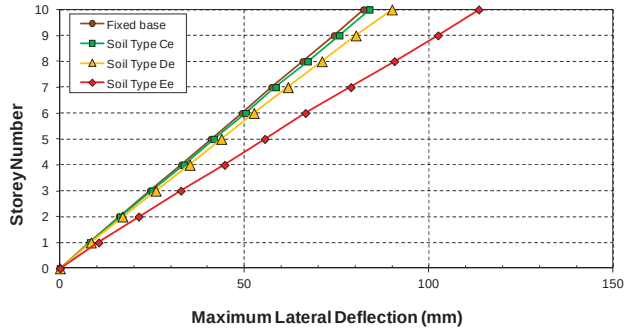

(b)

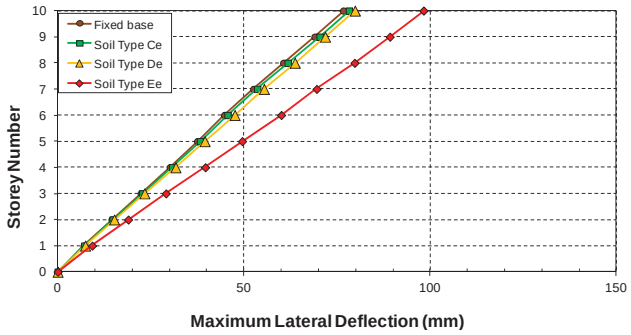

(c)

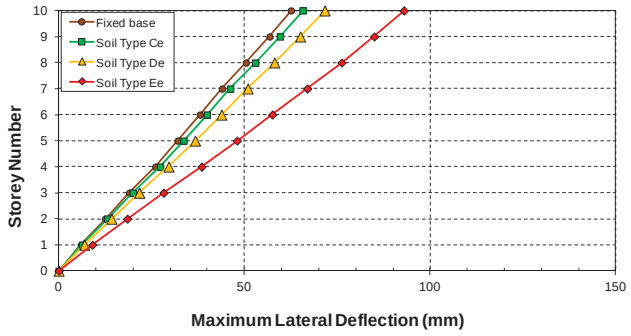

(d)

Figure A.3: Elastic storey deflections of model S10 resting on soil classes C_e, D_e, and E_e with bedrock depth of 30 metres; (a) Northridge (1994); (b) Kobe (1995); (c) El-Centro (1940); (d) Hachinohe (1968)

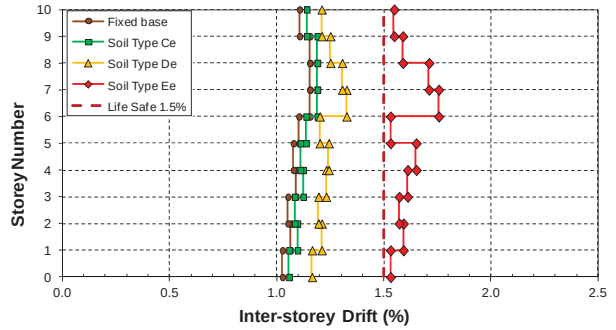

(a)

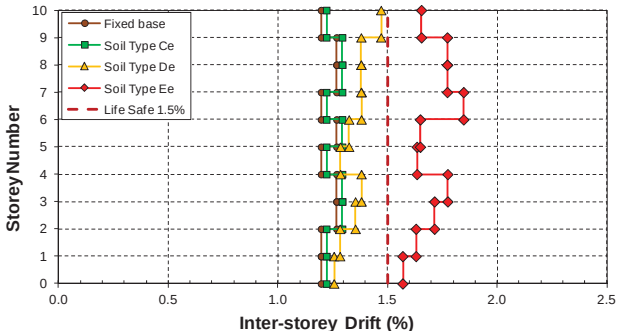

(b)

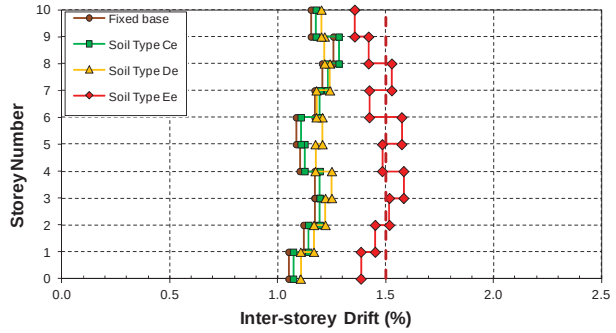

(c)

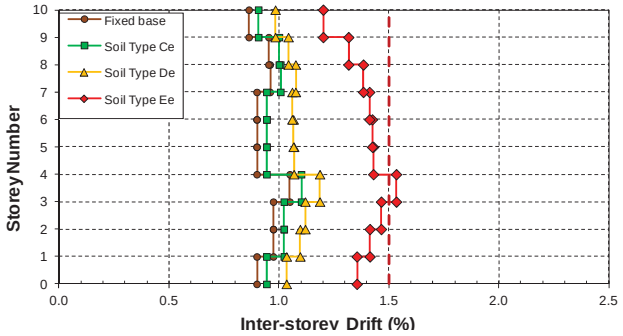

(d)

Figure A.4: Elastic inter-storey drifts of model S10 resting on soil classes C_e, D_e, and E_e with bedrock depth of 30 metres; (a) Northridge (1994); (b) Kobe (1995); (c) El-Centro (1940); (d) Hachinohe (1968)

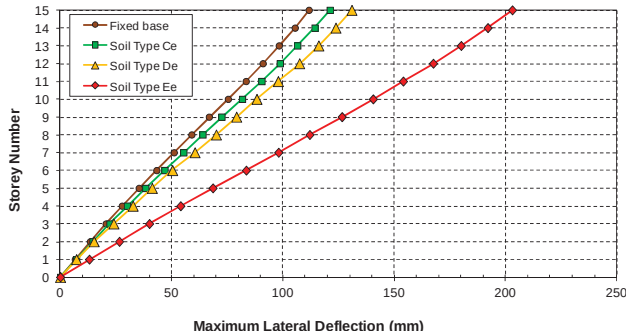

(a)

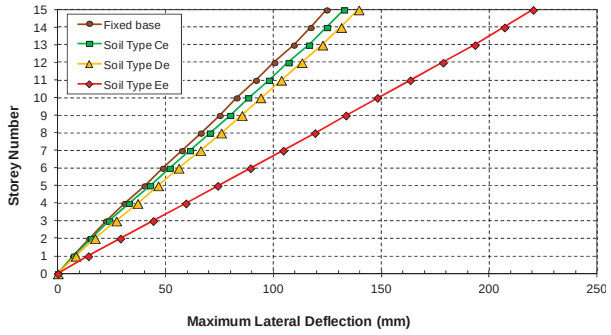

(b)

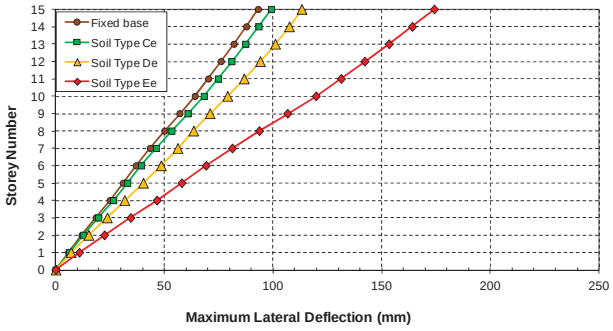

(c)

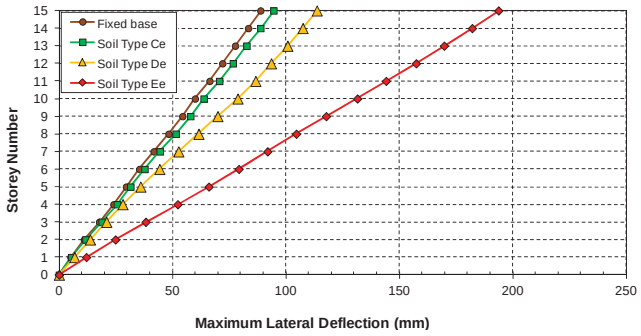

(d)

Figure A.5: Elastic storey deflections of model S15 resting on soil classes C_e, D_e, and E_e with bedrock depth of 30 metres; (a) Northridge (1994); (b) Kobe (1995); (c) El-Centro (1940); (d) Hachinohe (1968)

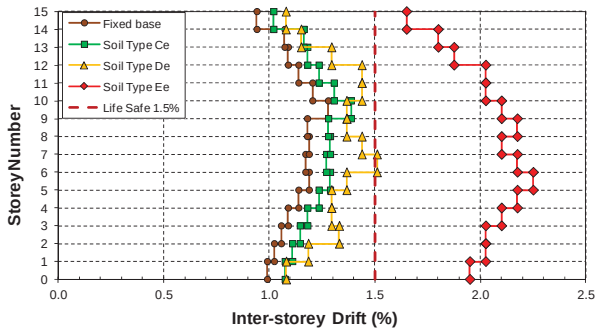

(a)

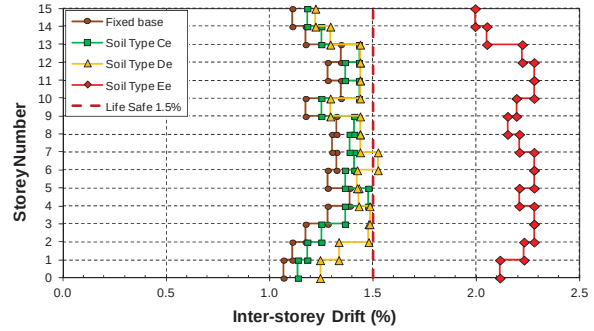

(b)

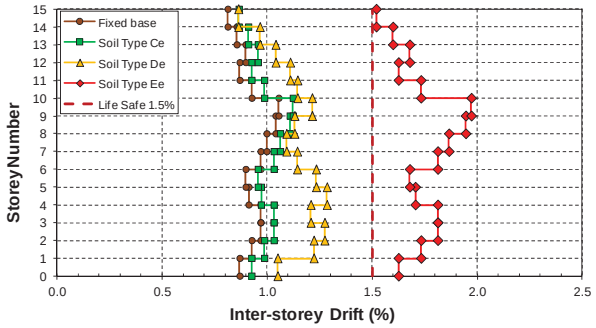

(c)

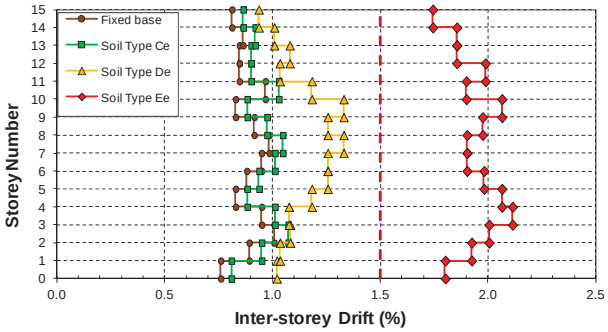

(d)

Figure A.6: Elastic inter-storey drifts of model S15 resting on soil classes C_e, D_e, and E_e with bedrock depth of 30 metres; (a) Northridge (1994); (b) Kobe (1995); (c) El-Centro (1940); (d) Hachinohe (1968)

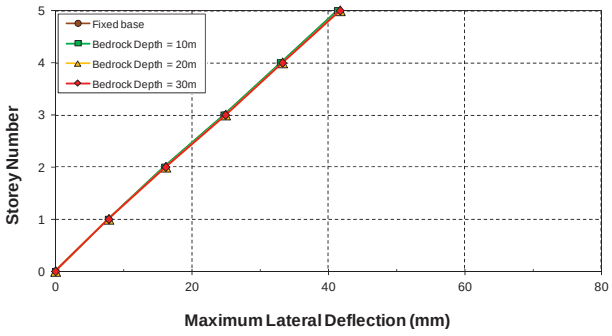

(a)

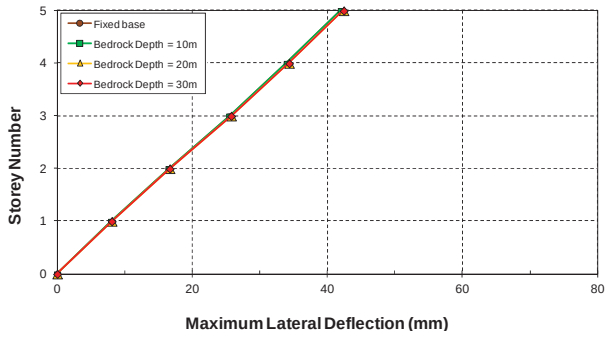

(b)

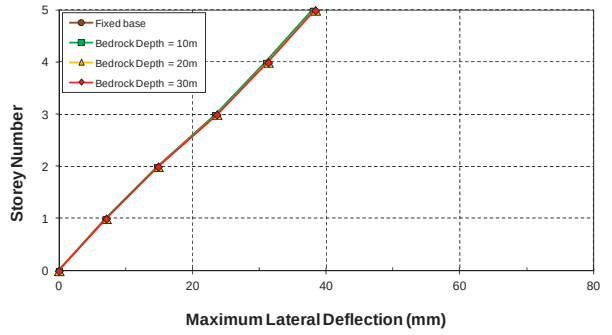

(c)

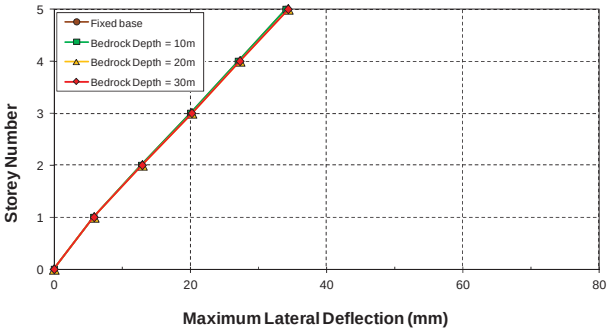

(d)

Figure A.7: Elastic storey deflections of model S5 resting on soil class C_e with variable bedrock depths; (a) Northridge (1994); (b) Kobe (1995); (c) El-Centro (1940); (d) Hachinohe (1968)

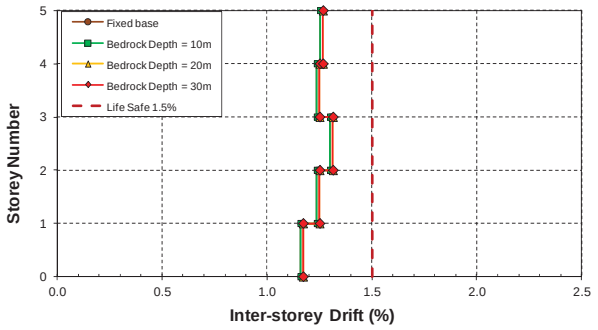

(a)

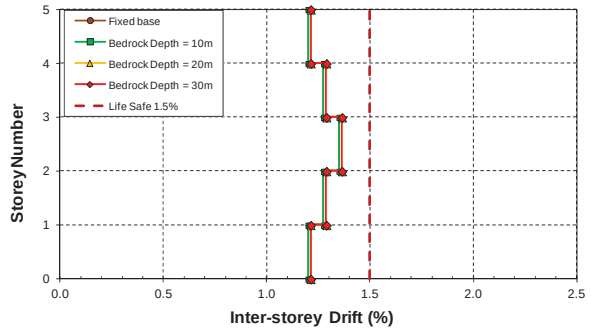

(b)

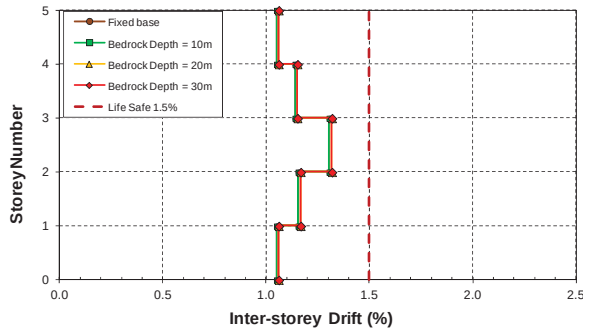

(c)

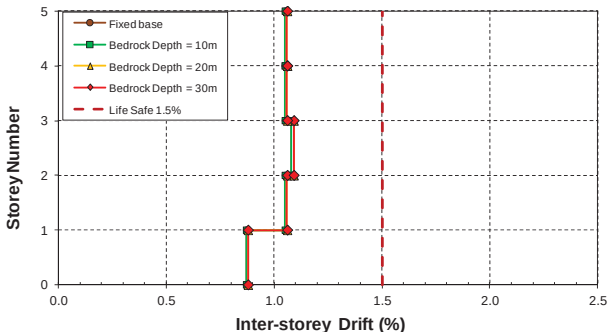

(d)

Figure A.8: Elastic inter-storey drifts of model S5 resting on soil class C_e with variable bedrock depths; (a) Northridge (1994); (b) Kobe (1995); (c) El-Centro (1940); (d) Hachinohe (1968)

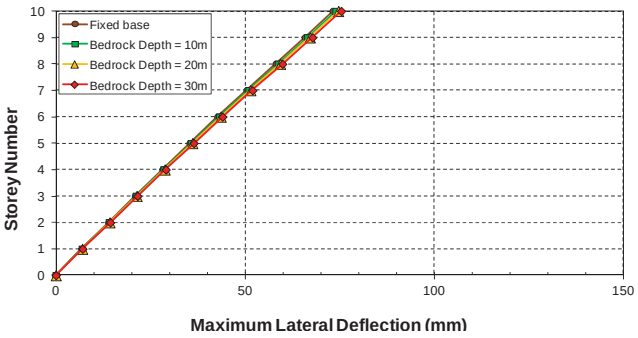

(a)

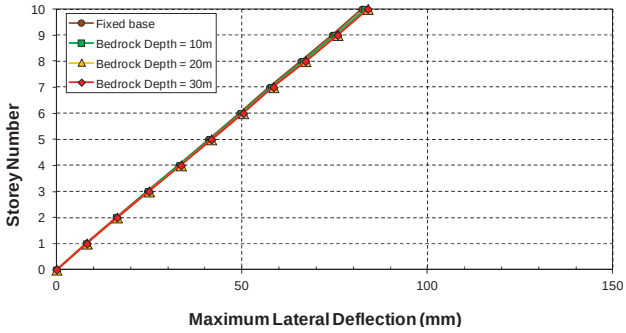

(b)

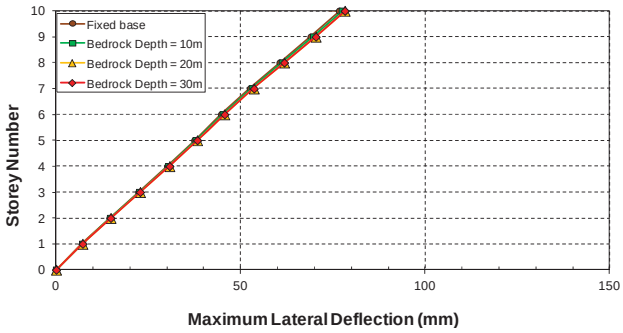

(c)

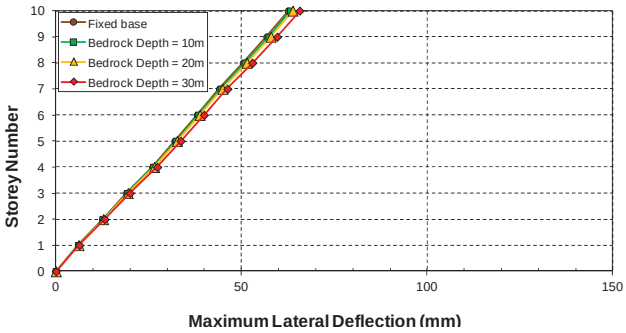

(d)

Figure A.9: Elastic storey deflections of model S10 resting on soil class C_e with variable bedrock depths; (a) Northridge (1994); (b) Kobe (1995); (c) El-Centro (1940); (d) Hachinohe (1968)

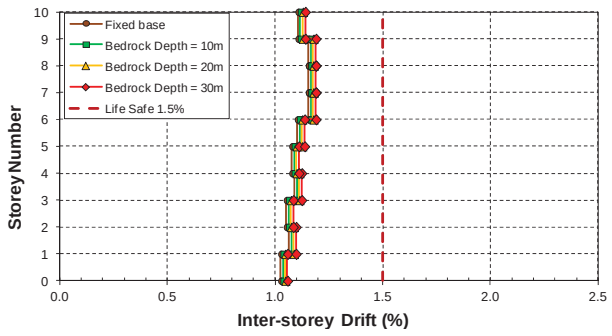

(a)

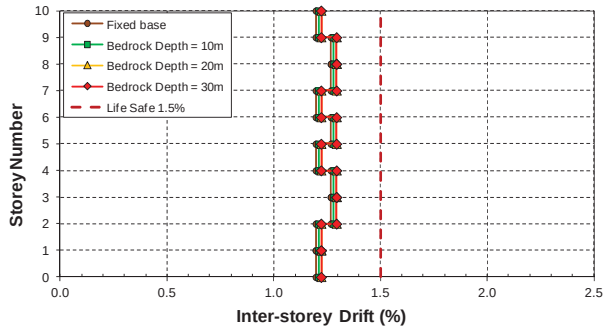

(b)

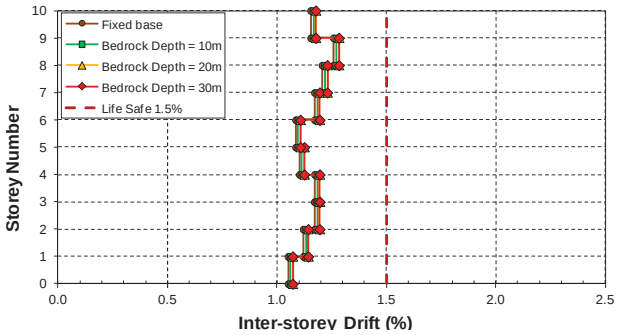

(c)

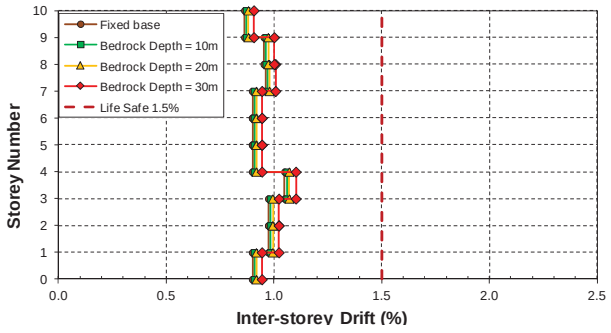

(d)

Figure A.10: Elastic inter-storey drifts of model S10 resting on soil class C_e with variable bedrock depths; (a) Northridge (1994); (b) Kobe (1995); (c) El-Centro (1940); (d) Hachinohe (1968)

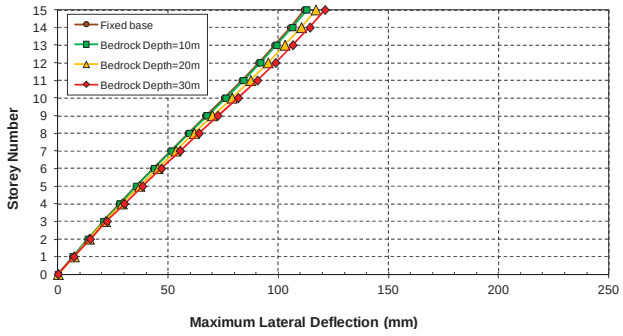

(a)

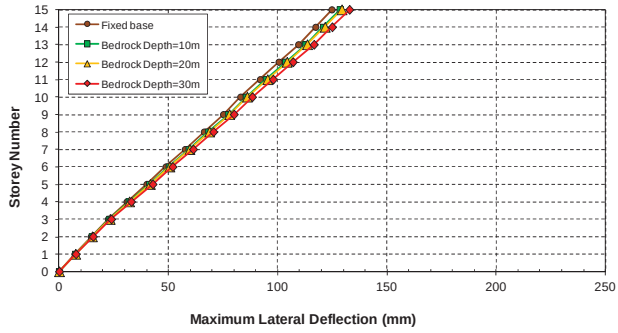

(b)

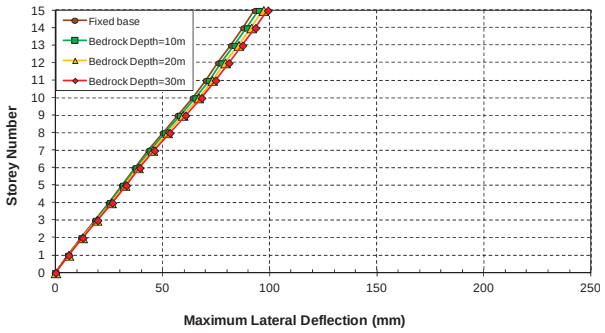

(c)

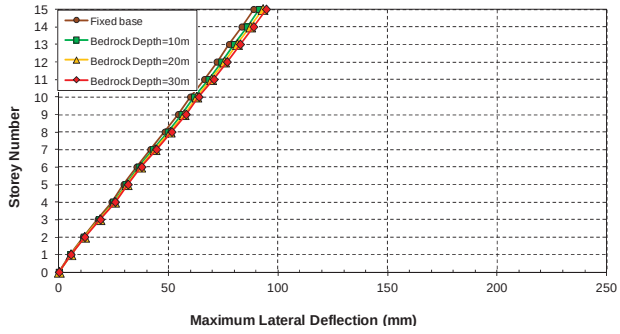

(d)

Figure A.11: Elastic storey deflections of model S15 resting on soil class C_e with variable bedrock depths; (a) Northridge (1994); (b) Kobe (1995); (c) El-Centro (1940); (d) Hachinohe (1968)

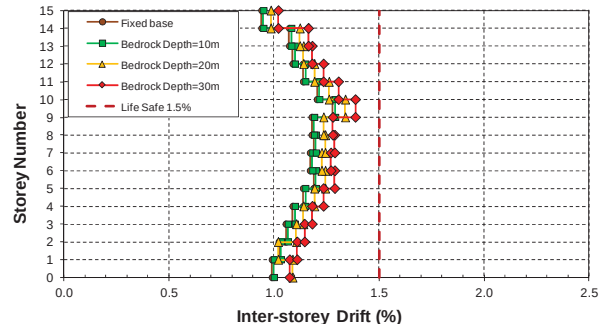

(a)

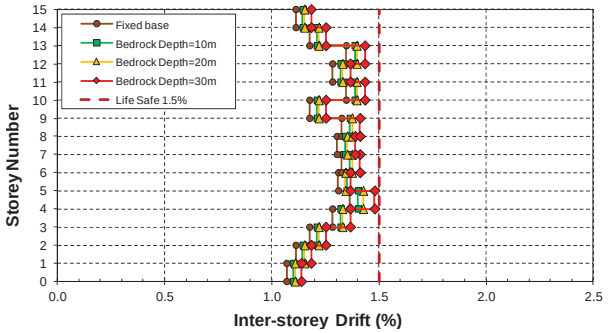

(b)

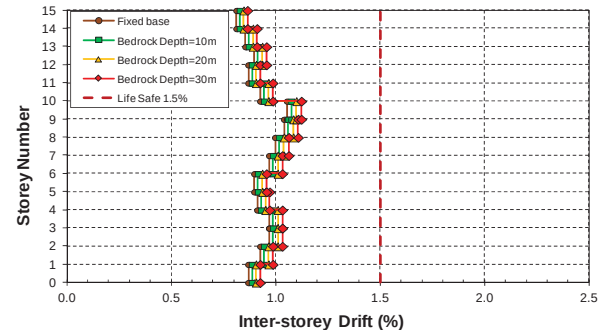

(c)

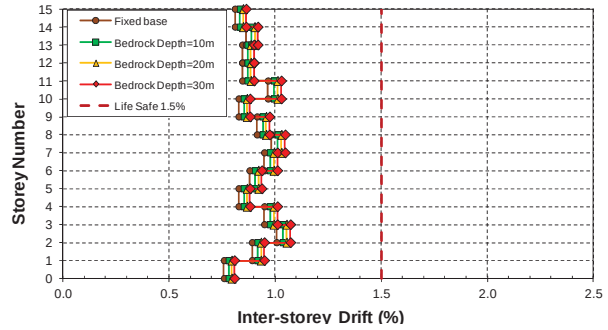

(d)

Figure A.12: Elastic inter-storey drifts of model S15 resting on soil class C_e with variable bedrock depths; (a) Northridge (1994); (b) Kobe (1995); (c) El-Centro (1940); (d) Hachinohe (1968)

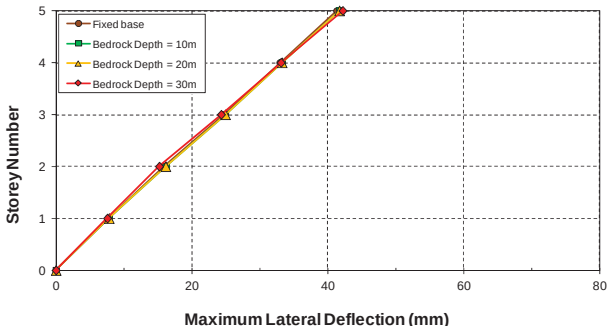

(a)

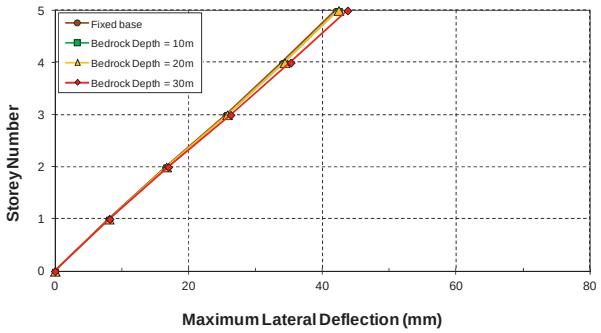

(b)

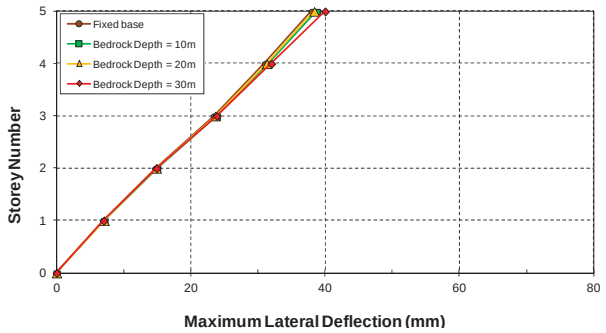

(c)

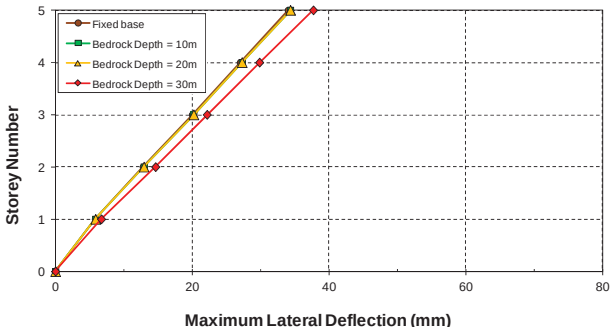

(d)

Figure A.13: Elastic storey deflections of model S5 resting on soil class D_e with variable bedrock depths; (a) Northridge (1994); (b) Kobe (1995); (c) El-Centro (1940); (d) Hachinohe (1968)

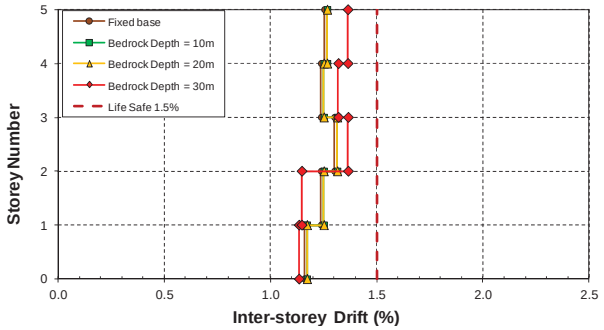

(a)

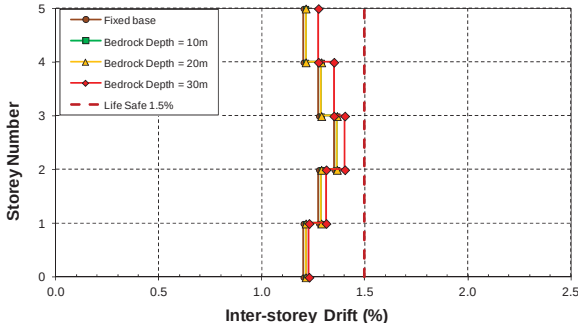

(b)

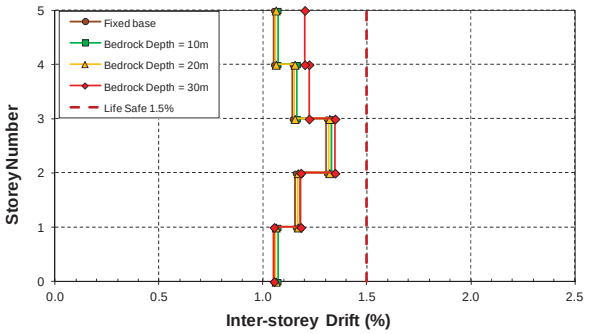

(c)

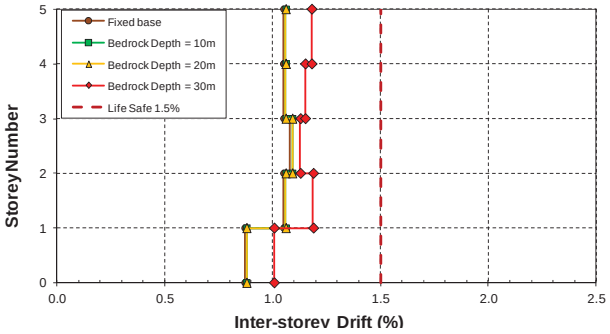

(d)

Figure A.14: Elastic inter-storey drifts of model S5 resting on soil class D_e with variable bedrock depths; (a) Northridge (1994); (b) Kobe (1995); (c) El-Centro (1940); (d) Hachinohe (1968)

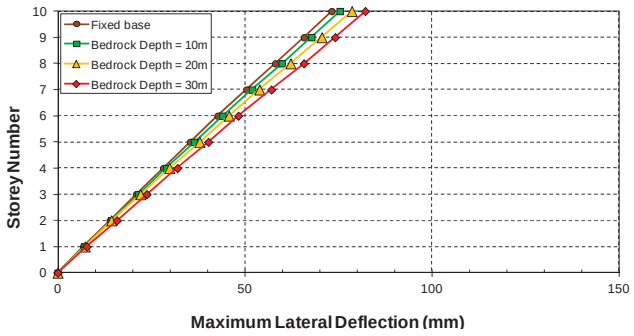

(a)

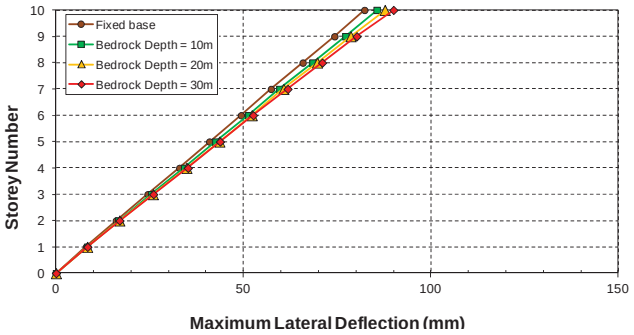

(b)

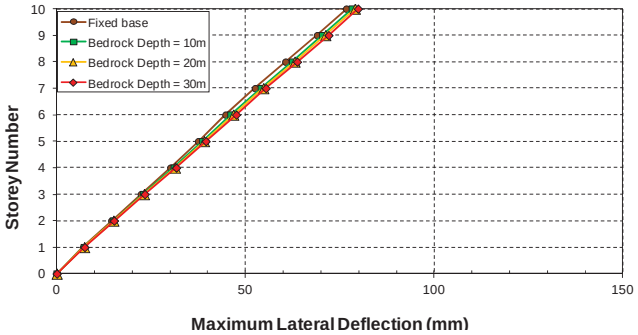

(c)

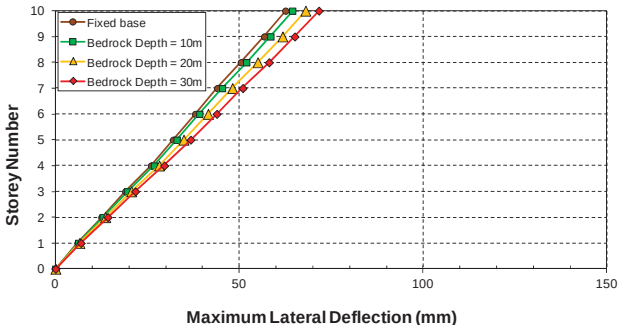

(d)

Figure A.15: Elastic storey deflections of model S10 resting on soil class D_e with variable bedrock depths; (a) Northridge (1994); (b) Kobe (1995); (c) El-Centro (1940); (d) Hachinohe (1968)

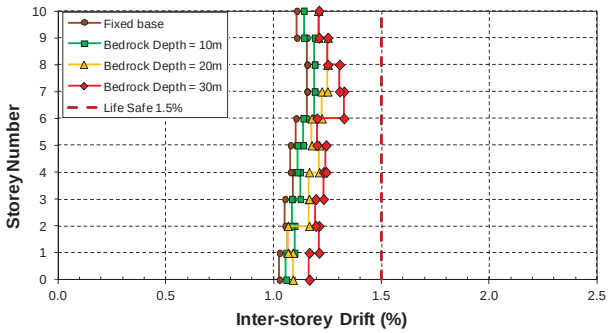

(a)

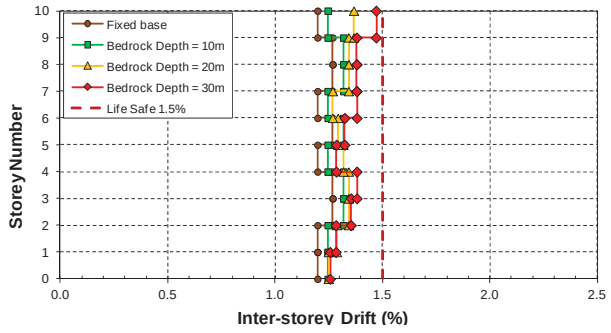

(b)

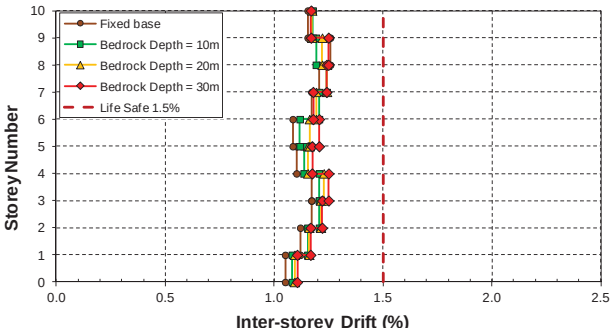

(c)

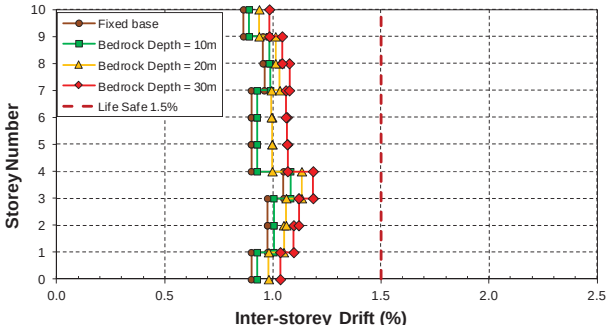

(d)

Figure A.16: Elastic inter-storey drifts of model S10 resting on soil class D_e with variable bedrock depths; (a) Northridge (1994); (b) Kobe (1995); (c) El-Centro (1940); (d) Hachinohe (1968)

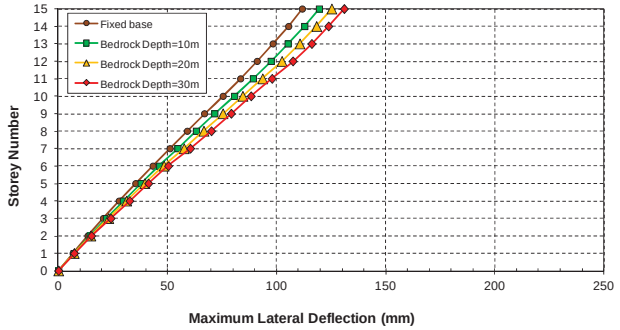

(a)

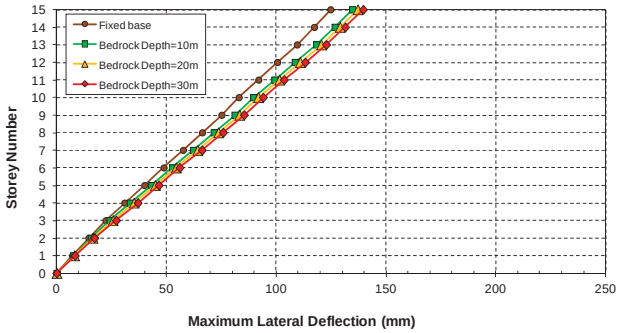

(b)

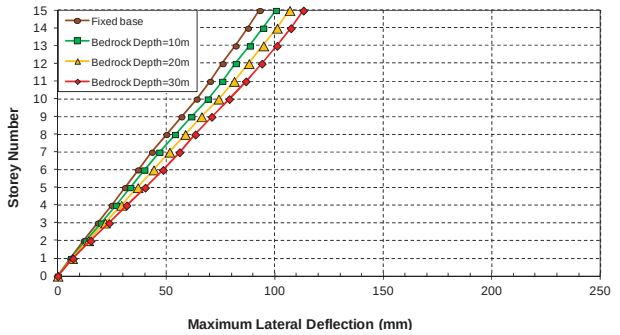

(c)

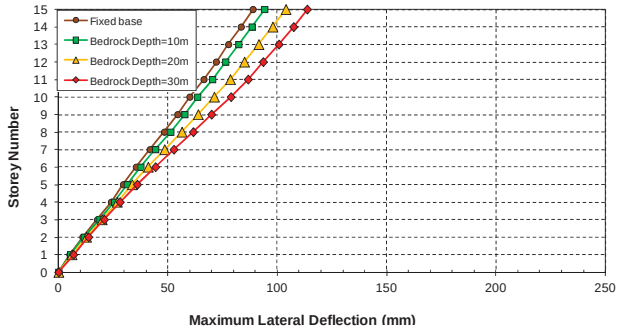

(d)

Figure A.17: Elastic storey deflections of model S15 resting on soil class D_e with variable bedrock depths; (a) Northridge (1994); (b) Kobe (1995); (c) El-Centro (1940); (d) Hachinohe (1968)

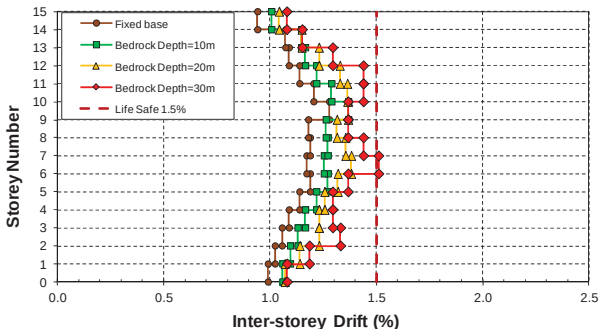

(a)

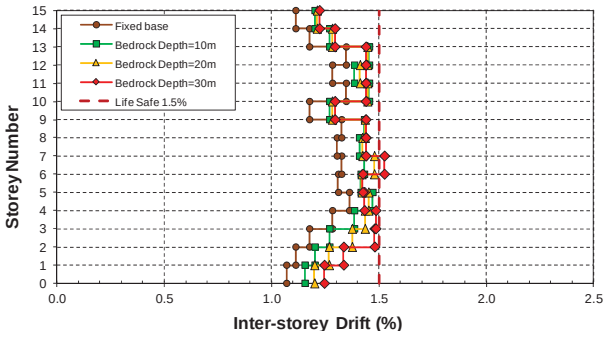

(b)

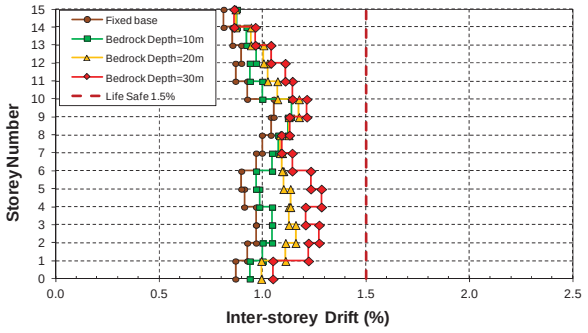

(c)

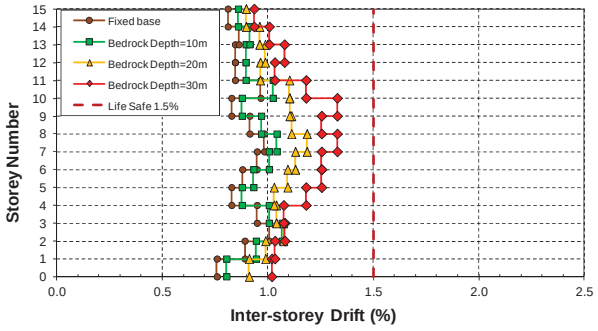

(d)

Figure A.18: Elastic inter-storey drifts of model S15 resting on soil class D_e with variable bedrock depths; (a) Northridge (1994); (b) Kobe (1995); (c) El-Centro (1940); (d) Hachinohe (1968)

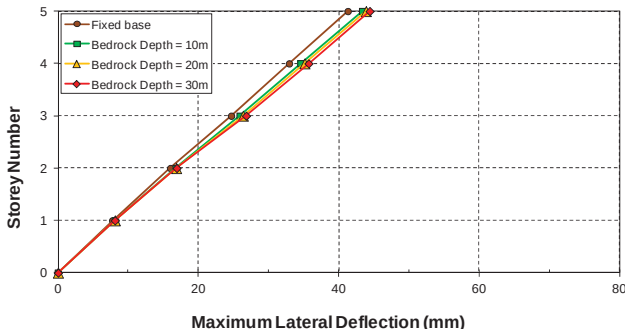

(a)

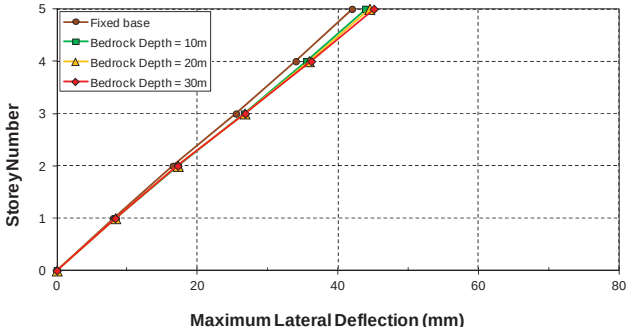

(b)

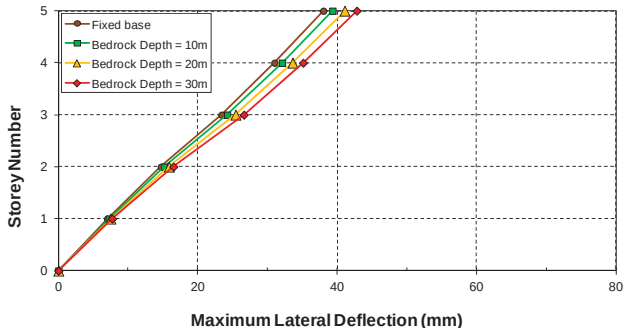

(c)

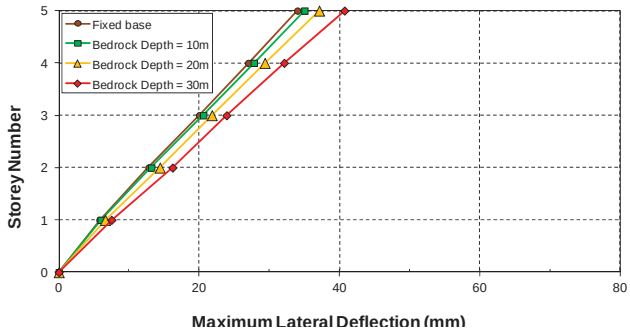

(d)

Figure A.19: Elastic storey deflections of model S5 resting on soil class E_e with variable bedrock depths; (a) Northridge (1994); (b) Kobe (1995); (c) El-Centro (1940); (d) Hachinohe (1968)

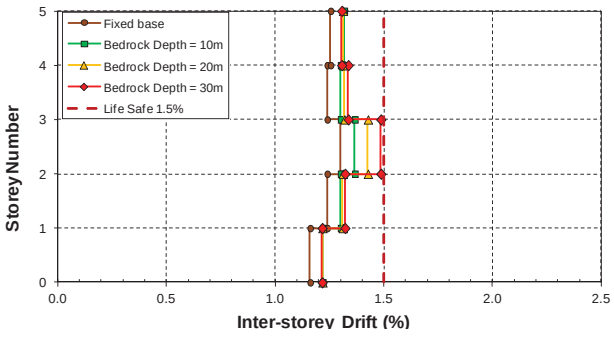

(a)

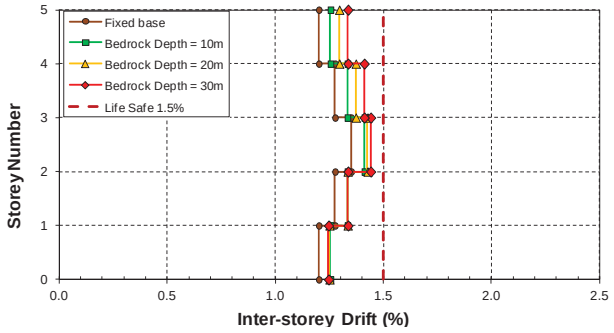

(b)

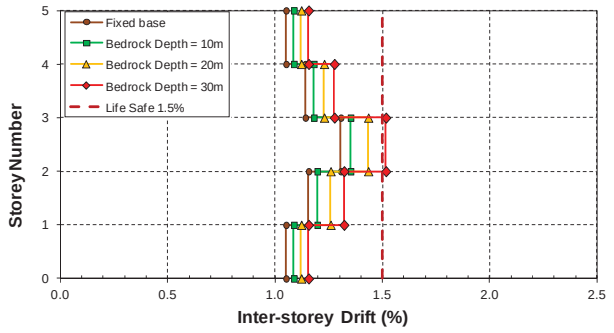

(c)

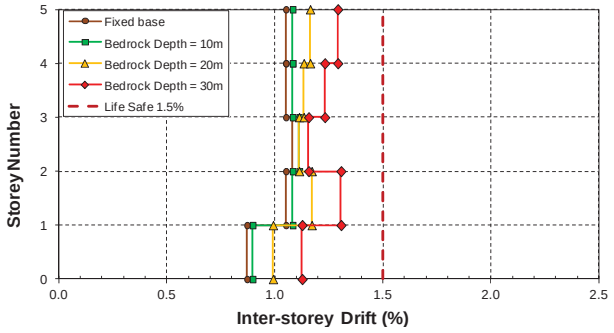

(d)

Figure A.20: Elastic inter-storey drifts of model S5 resting on soil class E_e with variable bedrock depths; (a) Northridge (1994); (b) Kobe (1995); (c) El-Centro (1940); (d) Hachinohe (1968)

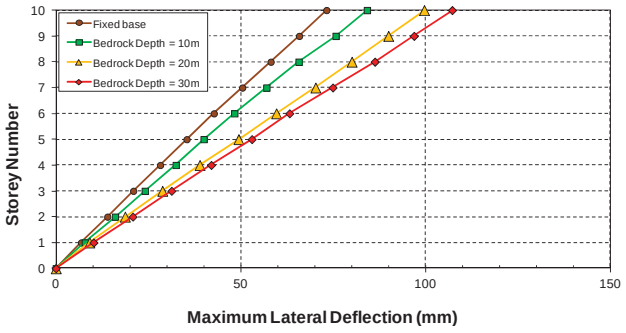

(a)

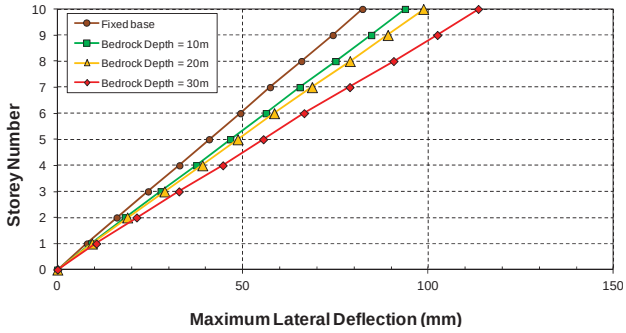

(b)

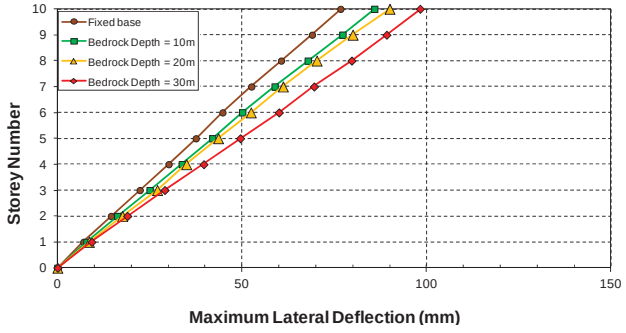

(c)

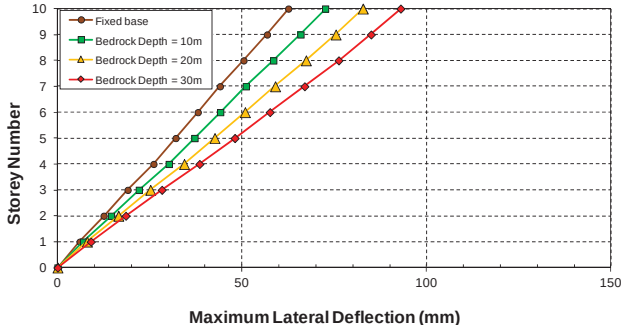

(d)

Figure A.21: Elastic storey deflections of model S10 resting on soil class E_e with variable bedrock depths; (a) Northridge (1994); (b) Kobe (1995); (c) El-Centro (1940); (d) Hachinohe (1968)

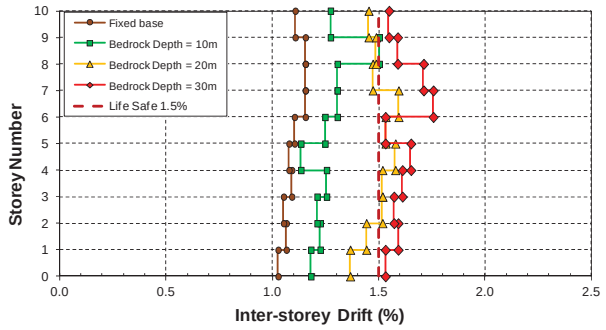

(a)

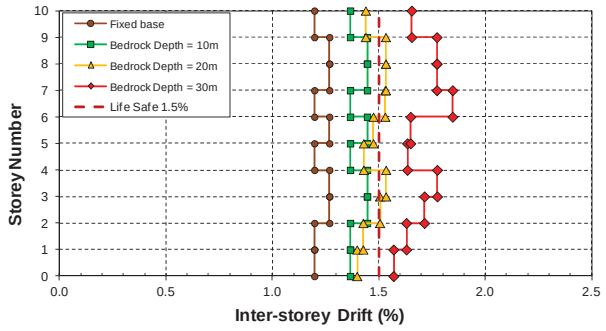

(b)

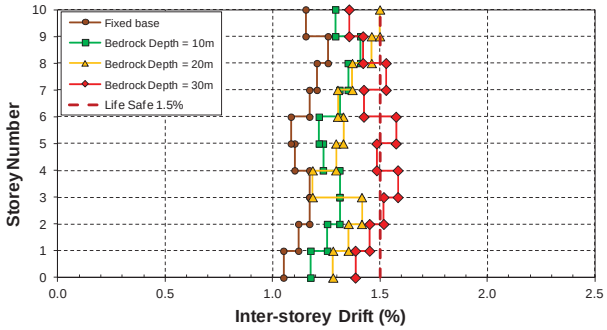

(c)

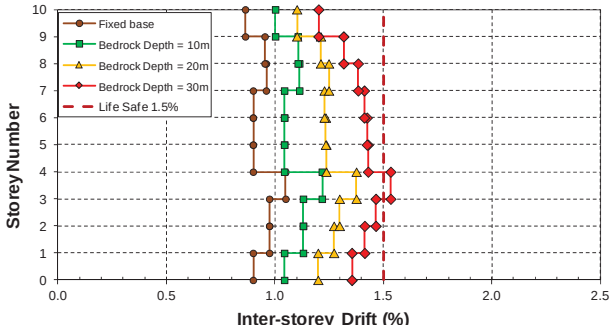

(d)

Figure A.22: Elastic inter-storey drifts of model S10 resting on soil class E_e with variable bedrock depths; (a) Northridge (1994); (b) Kobe (1995); (c) El-Centro (1940); (d) Hachinohe (1968)

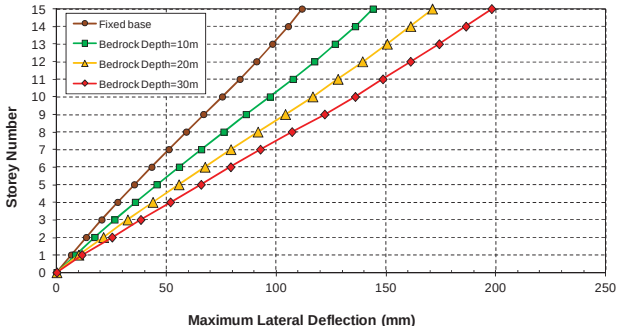

(a)

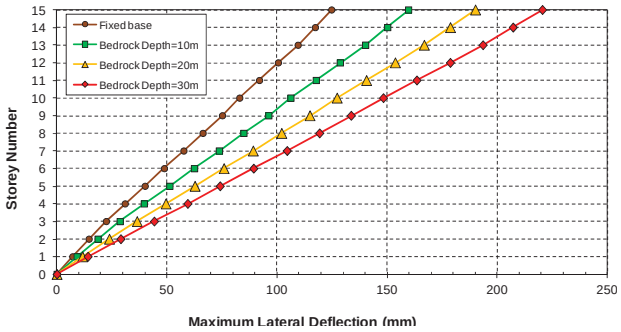

(b)

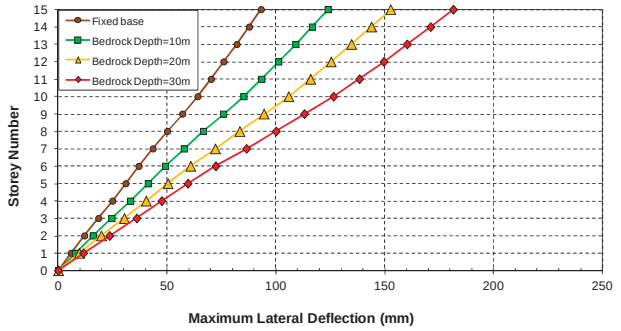

(c)

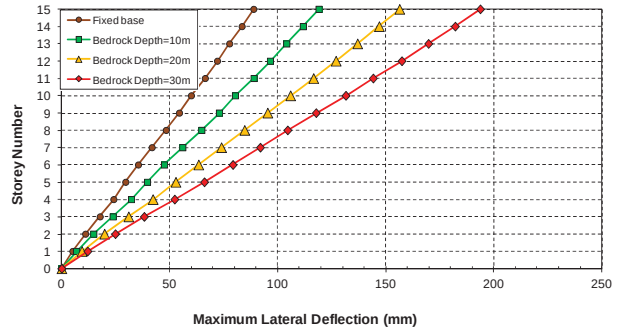

(d)

Figure A.23: Elastic storey deflections of model S15 resting on soil class E_e with variable bedrock depths; (a) Northridge (1994); (b) Kobe (1995); (c) El-Centro (1940); (d) Hachinohe (1968)

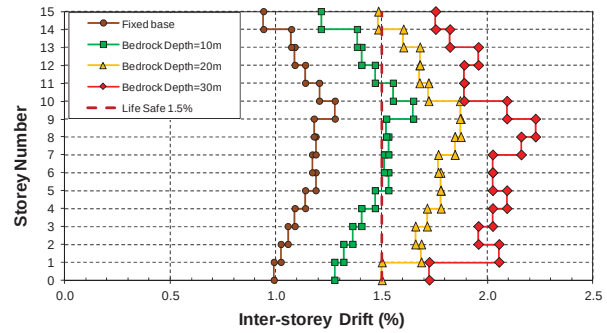

(a)

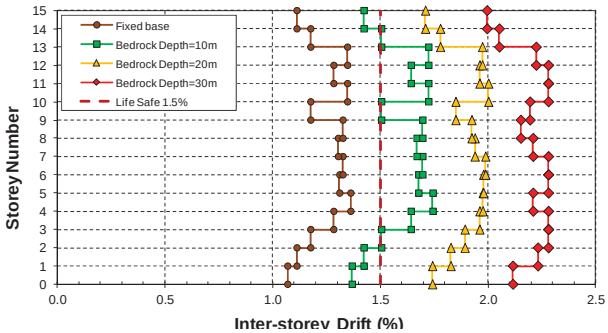

(b)

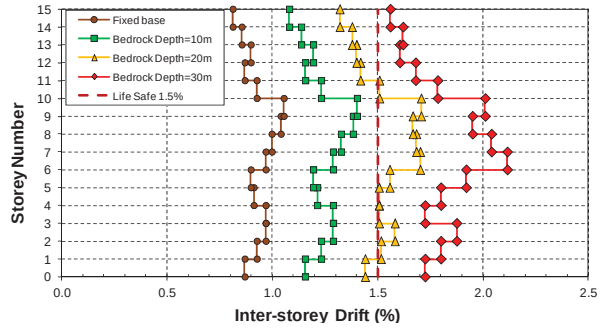

(c)

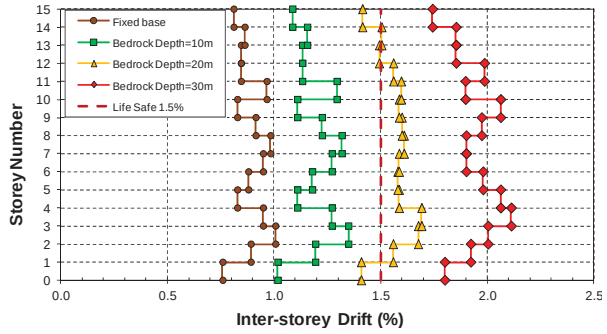

(d)

Figure A.24: Elastic inter-storey drifts of model S15 resting on soil class E_e with variable bedrock depths; (a) Northridge (1994); (b) Kobe (1995); (c) El-Centro (1940); (d) Hachinohe (1968)

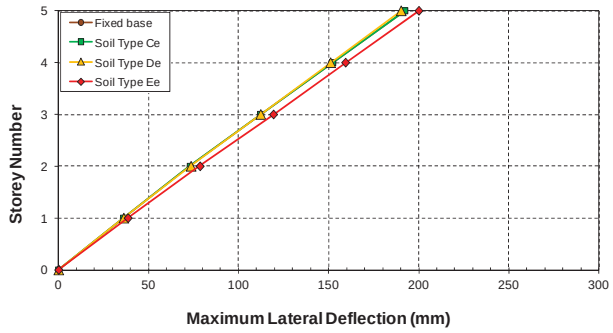

(a)

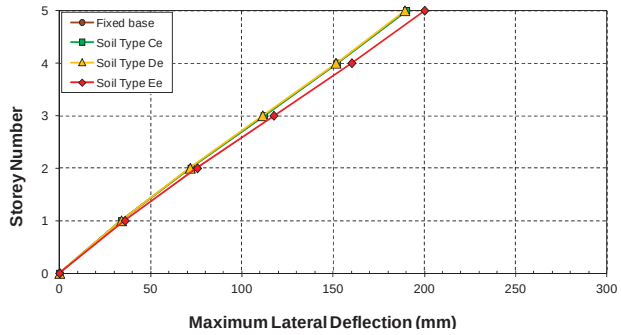

(b)

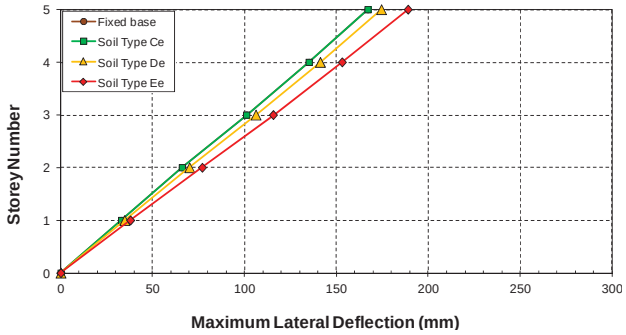

(c)

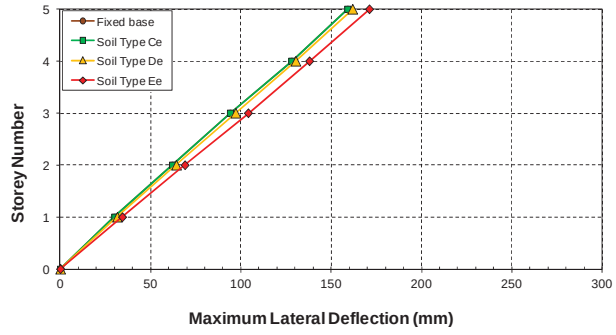

(d)

Figure A.25: Inelastic storey deflections of model S5 resting on soil classes C_e, D_e, and E_e with bedrock depth of 30 metres; (a) Northridge (1994); (b) Kobe (1995); (c) El-Centro (1940); (d) Hachinohe (1968)

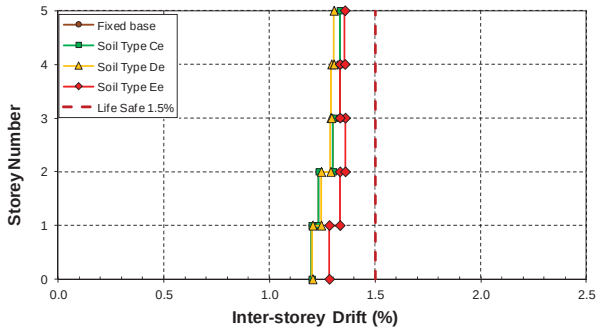

(a)

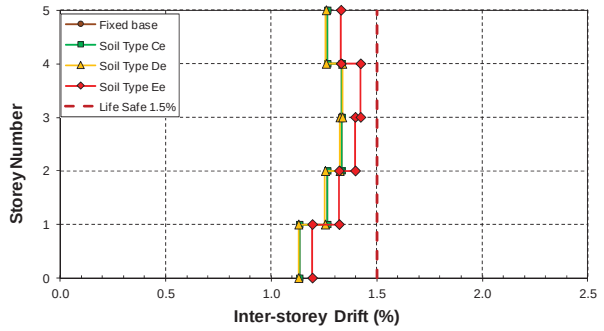

(b)

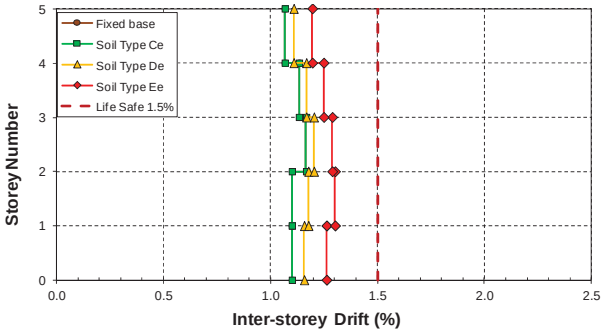

(c)

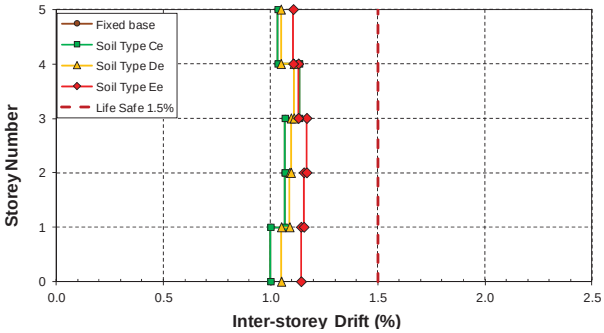

(d)

Figure A.26: Inelastic inter-storey drifts of model S5 resting on soil classes C_e, D_e, and E_e with bedrock depth of 30 metres; (a) Northridge (1994); (b) Kobe (1995); (c) El-Centro (1940); (d) Hachinohe (1968)

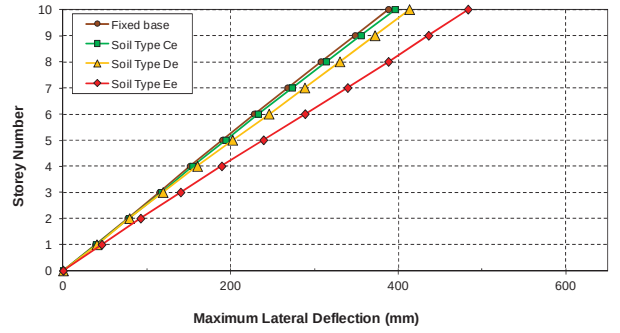

(a)

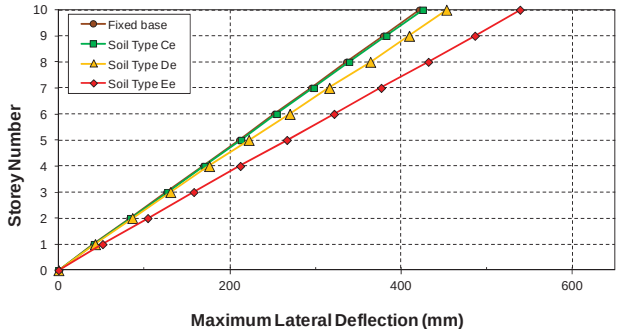

(b)

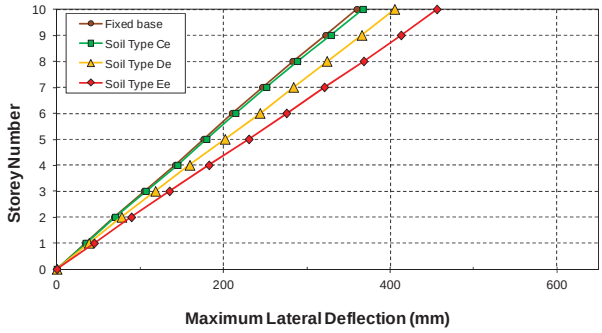

(c)

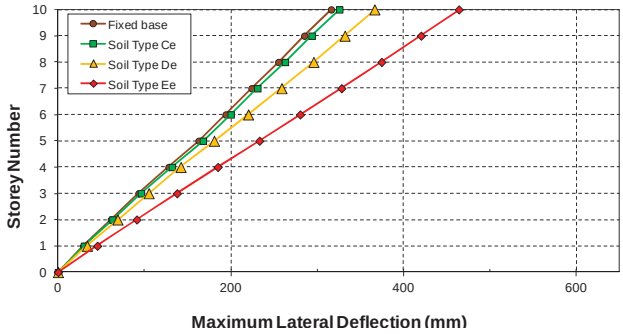

(d)

Figure A.27: Inelastic storey deflections of model S10 resting on soil classes C_e, D_e, and E_e with bedrock depth of 30 metres; (a) Northridge (1994); (b) Kobe (1995); (c) El-Centro (1940); (d) Hachinohe (1968)

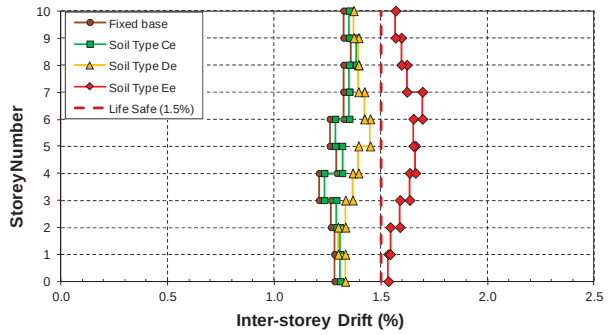

(a)

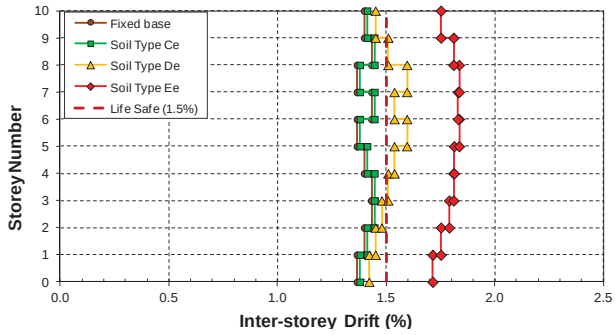

(b)

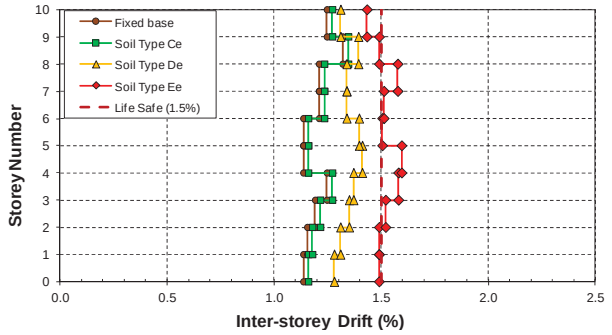

(c)

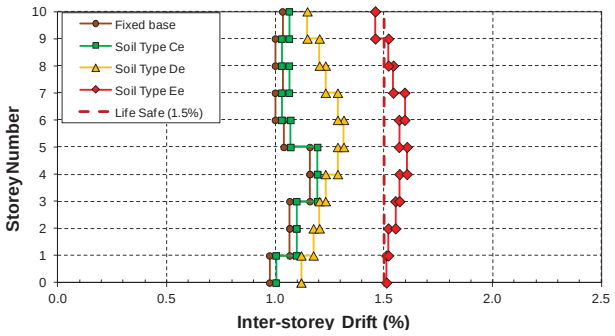

(d)

Figure A.28: Inelastic inter-storey drifts of model S10 resting on soil classes C_e, D_e, and E_e with bedrock depth of 30 metres; (a) Northridge (1994); (b) Kobe (1995); (c) El-Centro (1940); (d) Hachinohe (1968)

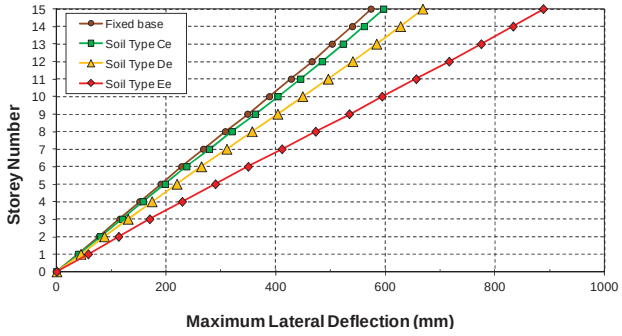

(a)

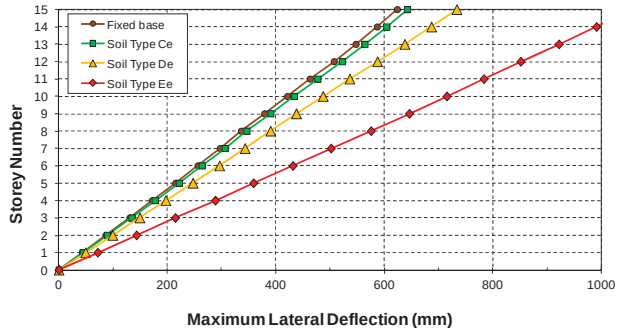

(b)

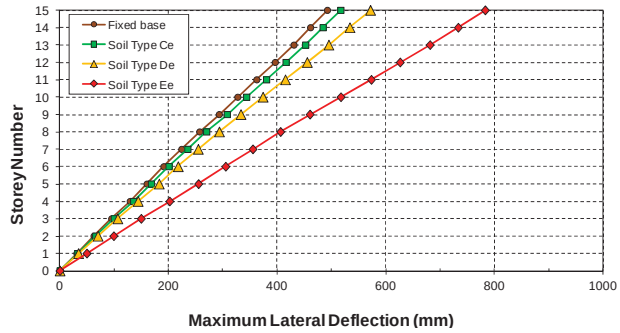

(c)

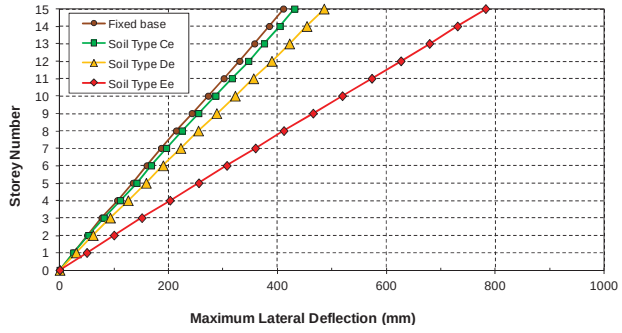

(d)

Figure A.29: Inelastic storey deflections of model S15 resting on soil classes C_e, D_e, and E_e with bedrock depth of 30 metres; (a) Northridge (1994); (b) Kobe (1995); (c) El-Centro (1940); (d) Hachinohe (1968)

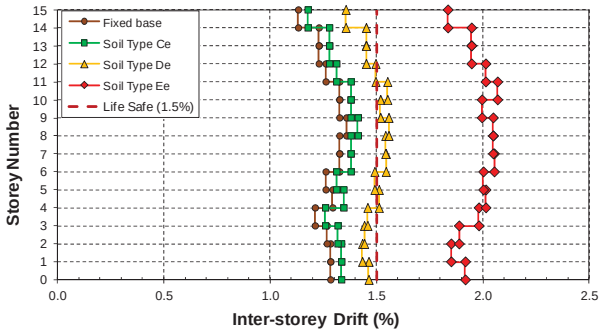

(a)

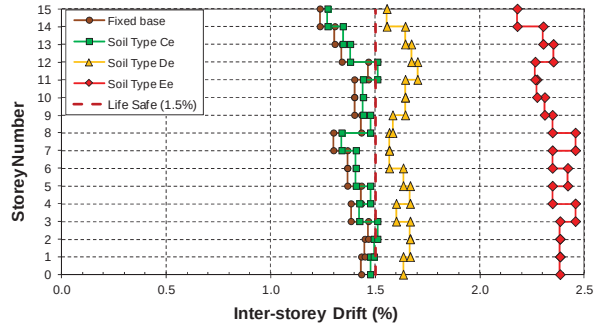

(b)

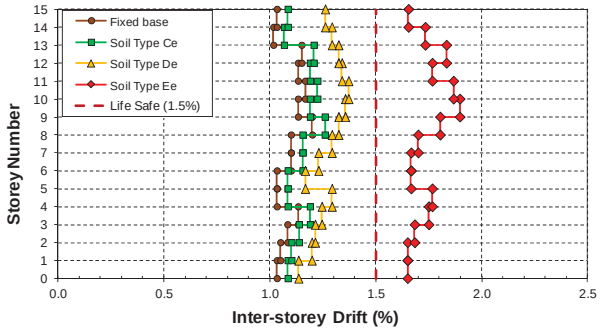

(c)

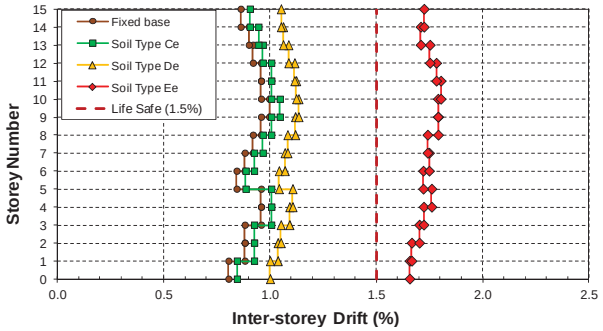

(d)

Figure A.30: Inelastic inter-storey drifts of model S15 resting on soil classes C_e, D_e, and E_e with bedrock depth of 30 metres; (a) Northridge (1994); (b) Kobe (1995); (c) El-Centro (1940); (d) Hachinohe (1968)

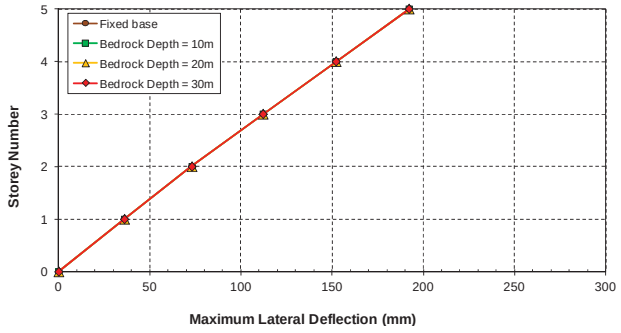

(a)

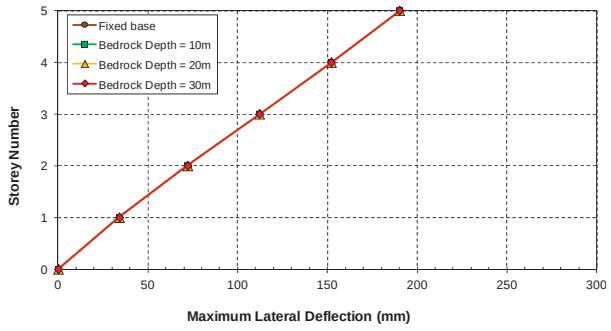

(b)

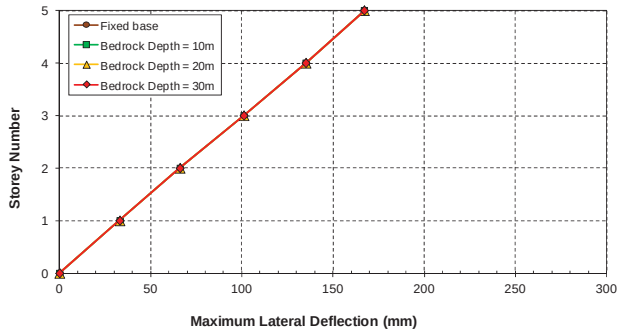

(c)

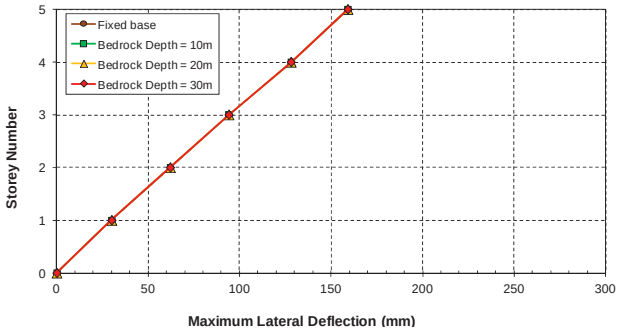

(d)

Figure A.31: Inelastic storey deflections of model S5 resting on soil class C_e with variable bedrock depths; (a) Northridge (1994); (b) Kobe (1995); (c) El-Centro (1940); (d) Hachinohe (1968)

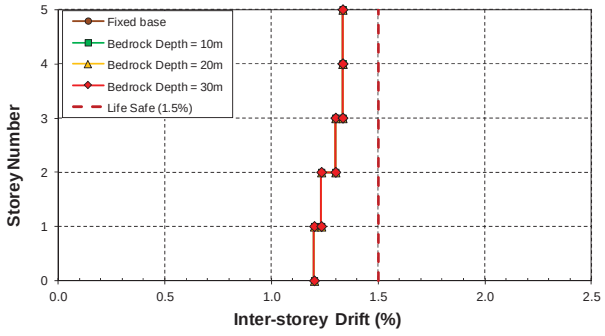

(a)

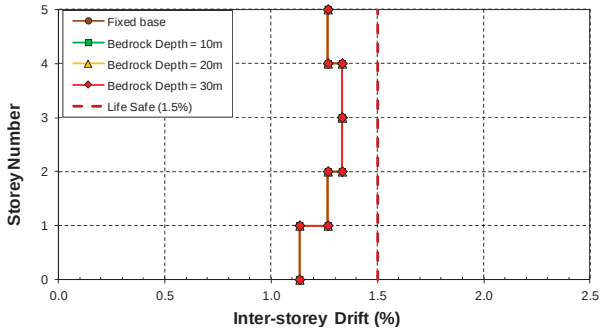

(b)

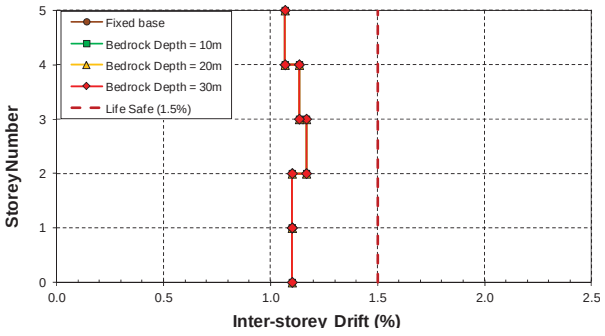

(c)

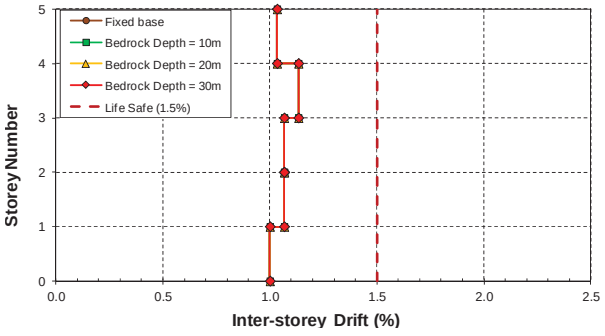

(d)

Figure A.32: Inelastic inter-storey drifts of model S5 resting on soil class C_e with variable bedrock depths; (a) Northridge (1994); (b) Kobe (1995); (c) El-Centro (1940); (d) Hachinohe (1968)

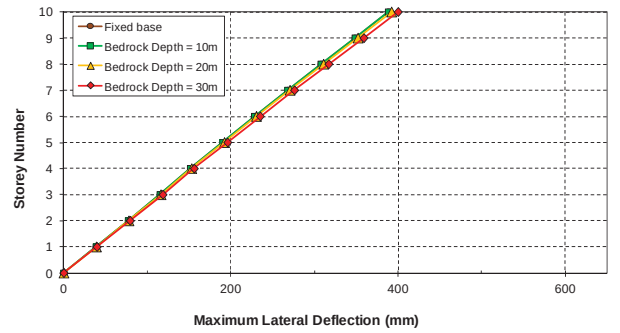

(a)

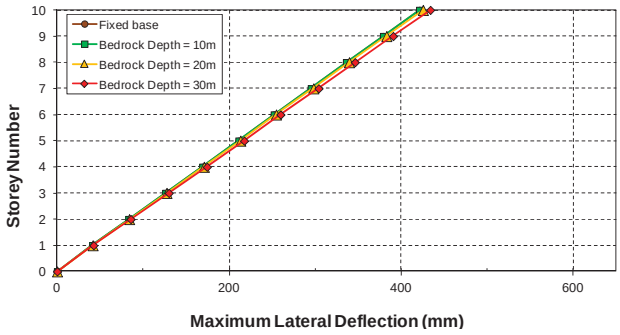

(b)

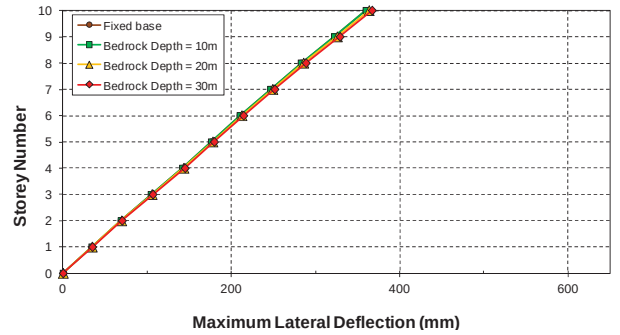

(c)

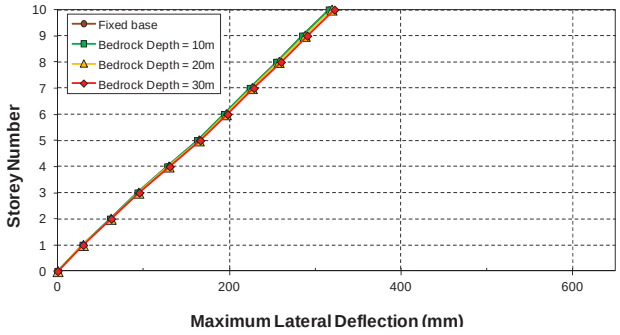

(d)

Figure A.33: Inelastic storey deflections of model S10 resting on soil class C_e with variable bedrock depths; (a) Northridge (1994); (b) Kobe (1995); (c) El-Centro (1940); (d) Hachinohe (1968)

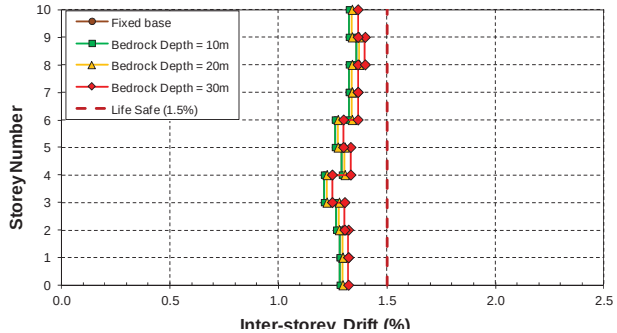

(a)

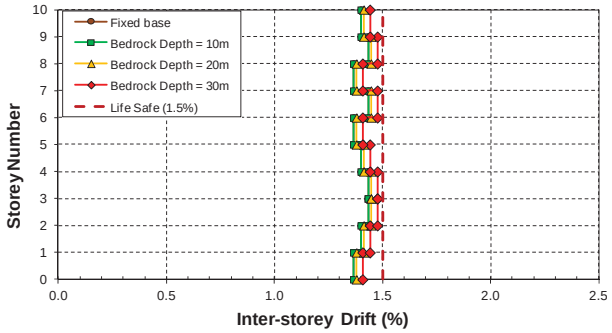

(b)

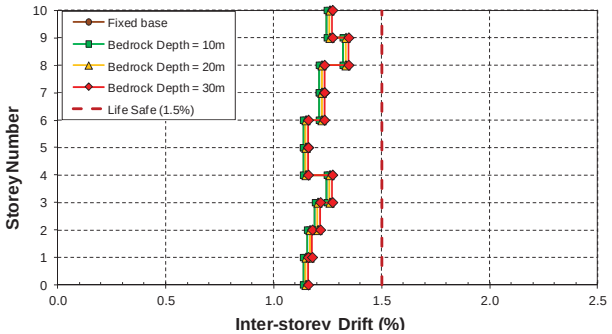

(c)

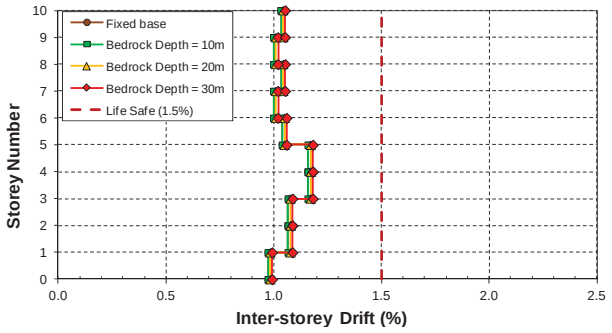

(d)

Figure A.34: Inelastic inter-storey drifts of model S10 resting on soil class C_e with variable bedrock depths; (a) Northridge (1994); (b) Kobe (1995); (c) El-Centro (1940); (d) Hachinohe (1968)

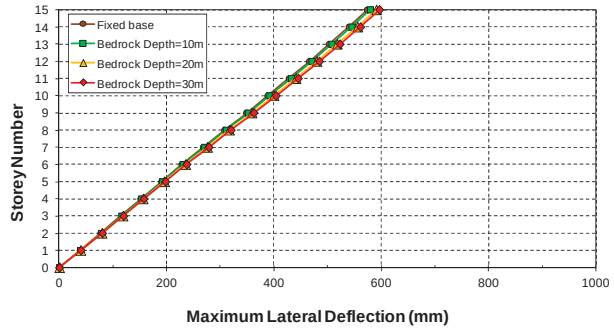

(a)

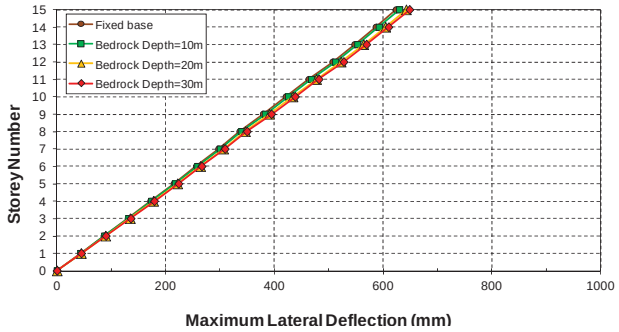

(b)

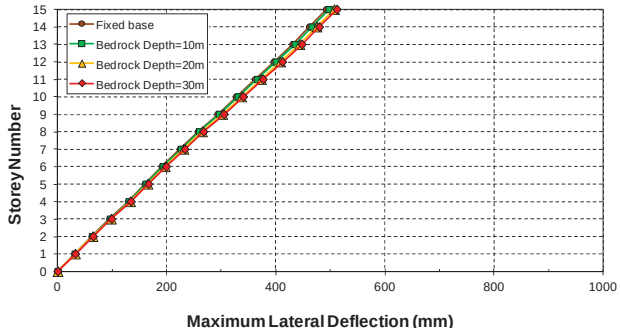

(c)

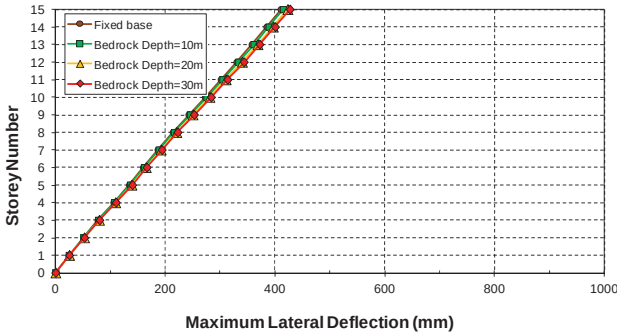

(d)

Figure A.35: Inelastic storey deflections of model S15 resting on soil class C_e with variable bedrock depths; (a) Northridge (1994); (b) Kobe (1995); (c) El-Centro (1940); (d) Hachinohe (1968)

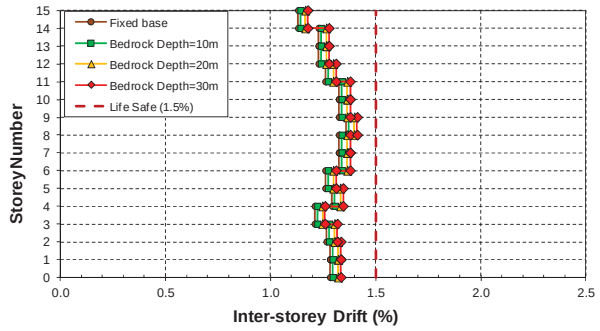

(a)

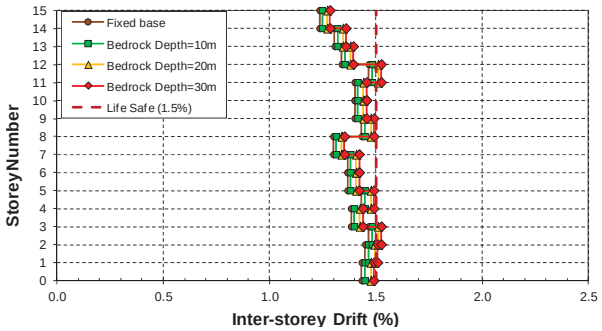

(b)

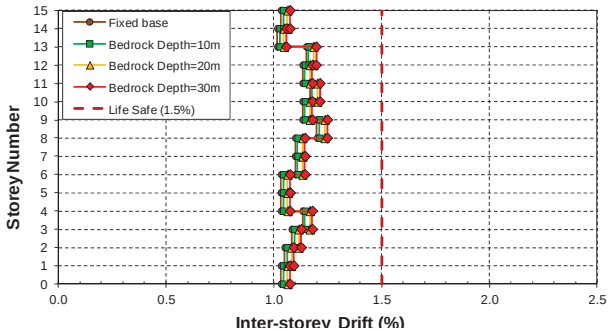

(c)

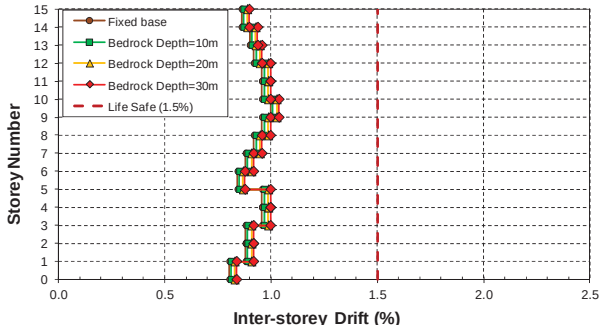

(d)

Figure A.36: Elastic inter-storey drifts of model S15 resting on soil class C_e with variable bedrock depths; (a) Northridge (1994); (b) Kobe (1995); (c) El-Centro (1940); (d) Hachinohe (1968)

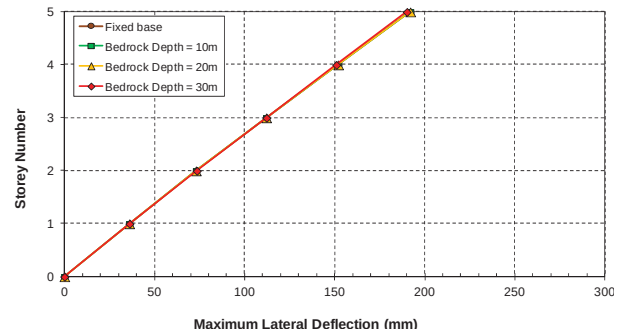

(a)

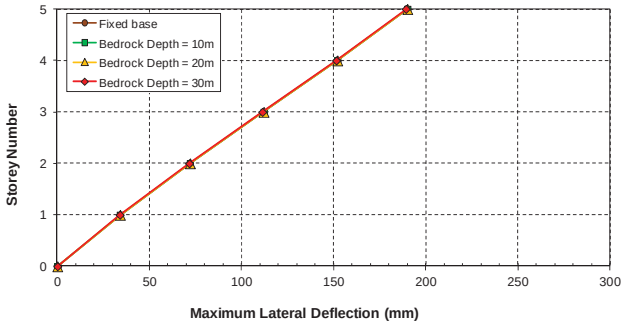

(b)

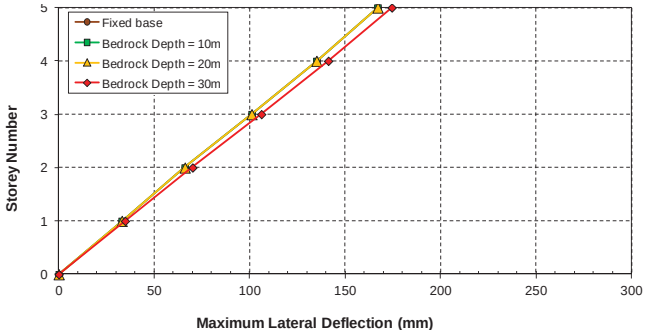

(c)

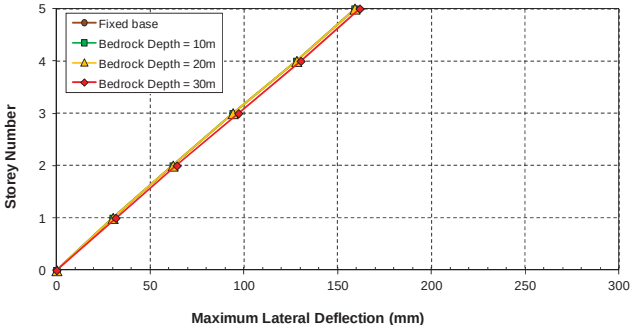

(d)

Figure A.37: Inelastic storey deflections of model S5 resting on soil class D_e with variable bedrock depths; (a) Northridge (1994); (b) Kobe (1995); (c) El-Centro (1940); (d) Hachinohe (1968)

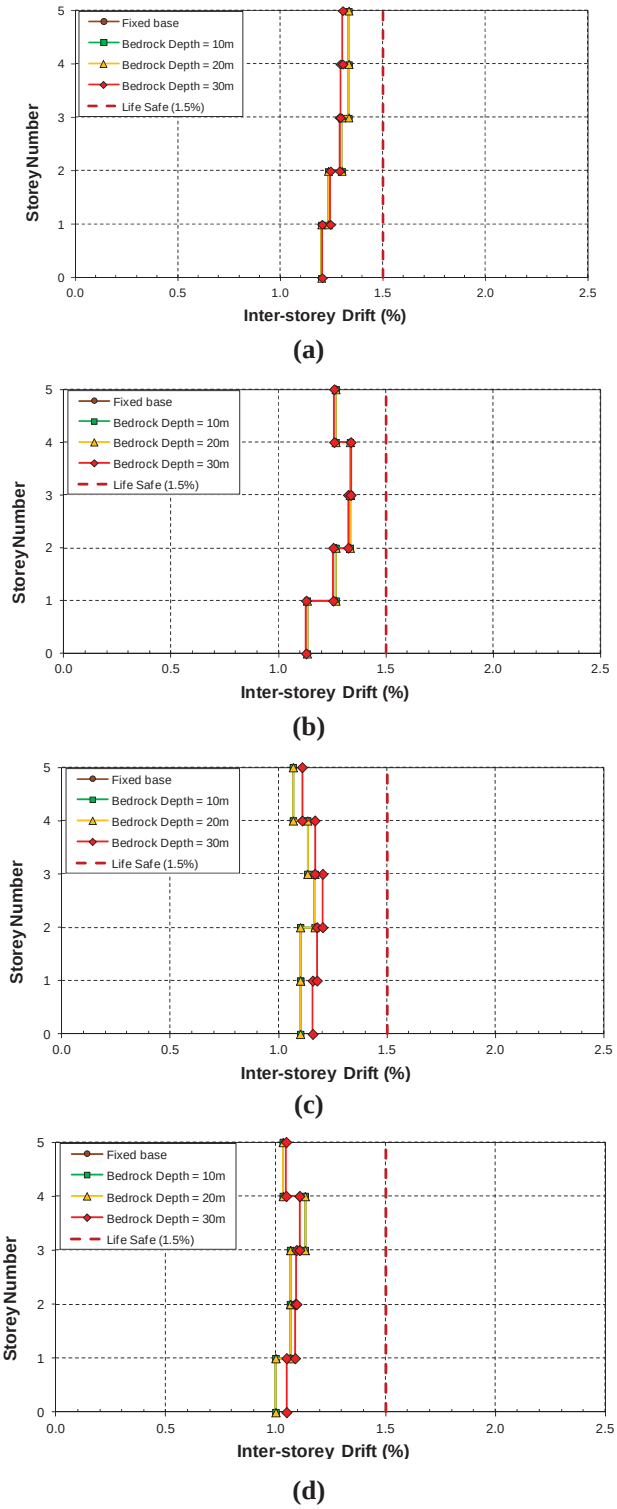

Figure A.38: Elastic inter-storey drifts of model S5 resting on soil class D_e with variable bedrock depths; (a) Northridge (1994); (b) Kobe (1995); (c) El-Centro (1940); (d) Hachinohe (1968)

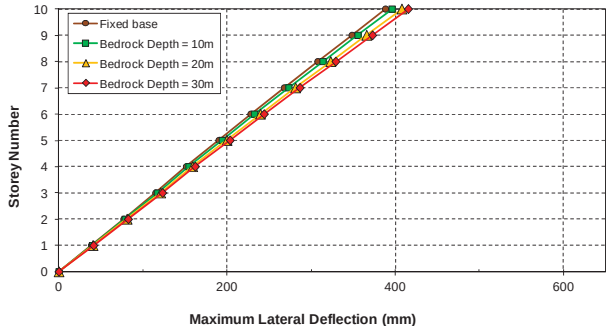

(a)

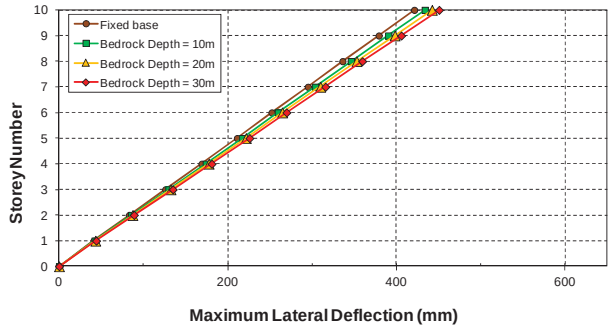

(b)

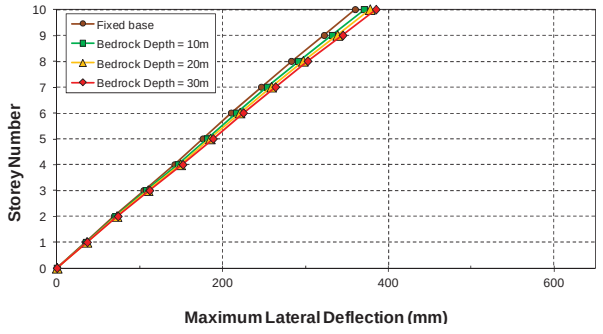

(c)

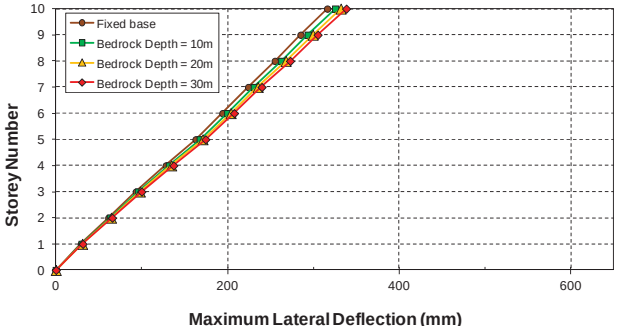

(d)

Figure A.39: Inelastic storey deflections of model S10 resting on soil class D_e with variable bedrock depths; (a) Northridge (1994); (b) Kobe (1995); (c) El-Centro (1940); (d) Hachinohe (1968)

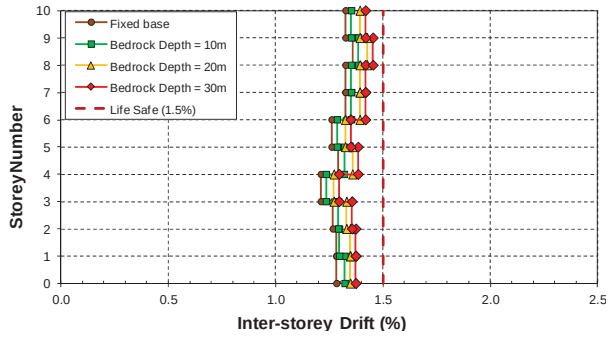

(a)

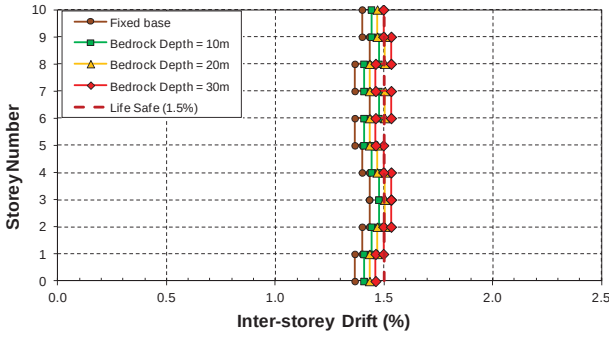

(b)

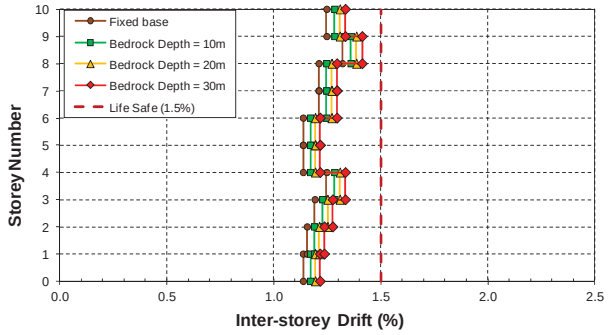

(c)

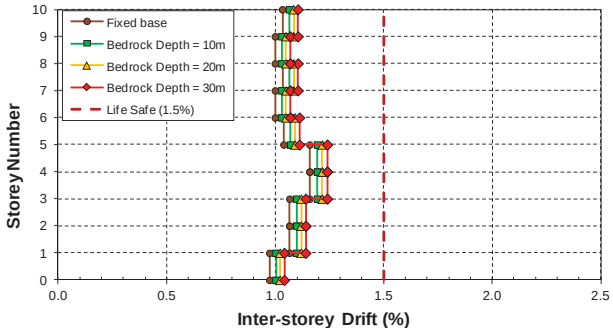

(d)

Figure A.40: Inelastic inter-storey drifts of model S10 resting on soil class D_e with variable bedrock depths; (a) Northridge (1994); (b) Kobe (1995); (c) El-Centro (1940); (d) Hachinohe (1968)

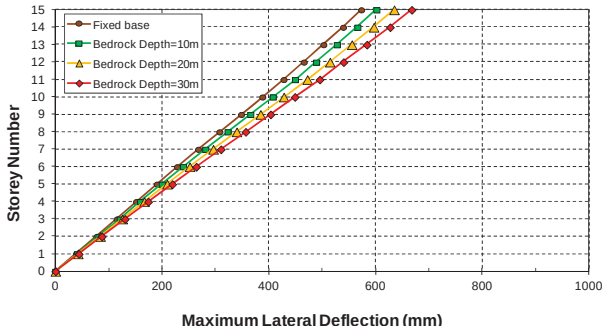

(a)

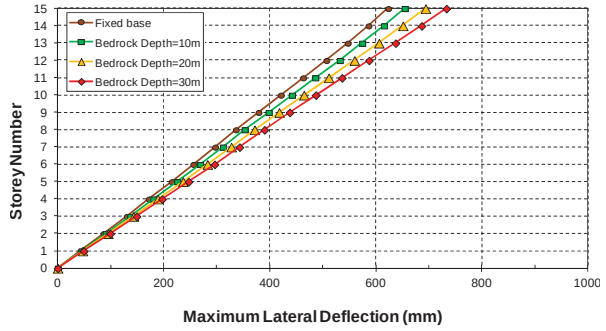

(b)

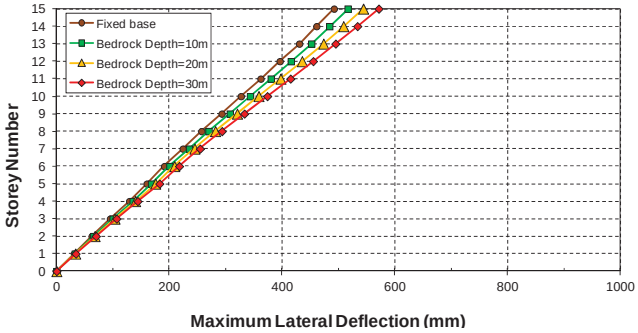

(c)

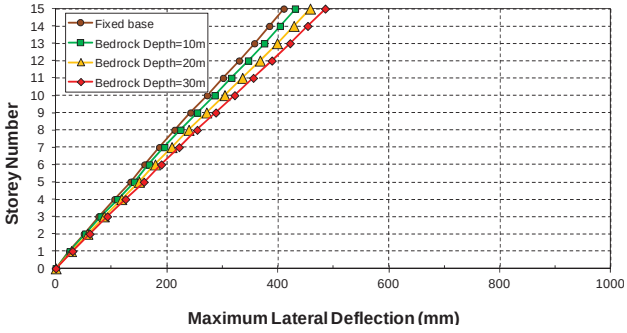

(d)

Figure A.41: Inelastic storey deflections of model S15 resting on soil class D_e with variable bedrock depths; (a) Northridge (1994); (b) Kobe (1995); (c) El-Centro (1940); (d) Hachinohe (1968)

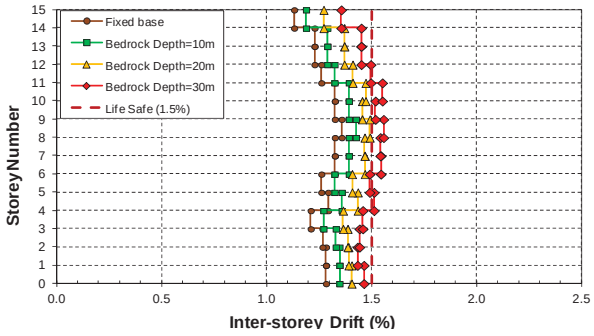

(a)

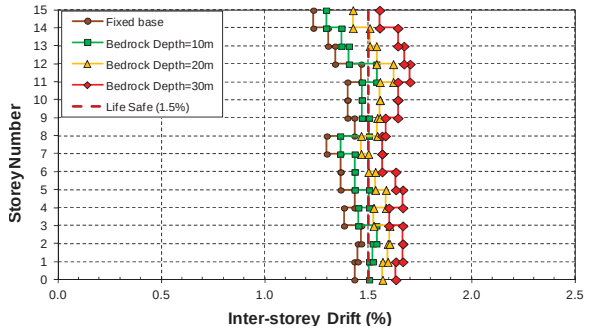

(b)

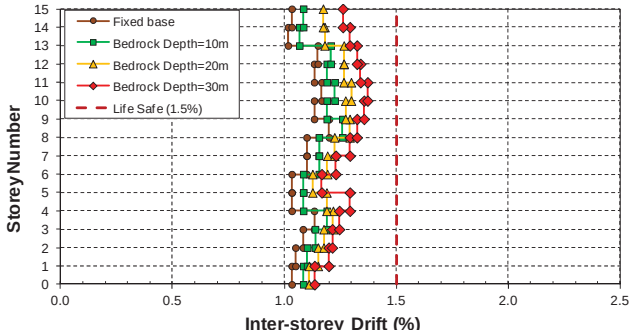

(c)

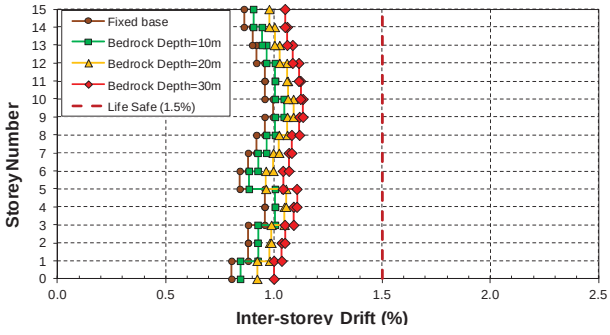

(d)

Figure A.42: Inelastic inter-storey drifts of model S15 resting on soil class D_e with variable bedrock depths; (a) Northridge (1994); (b) Kobe (1995); (c) El-Centro (1940); (d) Hachinohe (1968)

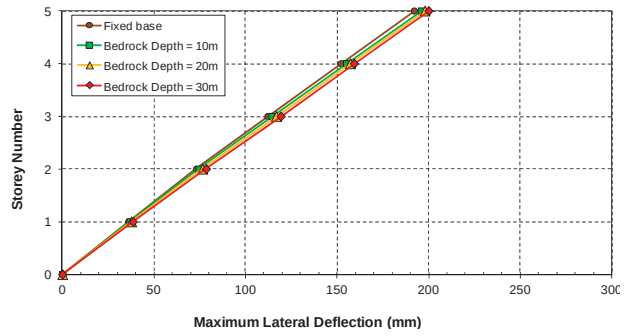

(a)

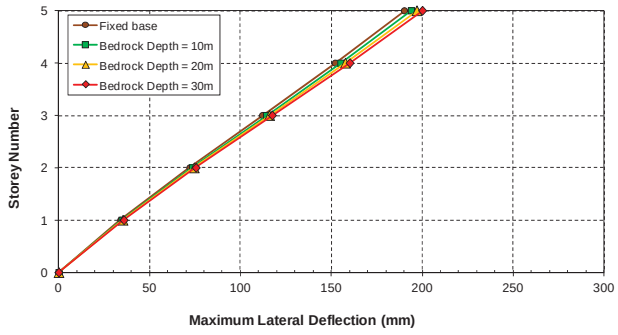

(b)

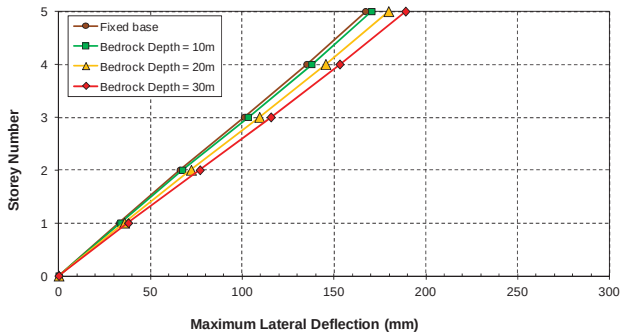

(c)

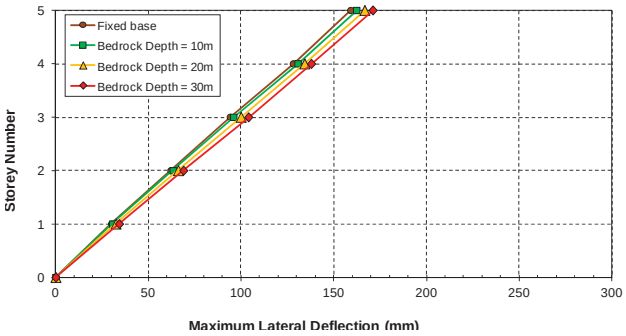

(d)

Figure A.43: Inelastic storey deflections of model S5 resting on soil class E_e with variable bedrock depths; (a) Northridge (1994); (b) Kobe (1995); (c) El-Centro (1940); (d) Hachinohe (1968)

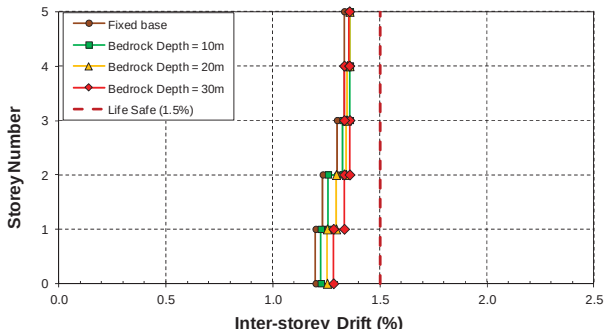

(a)

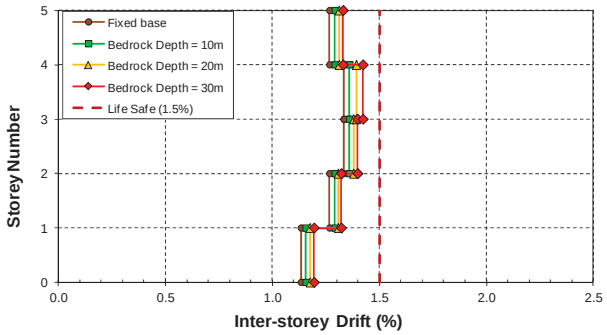

(b)

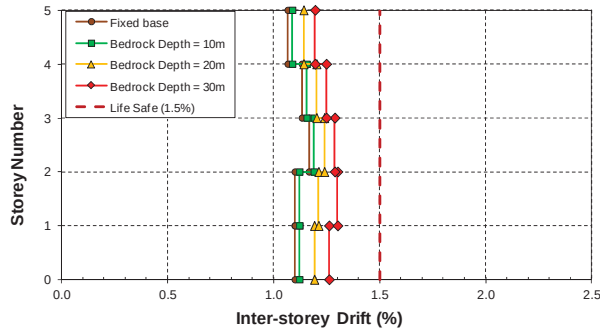

(c)

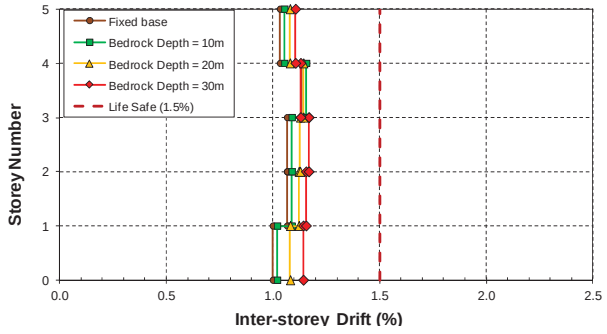

(d)

Figure A.44: Inelastic inter-storey drifts of model S5 resting on soil class E_e with variable bedrock depths; (a) Northridge (1994); (b) Kobe (1995); (c) El-Centro (1940); (d) Hachinohe (1968)

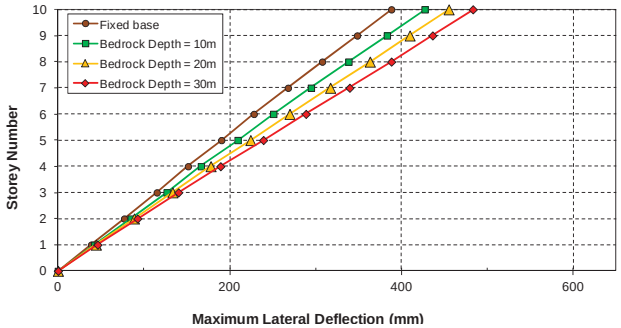

(a)

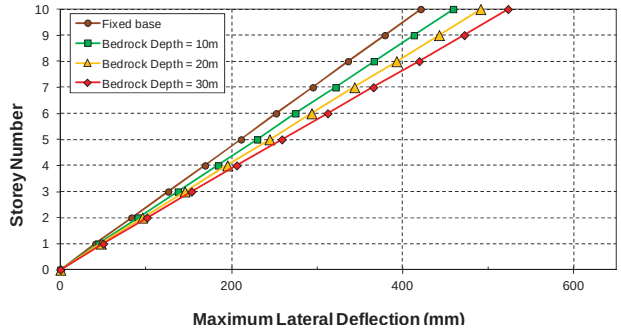

(b)

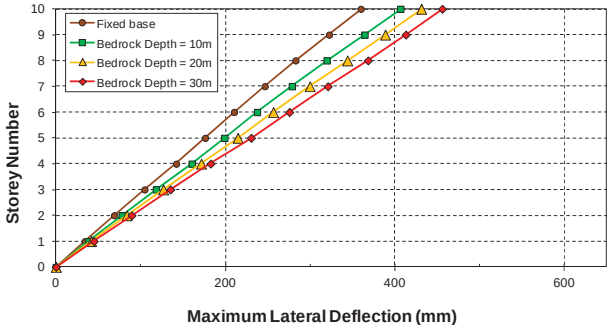

(c)

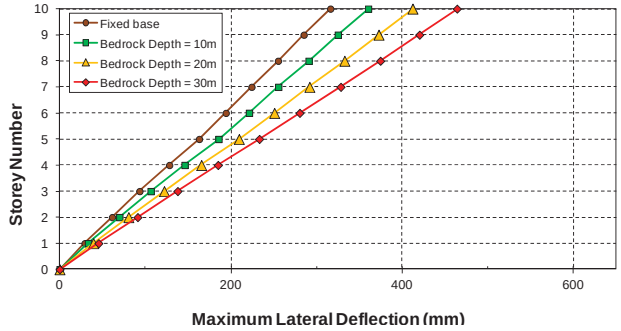

(d)

Figure A.45: Inelastic storey deflections of model S10 resting on soil class E_e with variable bedrock depths; (a) Northridge (1994); (b) Kobe (1995); (c) El-Centro (1940); (d) Hachinohe (1968)

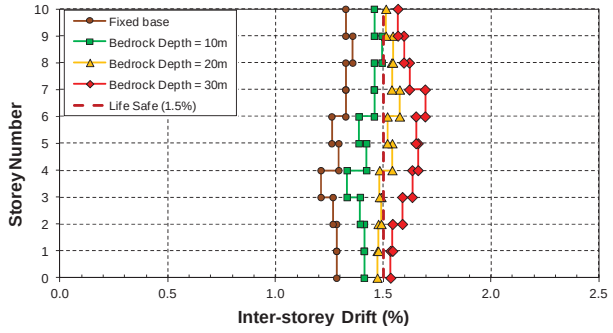

(a)

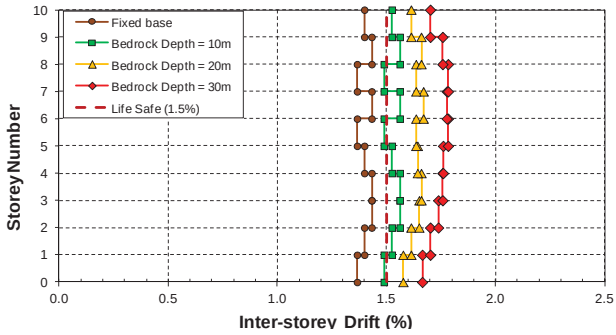

(b)

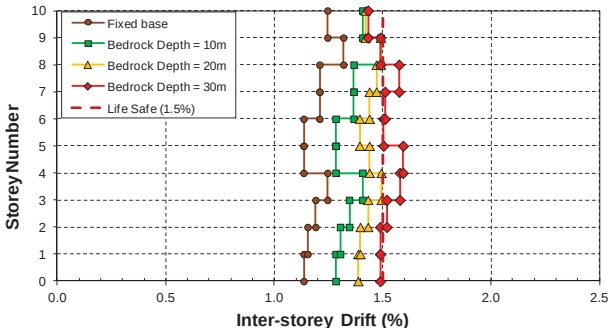

(c)

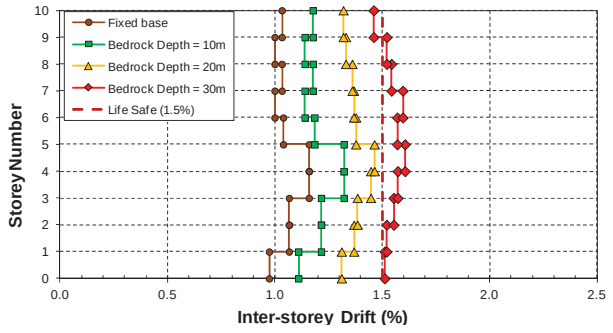

(d)

Figure A.46: Elastic inter-storey drifts of model S10 resting on soil class E_e with variable bedrock depths; (a) Northridge (1994); (b) Kobe (1995); (c) El-Centro (1940); (d) Hachinohe (1968)

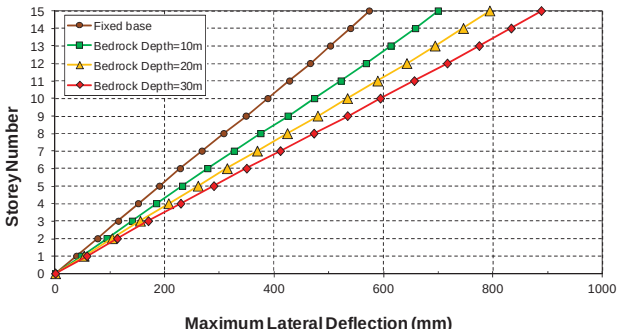

(a)

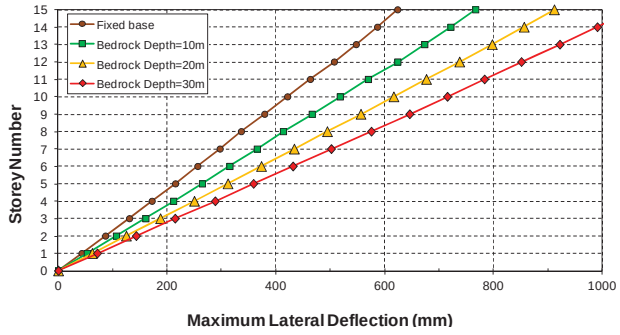

(b)

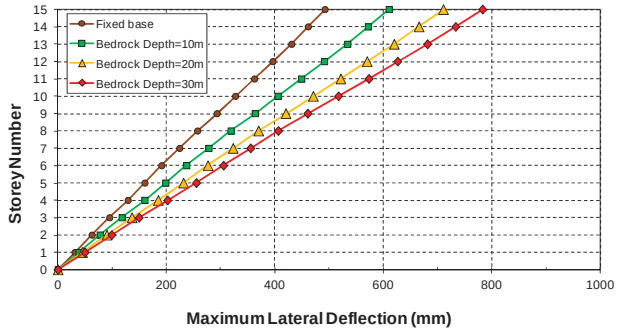

(c)

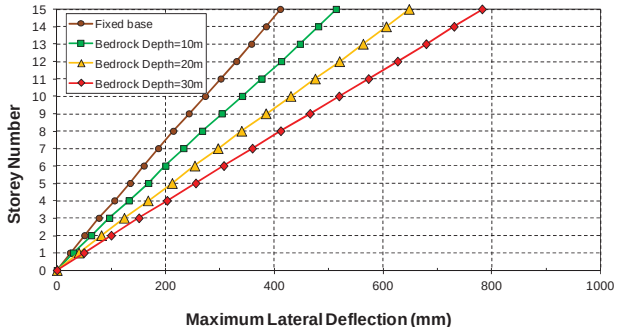

(d)

Figure A.47: Inelastic storey deflections of model S15 resting on soil class E_e with variable bedrock depths; (a) Northridge (1994); (b) Kobe (1995); (c) El-Centro (1940); (d) Hachinohe (1968)

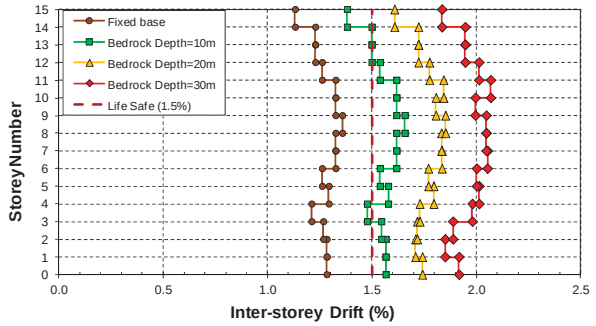

(a)

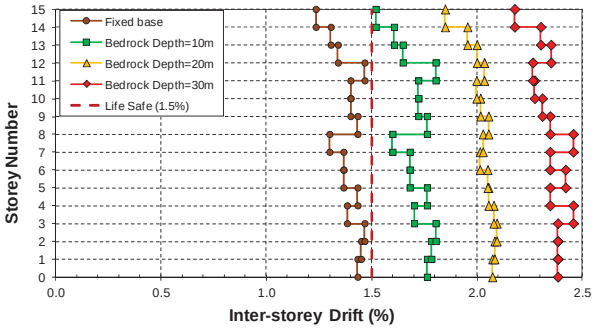

(b)

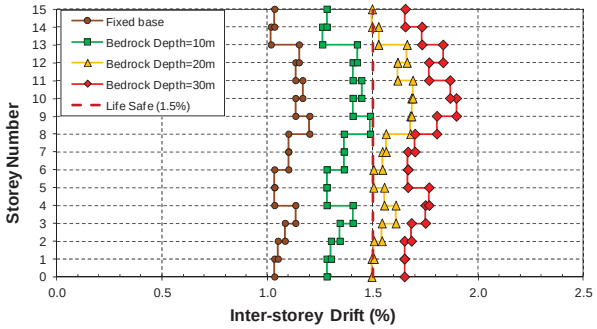

(c)

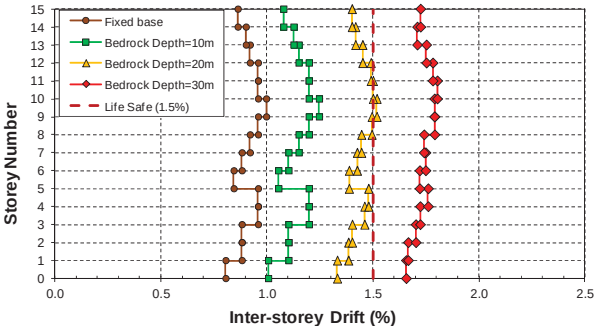

(d)

Figure A.48: Inelastic inter-storey drifts of model S15 resting on soil class E_e with variable bedrock depths; (a) Northridge (1994); (b) Kobe (1995); (c) El-Centro (1940); (d) Hachinohe (1968)